Adipose Tissue Remodeling in Response to Corticosterone and β3-Adrenergic Receptor Agonist Mirabegron

By JOCELYN SUSAN BEL

A dissertation submitted in partial fulfillment of the requirements of the degree

of Doctor of Philosophy in Biotechnology

Biotechnology PhD Program, Lakehead University Thunder Bay, Ontario, Canada

Abstract

With the rise of metabolic diseases including obesity and type 2 diabetes, the need to investigate one of the most dynamic endocrine organs is critical for combating these diseases. Adipose tissue (AT) exists predominantly in two forms: white AT (WAT) and brown AT (BAT). This study set out to investigate how chronic levels of glucocorticoids (GC), namely corticosterone, influence AT, and if the negative effects of GCs can be combated with a β3-adrenergic receptor (β3AR) agonist, mirabegron. Mice were subjected to oral treatments of either, corticosterone (500μg/day), mirabegron (either 0.024mg/day or 0.24mg/day), a combination of the two, or naïve or vehicle (<1% ethanol) controls for four weeks. The corticosterone dose was chosen to match the level of corticosterone circulating in Cushing's syndrome patients, and the mirabegron treatments were chosen to be a much lower dose (0.024mg/day) than or to closely resemble the maximal dosage approved (0.24mg/day) for overactive bladder patients. We hypothesized that mirabegron would offset the negative impacts of corticosterone-induced metabolic dysfunction and lipid accumulation within the AT depots. Corticosterone treatment resulted in BAT whitening, significantly ($p \leq 0.05$) increased body and AT weights, whole-body insulin resistance and circulating leptin levels. Mirabegron did not induce WAT beiging or influence any other factors. In the BAT, both mirabegron and surprisingly the corticosterone treatments resulted in significantly ($p \leq 0.05$) increased UCP1 protein expression. When combined, mirabegron failed to prevent the negative effects of corticosterone and resulted in metabolic parameters that closely matched the corticosterone treatment alone. Both the corticosterone and combination treatments had significantly ($p \leq 0.05$) less mitochondria per gram of tissue. None of the treatments influenced oxidative stress markers in BAT or WAT. This is the first study to report systemic metabolic effects in a short duration while also demonstrating that at the maximal approved dose,

mirabegron cannot counteract corticosterone-induced alterations in AT. Future work into examining the pathways directly involved with BAT and WAT in response to GCs will be vital for furthering our understanding and their effects on AT dysfunction, and then new therapeutic agents can be tested for their ability to offset these tissue-specific alterations.

Acknowledgments

I would like to thank my supervisors Dr. Simon Lees and Dr. Neelam Khaper for the amazing opportunity to pursue research in their labs and for their support throughout my studies. Your guidance and mentorship have been invaluable to my growth as a scientist and I will be eternally grateful for everything you have helped me accomplish. To my dissertation committee members, Dr. Marina Ulanova and Dr. Zacharais Suntres, your feedback really helped shape my project throughout the last four years, and I can't thank you enough for your expertise. I would also like to thank my comprehensive external examiner Dr. Chris Phenix. A huge thank you to my external dissertation examiner Dr. Ayesha Saleem who provided a very in-depth review of my dissertation and who's critiques helped shape the final document.

My project would not have been accomplished without Dr. Maki the Lakehead University veterinarian and the dedication of Trista King, our veterinary technician. I can't thank you both enough for being so diligent with the care of my mice and ensuring that everything (within our control) ran smoothly. I would also like to thank Jodi Morrison at the Ontario Veterinary College for her time and expertise with preparing my histological samples. To all the members of the Northern Ontario School of Medicine lab, thank you for your support during these last four years, and always being willing to troubleshoot experiments with me! I would specifically like to thank Sarah Niccoli, Shayen Sreetharan, Riley Voth and Jake Puskas for their assistance with completing my project.

A huge thank you goes out to my brother Nick Bel who helped me with every aspect of my project, including venturing out into the world of animal work and learning muscle dissections. I wouldn't have been able to execute everything without you Nick, thanks for being my best friend and lab partner! To my Mom and Dad, your continued encouragement and understanding over these last four years means everything to me! I would not have been able to finish this dissertation and get through the stress of completing it without your continued support. I can't begin to explain how much it meant to me that you were willing to re-read and listen to this dissertation repeatedly with a smile. To Carlos Chan, thanks for being a continued pillar of support during the last year of my PhD, this was likely the most stressful time in my life, but our relationship made it better then I could have imagined. Finally, to all my other family and friends, thanks for being apart of this journey and continually supporting my research endeavours. I also would like to thank all my four-legged friends who continually provided me with emotional support during my 11 years in university: Mia, Jasmine, Bella, Abby, Raymond, Simon and Kahleigh.

Dedication

I would like to dedicate this dissertation to my best friends Abby and Kahleigh. Their willingness to sit beside me while I worked out all aspects of this project, wrote manuscripts, put together presentations and listen to me practise them meant the world to me. They always knew when I needed a break, or just a moment to smile, especially when I was stressed. While Abby couldn't be here to finish my PhD with me, Kahleigh stepped into her big shoes and filled them flawlessly. I can't imagine doing this without their support.

Table of Contents

Abbreviations

[^{18}F]-FDG	^{18}F-Fluorodeoxyglucose
[^{18}F]-FDG-PET/CT	^{18}F-Fluorodeoxyglucose Positron Emission Tomography and Computed Tomography
11β-HSD1/2	11β-Hydroxysteroid Dehydrogenase Type 1/2
4-HNE	4-Hydroxynonenal/ 4-hydroxy-2-noneal
ACC	Acetyl Co-A Carboxylase
Acetyl CoA	Acetyl Coenzyme A
ACTH	Adrenocorticotropic hormone
ADRP	Adipocyte Differentiation Protein
AGRKO	Adipocyte-specific GR Knockout
AMPK	Adenosine Monophosphate Activated Protein Kinase
ANGPTL4	Angiopoietin-Like 4
AR	Adrenergic Receptor
AS1	Animal Study #1
AS2	Animal Study #2
AT	Adipose Tissue
ATF	Activating Transcription Factor
ATGL	Adipose Triglyceride Lipase
ATM	Adipose Tissue Macrophages
ATP	Adenosine Triphosphate
BAT	Brown Adipose Tissue
BMI	Body Mass Index
BMP	Bone Marrow Protein
cAMP	Cyclic Adenosine Monophosphate
CCL5	Chemotactic Chemokine Ligand 5
CD36	Cluster of Differentiation 36

CD4+ T-cells	Cluster of Differentiation 4 T-cells
CD8+ T-cells	Cluster of Differentiation 8 T-cells
CE	Cold Exposure
CCE	Chronic Cold Exposure
CEBP(β/α)	CCAAT/Enhancer-Binding Protein (β/α)
CIDEA/CIDEC	Cell Death Inducing DNA Fragmentation Factor α -like Effector A/C
CLS	Crown Like Structures
CNS	Central Nervous System
CORT	Corticosterone
CREB	cAMP Response Element-Binding Protein
CRH	Corticotropin-releasing hormone
CTBP	C-Terminal Binding Protein
DAG	Diacylglycerol
DGAT	Diacylglycerol acyltransferase
DIO	Diet Induced Obesity
DIT	Diet Induced Thermogenesis
ECL	Enhanced Chemiluminescence
EE	Energy Expenditure
ER	Endoplasmic Reticulum
ETC	Electron Transport Chain
FATP	Fatty Acid Transporter Protein
FFA/ FA	Free Fatty Acids/ Fatty Acid
FGF21	Fibroblast Growth Factor 21
FSP27	Fat Specific Protein 27
GC	Glucocorticoid
GLUT4	Glucose Transporter 4
GR	Glucocorticoid Receptor
GR-KO	Glucocorticoid Receptor Knock Out
GRE	Glucocorticoid response Element

H&E	Hematoxylin and Eosin
HDL	High density lipoprotein
HFD	High Fat Diet
HOMA-IR	Homeostatic Model of Assessment of Insulin Resistance
HPA Axis	Hypothalamic Pituitary Adrenal Axis
HSL	Hormone Sensitive Lipase
Hsp90	Heat Shock Protein 90
iBAT	Interscapular Brown Adipose Tissue
ICE	Intermittent Cold exposure
IL-1β/ α	Interleukin 1β/ α
IL-4	Interleukin 4
IL-5	Interleukin 5
IL-6	Interleukin 6
IL-10	Interleukin 10
IL-13	Interleukin 13
INFγ	Interferon γ
ingWAT	Inguinal White Adipose Tissue
IR	Insulin Resistance
IRE1	Inositol Requiring Enzyme 1
IRS	Insulin Receptor Substrate
JAK/STAT	Janus Kinases- Signal Transducer and Activator of Transcription
JNK	c-Jun N-terminal Kinase
KLF	Kruppel-Like Factor
KO	Knock Out
LD	Lipid Droplet
LPL	Lipoprotein Lipase
LDLP	Low Density Lipoprotein
Lipe	Gene encoding for Hormone Sensitive Lipase
MAG	Monoacylglycerol

MAPK	Mitogen-Activated Protein Kinase
MC	Mineralocorticoid
MCP-1	Monocyte Chemoattractant Protein 1
Mgll	Gene encoding for Monoglyceride lipase
MMe	Metabolic Macrophage
MR	Mineralocorticoid receptor
mRNA	Messenger RNA
mtDNA	Mitochondrial DNA
mTOR	Mammalian Target of Rapamycin
mtTFA/mtTFB	Mitochondrial transcription factor A / B
Myf5	Myogenic Factor 5
NE	Norepinephrine
NFkB	Nuclear Factor kappa-light-chain-enhancer of activated B cells
NK cells	Natural Killer Cells
NRF1/2	Nuclear Respiratory Factor 1/2
NST	Non-Shivering Thermogenesis
p38MAPK	p38 mitogen-activated protein kinase
PERK	Pancreatic EIF2-α kinase
PGC1α/ PGC1β	Peroxisome Proliferator Activated Receptor Gamma Coactivator 1 α/ β
PKA	Protein Kinase A
PLIN	Perilipin
PPARγ/ α	Peroxisome Proliferator Activated Receptor γ/ α
PRDM16	PR Domain Zinc Finger 16
RAAS	Renin Angiotensin Aldosterone System
RER	Respiratory Exchange Ratio
ROS	Reactive Oxygen Species
SAM	Sympathetic Neuron Associated Macrophages
scWAT	Subcutaneous White Adipose Tissue
SIRT1	Sirtuin Silent Mating Type Information Regulation 2 Homologue 1

SNS	Sympathetic Nervous System
SOCS3	Suppressor of Cytokine Signaling 3
SREBP1	Sterol Regulatory Element-Binding Protein 1
T2D	Type 2 Diabetes
TAG	Triglyceride
TLR	Toll-Like Receptors
TMEM26	Transmembrane Protein 26
TNFα	Tumor Necrosis Factor α
TRL	Triglyceride Rich Lipoprotein
TZD	Thiazolidinedione
UCP-1 / *Ucp-1*	Uncoupling Protein 1
UPR	Unfolding Protein Response
VEGF	Vascular Endothelial Growth Factors
VLDL	Very-Low-Density Lipoprotein
vWAT	Visceral White Adipose Tissue
WAT	White Adipose Tissue
WHO	World Health Organization
XBP1	X-box-Binding Protein 1
β2AR	β2-Adrenergic Receptor
β3AR	β3-Adrenergic Receptor

List of Figures

List of Tables

Chapter 1: Introduction

Study Rationale

Adipose tissue (AT) has been found to exist in two predominant forms, white adipose tissue (WAT) (the conventional storage organ) and brown adipose tissue (BAT) (the fat organ responsible for non-shivering thermogenesis (NST) which has specialized proteins that allow it to produce heat for the organism to regulate temperature) (Chait and den Hartigh, 2020; Luo and Liu, 2016). These two types of AT exist in distinct depots within the body that are well known and can be isolated. This study will specifically investigate the inguinal (ingWAT) and interscapular BAT (iBAT) depots in the context of metabolism. Studies examining AT metabolism have found that certain WAT depots can become "activated" to express predominantly BAT-associated genes and proteins, namely UCP1, and have higher metabolic function that may contribute to better overall health (Chait and den Hartigh, 2020). These "activated" WAT depots are called beige AT and may play a key role in whole-body metabolism (Chait and den Hartigh, 2020). The intricate relationship between AT signalling and metabolism may have connections to alterations in the mitochondria since UCP1 uncouples mitochondrial respiration. AT mitochondria have recently been studied in the context of obesity and researchers have found that mitochondrial control and metabolism are altered under different diseases (Holmström et al., 2012). Further research into this organelle's effect on metabolic diseases needs to be investigated more thoroughly.

Previous studies have reported that AT's role in metabolism and as an endocrine organ extends far beyond energy storage and its ability to influence overall health (Bartlet & Heeren, 2013; Bettini et al., 2019; Chait & den Hartigh, 2020; K. Y. Chen et al., 2020; Cummins et al.,

2014; Guilherme et al., 2019; R. Pan et al., 2020; Peng et al., 2015; Wu & Ballantyne, 2020). The cells that make up AT, adipocytes, are also responsible for secreting leptin, a satiety hormone that is produced in amounts proportional to the amount of triglycerides stored in the AT depots (L. Chen et al., 2015; Guilherme et al., 2019; Kahn et al., 2019; Kershaw & Flier, 2004; Kotzbeck et al., 2018; Luo & Liu, 2016; W. W. Pan & Myers, 2018). Links to AT and metabolic diseases such as obesity and type 2 diabetes (T2D) have also been emerging in recent years. Chronic stress has also been shown to negatively influence whole-body metabolism which can lead to detrimental health effects, poor quality of life and can culminate in metabolic syndrome (Di Dalmazi et al., 2012; Han & Lean, 2016; Tamashiro et al., 2011). Metabolic syndrome is a cluster of risk factors that includes insulin resistance, obesity, intra-abdominal fat accumulation, hypertension and dyslipidemia leading to the development of cardiovascular disease and diabetes (Han & Lean, 2016). Each of these risk factors has a direct association with AT, but the exact mechanisms linking this tissue to metabolic syndrome are not fully understood. AT's influence on whole-body metabolism and overall health has sparked interest in researchers who believe this endocrine organ may be a key factor in combatting the negative effects of metabolic syndrome and be related to the stress response. Links between oxidative stress, metabolic syndrome and inflammation have begun to be investigated in the context of AT. New therapies using cold exposure (CE) or pharmacological agents that act through the sympathetic nervous system (SNS) pathway (e.g., mirabegron, a β3-adrenergic receptor (β3AR) agonist) have been used to stimulate WAT to become more metabolically active, less of a chronic storage vesicle, and have been under investigation more so over the last ten years (Bel et al., 2021). In order to thoroughly

investigate the effects of stimulating WAT to become more metabolically active (this process is termed beiging), more research needs to be conducted.

Obesity is a comorbidity to a variety of other pathologies that can cause serious health effects, including death (Manna and Jain, 2015). Many of these pathologies have been linked to oxidative stress (Manna and Jain, 2015; Masschelin et al., 2020). The exact mechanisms between these pathologies and oxidative stress within AT are still unclear (Masschelin et al., 2020). Although the mitochondria is the largest source of ROS in mammalian cells, the role of lipid peroxidation, especially in adipocytes, plays a significant part in AT oxidative stress (Masschelin et al., 2020). With a focus on AT, this thesis aims to study the relationship between both corticosterone induced and mirabegron induced alterations to metabolism. Currently, there are minimal studies that examine the direct relationships each of these treatments can have on the amount of oxidative stress within AT.

Chronic treatment with corticosterone in mice has been previously deemed a model of metabolic syndrome mimicking diseases like T2D and Cushing's syndrome (Cassano et al., 2012; Do et al., 2019; van Donkelaar et al., 2014; Karatsoreos et al., 2010; Kinlein et al., 2017; Luijten et al., 2019; Wray et al., 2019). Patients with Cushing's syndrome have chronically high levels of GCs that have been linked to high levels of ROS and oxidative stress (Karamouzis et al., 2015). Masschelin et al. (2020) reviewed how oxidative stress impacts AT energy balance and note specifically how prolonged stress will influence metabolism through the enzymes involved in the Kreb's cycle and ETC (Masschelin et al., 2020). Oxidation of lipids in the stressed state also play a role in obesity where correlations have been noted in ROS levels and increased central AT in both humans and mice (Masschelin et al., 2020). WAT, due to its increased lipid storage capacity,

is more probe to lipid peroxidation than other types of AT (Masschelin et al., 2020). Obese mice show decreased 4-HNE metabolism and increased stress response proteins, both of which play a role in insulin signaling and may contribute to insulin resistance (Masschelin et al., 2020). The increased levels of ROS in obesity further restrict mitochondrial biogenesis and further render effects within the AT depot itself (Masschelin et al., 2020).

Do et al. (2019) used corticosterone in drinking water (100μg/ml) to investigate the WAT specific response to GCs in order to better understand the link between obesity related complications in metabolic syndromes (Do et al., 2019). Their study found vast differences in the stress response within different WAT depots (vWAT vs scWAT) but noted all WAT depots had increased 11β-HSD1 gene expression with corticosterone treatment. They also used flow cytometry to investigate the level of macrophage infiltration and found that increased macrophages (through Cd68 and F4/80 levels) were only increased in the AT depots, not in the intestine or liver (Do et al., 2019). The level of MCP-1 increased in both the mRNA and protein levels in the AT depots of corticosterone treated mice, which is consistent with increased macrophage infiltration in patients with obesity, mice fed HFDs, and genetically obese diabetic mice (Kanda et al., 2006; Weisberg et al., 2006).

Treatments examining mirabegron as a beiging agent do not widely investigate specific oxidative stress markers. Since its intended use is for overactive bladder, most studies have been focusing on that disease. A new review looking into overactive bladder and its connection to oxidative stress has provided some information about a possible role mirabegron could be playing in this context (Wu et al., 2021). Overactive bladder is associated with decreased nitric

oxide release, hypoxia and increased ATP, all of which decrease the ability of the bladder to contract (Wu et al., 2021). These factors also contribute to the increased oxidative stress and free radicals associated with the disease (Wu et al., 2021). Urine oxidative stress markers including 8-Hydroxy-2'-Deoxyguanosine, malondialdehyde, and isoprostanes have all been linked to bladder dysfunction, metabolic syndrome, obesity and diabetes in animal models (Wu et al., 2021). Mirabegron works to relax the bladder muscle through the β3AR pathway and the action of nitric oxide (Wu et al., 2021). With the ability to relax the smooth muscle and therefore facilitate nitric oxide action, mirabegron may be influencing the oxidative capacity through this mechanism and thereby render less oxidative stress. However more research needs to be done to fully understand this connection.

One recent study has started to inquire into mirabegron's mechanism in relation to its ability to counteract obesity. Peres Valgas da Silva et al. (2021) recently induced obesity in mice and then attempted to offset the negative side effects with a two-week treatment with mirabegron (10mg/kg)(Peres Valgas da Silva et al., 2021). They observed a partial rescuing effect on circulating thiobarbituic acid reactive substance, a marker of lipid peroxidation, within the mice receiving the mirabegron treatment (Peres Valgas da Silva et al., 2021). To our knowledge, this was one of the only studies to connect an oxidative stress marker to a mirabegron treatment, however, it was measured through circulating levels, not at the AT depot specifically. This is where our study hopes to add knowledge in this area.

An understanding of how β3AR stimulation therapy induces beiging or influences BAT within the context of elevated glucocorticoids (GCs) also needs to be investigated due to the

high prevalence of chronic stress in the world's population. The goal of this study is to determine how stress hormones (more specifically, corticosterone in mice) affect the beiging process, the adaptive response in BAT, metabolic dysfunction, and the AT phenotype. If AT can be stimulated to be metabolically active, the tissue's response to chronic stress may be diminished and therefore may lead to fewer metabolic diseases and its detrimental health effects. By investigating the interaction between stress and the NST pathways, steps can be undertaken to combat the many health conditions that are affected by AT.

This study aimed to investigate how AT metabolism responds to chronic stress and the NST pathway. In order to accomplish this, the stress hormone in mice, corticosterone, will be administered via drinking water to observe its effects on AT metabolism. To study the activation of AT, the β3AR pathway (the process responsible for the production of heat through NST in BAT) will be stimulated by the pharmacological compound mirabegron, a selective β3AR agonist that will also be administered in drinking water. Once the individual effects of corticosterone and mirabegron are determined for AT metabolism and activation, the combination of the two treatments will provide additional information regarding the interaction between stress and NST pathways interact, and how this interaction may be beneficial in combating metabolic diseases (depicted in Figure 1).

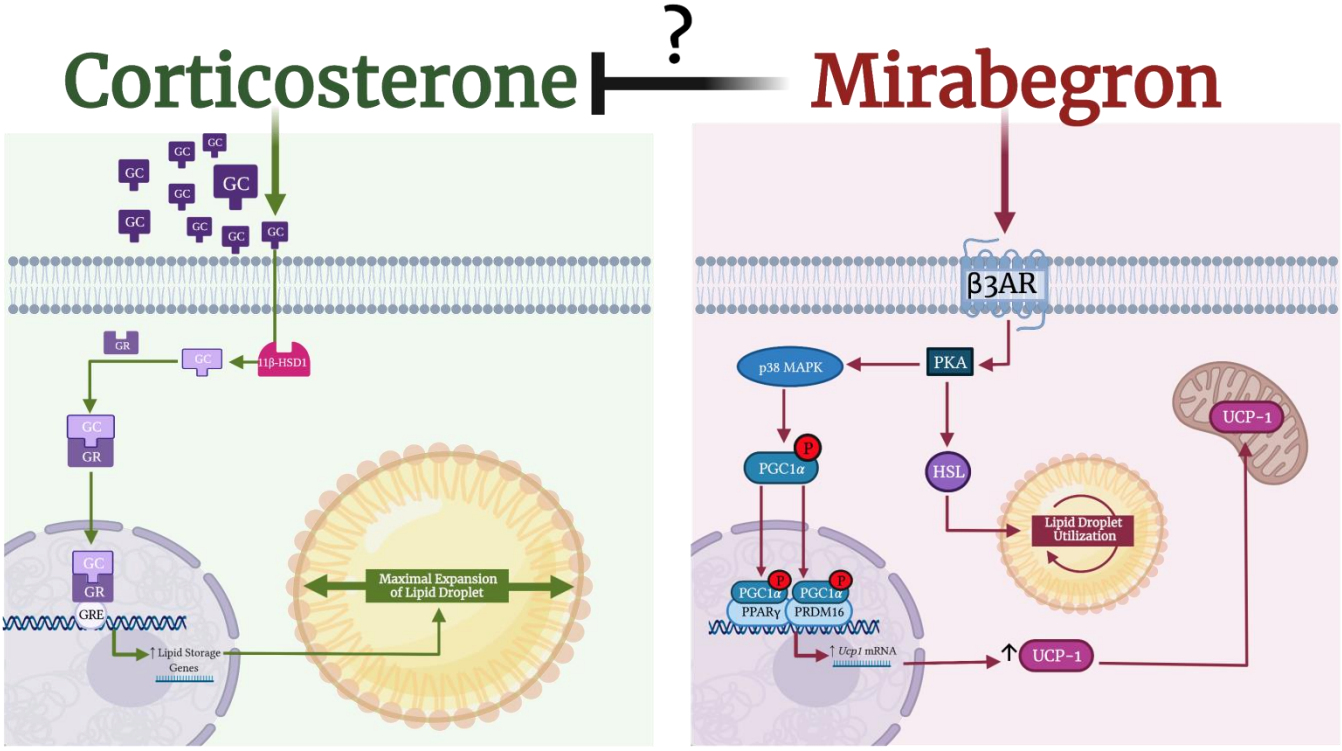

Figure 1: Metabolic pathways investigated in this study.

A graphical image representing the two competing metabolic pathways investigated in this study. Chronic exposure to glucocorticoid (GC) corticosterone excess (green) and activation of the β3-adrenergic receptor (β3AR) pathway via mirabegron (red arrows) may result in the following potential interactions. GCs will become activated by 11β-hydroxysteroid dehydrogenase type 1 (11β-HSD1). Once active, GCs will bind to the Glucocorticoid receptor (GR) where it will travel to the nucleus and bind to the glucocorticoid response element (GRE). Once bound inside the nucleus, the GRE will inhibit many pathways including mitochondrial biogenesis, transcription of inflammatory markers, and lipid storage genes. Increased lipid storage will then increase the size of the lipid droplet and storage capacity within the tissue. The β3AR is activated by mirabegron and will further activate protein kinase A (PKA) which will initiate a series of downstream reactions including activating protein p38 mitogen-activated protein kinase (p38MAPK). Active p38MAPK will subsequently phosphorylate peroxisome proliferator-activator receptor-gamma coactivator-1α (PGC1α). Phosphorylated PGC1α will enter the nucleus and bind to subsequent transcription factors allowing for the translation of proteins UCP1 and PGC1α, allowing for increased mitochondrial uncoupling and the production of heat. PKA can also increase the translocation of hormone-sensitive lipase (HSL) to the lipid droplet which will increase lipid utilization and metabolism.

Dissertation Goal, Hypothesis and Specific Aims

The overall goal of this project was to determine how the effects of chronic corticosterone and β3AR stimulation impact AT. Our central hypothesis was that the negative effects of excessive lipid accumulation induced by chronic corticosterone are alleviated by a β3AR agonist. The specific aims of this project are as follows:

1) Establish how corticosterone or β3AR stimulation impact AT and UCP1 expression
2) Determine how oxidative stress, immune cell infiltration, and leptin are influenced by corticosterone or under β3AR stimulation
3) Investigate the effects of corticosterone or β3AR stimulation on whole-body insulin resistance
4) Examine mitochondrial content in response to corticosterone and β3AR stimulation in both BAT and WAT

References

Bel, J.S., Tai, T.C., Khaper, N., Lees, S.J., 2021. Mirabegron: The most promising adipose tissue beiging agent. Physiol Rep 9. https://doi.org/10.14814/phy2.14779

Bartlet, A., & Heeren, J. (2013). Adipose Tissue Browning and Metabolic Health. *Nature Reviews Endocrinology*, *10*, 24–26. https://doi.org/doi:10.1038/nrendo.2013.204

Bettini, S., Favaretto, F., Compagnin, C., Belligoli, A., Sanna, M., Fabris, R., Serra, R., Dal Prà, C., Prevedello, L., Foletto, M., Vettor, R., Milan, G., & Busetto, L. (2019). Resting Energy Expenditure, Insulin Resistance and UCP1 Expression in Human Subcutaneous and Visceral Adipose Tissue of Patients With Obesity. *Frontiers in Endocrinology*, *10*, 548. https://doi.org/10.3389/fendo.2019.00548

Cassano, A.E., White, J.R., Penraat, K.A., Wilson, C.D., Rasmussen, S., and Karatsoreos, I.N. (2012). Anatomic, Hematologic, and Biochemical Features of C57BL/6NCrl Mice Maintained on Chronic Oral Corticosterone. Comparative Medicine by the American Association for Laboratory Animal Science *62*, 348–360.

Chait, A., & den Hartigh, L. J. (2020). Adipose Tissue Distribution, Inflammation and Its Metabolic Consequences, Including Diabetes and Cardiovascular Disease. *Frontiers in Cardiovascular Medicine*, *7*, 22. https://doi.org/10.3389/fcvm.2020.00022

Chen, K. Y., Brychta, R. J., Abdul Sater, Z., Cassimatis, T. M., Cero, C., Fletcher, L. A., Israni, N. S., Johnson, J. W., Lea, H. J., Linderman, J. D., O'Mara, A. E., Zhu, K. Y., & Cypess, A. M. (2020). Opportunities and challenges in the therapeutic activation of human energy expenditure and thermogenesis to manage obesity. *Journal of Biological Chemistry*, *295*(7), 1926–1942. https://doi.org/10.1074/jbc.REV119.007363

Chen, L., Chen, R., Wang, H., & Liang, F. (2015). Mechanisms Linking Inflammation to Insulin Resistance. *International Journal of Endocrinology*, *2015*, 1–9. https://doi.org/10.1155/2015/508409

Cummins, T. D., Holden, C. R., Sansbury, B. E., Gibb, A. A., Shah, J., Zafar, N., Tang, Y., Hellmann, J., Rai, S. N., Spite, M., Bhatnagar, A., & Hill, B. G. (2014). Metabolic remodeling of white adipose tissue in obesity. *American Journal of Physiology-Endocrinology and Metabolism*, *307*(3), E262–E277. https://doi.org/10.1152/ajpendo.00271.2013

Di Dalmazi, G., Pagotto, U., Pasquali, R., & Vicennati, V. (2012). Glucocorticoids and Type 2 Diabetes: From Physiology to Pathology. *Journal of Nutrition and Metabolism*, *2012*, 1–9. https://doi.org/10.1155/2012/525093

Do, T.T.H., Marie, G., Héloïse, D., Guillaume, D., Marthe, M., Bruno, F., and Marion, B. (2019). Glucocorticoid-induced insulin resistance is related to macrophage visceral adipose tissue infiltration. The Journal of Steroid Biochemistry and Molecular Biology *185*, 150–162. https://doi.org/10.1016/j.jsbmb.2018.08.010.

Guilherme, A., Henriques, F., Bedard, A. H., & Czech, M. P. (2019). Molecular pathways linking adipose innervation to insulin action in obesity and diabetes mellitus. *Nature Reviews Endocrinology*, *15*(4), 207–225. https://doi.org/10.1038/s41574-019-0165-y

Han, T. S., & Lean, M. E. (2016). A clinical perspective of obesity, metabolic syndrome and cardiovascular disease. *JRSM Cardiovascular Disease*, *5*, 204800401663337. https://doi.org/10.1177/2048004016633371

Holmström, M. H., Iglesias-Gutierrez, E., Zierath, J. R., & Garcia-Roves, P. M. (2012). Tissue-specific control of mitochondrial respiration in obesity-related insulin resistance and diabetes. *American Journal of Physiology-Endocrinology and Metabolism*, *302*(6), E731–E739. https://doi.org/10.1152/ajpendo.00159.2011

Kahn, C. R., Wang, G., & Lee, K. Y. (2019). Altered adipose tissue and adipocyte function in the pathogenesis of metabolic syndrome. *The Journal of Clinical Investigation*, *129*(10), 12.

Kanda, H., Tateya, S., Tamori, Y., Kotani, K., Hiasa, K., Kitazawa, R., Kitazawa, S., Miyachi, H., Maeda, S., Egashira, K., et al. (2006). MCP-1 contributes to macrophage infiltration into adipose tissue, insulin resistance, and hepatic steatosis in obesity. Journal of Clinical Investigation *116*, 1494–1505. https://doi.org/10.1172/JCI26498.

Karamouzis, I., Berardelli, R., D'Angelo, V., Fussotto, B., Zichi, C., Giordano, R., Settanni, F., Maccario, M., Ghigo, E., and Arvat, E. (2015). Enhanced oxidative stress and platelet activation in patients with Cushing's syndrome. Clin Endocrinol *82*, 517–524. https://doi.org/10.1111/cen.12524.

Karatsoreos, I.N., Bhagat, S.M., Bowles, N.P., Weil, Z.M., Pfaff, D.W., and McEwen, B.S. (2010). Endocrine and Physiological Changes in Response to Chronic Corticosterone: A Potential Model of the Metabolic Syndrome in Mouse. Endocrinology *151*, 2117–2127. https://doi.org/10.1210/en.2009-1436.

Kershaw, E. E., & Flier, J. S. (2004). Adipose Tissue as an Endocrine Organ. *The Journal of Clinical Endocrinology & Metabolism*, *89*(6), 2548–2556. https://doi.org/10.1210/jc.2004-0395

Kinlein, S.A., Shahanoor, Z., Romeo, R.D., and Karatsoreos, I.N. (2017). Chronic Corticosterone Treatment During Adolescence Has Significant Effects on Metabolism and Skeletal Development in Male C57BL6/N Mice. Endocrinology *158*, 2239–2254. .

Kotzbeck, P., Giordano, A., Mondini, E., Murano, I., Severi, I., Venema, W., Cecchini, M. P., Kershaw, E. E., Barbatelli, G., Haemmerle, G., Zechner, R., & Cinti, S. (2018). Brown adipose tissue whitening leads to brown adipocyte death and adipose tissue inflammation. *Journal of Lipid Research*, *59*(5), 784–794.

Luo, L., & Liu, M. (2016). Adipose tissue in control of metabolism. *Journal of Endocrinology*, *231*(3), R77–R99. https://doi.org/10.1530/JOE-16-0211

Luijten, I.H.N., Brooks, K., Boulet, N., Shabalina, I.G., Jaiprakash, A., Carlsson, B., Fischer, A.W., Cannon, B., and Nedergaard, J. (2019). Glucocorticoid-Induced Obesity Develops Independently of UCP1. Cell Reports *27*, 1686-1698.e5. https://doi.org/10.1016/j.celrep.2019.04.041.

Manna, P., and Jain, S.K. (2015). Obesity, Oxidative Stress, Adipose Tissue Dysfunction, and the Associated Health Risks: Causes and Therapeutic Strategies. Metabolic Syndrome and Related Disorders *13*, 423–444. https://doi.org/10.1089/met.2015.0095.

Masschelin, P.M., Cox, A.R., Chernis, N., and Hartig, S.M. (2020). The Impact of Oxidative Stress on Adipose Tissue Energy Balance. Front. Physiol. *10*, 1638. https://doi.org/10.3389/fphys.2019.01638.

Pan, R., Zhu, X., Maretich, P., & Chen, Y. (2020). Combating Obesity With Thermogenic Fat: Current Challenges and Advancements. *Frontiers in Endocrinology*, *11*, 185. https://doi.org/10.3389/fendo.2020.00185

Pan, W. W., & Myers, M. G. (2018). Leptin and the maintenance of elevated body weight. *Nature Reviews Neuroscience*, *19*(2), 95–105. https://doi.org/10.1038/nrn.2017.168

Peng, X.-R., Gennemark, P., O'Mahony, G., & Bartesaghi, S. (2015). Unlock the Thermogenic Potential of Adipose Tissue: Pharmacological Modulation and Implications for Treatment of Diabetes and Obesity. *Frontiers in Endocrinology*, *6*. https://doi.org/10.3389/fendo.2015.00174

Peres Valgas da Silva, C., Calmasini, F., Alexandre, E.C., Raposo, H.F., Delbin, M.A., Monica, F.Z., and Zanesco, A. (2021). The effects of mirabegron on obesity-induced inflammation and insulin resistance are associated with brown adipose tissue activation but not beiging in the subcutaneous white adipose tissue. Clin Exp Pharmacol Physiol *48*, 1477–1487. https://doi.org/10.1111/1440-1681.13566.

Tamashiro, K. L., Sakai, R. R., Shively, C. A., Karatsoreos, I. N., & Reagan, L. P. (2011). Chronic stress, metabolism, and metabolic syndrome. *Stress*, *14*(5), 468–474. https://doi.org/10.3109/10253890.2011.606341

van Donkelaar, E.L., Vaessen, K.R.D., Pawluski, J.L., Sierksma, A.S., Blokland, A., Cañete, R., and Steinbusch, H.W.M. (2014). Long-Term Corticosterone Exposure Decreases Insulin Sensitivity and Induces Depressive-Like Behaviour in the C57BL/6NCrl Mouse. PLoS ONE *9*, e106960. https://doi.org/10.1371/journal.pone.0106960.

Weisberg, S.P., Hunter, D., Huber, R., Lemieux, J., Slaymaker, S., Vaddi, K., Charo, I., Leibel, R.L., and Jr., A.W.F. (2006). CCR2 modulates inflammatory and metabolic effects of high-fat feeding. J. Clin. Invest. *116*, 115–124. https://doi.org/10.1172/JCI24335.

Wray, J.R., Davies, A., Sefton, C., Allen, T.-J., Adamson, A., Chapman, P., Lam, B.Y.H., Yeo, G.S.H., Coll, A.P., Harno, E., et al. (2019). Global transcriptomic analysis of the arcuate nucleus following chronic glucocorticoid treatment. Molecular Metabolism *26*, 5–17. https://doi.org/10.1016/j.molmet.2019.05.008.Wu, H., & Ballantyne, C. M. (2020). Metabolic Inflammation and Insulin Resistance in Obesity. *Circulation Research*, *126*(11), 1549–1564. https://doi.org/10.1161/CIRCRESAHA.119.315896

Chapter 2: Literature Review

Adipose Tissue

Introduction

Once thought of as just a reservoir for energy storage, adipose tissue (AT) knowledge has evolved to include major roles in the endocrine system and whole-body metabolism (Guilherme et al., 2019; Kershaw and Flier, 2004; Luo and Liu, 2016). This tissue depot was found to be an active site in sex steroid metabolism, an endocrine organ, and today is known to coordinate many biological processes including energy metabolism, immune and even neuroendocrine functions (Kershaw and Flier, 2004). Metabolically active organs, such as the liver, muscle, pancreas and brain all depend on AT to send information through adipokines which are AT secreted mediators of metabolic processes (Chait and den Hartigh, 2020; Guilherme et al., 2019; Luo and Liu, 2016; Maximus et al., 2020). AT is morphologically classified into white, brown, and beige subsets, and each of these depots have distinct physiological roles (Chait and den Hartigh, 2020; Luo and Liu, 2016). Each AT depot is innervated by the sympathetic nervous system (SNS) and is comprised of adipocytes, pre-adipocytes, macrophages, endothelial cells, and fibroblasts, all of which play a part in the various depot-specific actions (Luo and Liu, 2016). Dysfunction of any of these cells could result in conditions ranging from obesity, Type 2 Diabetes (T2D), cardiovascular disease and even cancer (Ahmad et al., 2020).

Physiological Significance of Adipose Tissue

An essential energy storage organ, AT stores triglycerides (TAGs) through lipogenesis and will release them as free fatty acids (FFAs) through lipolysis (Luo and Liu, 2016). AT integrates and services the energy for several organ systems including the liver, skeletal muscle, heart, pancreas and brain (Chait and den Hartigh, 2020; Guilherme et al., 2019). The primary function of this organ is to store excess energy when nutrients are available, in the form of TAGs in adipocytes that will grow in size (hypertrophy) and in number (hyperplasia) (Chait and den Hartigh, 2020; Luo and Liu, 2016). The AT depot is comprised of many different cell types that can secrete cytokines, chemokines, and hormones (Chait and den Hartigh, 2020). AT functions as an endocrine organ where it secretes adipokines, growth factors, cytokines and chemokines, some of which are distinct to the AT depots (Chait and Hartigh, 2020). One-third of the cells in these AT depots are adipocytes with the other two-thirds being comprised of fibroblasts, macrophages, endothelial cells, stromal cells, mesenchymal stem cells, vascular cells, immune cells and pre-adipocytes (Chait and den Hartigh, 2020; C. R Kahn et al., 2019). Within each of these types of AT depots, adipocytes can be heterogeneous both genetically and metabolically, fueling the need for more research to fully determine how this tissue affects whole-body health (C. R Kahn et al., 2019).

White Adipose Tissue

One of the most dynamic tissues in the body, white adipose tissue (WAT) accounts for 2-70% of total body weight (C. R Kahn et al., 2019). WAT is classified by location as either subcutaneous (scWAT) or visceral (vWAT) where it is either located directly under the skin or intra-abdominally and next to internal organs respectively (Chait and den Hartigh, 2020; C. R Kahn et al., 2019). Visceral adipocytes make up the mesenteric, gonadal, epicardial, retroperitoneal and omentum AT depots (Jeanson et al., 2015; C. R Kahn et al., 2019; Luo and Liu, 2016). This vWAT depot has been found to promote metabolic disease development in rodents (Luo and Liu, 2016). Primarily found in the upper and lower body regions of humans, scWAT makes up approximately 80% of all AT in healthy humans (Chait and den Hartigh, 2020; C. R Kahn et al., 2019). The depot is a metabolic "sink" for excess lipid storage that can be used in times of limited energy sources (Chait and den Hartigh, 2020; Guilherme et al., 2019; Jeanson et al., 2015; C. R Kahn et al., 2019). It is also a site for TAG synthesis in the body (Ahmad et al., 2020). The stored excess energy is then later utilized by the body when FAs are needed for energy utilization, for example in a postabsorptive state, or during exercise (Chait and den Hartigh, 2020; Leiria and Tseng, 2020). All WAT depots function to store excess TAGs in the cytoplasmic lipid droplet (LD), insulate the body, prevent heat loss, act as a barrier against infection, protect organs from lipotoxicity, and even serve as a protective layer against physical stress (Chait and den Hartigh, 2020; Heeren and Scheja, 2018; Jeanson et al., 2015; Luo and Liu, 2016).

The adipocytes that make up WAT are variable in size, 25-200μm, have a unilocular LD to store energy as TAGs, have very few mitochondria, and maintain a low oxidative rate (Jeanson et

al., 2015; Luo and Liu, 2016). The LD in white adipocytes occupies over 95% of the adipocyte volume (Leiria and Tseng, 2020).

The strong endocrine capacity of the WAT depot in secreting adipokines highlights that this organ plays a key role in metabolism and whole-body health (Jeanson et al., 2015; Kiefer, 2016). WAT has also been found to modulate immune cells within the depot by attracting macrophages through secretion of monocyte chemoattractant protein-1 (MCP-1) and tumour necrosis factor-α (TNFα), especially in times of adipocyte death (Guilherme et al., 2019) (to be discussed below). They also activate T and B cells that will further secrete cytokines and affect insulin signalling within the tissue (Guilherme et al., 2019).

WAT has become increasingly important to research due to the rise in obesity-related metabolic disorders. When there is excess energy intake, WAT will store the lipids within the depots (Chait and den Hartigh, 2020). When the storage capacity is exceeded, the adipocytes will undergo hypertrophy or generate new adipocytes until the capacity is reached (Chait and den Hartigh, 2020; C. R Kahn et al., 2019). When the storage capacity is exceeded, fat begins to accumulate in areas outside of the scWAT depot (Chait and den Hartigh, 2020). Generally, an individual's number of fat cells will remain constant from childhood through adulthood, however, obesity and overeating can alter this overall number within the body (C. R Kahn et al., 2019). In conditions like obesity, WAT increases ectopically, increasing in locations within the visceral cavity, which is linked to an increased susceptibility to comorbidities such as diabetes and atherosclerosis (Chait and den Hartigh, 2020). While lowering the amount of scWAT has been shown to be metabolically protective, there have been studies demonstrating that liposuction has little metabolic benefits in humans (Chait and den Hartigh, 2020). Rodent studies

have shown the improved metabolic outcomes, including glucose tolerance and insulin sensitivity, when scWAT is transplanted to obese mice, whereas the opposite effects are found when vWAT is transplanted, illustrating that the scWAT depot plays an important role in obesity and metabolic diseases that is not fully understood (Foster et al., 2013; Luo and Liu, 2016).

Brown Adipose Tissue

Brown Adipose Tissue (BAT) was first described by Conrad Gessner in 1551 as a hibernating gland thought to have developed for three reasons: 1) to facilitate non-shivering thermogenesis (NST) in newborns, 2) as a thermostabilizer under chronic/transient cold exposure (CE), and 3) as a bio-thermic effector organ that will facilitate hibernating animals to wake (Smith and Horwitz, 1969). With multilocular LDs, BAT is able to mobilize lipids quickly and oxidize FAs (Kiefer, 2016; Marlatt and Ravussin, 2017; Reddy et al., 2014). The ability for rodents to undergo cold-induced adaptive thermogenesis is largely due to BAT (Lowell and Spiegelman, 2000). In recent years, BAT became a prominent research topic due to its strong connection to the stress response, albeit this stress in most cases was CE, and researchers began to observe its increased respiratory rate, and influence on metabolic parameters under chronic CE (Smith and Horwitz, 1969). The first review of BAT was by Johansson in 1959, and research into this tissue has only grown exponentially since (Smith and Horwitz, 1969; Trayhurn, 2017).

Originally thought to only be found during the infant stage of human development, due to their inability to produce heat from shivering, BAT has now been found to be present in adults and has physiological relevance even though it only represents 1-2% of total AT mass (C. R Kahn et al., 2019). The identification of adult human BAT was found by three independent research

groups in 2009 during cold exposure studies using ^{18}F-Fluorodeoxyglucose Positron Emission Tomography and Computed Tomography ([^{18}F]-FDG-PET/CT) (Cypess et al., 2009; Saito et al., 2009; Virtanen et al., 2009). BAT is defined as a distinct type of AT that is morphologically and functionally different from WAT in many ways and has been reviewed elsewhere (Chait and den Hartigh, 2020; Kiefer, 2016; Leiria and Tseng, 2020; Luo and Liu, 2016; Marlatt and Ravussin, 2017; Trayhurn, 2017; Virtue and Vidal-Puig, 2013). In rodents, this depot plays a critical role in adaptive thermogenesis and its innervation of sympathetic nerves allows it to respond to cold temperatures through adrenergic receptors (ARs) (Lowell and Spiegelman, 2000). When the peripheral and thermoreceptors sense cold, the information is processed by the SNS, specifically in the hypothalamus (Münzberg et al., 2021). This leads to the release of sympathetic transmitter norepinephrine (NE) that will bind to the β3-Adrenergic receptors (β3AR) and further render a response (discussed below) (Lowell and Spiegelman, 2000; Münzberg et al., 2021). Normally found in the cervical, axillary and paraspinal regions, functionally, BAT displays a high metabolic rate when activated that contributes to whole-body metabolism (Heeren and Scheja, 2018; C. R Kahn et al., 2019). In fact, nutrient oxidation in BAT can be responsible for over 60% of the total energy expenditure (EE) in mice exposed to cold temperatures (Virtue and Vidal-Puig, 2013). BAT depots are rich in iron-containing mitochondria, which gives them the brown colour (Chait and den Hartigh, 2020; Kiefer, 2016; Luo and Liu, 2016). These mitochondria generate heat by uncoupling the Adenosine Tri-Phosphate (ATP) energy production from the electron transport chain (ETC) for NST through a specialized protein called Uncoupling Protein-1 (UCP1) that is in abundance within this depot (Chait and den Hartigh, 2020; Heeren and Scheja, 2018; Lowell and Spiegelman, 2000; Luo and Liu, 2016; Ro et al., 2014). This anion-carrier protein,

located on the inner mitochondrial membrane, allows the depot to use circulating FFA to generate heat by implementing a proton shunt that will disconnect ATP synthesis through oxidative phosphorylation, and in turn help with decreasing the number of lipids stored (Chait and den Hartigh, 2020; Heeren and Scheja, 2018; M.J. Lee et al., 2014; Luo and Liu, 2016; Ro et al., 2014).

Acute cold-induced activation of BAT allows for increased lipolysis of stored TAGs within the tissue and increased UCP1 activity allowing the organism to produce heat (Lowell and Spiegelman, 2000). Chronic activation will lead to increased *Ucp1* gene transcription, mitochondrial biogenesis, hyperplasia of BAT, and recruitment of brown adipocytes to WAT depots, called beiging (Lowell and Spiegelman, 2000; Okamatsu-Ogura et al., 2013; Peng et al., 2015). Continued stimulation of the β3AR will increase BAT mass and further allow for NST to occur (Heeren and Scheja, 2018). Heeren and Scheja (2018) note that in rodents the release of FFA from WAT can activate the sympathetic nerves which can increase the sympathetic activity of BAT serving as a feed-forward signalling mechanism between WAT FFA release and BAT consumption (Heeren and Scheja, 2018; Jeanson et al., 2015) This increase in stimulation will further amplify the oxidative potential of the BAT depot, which can play a role in burning calories (Jeanson et al., 2015).

BAT uses FFA for approximately 90% and glucose for approximately 10% of its heat production capabilities (Chait and den Hartigh, 2020; Heeren and Scheja, 2018). However, BAT is implicated in glucose clearance due to its ability to remove large amounts of glucose from the circulation and will reduce the amount of insulin secreted from the pancreatic β-cells, after a meal (Chait and den Hartigh, 2020). BAT has high levels of the insulin receptor within the depot

which contributes to it being a very important tissue for glucose disposal (Chait and den Hartigh, 2020). This ability to lower the amounts of circulating glucose, reduce insulin resistance (IR), and in turn provide a better metabolic phenotype are just some of the major reasons for investigating the BAT depot and the beiging process of AT. IR can be defined as a complex condition whereby tissues normally sensitive to insulin are less sensitive, thereby requiring more insulin to elicit the same response under normal serum glucose levels (Chen et al., 2015). Animal models have shown that BAT transplanted into both high fat diet (HFD) induced obese and leptin deficient ob/ob mice improves insulin sensitivity, glucose metabolism, and obesity (Chait and den Hartigh, 2020; Jeanson et al., 2015; Liu et al., 2015; Stanford et al., 2013). Gene expression of *Ucp1* has been shown to be significantly reduced in obese mice and its upregulation has been associated with leanness in humans (Ro et al., 2014).

Beige Adipose Tissue

Beige (brown-in-white) AT shares some physiological features of BAT and some with classical WAT (Chait and den Hartigh, 2020; Kiefer, 2016; Leiria and Tseng, 2020; Okamatsu-Ogura et al., 2013). Researchers have found that scWAT, especially inguinal WAT (ingWAT), can contain considerable amounts of beige adipocytes, with vWAT also being susceptible to thermogenic remodeling (Kiefer, 2016). Wu et al. (2012) describe beige adipocytes as "brown-like thermogenic adipocytes" that contain multilocular LDs and UCP1 expression but originate from Myogenic Factor 5 (Myf5) negative cells (Jeanson et al., 2015; Luo and Liu, 2016; Wu et al., 2012). The beige cells appear in traditional WAT depots, especially scWAT, with brown adipocytes that contain UCP1 positive cells and therefore harness the ability to lower the

number of FFAs circulating within the body (Chait and den Hartigh, 2020; Kiefer, 2016; Leiria and Tseng, 2020; Okamatsu-Ogura et al., 2013). Discovered in the 1980s-1990s in rodents, beige adipocytes could respond to β3AR stimulation within traditional WAT depots (Jeanson et al., 2015). Beige adipocytes were originally thought to have risen from trans differentiation from WAT cells, and that these beige cells had the ability to revert to this "white-like" cell type if it was left unstimulated (Chait and den Hartigh, 2020; Jeanson et al., 2015; Kiefer, 2016; Luo and Liu, 2016). *In vitro* studies have suggested that the cells most likely originate from de novo adipogenesis from specific progenitor cells that were stimulated by CE but remain dormant until they are activated again (Chait and den Hartigh, 2020; Jeanson et al., 2015; Kiefer, 2016; Luo and Liu, 2016; Shao et al., 2019). It was previously postulated that the beige adipocytes contained within scWAT most likely evolved from trans differentiation, whereas epididymal beige cells would have more likely risen from Myf5 positive cells (Jeanson et al., 2015; Kiefer, 2016; Lee et al., 2012; Y. H. Lee et al., 2014b). However, other papers have since disputed the idea of trans differentiation since the small changes in EE would not be reasonable for such a complex process (Giralt and Villarroya, 2013; Shao et al., 2019). There are still many questions on the underlying mechanisms involved in beige adipocyte commitment, but their role in metabolism has been investigated in multiple stimulated studies.

Beiging of AT has been reported to occur from numerous physiological stressors including CE, β3AR agonists, exercise, severe burns and pharmacological compounds to name a few (Chait and den Hartigh, 2020; Kiefer, 2016; Luo and Liu, 2016; Münzberg et al., 2021). Sustained CE will activate UCP1 in beige adipocytes and allow for the appearance of multilocular LDs inside these cells (Heeren and Scheja, 2018). Beiging studies use a variety of beige adipocyte markers,

metabolic parameters, and whole-body measurements to determine the degree to which WAT is deemed to be beige.

Cells of the Adipose Tissue Depots

Adipocytes and Pre-Adipocytes

AT is comprised of different types of cells including adipose stem cells, adipocytes, and endothelial cells to name a few (Berry et al., 2013; Chait and den Hartigh, 2020; C. R Kahn et al., 2019). Adipocytes are thought of as the fat storing cells within the AT depot, and arise from the stem cells (Berry et al., 2013). Originally formed from the mesoderm and neuroectoderm, adipocytes are generated throughout a mammal's life (Berry et al., 2013). Brown adipocytes develop earlier during gestation, during the second trimester in humans and during the embryonic days 15-16 in rodents (Brandão et al., 2021). Subcutaneous white adipocytes develop towards the end of gestation with complete formation at 56 days postpartum in humans, whereas visceral white adipocytes form after birth (Brandão et al., 2021). For a long time, it was believed that brown and white adipocytes developed from distinct progenitors with only brown originating from the Myf5 lineage and white adipocytes originating from non-Myf5 lineages (Brandão et al., 2021; Luo and Liu, 2016; Shan et al., 2013). However, recent lineage tracing studies reviewed by Brandao et al. (2021) reveal that adipocytes originate from different mesenchymal stem cells depending on their function (Brandão et al., 2021). Subcutaneous adipocytes originate from paired related homeobox 1 progenitors and visceral adipocytes originate from Wilms tumor 1 progenitors (Brandão et al., 2021). Myf5 progenitors are also

present in scWAT depots and some white adipocytes share a common progenitor with the conventional brown adipocyte progenitor (Brandão et al., 2021). Differentiation into the different types of adipocytes occurs following the multipotent stem cells committing to forming pre-adipocytes (Brandão et al., 2021). Activation of the development of both brown and beige adipocytes follows similar patterns with transcriptional factors and co-factors that are reviewed by Brandao et al. (2021) to include PR domain zinc finger 16 (PRDM16), Peroxisome Proliferator Activated Receptor Gamma Coactivator 1 α (PGC1α), and the cAMP-responsive element-binding and activating transcription factor 2 (CREB-ATF2) to name a few (Brandão et al., 2021).

Lipid Droplet and Cellular Morphology

LDs were defined by Greenberg et al. (2011) to be "*intracellular organelles that store neutral lipids within cells*" (Greenberg et al., 2011). These neutral lipids, TAGs and cholesterol esters, are stored within adipocytes until energy is needed by the cell (Brasaemle, 2007; Greenberg et al., 2011; Welte, 2009). LDs are described as spherical in shape to hold large amounts of lipids at the core (i.e. TAGs) with the surface of the LD being composed of a monolayer of phospholipids with regulatory proteins and cholesterol molecules (Konige et al., 2014; Xu et al., 2018; Yu et al., 2015). LDs are important for lipid metabolism, especially within adipocytes and can range from 0.1-100µm in diameter (Jarc and Petan, 2020; Xu et al., 2018; Yu et al., 2015). LDs can act as a metabolic sink for molecules including FAs, cholesterol, ceramides, and polyunsaturated FAs, removing them from circulation and thereby reducing inflammation and cell damage (Jarc and Petan, 2020). They can also be a source for all of these molecules, releasing them into circulation and increasing inflammation in times of stress (Jarc and Petan,

2020). There have been over 200 proteins associated with the LD surface, however, Kongie et al. (2014) describe four main types of enriched AT specific LDs regulatory proteins including perilipins (PLIN), Fat Specific Protein 27/ Cell Death Inducing DNA Fragmentation Factor α -like Effector-C (FSP27/CIDEC), caveolins and cavins (Gong et al., 2009; Konige et al., 2014). PLINs are localized to the surface of the LD to contribute to lipid storage and liberation (Konige et al., 2014; Ramos et al., 2016; Welte, 2009; Xu et al., 2018). PLINs are the most abundant family of proteins associated with the AT LDs and is composed of 5 members (Konige et al., 2014; Ramos et al., 2016; Welte, 2009; Xu et al., 2018). Perilipin 1 (PLIN1), the most abundant PLIN found in AT, was the first LD associated protein identified, and is the only member of this family that has been found to play a role in lipolysis (Ramos et al., 2016; Xu et al., 2018). This protein will become phosphorylated through the cAMP-PKA pathway in order to promote lipolysis in the cell (Xu et al., 2018). The adipocyte differentiation related protein (ADRP/PLIN2) has also been identified as a major LD protein (Welte, 2009; Xu et al., 2018). PLIN2 is primarily found in the muscle and liver, however, it is also found in adipocytes with it playing a role in hindering lipid turnover in adipocytes (Ramos et al., 2016; Xu et al., 2018). PLIN3 and PLIN5 expression is reported in all AT depots with more expression found in WAT compared to BAT, while the PLIN4 protein is primarily found in WAT (Ramos et al., 2016). PLIN5 is expressed in FA oxidizing tissues such as BAT or stimulated beige AT (Konige et al., 2014; Ramos et al., 2016; Xu et al., 2018). In situations where lipids need to be stored quickly, PLIN3, PLIN4, and PLIN5 exhibit increased expression in the AT LD to facilitate lipid storage in the cell (Xu et al., 2018).

The CIDE family of proteins are involved in metabolic processes including lipolysis, LD formation and FA oxidation (Gong et al., 2009). They are also found in adipocytes with CIDEA

being found in BAT, and FSP27 (murine) or CIDEC (human) being found in WAT (Gong et al., 2009; Konige et al., 2014). These proteins are found in the endoplasmic reticulum (ER) and LD surface that aid in the growth of the LD by promoting clustering within the cell (Konige et al., 2014). CIDEA is shown to activate CAAT/Enhancer-Binding Protein β (CEBPβ) in BAT and act as a transcription coactivator, whereas FSP27 has been found to be involved in upregulating genes involved in the inflammatory response and may play a role in both LD size and TAG synthesis (Konige et al., 2014; Nishimoto and Tamori, 2017). Calevolins and cavins are proteins found in all mammalian cell plasma membranes but are also found in WAT and appear to be a part of lipid metabolism (Konige et al., 2014; Welte, 2009). They may regulate hormone sensitive lipase (HSL) and therefore may affect LD size, but further research needs to be conducted in order to establish this connection (Konige et al., 2014). The LD is thought to originate from within the membranes of the ER where it is believed that lipids will be naturally synthesized and accumulate within the cell eventually leading to LD formation (Brasaemle, 2007; Welte, 2009). LDs can interact with other cellular organelles including the ER and mitochondria which allows for efficient use of the FFAs from LD lipolysis to be utilized more efficiently by the cell (Welte, 2009; Xu et al., 2018; Yu et al., 2015). The most common theory in LD biogenesis hypothesizes that LDs originate from the ER, specifically the PLIN2-enriched domain of this cellular organelle (Nettebrock and Bohnert, 2020; Xu et al., 2018). From the ER, the LDs will receive TAG and grow in size and retain lipid synthesis enzymes before becoming a fully functioning LD (Nettebrock and Bohnert, 2020; Xu et al., 2018). These functioning LDs can grow in harmony with other LDs by creating a channel connection between them using PLIN1 and FSP27 (Xu et al., 2018). The

neutral lipids in the LD core can also come from caveolae from the plasma membrane where PLIN1 will work to facilitate LD storage (Xu et al., 2018).

In adipocytes, the TAG filled LD is the largest storage depot for energy in the body that will be liberated as FFA and glycerol (Brasaemle, 2007; Greenberg et al., 2011). The FFA will be transported to tissues to be used for ATP production while the glycerol will be transported to the liver for gluconeogenesis or glycolysis (Brasaemle, 2007; Greenberg et al., 2011). The regulation of this liberation process occurs partially through PLIN localized to the surface of the LD (Brasaemle, 2007; Greenberg et al., 2011; Konige et al., 2014; Rutkowski et al., 2015; Tansey et al., 2004; Xu et al., 2018). cAMP-PKA activation will, in turn, lead to the phosphorylation of PLIN1 on the surface of the LD (Brasaemle, 2007; Konige et al., 2014; Tansey et al., 2004). Phosphorylation of this protein will allow for HSL to be translocated from the cytosol to the LD where it will initiate lipolysis (Brasaemle, 2007; Greenberg et al., 2011; Konige et al., 2014; Rutkowski et al., 2015; Tansey et al., 2004). The activation of the cAMP-PKA pathway is initiated by the β3AR through catecholamine binding, which occurs in times of immediate physical (cold) or physiological (fasting) stress (Tansey et al., 2004). This induction of lipolysis is vital for whole body functioning in times where the tissue requires increased energy demands.

Previously described by numerous review papers, the morphology of BAT, induced beige, and WAT cells are very different (Figure 2) (Cinti, 2005; Luo and Liu, 2016; Sanchez-Gurmaches et al., 2016). WAT cells are conventionally depicted containing few mitochondria with a unilocular LD where the storage of TAGs are contained (Sanchez-Gurmaches et al., 2016). The single LD in WAT cells can range from 25-150μm in diameter (Konige et al., 2014; Weidlich et al., 2019). Whereas BAT cells are mitochondrial rich that contain much smaller multi-locular LDs that

are less than 10μm in diameter, thereby only facilitating storage of a small amount of TAGs (Sanchez-Gurmaches et al., 2016; Weidlich et al., 2019). These BAT cells have the main function of facilitating NST, rather than lipid storage, through the expression of the UCP1 protein (Cinti, 2005; Sanchez-Gurmaches et al., 2016). This large difference in cellular morphology can be bridged with the inducible beige cells. Beige cells, UCP1-expressing brown-like adipocytes found within particular WAT depots, especially scWAT or ingWAT depots, can be stimulated through β3AR to alter their cellular morphology to contain multilocular LDs and more mitochondria (M.J. Lee et al., 2014; Y. H. Lee et al., 2014b; Luo and Liu, 2016; Okamatsu-Ogura et al., 2013; Sanchez-Gurmaches et al., 2016). It is thought that these beige cells exist as adipocytes within the WAT depot and remain dormant until they are activated (Chait and den Hartigh, 2020). LDs in WAT have been studied previously, however much less is understood about BAT LDs (Konige et al., 2014; Yu et al., 2015). BAT LDs are known to be different from WAT LDs due to their role in cellular metabolism (Yu et al., 2015). Yu et al. (2015) conducted a study where they attempted to isolate BAT LDs and characterize them based on morphology, biochemical and proteome experiments. They were able to show increases in PLIN1 protein expression and UCP1 in mice under CE (Yu et al., 2015). The PLIN family of proteins and lipases were found to show significant increases in their expression with CE, which will increase the TAG hydrolysis that occurs within these cells, further illustrating their distinct function from WAT cells (Yu et al., 2015). Exercise training of Sprague-Dawley rats was found to increase the PLIN5 protein expression in BAT and PLIN3 expression in ingWAT indicating that these proteins will respond to changes occurring systemically (i.e. exercise training) (Ramos et al., 2016). These changes occurring within the AT may be key to understanding the roles these proteins play in the beiging of WAT. Previous

research has described the presence of small multilocular LDs in BAT allowing the tissue to increase the interaction between lipases and the LD to facilitate lipolysis within these cells (Nishimoto and Tamori, 2017). While the exact mechanism for the LD formation difference between WAT and BAT is still unknown, the CIDE proteins may play a key role in this difference (Nishimoto and Tamori, 2017). Nishimoto and Tamori (2017) speculate that FSP27 and its two isoforms, α and β, is involved in regulating the size of LDs in adipocytes (Nishimoto and Tamori, 2017). FSP27α is found to be expressed in WAT and when activated through Peroxisome Proliferator Activated Receptor γ (PPARγ) will promote large LDs to form, whereas FSP27β is found to be primarily expressed in the liver and BAT and will increase the EE in BAT through an unknown transcription factor (Nishimoto and Tamori, 2017). LDs are constantly changing in size with the stimulation of lipolysis causing a shrinking of the unilocular LD overall. This alteration in LD size should be further investigated in order to monopolize the beneficial effects of breaking down stored amounts of fat.

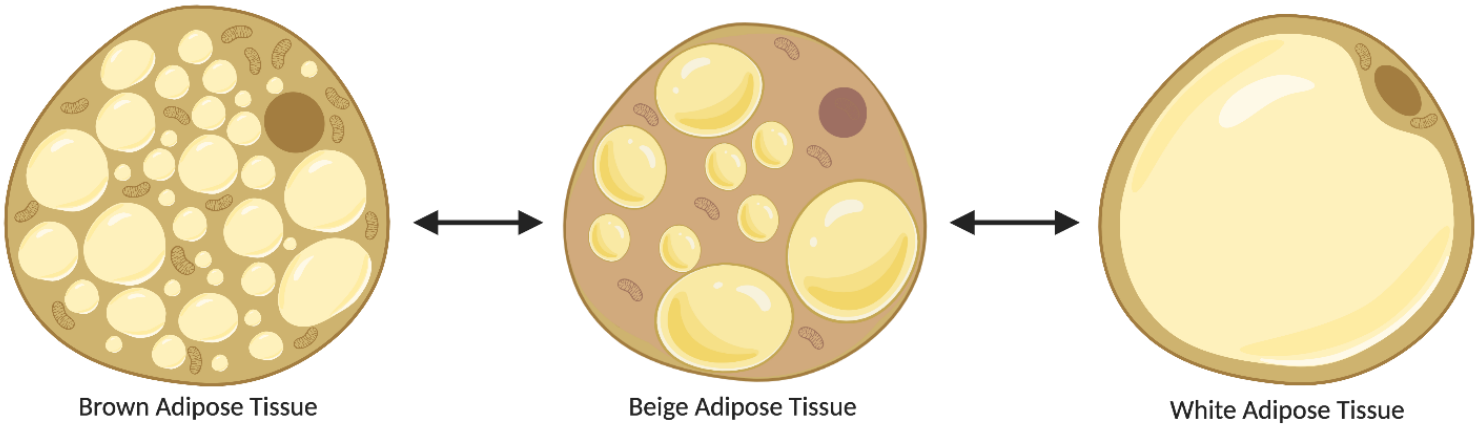

Figure 2: Adipocyte and lipid droplet morphology

Visual representation of the lipid droplet morphology in brown, beige and white adipocytes.

Key Metabolic Processes within Adipose Tissue

Lipid Metabolism

When fuel is fed to the body, the lipogenic pathway will allow for the storage of excess energy in the form of TAG within AT (Luo and Liu, 2016). The AT depot will efficiently store TAGs that will accumulate and remain in the LD of the adipocyte (Luo and Liu, 2016). This storage of TAGs, in combination with the tissue's ability to clear plasma TAGs, further exemplify the vital role the AT depot plays in whole-body health (Guilherme et al., 2019; Luo and Liu, 2016). It is important to note that in addition to storing lipids, the AT depot also aids in decreasing the number of lipids accumulating in other tissues and the extent of lipotoxicity that will occur (Guilherme et al., 2019).

When energy is required by tissues, for example during periods in between meals or in times of fasting, the TAGs stored in the cytosolic lipid droplet will be broken down through the lipolytic pathway into FFAs and glycerol (Heeren and Scheja, 2018; Luo and Liu, 2016). The FFAs and glycerol will travel through the blood to the tissues that require them for energy balance including the muscles and liver (Luo and Liu, 2016).

In times of fasting, other organs will require energy, and AT will provide this energy from its LDs (Luo and Liu, 2016). The activation of lipolysis will occur due to a decrease in insulin levels circulating in the blood and an increase in counterregulatory controls (including increases in NE and cortisol), which will signal the AT to undergo lipolysis. Lipolysis is the catabolic process where stored TAG inside the AT are broken down into FFAs and glycerol (Luo and Liu, 2016). This process will occur in a stepwise fashion where the TAGs will be broken down into

diacylglycerides (DAG) and then monoacylglycerides (MAGs) by adipocyte triglyceride lipase (ATGL) and HSL respectively before being further broken down to FFAs and glycerol (Heeren and Scheja, 2018; Luo and Liu, 2016). Glycerol and FFAs will be used for hepatic gluconeogenesis and oxidation by other organs for energy respectively (Luo and Liu, 2016). Glycerol can be a substrate for gluconeogenesis in the liver, which will allow it to supply the brain with glucose for energy (Luo and Liu, 2016). In periods of prolonged fasting, FFAs can also be used to synthesize ketone bodies in the liver that can also be utilized by the brain for energy (Luo and Liu, 2016). This process will not occur as effectively if there is a state of minimal carbohydrates but high amounts of FAs available for the liver. Instead, ketogenesis will occur when ketone bodies will be produced from the FFAs to supply the brain with energy (Luo and Liu, 2016). Fasting will also increase the amount of glucagon circulating in the body, which will activate the cAMP-PKA pathway in adipocytes (Luo and Liu, 2016). This pathway will allow for LD proteins, like PLIN, to become phosphorylated and allow for HSL to be translocated to the LD for lipolysis to occur (Luo and Liu, 2016). The FAs released from lipolysis are used for activating transcription factor receptors, such as PPARγ that aid in promoting the expression of other genes required for heat generation (Heeren and Scheja, 2018). Fasting will also increase the catecholamine released from the SNS, which will bind to β3ARs and in turn further activates the lipolysis and PKA pathways (Luo and Liu, 2016).

Lipogenesis occurs by combining the de novo FA synthesis from acetyl coenzyme A (acetyl-CoA) and TAG biosynthesis (Luo and Liu, 2016). Glucose provides acetyl-CoA as a substrate that will induce the expression of the rate-limiting enzyme of lipogenesis, acetyl-CoA carboxylase (ACC), in order to stimulate insulin to be released from the pancreas and in turn,

stimulate glucose uptake in adipocytes through the glycolytic and lipogenic enzymes and lipogenic genes (Luo and Liu, 2016). One gene, in particular, the sterol regulatory element-binding protein 1 (SREBP1) will control genes that are needed for fatty acids, TAG, phospholipid and cholesterol synthesis (Luo and Liu, 2016). Glycerol will be utilized by esterifying FAs from circulating TAGs in the form of chylomicrons and very-low-density lipoproteins (VLDL) to combine and form TAGs that can be stored by the adipocytes (Luo and Liu, 2016). The enzyme that will facilitate the hydrolyzing of the FAs from circulating TAGs is called lipoprotein lipase (LPL) (Heeren and Scheja, 2018; Luo and Liu, 2016). This enzyme is secreted from adipocytes and its expression is dependent on posttranslational factors like angiopoietin-like 4 (ANGPTL4) that are actively degraded in times of fasting (Luo and Liu, 2016). ANGPTL4 has also been found to promote intracellular lipolysis in WAT to allow for more beige adipocytes to occur in WAT depots and enhance the EE (Heeren and Scheja, 2018). Fatty acid transporter proteins (FATPs) are abundantly present on the surface of activated adipocytes, which allow FFAs uptake at a much more effective rate from circulation (Heeren and Scheja, 2018). Fatty acid transport protein-1 (FATP1) and the cluster of differentiation 36 (CD36) are both located on the plasma membrane that intake non-esterified FAs from circulation that were broken down by LPL (Heeren and Scheja, 2018). Insulin will also play a large role in FA uptake by activating LPL, inducing FATPs and upregulating associated genes within the adipocytes (Luo and Liu, 2016). Once the fatty acids are combined with glycerol, further esterification will occur through diacylglycerol acyltransferase (DGAT) (Luo and Liu, 2016). The synthesized TAGs will then accumulate inside the LD to remain until the body requires them. As the LD size increases in size, this expansion can result in obesity (Luo and Liu, 2016). Due to their interplay within the

body, systemic energy homeostasis and insulin sensitivity are a balancing act between lipogenesis and lipolysis that must be regulated by the adipocyte (Luo and Liu, 2016).

Conditions, where the body is unable to maintain and produce AT, are called lipodystrophies (C. R Kahn et al., 2019). These conditions show similar metabolic outcomes to those with excess AT, such as obesity, where there is severe IR, hypertriglyceridemia, and metabolic syndrome (C. R Kahn et al., 2019). The similar metabolic outcomes with these two extremes showcase the need to maintain an ideal balance between too much and too little AT for whole-body health (C. R Kahn et al., 2019).

Obesity, Immune Cells and Metabolic Homeostasis

Metabolic homeostasis is tightly connected to the immune response, especially in AT (Brestoff and Artis, 2015). WAT has been most closely linked with the regulation of the immune cell network related to metabolism (Brestoff and Artis, 2015). White adipocytes produce many types of adipokines including leptin, resistin, fibroblast growth factor 21 (FGF21) and adiponectin, all of which play key roles in regulating satiety and metabolism in the brain, kidney, liver, pancreas and skeletal muscle (Brestoff and Artis, 2015).

WAT in lean mammals generally contains immune cells including alternately activated macrophages, eosinophils, T-helper-type-2 cells, regulatory T-cells, and invariant natural killer T-cells (Brestoff and Artis, 2015). While WAT in obese mammals contains classically activated macrophages, that are recruited by adipocyte derived inflammatory mediators including MCP-1, C-X-C motif chemokine 12, and prostaglandins (Brestoff and Artis, 2015). Once recruited, these classically activated macrophages will engulf the hypoxic or dying cell to form crown-like

structures (CLS) comprised of a ring of immune cells around the adipocyte (Brestoff and Artis, 2015). These immune cells will not only break down the dying adipocyte, but they will also produce inflammatory cytokines, including TNFα, Interleukin 6 (IL-6), Interleukin 1β (IL-1β) and other immune cells to evoke the inflammatory response (Brestoff and Artis, 2015). The main inflammatory cytokines produced by the immune cells in obese AT will render effects throughout the entire body, discussed in detail below. For example, circulating TNFα has been tightly associated with obesity and IR (Brestoff and Artis, 2015). IR is especially prevalent in skeletal muscle, liver and WAT and is associated with metabolic diseases like obesity, hypertension, hyperglycemia, cancer and T2D (Ahmad et al., 2020; Chen et al., 2015).

Obesity

The World Health Organization (WHO) defines obesity as "*an abnormal or excessive fat accumulation that may impair health*" (World Health Organization, 2022). Classification of obesity has been classically determined through the Body Mass Index (BMI) where an individual's weight in kilograms is divided by the square measure of their height in meters (World Health Organization, 2022). People with BMI's greater than or equal to 25 are overweight and a BMI of greater than or equal to 30 is considered obese (World Health Organization, 2022). In terms of AT specifically, obesity is defined by Chait and Hartigh (2020) as "*dysfunctional AT, where adipocytes become hypertrophic during periods of caloric excess and secrete adipokines that result in the recruitment of pre-adipocytes which differentiate into mature adipocytes as compensatory protection against some of the adverse metabolic consequences of obesity*" (Chait and den Hartigh, 2020). The dysfunction that occurs in AT with obesity is normally characterized

as a low-grade chronic inflammatory state where the high amounts of immune cells that are localized in obese AT of both rodents and humans (Guilherme et al., 2019). The increased cytokine levels within the obese AT will affect the nerves and therefore impair the signalling needed for AT to communicate effectively with the brain (Guilherme et al., 2019; Villarroya et al., 2018). This impaired signalling will affect insulin secretion, the overall function of the tissue, and whole body metabolism (Guilherme et al., 2019).

In both obese and insulin resistant states, the increase in FAs circulating and WAT lipolysis will amplify liver gluconeogenesis (Guilherme et al., 2019). These effects will cause the pancreatic cells to produce insulin at a higher rate in order to counter the increased circulating glucose. This increased insulin production cannot be maintained indefinitely, and will eventually cause the pancreatic beta cells to lose functionality and decrease insulin production, further promoting glucose intolerance and can lead to T2D (Guilherme et al., 2019). T2D and metabolic syndrome are not only related to the energy balance within the tissue but also the balance between WAT and BAT within the body (C. R Kahn et al., 2019).

The expansion of WAT depots due to the increase in TAG storage and decreased lipid turnover can lead to hypertrophy of AT (Ghazarian et al., 2015). Hypertrophy can increase both the inflammatory cytokines and adipokine secretions, which can further result in lead to IR and disrupted metabolism. Glucose concentrations are also affected by WAT metabolism due to the chronic low-grade inflammatory state, defined as mildly elevated levels of circulating cytokines and chemokines (Chait and den Hartigh, 2020). This inflammatory state will cause the upregulation of various immune responses which influence both glucose and insulin homeostasis

(reviewed by Mraz and Haluzik and Ghazarian et al.) (Ghazarian et al., 2015; Mraz and Haluzik, 2014).

The macrophages within AT depots seem to be able to switch between two major subtypes, M1 and M2, depending on the stimulation occurring within the body towards a pro or anti-inflammatory state respectively (Guilherme et al., 2019; Villarroya et al., 2018). Both M1 and M2 macrophages are present in the tissue, however, the ratio of the two can shift in either direction to promote or hinder whole-body metabolism (Guilherme et al., 2019). In obesity, M1 macrophages increase due to the rise in pro-inflammatory mediators, such as TNFα and Interferon γ (INFγ), that will ultimately alter the composition of the depot where AT macrophages (ATM) will render microbicidal actions (C. R Kahn et al., 2019; Villarroya et al., 2018). This phenotype will increase the release of type 1 cytokines (such as MCP-1 and chemotactic chemokine ligand 5 (CCL5) which will further trigger more immune cells, such as cluster of differentiation 4 and 8 (CD4+ and CD8+) T-cells and Natural Killer cells (NK cells) to be recruited to the AT depot and further exacerbate the inflammation (C Ronald Kahn et al., 2019; Villarroya et al., 2018). This self-perpetuating inflammatory effect will influence the entire body and lead to many negative metabolic outcomes (C Ronald Kahn et al., 2019; Villarroya et al., 2018).

In situations of stress, catecholamines will act through β2-Adrenergic Receptor (β2AR) on M1 macrophages to shift to an M2 phenotype and decrease inflammation occurring within the body (Guilherme et al., 2019). M2 macrophages are formed when type 2 cytokines, such as interleukins 4 or 13 (IL-4 or IL-13 respectively), circulate in the tissue and polarize the M1 macrophages to exert homeostatic properties (Villarroya et al., 2018). These M2 macrophages

are also largely found in healthy and lean AT (Villarroya et al., 2018). It is also important to note a third group of macrophages termed metabolic macrophages (MMe) are found in WAT of obese mammals and express high amounts of lipid metabolism proteins and are associated with anti-infectious immune responses (Villarroya et al., 2018).

Sympathetic neuron-associated macrophages (SAMs) are a new subtype of macrophage that will affect the sympathetic signalling from the tissue to the rest of the body (Guilherme et al., 2019). These SAMs will decrease the sympathetic signal by lowering the availability of catecholamines released into circulation and increasing inflammation (Guilherme et al., 2019).

The impaired signaling that occurs in obese AT will affect glucose signaling, insulin secretion, and the overall function of the tissue (Chen et al., 2015; Guilherme et al., 2019). Guilherme et al. (2019) hypothesize that the expansion of AT in obesity could also lead to the hyperactivation of local sensory nerve fibers resulting in pro-inflammatory mediators to be released leading to more inflammation in other body tissues (Guilherme et al., 2019). A great deal is still unknown of the relationship between obesity and glucose metabolism, however, the dysfunction that occurs in the entire body from this increased lipid storage is not disputed.

WAT dysfunction in obesity (i.e. storing more lipids within the LD) in combination with decreased levels of lipolysis proteins found on the LD (i.e. PLIN) will result in obesity (Chen et al., 2015; Czech, 2020). These dysfunctional WAT cells will decrease their rate of glucose uptake and glycerolneogenesis in order to increase lipid storage (Czech, 2020). This decrease in glucose uptake, in addition to an increase in FFA uptake, will have a profound impact on insulin signaling and whole-body glucose tolerance (Czech, 2020). Lipolysis in WAT that occurs in obesity can lead to increased glycerol and FFA that are circulating and accumulate in the liver to enhance

glucose output through gluconeogenesis, which will further increase circulating glucose concentrations (Czech, 2020; Guilherme et al., 2019). These effects will eventually cause pancreatic cells to decrease insulin production (as discussed above) while inhibiting glucose transport and further promote glucose intolerance, which can lead to T2D (Guilherme et al., 2019). The role of T2D and metabolic syndrome may not only be related to the energy balance within the tissue but also the relationship between WAT and BAT within the body (C. R Kahn et al., 2019). BAT depots serve as an important point in the glucose disposal whereby active BAT will be able to contribute to glucose disposal and oxidizing lipids in the body (Czech, 2020). Beige AT has also been found to contribute to glucose tolerance in rodents and humans and therefore may be a key player in the fight against metabolic diseases (Czech, 2020).

BAT has been studied for its beneficial effects on obesity and glucose metabolism. When BAT is in an environment of chronic inflammation, studies have reported that the depot will switch from an M2 type depot to an M1 type where macrophages and immune cells secrete type 1 cytokines thereby further enhancing the inflammatory response (Villarroya et al., 2018).

In times of stress or inflammation, adipocytes have been found to express toll-like receptors (TLRs) (TLR4 and TLR2) that when activated, will ultimately impair *Ucp1* gene expression and activation, and hence may be involved in inhibiting the thermogenic response (Okla et al., 2015; Rogero and Calder, 2018; Villarroya et al., 2018). This activation of TLRs will induce a pro-inflammatory phenotype through the Nuclear Factor kappa-light-chain-enhancer of activated B cells (NF-kB) and Mitogen-Activated Protein Kinase (MAPK) signalling pathways that will result in ER stress and further promote the release of pro-inflammatory cytokines which may hinder thermogenic genes from being transcribed (Okla et al., 2015; Rogero and Calder, 2018).

Due to the interaction between these inflammatory pathways and the thermogenesis response, the connection between stress and less AT beiging is evident.

Metabolic Stress and Inflammatory Cells

When AT expands during obesity, there are inflammatory changes that occur within the depot that contribute to chronic low-grade systemic inflammation (Chait and den Hartigh, 2020). When the AT expands, it will be accompanied by the accumulation of inflammatory cells, with the most predominant cell type being macrophages (Chait and den Hartigh, 2020; Kershaw and Flier, 2004). In AT of lean mammals, 5-10% of the cells are macrophages whereas in obese AT, this amount is greater than 60% of all cells present (Chait and den Hartigh, 2020). B-cells and mast cells also increase in obese AT.

Metabolic disarray is associated with increasing adipocyte size and this is connected with an increase in the inflammatory response. AT cells are associated with multiple immune cells including T-cells, macrophages, eosinophils, neutrophils and dendritic cells. All of these cells are present in the AT depot and help with its endocrine function. Normally, AT has cytokines IL-4, 5, 10 and 13 that are anti-inflammatory. Whereas when the tissue grows in size to the point where it has become hypoxic, the cytokine population shifts to pro-inflammatory cytokines such as IL-1β, IL-6 and TNFα (Hotamisligil, 2006).

The inflammatory cells are recruited to the depot in response to MCP-1 that is produced by hypertrophic adipocytes (Chait and den Hartigh, 2020; Kershaw and Flier, 2004). MCP-1 allows for macrophages to be recruited to the tissue and accumulate around the dead or dying adipocytes to form CLS (Chait and den Hartigh, 2020). The macrophages undergo a phenotype

change from anti- to pro-inflammatory where they will recruit more pro-inflammatory cells to the tissue and exacerbate the inflammation process (Chait and den Hartigh, 2020). MCP-1 promotes macrophages and monocytes to sites of inflammation during periods of tissue injury and infection (Chait and den Hartigh, 2020). In animal studies, the circulating amounts of MCP-1 are increased in obesity which is thought to contribute to metabolic issues associated with obesity and IR (Kershaw and Flier, 2004).

IL-6

A cytokine that can be derived from AT is IL-6, which circulates in two glycosylated forms has a receptor that is homologous to the leptin receptor (Kershaw and Flier, 2004). AT depots and adipocytes express IL-6 itself and the IL-6 receptors with scWAT expressing and secreting 2 to 3X times more IL-6 than vWAT (Kershaw and Flier, 2004). IL-6 circulates in high amounts in the bloodstream with about one-third of these cytokines found to be originating from the AT depot (Kershaw and Flier, 2004; Mauer et al., 2014). Unsurprisingly, the amount of circulating IL-6 and its expression are positively correlated with obesity, impaired glucose tolerance and IR (Chait and den Hartigh, 2020; Kershaw and Flier, 2004). IL-6 has been linked to IR through its ability to reduce the expression of glucose transporter 4 (GLUT4) and the insulin receptor substrate (IRS) 1 (Chen et al., 2015). IL-6 from AT is involved in obesity due to its role in adipocyte expansion (Chait and den Hartigh, 2020). When adipocytes expand and undergo excessive lipolysis, the FFA levels circulating will become elevated, which will activate IL-6 secretion (Chait and den Hartigh, 2020). Rodent studies have shown that AT-derived IL-6 promotes IR and glucose intolerance, while other studies have shown that IL-6 signalling in the

WAT and liver may be protective against metabolic disease (Chait and den Hartigh, 2020). Both decreased expression and circulating levels of IL-6 are associated with weight loss and the change in plasma levels of this cytokine has been used as a predictive molecule for T2D and the development of heart disease (Kershaw and Flier, 2004). Therefore, the body must maintain a key concentration of IL-6 in order to mitigate chronic low-grade inflammation and macrophage polarization (Mauer et al., 2014). Mauer et al. (2014) was able to show this balancing effect in mice through inactivation of one of the chains of the IL-6 receptor and found that this cytokine is an essential regulator of macrophage polarization to an M2 phenotype during inflammatory responses. They were able to show that IL-6 is a regulator of IL-4, which is a type 2 cytokine thereby resulting in limiting the inflammatory effect (Mauer et al., 2014).

IL-6 has been described as a batokine where BAT cells express and release this cytokine without being released from immune cells (Villarroya et al., 2018). The role of IL-6 in BAT activation may have positive effects on metabolism where it can sensitize the tissue to the effects of insulin similar to the IL-6 released from skeletal muscle and ultimately act as a regulator of inflammation via M2 macrophages in cases of obesity (Mauer et al., 2014; Stanford and Goodyear, 2013; Villarroya et al., 2018). Previous work in Dr. Lees' lab highlighted the tissue specific changes in response to HFD for four weeks and the roles IL-6 and voluntary physical activity plays in glucose tolerance and the prevention of insulin resistance (Sarvas et al., 2015). In the study with IL-6 KO mice, lack of IL-6 results in significantly higher circulating glucose levels in the animals who exercised compared to sedentary animals (Sarvas et al., 2015). Physical activity prevented insulin resistance in a tissue-specific manner with the gastrocnemius and plantaris muscles of exercised wildtype mice, however, the IL-6 KO exercised mice failed to show

increased insulin-stimulated protein kinase B phosphorylation (Sarvas et al., 2015). These results indicate that the beneficial effects of physical activity in skeletal muscle rely on IL-6 in order to prevent insulin resistance under HFDs (Sarvas et al., 2015). The findings from this study demonstrate the important role IL-6 can play in mediating insulin resistance in obesity models, especially in skeletal muscle, but more is still to be learned. The role of IL-6 is not completely established in BAT, however cold stimulus has been found to increase the production of IL-6 in BAT cells and is, therefore, a key player in the AT depot's response to different stimuli (Villarroya et al., 2018). The role of IL-6 may prove to be just as critical for BAT as it is in skeletal muscle for proper tissue functioning, but more research needs to be conducted in this area.

TNFα

TNFα is another cytokine that can be derived from AT (Chen et al., 2015). The active protein that will render its effects through the type I and type II TNFα receptors (Kershaw and Flier, 2004). These receptors, both of which are expressed in adipocytes, allow for it to repress genes that are involved in uptake and storage of nonessential FAs and glucose, in addition to suppressing genes involved in adipogenesis and lipogenesis (Kershaw and Flier, 2004).

TNFα will also suppress genes for glucose uptake, metabolism, and FA oxidation in the liver (Kershaw and Flier, 2004). This protein will increase the amount of serum nonesterified FAs which will impair insulin signalling pathways, causing IR in many tissues throughout the body (Chen et al., 2015; Kershaw and Flier, 2004). Emerging evidence points to this impairing insulin signalling in the liver through the increased serine phosphorylation of IRS1 and IRS2, thereby reducing their effectiveness with insulin receptor kinases, and increasing their degradation (Chen

et al., 2015; Kershaw and Flier, 2004). This impaired insulin signalling can ultimately result in IR (Chen et al., 2015; C Ronald Kahn et al., 2019).

TNFα is also related to obesity with the levels of it being connected to adiposity, IR and a high body mass index (Chait and den Hartigh, 2020). The majority of TNFα is secreted by the immune cells in the stromal vascular fraction of AT, even though the adipocytes themselves can also secrete TNFα (Chait and den Hartigh, 2020). Obesity increases the level of TNFα due to the macrophages adopting a pro-inflammatory phenotype, which then activates the enzyme HSL that increases the release of FFA from the adipocytes and promotes IR (Chait and den Hartigh, 2020).

Adipokines

Adipokines are mediators of metabolic processes in the body that are secreted from AT for distinct functions (Chait and den Hartigh, 2020; Luo and Liu, 2016). Some adipokines are related to FA oxidation, gluconeogenesis, glucose uptake, insulin signalling, and even EE in active tissues including the liver, skeletal muscle and brain (Chait and den Hartigh, 2020). Adipokines are either pro- or anti-inflammatory in their classification and any imbalance is associated with metabolic disease (Maximus et al., 2020). Many studies have noted that any impairment in the biosynthesis of these adipokines is associated with obesity (Luo and Liu, 2016). At a cellular level, all adipokines exert their action through receptor binding on the cell membrane that will trigger intracellular signalling pathways within the different tissues (Luo and Liu, 2016). The two main adipokines released from the adipocyte are leptin and adiponectin.

Leptin

Leptin is essential for body weight regulation and energy balance as it is a satiety hormone (Chen et al., 2015; Luo and Liu, 2016). This satiety effect is due to its ability to cross the blood-brain barrier and target the hunger center in the brain in the hypothalamus (Guilherme et al., 2019; C Ronald Kahn et al., 2019; Luo and Liu, 2016). This peptide hormone, expressed exclusively by adipocytes, is released from AT to exert effects on target organs (Chait and den Hartigh, 2020; C Ronald Kahn et al., 2019). The primary role of leptin is to act as a metabolic signal in the body indicating energy stores are sufficient and the regulation of EE (C Ronald Kahn et al., 2019; Kershaw and Flier, 2004; Luo and Liu, 2016). When food intake decreases, leptin levels decrease which signals to the body that it must adapt to different physiological conditions (i.e. increased appetite and decreased EE) (Kershaw and Flier, 2004; Luo and Liu, 2016; Simonds et al., 2012). Leptin is secreted by adipocytes in proportion to AT mass and nutritional status (Chen et al., 2015; Guilherme et al., 2019; Kershaw and Flier, 2004; Luo and Liu, 2016; Simonds et al., 2012). Leptin has been found to play roles in energy homeostasis with its secretion being influenced by many other biological factors including increasing with concentrations of insulin, glucocorticoids (GCs), TNFα, estrogens, and decreasing with concentrations of β3AR activity, and FFAs (Kershaw and Flier, 2004; Simonds et al., 2012).

The secretion of leptin is greater in the scWAT compared to the vWAT depot (Kershaw and Flier, 2004). However, leptin can also be secreted from other organs like the skeletal muscle, intestine and stomach (Luo and Liu, 2016; Park et al., 2018; Simonds et al., 2012). It was previously thought that leptin gene mutations were a causative factor in obesity (Khan et al., 2019), but now it is thought of as a possible diagnostic and treatment agent inpatients with

obesity, not the cause of obesity (Salum et al., 2021) . However, human obesity is a multifactorial disease and has been found to be linked with leptin resistance due to insufficient response to exogenous leptin (C Ronald Kahn et al., 2019) and leptin replacement therapy has been indicated as a possible treatment for IR or metabolic diseases in combination with other clinical strategies (Chen et al., 2015; Salum et al., 2021). All that being said, the exact role that leptin plays in mediating obesity is yet to be fully uncovered.

Leptin also affects the immune system by normalizing the immune function that is associated with malnutrition and leptin deficiency (Kershaw and Flier, 2004). Leptin will alter the cytokine production of immune cells that will accelerate wound healing within tissues (Kershaw and Flier, 2004). Leptin has shown protective effects in colon cancer and Alzheimer's but has also been negatively associated with diseases like arthritis, hypertension and atherosclerosis (Maximus et al., 2020). Leptin also regulates neuroendocrine functions by interacting with the Hypothalamic-Pituitary-Adrenal axis (HPA axis) (C Ronald Kahn et al., 2019; Kershaw and Flier, 2004). When fasting, leptin levels become low, signaling to the body to decrease EE and increase food intake (C Ronald Kahn et al., 2019).

Adiponectin

Specifically expressed in high amounts within AT (especially scWAT), adiponectin is a polypeptide that is an insulin-sensitizing hormone that affects many tissues including the heart, skeletal muscle and liver (Chait and den Hartigh, 2020; C Ronald Kahn et al., 2019; Kershaw and Flier, 2004; Luo and Liu, 2016). Adiponectin signals through two receptors, ADIPOR1 (primarily expressed in muscle) and ADIPOR2 (primarily expressed in the liver) that allow for docking of the

adaptor protein APPL1 which will activate the signalling pathway of Peroxisome Proliferator Activated Receptor α (PPARα) leading to several metabolic effects. PPARα leads to reduced liver gluconeogenesis, reduced WAT inflammation, increased glucose uptake in the skeletal muscle and WAT, and increased FA oxidation in the liver and skeletal muscle (Chait and den Hartigh, 2020; Chen et al., 2015; C Ronald Kahn et al., 2019; Kershaw and Flier, 2004; Luo and Liu, 2016). This polypeptide is inversely related to adiposity and demonstrates variations between the sexes, with females showing higher adiponectin levels compared to males (Chait and den Hartigh, 2020). There are also inverse relationships with IR (from either obesity or lipodystrophy) where administration of adiponectin to patients with these conditions will improve their metabolic health (Chen et al., 2015; Kershaw and Flier, 2004). Adiponectin can also stimulate a person's appetite and reduce EE through actions in the central nervous system (CNS) and SNS (C Ronald Kahn et al., 2019). Adiponectin has protective effects on IR, obesity, cancers (namely breast, colon, and lung), atherosclerosis and hypertension (Maximus et al., 2020). Moreover, adiponectin levels have been implicated in the pathogenesis of joint inflammation and cervical cancer (Maximus et al., 2020). In nonhuman primates, plasma adiponectin levels decline before IR and obesity sets in (Kershaw and Flier, 2004). This adipokine has been found to circulate in high levels and has been shown to have anti-inflammatory and insulin-sensitizing effects (Luo and Liu, 2016). The insulin-sensitizing effect arises from the primary target of this hormone, the liver (Luo and Liu, 2016). Adiponectin activates Adenosine Monophosphate Activated Protein Kinase (AMPK) and downregulates the expression of gluconeogenic enzymes, like glucose-6-phosphate and phosphoenolpyruvate carboxylase thereby suppressing gluconeogenesis (Luo and Liu, 2016).

Resistin

Resistin got its name from "resistance to insulin" and is a polypeptide that plays a role in insulin signalling and metabolism (Jamaluddin et al., 2012; C Ronald Kahn et al., 2019; Kershaw and Flier, 2004; Luo and Liu, 2016). Resistin is the hormone secreted by activated macrophages (in mice) and circulating monocytes and tissue macrophages and bone marrow cells (in humans) contained within obese AT (Chait and den Hartigh, 2020; C Ronald Kahn et al., 2019; Luo and Liu, 2016). Resistin is related to insulin signalling as it has been correlated with IR in both mice and humans, with increased plasma concentrations found within obese models (Chait and den Hartigh, 2020; Luo and Liu, 2016). Resistin can also upregulate inflammatory cytokines like TNFα and IL-6 in macrophages and monocytes and is positively associated with circulating TNFα (Chait and den Hartigh, 2020). Resistin has shown protective effects in Alzheimer's disease but is associated with IR, kidney failure, arthritis and depression (Maximus et al., 2020).

Fibroblast Growth Factor 21 (FGF21)

FGF21 is an endocrine hormone that is involved in the regulation of lipids, glucose, and overall energy homeostasis (Chait and den Hartigh, 2020; Huang et al., 2017). Due to its diverse range of effects on metabolism, FGF21 has been linked to the liver, skeletal muscle and AT (Luo and Liu, 2016). The main source of FGF21 is from the liver which secretes it when it is metabolically stressed, such as during times of fasting, or protein restriction (Chait and den Hartigh, 2020; Huang et al., 2017). In its role as an adipokine, FGF21 will induce the thermogenic gene program in both BAT and ingWAT when exposed to cold temperatures (Huang et al., 2017;

Luo and Liu, 2016). The exact mechanism is unclear, however, FGF21 will upregulate PGC1α in ingWAT, thereby facilitating beiging (Huang et al., 2017; Luo and Liu, 2016). There is some speculation that WAT and BAT may also secrete FGF21 as the levels of this hormone become elevated as obesity develops in both mice and humans (Chait and den Hartigh, 2020; Huang et al., 2017).

Other Factors

Other important growth factors in the AT depot include bone morphogenic proteins (BMPs) and vascular endothelial growth factors (VEGFs) (Khan et al., 2019). BMPs play roles in differentiation and adrenergic response in both WAT and BAT (Khan et al., 2019). BMP2 and BMP4 are important for WAT differentiation, BMP7 for BAT development, and BMP8b enhances the β3AR response of BAT (C Ronald Kahn et al., 2019). VEGF-A is an angiogenic factor within WAT and BAT that is essential for circulation within the AT depot (C Ronald Kahn et al., 2019).

Inflammatory responses are also found to affect the lymphatic system which is linked to obesity and associated metabolic syndromes (Kataru et al., 2020). Obesity increases the amount of low-grade chronic inflammation, which will lead to the accumulation of inflammatory cells around the lymphatic vessels found in scWAT, resulting in their impaired function (Kataru et al., 2020). Kataru et al. (2020) note studies involving the lymphatic response with AT inflammation (Kataru et al., 2020). VEGF-A and VEGF-C are increased in obese individuals and VEGF-C has been found to be linked to macrophage infiltration and IR in scWAT (Kataru et al., 2020). It appears as though overexpression of any of the VEGF subtypes in AT may lead to increase lymphangiogenesis in WAT which can result in improved lymphatic function and therefore

decrease metabolic associated problems (Kataru et al., 2020). In vivo experiments noted by Kataru et al. (2020) show that obesity-induced lymphatic dysfunction may be reversible as HFD studies whose subjects are either undergoing caloric restriction or exercise will show improved lymphatic function (i.e. less lipids leaking from damaged lymphatic vessels, which in turn will cause increased adipogenesis) (Kataru et al., 2020). If obesity can be mitigated, through pharmaceutical or lifestyle changes, it is believed that the inflammatory changes will have a wide range of systemic effects (Kataru et al., 2020).

Adipogenesis

The cellular process by which pre-adipocytes commit to becoming mature adipocytes is defined as adipogenesis (Lowe et al., 2011; Luo and Liu, 2016; Rosen et al., 2002). This process is critical for the energy homeostasis and balance of mammals and must be regulated to effectively regulate metabolic function (Ahmad et al., 2020; Luo and Liu, 2016). Each year, approximately 10% of adipocytes turn over, so ensuring proper functionality of these cells is critical for healthy metabolism (Ahmad et al., 2020; Lowe et al., 2011). Adipogenesis is a regulatory process known to involve numerous transcriptional factors including PPARγ and CEBPα (Rosen et al., 2002). PPARγ has been thought of as the master regulator of adipogenesis due to its ability to induce fibroblast differentiation (Luo and Liu, 2016; Rosen et al., 2002). This regulator is involved in all adipogenic mechanisms including CEBPs, PRDM16, Kruppel-like factors (KLFs) and GATA transcription factors (named after the consensus DNA-binding sequence) that together play a role in adipocyte gene expression, lipid accumulation and insulin sensitivity (Luo and Liu, 2016; Rosen et al., 2002). Due to its central role in adipogenesis, PPARγ is a potential therapeutic

target for obesity-linked metabolic disorders (Luo and Liu, 2016). One of the classes of PPARγ agonists is thiazolidinediones (TZDs), which were originally shown to improve insulin sensitivity and glucose tolerance through PPARγ stimulation, however, these drugs had severe side effects and could not be directly used to target obesity-related illnesses (Luo and Liu, 2016).

The adipogenic agonist, CEBP is a transcription factor that works together with PPARγ to allow for adipogenesis and adipocyte differentiation to occur (Luo and Liu, 2016; Rosen et al., 2002). Isoforms of CEBPs are upregulated by PPARγ which then leads to further PPARγ transcription and other adipogenic essential genes (Luo and Liu, 2016) that promote pre-adipocytes to mature and contribute to whole-body metabolism.

In primary cell culture, PRDM16 is a transcriptional co-regulator that forms a transcriptional complex with CEBPβ and selectively initiates myoblasts to switch to brown adipocytes (Luo and Liu, 2016). PPARγ has a central role in regulating this gene where rodent studies have indicated that without a functional version of this transcription factor, brown adipocytes exposed to cold will appear as white adipocytes with a unilocular LD and decreased UCP1 expression (Jeanson et al., 2015). White adipocyte genes are suppressed by PRDM16 by its binding with C-terminal binding proteins (CTBP1 and CTBP2) but can be displaced when PPARγ co-activators PGC1α and PGC1β are recruited to the cells and activate brown adipocyte genes (Luo and Liu, 2016). PGC1α is essential for thermogenesis, not differentiation, as it is the co-activator of thermogenic and mitochondrial biogenesis genes (Luo and Liu, 2016). A co-regulator of PRDM16 is PGC1α, which been found to be essential for UCP1 activation (Jeanson et al., 2015).

Adipogenesis is also influenced by the unfolded protein response (UPR) that is activated when stress causes the unfolded proteins to accumulate in the ER (Lowe et al., 2011). This response has multiple arms that are all implicated in adipocyte development (Lowe et al., 2011). One arm is the Pancreatic EIF2-α kinase (PERK) that will reduce the rate of protein synthesis to and in turn reduce the expression of lipolytic enzymes and therefore amplify lipid accumulation within the adipocyte (Lowe et al., 2011). Another arm of the UPR involves the inositol requiring 1 (IRE1) enzyme and x-box-binding protein 1 (XBP1) that will target CEBPβ in adipogenesis and causes increased lipid accumulation and a decrease in UCP1 expression in BAT (Darlington et al., 1998; Lowe et al., 2011).

Mitochondrial Biogenesis

Being the powerhouse of the cell, the mitochondria are essential in cellular functions ranging from energy production to homeostasis of biomolecules and antioxidants (Cameron et al., 2016; Dominy and Puigserver, 2013). Located in the cell as a double membrane-enclosed organelle, the mitochondria have their own circular DNA molecule (mitochondrial DNA) and can auto replicate (Dominy and Puigserver, 2013; Jornayvaz and Shulman, 2010). Mitochondrial biogenesis was defined to be the "*growth and division of pre-existing mitochondria"* (Jornayvaz and Shulman, 2010). The ability for this biogenesis to occur will require many proteins, encoded in the nucleus and synthesized in the cytosol, in order to efficiently increase the size and mass of mitochondria within the cell (Jornayvaz and Shulman, 2010). Mitochondrial biogenesis is affected by changes in temperature, oxidative stress, and caloric restriction (Jornayvaz and Shulman, 2010). This process is regulated by nuclear-based gene expression of signalling

pathways that will allow the mitochondria to respond to the different stimuli that will promote the mitochondrial mass and size to increase. Nuclear respiratory factor 1 (NRF-1) is an important regulator of the many proteins that make up the ETC, and proteins that are important for mitochondrial biogenesis (Dominy and Puigserver, 2013). NRF-2 is another nuclear factor that will regulate the expression of mitochondrial complex IV cytochrome c oxidase (Dominy and Puigserver, 2013). Both of these NRFs will promote the expression of mitochondrial transcription factor A (mtTFA) and factor B (mtTFB) which will regulate and increase the transcription of mitochondrial DNA (mtDNA) (Dominy and Puigserver, 2013; Jornayvaz and Shulman, 2010). Nuclear hormone receptors also play a role in mitochondrial biogenesis, especially the perioxisome proliferator-activated receptors (PPARs) (Dominy and Puigserver, 2013). Most notably, PPARγ will induce mitochondrial biogenesis in the BAT and WAT depots (Dominy and Puigserver, 2013). The cAMP activator transcription factor CREB will also promote mitochondrial biogenesis through its effect on various genes and proteins involved in β-oxidation (Dominy and Puigserver, 2013; Lowell and Spiegelman, 2000).

Another one of the major regulators of this process is the PGC1α (Cao et al., 2004; Dominy and Puigserver, 2013; Jornayvaz and Shulman, 2010; Wang et al., 2019). PGC1α will activate NRF-1 and NRF-2 which will increase mitochondrial transcription factors to stimulate mitochondrial biogenesis and enhance the activation of these biogenesis genes (Dominy and Puigserver, 2013; Jornayvaz and Shulman, 2010). When the PGC1α protein is phosphorylated, it will act as a co-activator for PPARγ, which is bound to the UCP1 promoter, and this will allow for *Ucp1* and other thermogenic genes to be transcribed (Cao et al., 2004). PRDM16 is a regulator of BAT's selective transcription factors like PPARγ, CEBP, and PGC1α (Wang et al., 2019).

PRDM16 can be bound to both PPARγ and CEBPs which makes it a co-regulator of these factors (Wang et al., 2019). CEBPβ is especially important for beiging, as it will bind with PRDM16 and induce PPARγ and PGC1α in preadipocytes (Y. H. Lee et al., 2014b, 2014a). When PRDM16 is activated through CREB/ATF2, it will also activate the transcription of thermogenic genes like *Ucp1* and *Pgc1*α (Wang et al., 2019). PGC1α has been deemed essential for the mitochondrial biogenesis pathway to occur in response to cold and exercise and has been a key target of this process (Jornayvaz and Shulman, 2010).

The cAMP-PKA pathway has been heavily involved in the activation of mitochondrial biogenesis as it will phosphorylate the CREB transcription factor and promote mitochondrial gene transcription (Dominy and Puigserver, 2013). The protein p38 mitogen-activated protein kinase (p38MAPK) will also increase the expression of PGC1α and mitochondrial proteins (Jornayvaz and Shulman, 2010). The sirtuin silent mating type information regulation 2 homologue 1 (SIRT1) has also been found to play a role in activating PGC1α for mitochondrial biogenesis and respiration (Dominy and Puigserver, 2013; Jornayvaz and Shulman, 2010). The SIRT1 protein can be imported into the mitochondria and will increase during fasting to activate PGC1α directly (Dominy and Puigserver, 2013; Jornayvaz and Shulman, 2010). AMPK has also been found to play a role in mitochondrial biogenesis when it is chronically activated (Dominy and Puigserver, 2013). When this signalling molecule is phosphorylated at a high rate, PGC1α will become activated and in turn increase mitochondrial biogenesis (Dominy and Puigserver, 2013). The activation of PKA through this pathway will also enhance PGC1α expression through CREB, which will account for 30% of the cAMP response in BAT cells (Dominy and Puigserver, 2013).

Pharmacological compounds known to target the mitochondrial biogenesis pathways have gained popularity for their possible beneficial effects in treating metabolic syndromes. Activators of PPARγ, TZDs, namely rosiglitazone and pioglitazone have been found to increase the activation of PGC1α in human scWAT (Jornayvaz and Shulman, 2010). These drugs normally used in the treatment of T2D will lead to increased mtDNA, reduced mitochondrial reactive oxygen species (ROS), and increased activity of AMPK (Jornayvaz and Shulman, 2010). Metformin has also demonstrated increased mitochondrial biogenesis indicating that these PPARγ agonists are potentially useful in stimulating this biological process in humans (Jornayvaz and Shulman, 2010). More work is currently being done in this area to investigate possible therapeutics that can increase mitochondrial biogenesis and mitigate metabolic diseases.

Central Nervous System and Adipose Tissue

Recent advances in AT's role in paracrine signalling have been reviewed by Guilherme et al. (2019) which indicate the potential for novel metabolic therapies. In addition to BAT being highly innervated, the emergence of beige AT proves the CNS's role in combating prevalent metabolic diseases (Guilherme et al., 2019). The lipid metabolism in adipocytes communicates with the local nerve fibers that send signals to the CNS and cause the activation of many pathways (Guilherme et al., 2019). If beiging is activated in WAT to increase lipolysis, the CNS might communicate with BAT depots to regulate its metabolic activities (Guilherme et al., 2019).

The state of AT is communicated to the brain through two mechanisms, through leptin and adiponectin, and through the sensory innervation of AT to signal to the CNS (Guilherme et al., 2019). When a white adipocytes store lipids during food intake, leptin will be secreted from

the WAT depot in proportion to the adipocyte size, and act on the hypothalamus to regulate appetite (Guilherme et al., 2019). When leptin is secreted, appetite decreases and promote increased EE (Guilherme et al., 2019). This key process where AT communicates with the brain gives way for tissue activation and for NST to occur.

BAT Activation and Nonshivering Thermogenesis

BAT is able to render the ability to produce heat through the induction of the NST pathway. In this pathway, cold temperatures will signal the SNS to release NE from the nerve fibers that are within the AT depot, which in turn will start the NST signalling pathway (Heeren and Scheja, 2018; Lowell and Spiegelman, 2000; Luo and Liu, 2016). NE will bind with the β3AR and in turn, will activate adenylyl cyclase, an enzyme with key regulatory roles in essentially all cells (Luo and Liu, 2016). ATP will be converted to 3',5'-cyclic AMP (cAMP) and pyrophosphate where PKA will be activated by cAMP (Luo and Liu, 2016). PKA will stimulate the gene transcription of *Ucp1* and induce lipolysis to release FFAs from the LD which will be transported to the mitochondria and activate thermogenic protein UCP1 (Luo and Liu, 2016). UCP1 dissipates the proton gradient from the ETC to produce heat rather than ATP from the oxidation of FFAs (Ro et al., 2014). Thermogenic genes are enhanced through PPARγ, thereby allowing for more thermogenesis to occur (Luo and Liu, 2016). Acutely, activation of the β3ARs will increase lipolysis and the activation of UCP1 (Lowell and Spiegelman, 2000). Whereas chronic activation of β3ARs will increase *Ucp1* gene transcription, mitochondrial biogenesis, hyperplasia of BAT, and will recruit beige adipocytes into WAT depots (Lowell and Spiegelman, 2000).

When brown adipocytes use their intracellular energy stores, they use de novo lipogenesis and glycogen synthesis to uptake circulating glucose and FFAs from either WAT or triglyceride-rich lipoproteins (Peng et al., 2015). PKA will also activate the CREB transcription factor to further regulate the *Ucp1* gene transcription (Cao et al., 2004; Y. H. Lee et al., 2014b, 2014a; Wang et al., 2015). PKA will also activate the p38MAPK signaling pathway which will become phosphorylated and further induce *Ucp1* transcription (Cao et al., 2004; Collins, 2011; Jeanson et al., 2015; Wang et al., 2019). This transcription is described by Cao et al. (2004) to be a combination of the phosphorylation of Activating Transcription Factor 2 (ATF-2) and PGC1α together to directly allow for *Ucp1* transcription (through PPARγ), while the phosphorylation of ATF-2 will further enhance the mitochondrial biogenesis to occur by allowing for more *Pgc1*α genes to be transcribed (Cao et al., 2004; Y. H. Lee et al., 2014b, 2014a).

The NST that occurs within BAT and beige AT contributes to glucose uptake in the body which further exemplifies its role in whole-body metabolism (Luo and Liu, 2016). BAT contributes to glucose uptake in the body due to it being an insulin-responsive tissue. When blood glucose concentrations rise in the body, insulin will also increase and bind to the adipocyte stimulating the GLUT4 receptor to bring more glucose into the adipocyte. The glucose will be converted to glucose-6-phosphate and then undergo glycolysis where it will be converted by pyruvate dehydrogenase into acetyl CoA that can enter the Kreb's cycle or form FFAs. Once in the Kreb's cycle, acetly CoA will undergo a series of chemical reactions that will eventually lead to the formation of ATP. The Kreb's cycle will also allow the cell to make more ATP through the ETC, or the FFAs will stimulate UCP1 further, thereby inducing NST even more.

Beiging/ Browning

Introduction

The beiging process of AT is completely facilitated through the UCP1 protein, originally only thought to be found in BAT. The thermogenic potential this protein extends to the body has huge implications in metabolism and with metabolic diseases. The process of stimulating beiging has gained increasing interest from the research community as beige AT cells could contribute to fat catabolism and potentially reduce the number of lipids stored in WAT depots (Chait and den Hartigh, 2020). Activating these types of cells within the AT could be a possible treatment for promoting weight loss in patients with obesity (Chait and den Hartigh, 2020). The high level of FA oxidation that occurs in BAT and beige cells will decrease the number of lipids stored in peripheral tissues and increase glucose tolerance, which can impact whole-body metabolism (Guilherme et al., 2019). Activation of the beige adipocytes can occur through repeated activation of the β3AR pathway with CE, or with β3AR agonists that are pharmaceutically derived (Chait and den Hartigh, 2020; Luo and Liu, 2016). The process of beiging occurs through the NST pathway where the β3AR will activate PKA to induce lipolysis and activate UCP1 (Luo and Liu, 2016).

An important peptide secreted by adipocytes to stimulate angiogenesis and promote sensory nerve density to increase within the cells is VEGF (Guilherme et al., 2019). This hormone's role in AT has been investigated over the last decade and proven to be important for the control of energy metabolism and glucose tolerance, but further investigations are needed to fully understand its effects (Guilherme et al., 2019).

The beiging of AT is an adaptive and reversible response to environmental challenges put onto the tissue (Bartlet and Heeren, 2013). Specific WAT depots are prone to altering their phenotype to develop a higher number of mitochondria and have more thermogenic potential (beiging) (Bartlet and Heeren, 2013). Brown adipocytes can also be altered to increase their lipid storage to morphologically resemble white adipocytes that are less thermochemically active, called whitening (to be discussed below) (Bartlet and Heeren, 2013). These processes are dependent on environmental challenges, such as cold temperatures for browning or a HFD for whitening. Adaptation to cold can also be pharmacologically mimicked by treatment with a β3AR agonist, whereas the absence of cold stress (thermoneutrality) reduces the rate of thermogenesis and leads to deposition of excess calories as lipids (Bartlet and Heeren, 2013). Activating beige adipocytes within the AT could be a possible treatment for promoting weight loss in patients with obesity (Chait and den Hartigh, 2020). Activation of the beige adipocytes can occur through repeated activation of the β3AR pathway with CE, exercise, or with β3AR agonists that are pharmaceutically derived (Chait and den Hartigh, 2020).

The study of inducing beige AT has gained popularity given today's obesity pandemic. Two natural stimuli that have been examined are exercise training and CE as both are involved in BAT activation and metabolism (Jeanson et al., 2015; Peres Valgas da Silva et al., 2019). CE is the conventional stimulator of BAT due to the thermogenic capabilities to consume glucose and FFAs for thermogenesis and EE (Peres Valgas da Silva et al., 2019). But exercise also causes adaptations in the body, and in AT, that lead to increased physiological stress, BAT activity, and possibly beiging in WAT (Boström et al., 2012; De Matteis et al., 2013; Jeanson et al., 2015; Peres Valgas da Silva et al., 2019). Pfeifer and Hoffman (2014) note the anti-obesity effect of β3AR

agonists for inducing lipolysis and brown adipocytes found in humans, dogs, rats and mouse scWAT depots.

The effects of exercise on BAT has shown conflicting results in regards to its effects on glucose uptake (Peres Valgas da Silva et al., 2019). Exercise has been shown to cause changes such as altering mitochondrial content and activity that indicate it could be implicated in beiging of WAT (Jeanson et al., 2015; Peres Valgas da Silva et al., 2019). However, there have been studies demonstrating that exercise induces changes in metabolic parameters such as BAT lipid structure and decreased lipid metabolism, which are opposite to the effects exerted by CE (Peres Valgas da Silva et al., 2019). Rodent studies with both lean and obese animals show conflicting results with exercise-induced beiging studies, which furthers the need for research in this area (Peres Valgas da Silva et al., 2019). Current studies with acute and chronic exercise models yield varying effects on the markers of beiging, such as UCP1, PGC1α and PRDM16 (Peres Valgas da Silva et al., 2019). Muscle hormones irisin, lactate and meteorin-like hormone have also been found to have beiging effects in WAT, however, studies yield conflicting results on the exact mechanism for this pathway (Jeanson et al., 2015).

Other conditions inducing beiging that have been identified cachexia and severe burn (Jeanson et al., 2015). Cachexia and the associated chronic inflammation will cause atrophy of the muscles and fat depots which will result in wasting syndromes (Evans et al., 2008; Jeanson et al., 2015). Saraf et al.(2016) demonstrated the morphological effects of the severe burn injury on scWAT in children and classify their associated tissue level cytokine concentrations (Saraf et al., 2016). Even though the scWAT decreased in size from the burn injury, the morphological changes that occurred in the WAT depot that remained beige-like in their phenotype where they

observed multilocular LDs and showed significantly reduced cell size (Saraf et al., 2016). They also reported significant increases in the cytokines IL-6, IL-8, IL-13, IL-1α, IL-1β, MCP-1 and TNFα, which are associated with tissue inflammation (Saraf et al., 2016). IL-6 is a key regulator of beiging in cases of inflammation, and may also be part of the pathways amplified in patients with severe burns in addition to hypermetabolic and hyperthermia body responses (Jeanson et al., 2015; Porter et al., 2015; Saraf et al., 2016; Sidossis et al., 2015). Song et al. (2017) also noted that chronic inflammation from cancer can induce beiging, possibly from increased IL-6 concentrations (Song et al., 2017). The level of stress associated with both cachexia and severe burn injuries also gives the possibility of the HPA axis and prolonged stress response playing a role in the beiging response (Jeanson et al., 2015; Saraf et al., 2016; Sidossis et al., 2015).

Cold Exposure Studies for Inducing Beiging

CE studies on BAT and now beige AT have gained popularity in recent years. These studies in rodents utilized temperatures ranging from 4-7°C. Notable rodent studies have found CE can affect body size, adipokine secretion, circulating metabolites and induce beiging genes (Beaudry et al., 2019; Defour et al., 2018; Flachs et al., 2017; Hui et al., 2015; Imai et al., 2006; Schulz and Tseng, 2013). One study exposed mice to varying durations of CE and reported that messenger ribonucleic acid (mRNA) changes in adiponectin will occur as early as 6 hours post CE and increase exponentially with longer cold acclimation, with protein adiponectin levels increasing with time (Hui et al., 2015). This study also observed that CE will selectively induce adiponectin production in scWAT which will mediate the cross-talk between M2 macrophages and the adipocytes and therefore plays a key role in signaling during adaptive thermogenesis

(Hui et al., 2015). Acute CE shows promising metabolic effects as early as 2 hours where lipid metabolism becomes activated in both BAT and WAT (Lu et al., 2017). Schultz et al. (2013) demonstrated that under chronic cold challenge for 48 hours, mice can achieve normal body temperature through rapid activation of NST (Schulz and Tseng, 2013). Imai et al. (2006) reported that the bodyweight of mice was decreased after 12 hours of CE but this decrease did not remain at 24 hours, possibly due to increased food intake in CE mice (Imai et al., 2006). Another study found that the mass of WAT was decreased with CE of 2 and 7 days, although TAG-rich lipoprotein levels initially decreased, they were normalized by day 7 of the study (Flachs et al., 2017). Flachs et al. (2017) also noted that there were only small differences observed with C57BL/6J mice in their CE studies, whereas A/J obesity-resistant mice illustrated larger changes in response to cold. Indicators of beiging, such as PPAR genes, have been found to increase in CE within the ingWAT depot when mice were exposed to cold for 10 days (Defour et al., 2018; Flachs et al., 2017). CE for 3.5 weeks continuously has been found to significantly decrease ingWAT mass and BAT adipocyte size (Cline et al., 2019).

CE studies have also gained popularity within the microbiology community where gut microbiota has been found to drastically change with CE (Chevalier et al., 2015). Prolonged CE appears to induce changes within the intestine where villi increase in length and the microbiota profile is altered due to the increased energy demand of the cold temperature (Chevalier et al., 2015). This altered microbiota appears to increase the insulin sensitivity and beiging of WAT, even when transplanted to a non-cold induced mouse (Chevalier et al., 2015).

Obesity has been a promising target of cold-induced beiging, so intermittent CE (ICE) studies have been conducted as a more physiologically relevant method of AT stimulation.

Ravussin et al. (2014) conducted ICE studies on diet-induced obesity (DIO) mice for 11 weeks. They determined that ICE activated BAT and had a transient effect on improved glucose homeostasis (Ravussin et al., 2014). Increased EE was noted in other studies when animals were exposed to cold temperatures, with some studies noting increased food intake as well (Presby et al., 2019; Ravussin et al., 2014). If accompanied by decreased food intake, ICE could be a possible means to achieve weight loss and better metabolic status (Ravussin et al., 2014). ICE for 2 hours a day for 14 weeks was found to induce beiging in ingWAT (indicated through increased UCP1 and PGC1α expression), improve glucose tolerance, and enhance insulin sensitivity in C57BL/6J mice (Wang et al., 2015). The body weight gain of these mice did not change, however, the average cell size of ingWAT was decreased with CE (Wang et al., 2015). This study did note that the ICE had to be applied for more than 7 weeks to see significant effects, less than this time would not yield any promising results (Wang et al., 2015). The timing of beiging is a very important factor as the ability for adipocytes to be induced to express UCP1 declines with age. Yoo et al. (2014) conducted ICE experiments where they gradually increased the number of times mice were subjected to cold from 3 hours on the first day, to up to 6 hours for 8-10 days (Yoo et al., 2014). This study found beige adipocytes in scWAT with enhanced *Ucp1* gene expression, however, they also found that CE appeared to increase lipogenesis between the exposure times and led to increased fat accumulation (Yoo et al., 2014). Berry et al. (2017) conducted a study on mice either 2 or 7 months old and exposed them to cold temperatures for 7 days (Berry et al., 2017). The cold increased BAT weight in both sets of mice, but the older mice did not have as many WAT UCP1 positive cells and the ability to become beige declined significantly (Berry et al., 2017). If this aging effect observed in the mouse model can be

translated to humans, a 7-month-old mice might approximate a human in their mid-30s, (Berry et al., 2017). This effect has been observed in human stromal cells where their beiging capabilities were found to decrease with age (Berry et al., 2017).

Since obesity is accompanied by hypertrophic and stressed adipocytes, Kotzbeck et al. (2018) investigated the effects of inflammation in C57BL/6J and ATGL knock-out (KO) mice exposed to 10 days of CE (Kotzbeck et al., 2018). They were able to see fewer CLS and more multilocular adipocytes in BAT in mice that were exposed to cold temperatures compared to warm-temperature mice (Kotzbeck et al., 2018). This study also examined the whitening effect of AT where warm temperatures induce phenotype changes transitioning the active BAT to increase its amount of lipids store (Kotzbeck et al., 2018). CLS were found to drastically increase in both BAT and ingWAT depots of warm temperature treated mice indicating that macrophages infiltrated both tissues, leading to a more inflammatory state (Kotzbeck et al., 2018).

A notable human study with beiging induced through cold temperatures was conducted by Chen et al. (2013) where they used ^{18}F-Fluorodeoxyglucose ([^{18}F]-FDG) imaging to determine if a mild decrease in ambient temperature was enough to induce BAT activation (Chen et al., 2013). They exposed participants to 19°C for 36 hours before undergoing [^{18}F]-FDG imaging (Chen et al., 2013). The mild decrease in temperature was found to increase BAT activity and activate the SNS (determined through increased cortisol and NE concentrations) (Chen et al., 2013). Blondin et al. (2014) found that the oxidative capacity of BAT in cold-acclimated humans, exposed to 10°C for 2 hours per day for 4 weeks, 5 days per week (Blondin et al., 2014). This study reported a 45% increase in BAT volume and activity throughout the experiment in addition to increased glucose uptake, measured through [^{18}F]-FDG imaging, yielding the possible

implications for activating BAT in humans (Blondin et al., 2014). The application of CE studies in diseased human populations has been observed in patients with T2D where 10 days of daily CE was able to increase the amount of glucose removed from circulation through insulin-mediated uptake (Chondronikola et al., 2014; Fernández-Verdejo et al., 2019). However, in order to use CE as a means to activate human AT, the compliance with repeated exposure to cold temperatures would not yield much tolerance, making the feasibility of this methodology relatively low. Fernandez-Verdejo et al. (2019) make a notable point when reviewing human studies that have investigated BAT's role in energy metabolism in that thermoneutral conditions are likely a common condition when measuring active BAT and may be the reason for such a small amount of BAT being detected (Fernández-Verdejo et al., 2019). CE that does not induce shivering, for humans being between 16-19°C, has been now deemed the standard for BAT determination hopefully alleviating this possible error in BAT measurements (Chen et al., 2016; Fernández-Verdejo et al., 2019). Another issue when determining active BAT or beige AT in humans is the lack of understanding when it comes to how long these beige cells will take to become fully activated with CE (Fernández-Verdejo et al., 2019). Leitner at al. (2017) note that some beige AT (as measured through [^{18}F]-FDG imaging) is inactive with 5 hours of CE in humans, thus indicating that long term CE may be needed for this tissue to become fully active, which would not be achievable or pragmatic in human subjects (Fernández-Verdejo et al., 2019; Leitner et al., 2017).

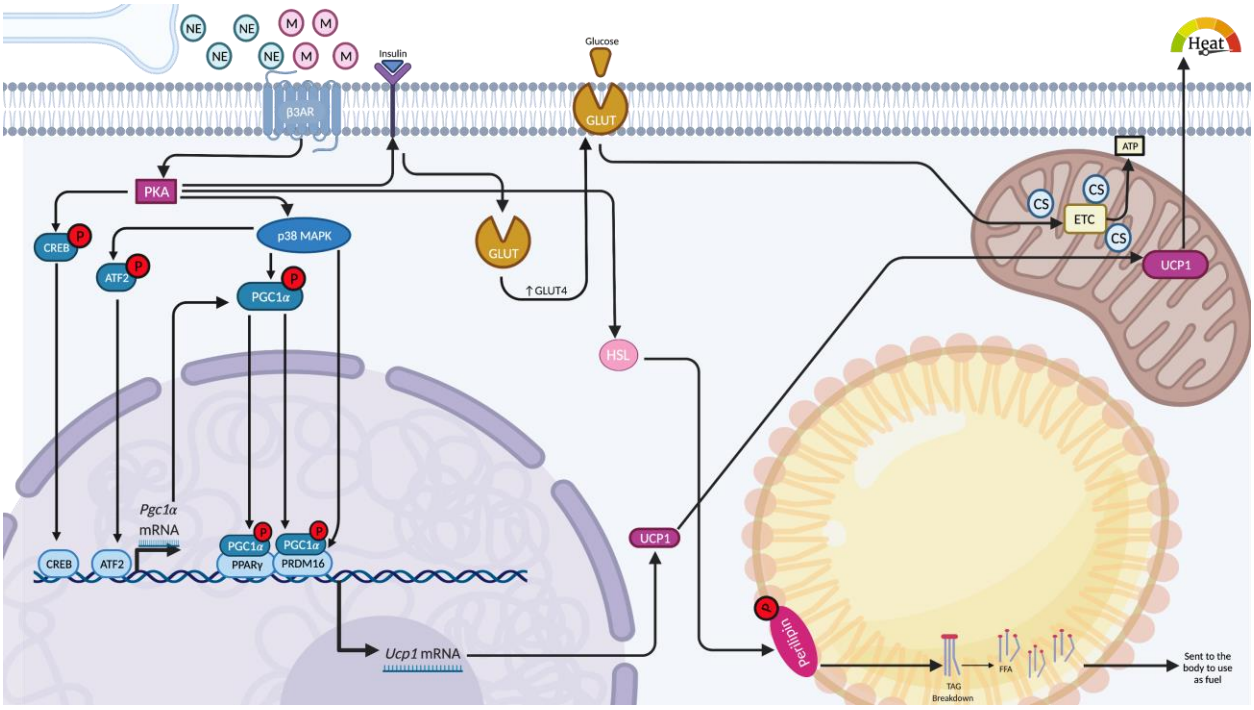

Figure 3: β3-Adrenergic signaling in BAT in response to cold and mirabegron.

The β3-adrenergic receptor (β3AR) is activated by either mirabegron (M) or Norepinephrine (NE) which will cause a confirmational change of the G-protein coupled receptor and initiate a signaling cascade. Protein kinase A (PKA) will phosphorylate the cAMP response element binding protein (CREB) or activate protein p38 mitogen-activated protein kinase (p38MAPK). Active p38MAPK will subsequently phosphorylate activating transcription Factor 2 (ATF2) or peroxisome proliferator-activator receptor-gamma coactivator-1α (PGC1α). Phosphorylated CREB, ATF2, or PGC1α will enter the nucleus and bind to subsequent transcription factors including including Peroxisome Proliferator Activated Receptor γ (PPARγ) and PR domain zinc finger 16 (PRDM16) allowing for the translation of proteins UCP1 and PGC1α. UCP1 will travel to the mitochondria where it will uncouple the electron transport chain (ETC) and allow for the production of heat. PKA will also activate hormone sensitive lipase (HSL) which will be translocated from the cytosol to the lipid droplet where it will phosphorylate perilipin allowing for the breakdown of stored triglycerides (TAG) to occur. The mitochondria contains high amounts of the enzyme citrate synthase (CS). When insulin binds to the insulin receptor, a series of reactions will allow for translocation of glucose transporter 4 (GLUT4) to the cell membrane allowing for increased amounts of glucose to enter the cell in order to be used to make ATP in the mitochondria.

Other Models for Inducing Beiging

In order to combat the discomfort and likely limited participation associated with subjecting humans to CE, pharmacological treatments have been investigated to mimic the effects CE has on the body. β3AR agonists have been reported to increase heart rate, systolic blood pressure and induce non-selective activation of other βARs, while others have been deemed impractical (Chait and den Hartigh, 2020; Fernández-Verdejo et al., 2019). However, mirabegron is the one compound that shows promising results with less unwanted side effects observed. Figure 3 illustrates the signaling occurring within BAT when CE or mirabegron are administered (Bel et al., 2021). For this reason, β3AR agonists in the form of pharmaceutical compounds have begun to be explored in order to have a greater effect on patients in need of AT activation (to be discussed further below).

A wide variety of natural and pharmaceutical compounds, immune responses and methods of gene therapy have been explored for their thermogenic inducing capacity. Natural compounds including berberine, capsaicin and capsinoid, curcumin, green tea and resveratrol have shown some thermogenic properties (Brandão et al., 2021). Pharmacological compounds including β3AR agonists and Glucagon-like peptide 1 receptor agonists have been explored for their their thermogenic/ anti-obesity capabilities (Brandão et al., 2021; Schena and Caplan, 2019; Warner and Mittag, 2016). β3AR agonists can induce thermogenesis but have been reported to increase heart rate, systolic blood pressure and induce non-selective activation of other βARs (Chait and den Hartigh, 2020; Fernández-Verdejo et al., 2019). However, mirabegron is the one compound that shows promising results with fewer unwanted side effects observed.

Mirabegron and Beiging

Mirabegron, a β3AR agonist originally intended as an over-active bladder drug, has been identified as a potential beiging agent for AT. Numerous studies have noted the possible use of mirabegron to increase beige AT (Finlin et al., 2018). In healthy individuals, Cypess et al. (2017) found that 200mg of mirabegron was able to increase the EE, glucose uptake in BAT, and BAT thermogenesis which led them to investigate whether this agent could be used in the treatment of obesity (Cypess et al., 2015). Calmasini et al. (2017) used mirabegron in C57BL/6 mice to determine its effects in cases of obesity (Calmasini et al., 2017). Mirabegron was administered through oral gavage daily at a dose of (10mg/kg/day) over the last two weeks of 12 weeks on a HFD (Calmasini et al., 2017). Their results indicated that low density lipoprotein (LDLP) and high-density lipoprotein (HDL) plasma levels were reduced with mirabegron treatment, proving its beneficial cardiovascular effects, in addition to a reduction in epididymal AT (Calmasini et al., 2017). A recent study conducted by Hao et al. (2019) used both in vivo and in vitro methods to determine the metabolic effects of mirabegron in cases of HFD-induced obesity (Hao et al., 2019). Through their in vivo studies, mirabegron was administered for 3 weeks at 2mg/kg/day through ALZET osmotic pumps to male C57BL6/J mice before metabolic and histological parameters were investigated (Hao et al., 2019). The histological results indicated that the BAT of mirabegron treated mice displayed smaller LDs and were fewer in number, in addition to an appearance of beige cells within the ingWAT depot compared to vehicle-treated mice (Hao et al., 2019). The gene expression of *Ucp1* was significantly increased in ingWAT, indicating beiging occurred within this depot (Hao et al., 2019). Glucose tolerance and insulin sensitivity were also

improved with mirabegron treatment indicating beneficial effects on whole-body metabolism (Hao et al., 2019). Mirabegron-treated mice displayed lower body weights and less adiposity than vehicle mice (Hao et al., 2019), indicating this drug can mitigate some of the effects on DIO. However, the mechanism of mirabegron action on glucose homeostasis and insulin signalling remains unknown (Hao et al., 2019). A study conducted on humans by Baskin et al. (2018) found that mirabegron can mitigate some of the obesity-related complications through increasing WAT lipolysis, and BAT thermogenesis (Baskin et al., 2018). This study noted that the BAT activity and resting EE of healthy subjects was increased acutely (Baskin et al., 2018). Finlin et al. (2018) compared the response of AT in humans to both mirabegron (50mg/day) and CE for 10 weeks (Finlin et al., 2018). The study demonstrated that beiging proteins UCP1 and transmembrane protein 26 (TMEM26) expression were increased in response to both stimuli in human scWAT (Finlin et al., 2018). The increase in expression of these proteins in both lean and obese subjects indicates beiging within this tissue depot, however, the protein PGC1α failed to be induced in obese subjects overall which may show limitations in its beiging capacity (Finlin et al., 2018).

The positive metabolic effects of using β3AR agonists should not be overlooked in the treatment of obesity and metabolic diseases (Schena and Caplan, 2019). Mirabegron has been shown to have better potency for the β3AR than known agonist CL316243 and has been shown to effectively activate both rodent BAT and human BAT. Roberts-Toler et al. (2015) investigated the effects mirabegron can have on BAT changes associated with DIO (Roberts-Toler et al., 2015). The C57BL/6 mice were fed either a normal or HFD for 16 weeks before metabolic parameters including body fat, glucose tolerance, mRNA markers of inflammation were assessed in response to both insulin and mirabegron (Roberts-Toler et al., 2015). As expected, the HFD

led to increased body weight and impaired glucose tolerance with both WAT and BAT displaying higher levels of TNFα and macrophage marker F4/80, indicating increased inflammation within these depots (Roberts-Toler et al., 2015). They were also able to show that BAT is resistant to DIO changes such as macrophage infiltration with inflammatory markers in BAT being 10-100-fold lower than perigonadal WAT irrespective of diet (Roberts-Toler et al., 2015).

Another recent study investigating BAT mediated lipolysis with mirabegron was conducted by Sui et al. (2019) at doses of 0.8mg/kg and 8 mg/kg administered daily for four weeks in mice (Sui et al., 2019). Their results indicated that both doses of mirabegron increased food intake significantly, but body weight and body mass index were reduced, especially with the high dose (Sui et al., 2019). The physical appearance of the ATs in the mirabegron treated mice displayed a more brownish colour for the BAT, ingWAT and epididymal WAT, in combination with lower tissue weights (Sui et al., 2019). BAT also yielded increased [^{18}F]-FDG uptake indicating increased BAT-mediated glucose uptake in these mirabegron-treated mice (Sui et al., 2019). Even metabolic changes were observed in the mirabegron-treated mice with increased insulin sensitivity and decreased blood glucose levels, illustrating a more metabolically favourable plasma profile (Sui et al., 2019). Cypess et al. (2015) conducted a study using human participants to investigate the activation of BAT through a one-time 200mg dose of mirabegron (Cypess et al., 2015). This was one of the preliminary studies to demonstrate results in humans that could be translated into treatments for obesity and diabetes (Cypess et al., 2015). They were able to demonstrate that mirabegron can lead to higher BAT metabolic activity and increase their resting metabolic rate (Cypess et al., 2015).

Mirabegron has high bioavailability and shows high in vitro binding affinity for the β3AR in humans compared to other drugs in the β3AR agonist class (Cypess et al., 2015). Current concerns with other β3AR agonists involve cardiac specific side effects, however, minimal effects have been observed with mirabegron at the doses used for overactive bladder (Cypess et al., 2015). Cypess et al. (2015) conclude that mirabegron shows promising results in increasing EE and treating diabetes and metabolic diseases (Cypess et al., 2015). Peng et al. (2015) reviewed numerous studies examining the implications of treating patients with drugs targeting the thermogenic potential of AT (Peng et al., 2015). When Peng et al. (2015) looked into the study conducted by Cypess et al. (2015), they anticipated that treatment with mirabegron could lead to an 8% reduction in body weight per year in BAT-positive healthy men (Cypess et al., 2015; Peng et al., 2015). However, functional tolerance and chronic β3AR mediated stimulation of BAT remain to be determined (Cypess et al., 2015). The beiging pathway is mediated through NE by increasing the intracellular cAMP concentration that will stimulate lipolysis in brown adipocytes through the PKA pathway (Peng et al., 2015). During lipolysis, ATGL hydrolyzes triglycerides to DAGs, which will then be hydrolyzed by HSL to MAG and then to glycerol and FFAs, which will, in turn, activate UCP1 for NST (Peng et al., 2015).

O'Mara et al. (2020) conducted a study on humans where chronic treatment with mirabegron (100mg daily for 14 days) increased the glucose uptake during the glucose tolerance test and HOMA-IR of healthy females, further exemplifying how this pharmaceutical agent could be used to treat metabolic diseases (O'Mara et al., 2020). Using [^{18}F]-FDG imaging, the activation of BAT was increased, as well as resting EE and glucose tolerance (O'Mara et al., 2020). The anti-inflammatory properties of the mirabegron treatment were also noted with

adiponectin increasing in the circulation by up to 35% when mirabegron treatment was administered (O'Mara et al., 2020).

A detailed review on the benefits of mirabegron as a beiging agent over chronic cold exposure (CCE) and exercise are outlined by Bel et al. (2021) (Bel et al., 2021). Briefly, this β3AR agonist, along with a healthy diet and exercise, warrants further investigation into its beiging capabilities and use in the treatment of metabolic disorders (Bel et al., 2021).

Immune Cells and the Beiging Process

A range of immune cells including macrophages, eosinophils, and lymphocytes have been implicated in the beiging of WAT (Villarroya et al., 2018). The review by Villarroya et al. (2018) outlined the direct involvement that each of these immune cells plays in the beiging process, but most importantly, macrophages have been found to play the most critical role in adipobiology (Villarroya et al., 2018). Due to their highly adaptive nature, WAT and BAT depots will contain macrophages that can become activated by several different stimuli (Villarroya et al., 2018). In obesity, the LD expansion stress will cause AT to contain more M1 macrophages that will secrete type 1 cytokines and pro-inflammatory mediators such as TNFα, MCP-1, CCL5, and IL-1β (Villarroya et al., 2018). These cytokines will suppress the *Ucp1* gene expression and protein activation within these AT depots (Villarroya et al., 2018). The inflammatory response in BAT has been found to cause IR and affect the thermogenic response (Villarroya et al., 2018). Brestoff and Artis (2015) illustrated the increase in inflammatory markers when exposed to cold temperatures (Brestoff and Artis, 2015; Jeanson et al., 2015). Upon CE, the eosinophils residing in the WAT depot can secrete IL-4 and IL-13 that will, in turn, recruit M2 macrophages to the

depot and respond to the cold (Jeanson et al., 2015). The macrophages will secrete catecholamines, which will activate the beiging process through traditional β3AR pathways (Jeanson et al., 2015). Ngyuen et al. (2011) were the first to describe the role of the M2 macrophage in promoting thermogenesis in BAT depots (Nguyen et al., 2011). Upon thermogenesis activation, the expression level of anti-inflammatory cytokines increases and levels of pro-inflammatory cytokines decrease (Nguyen et al., 2011). This finding has been noted by others where WAT depots exposed to cold or undergoing beiging, will also display this change in cytokine expression with a more anti-inflammatory phenotype (Qiu et al., 2014; Villarroya et al., 2018). Villarroya et al. (2018) describe how M2 polarization can occur through two mechanisms of direct or indirect activation through cytokine or eosinophil action (Villarroya et al., 2018). IL-6 can directly activate the SNS to release NE and therefore stimulate beiging (Villarroya et al., 2018). In essence, brown or beige cells have resident eosinophils that will be activated upon cold stimulation that will recruit anti-inflammatory cytokines IL-4 to promote the polarization to M2 macrophages (Villarroya et al., 2018). The link between immune cells and beiging have not been fully investigated and warrant further understanding (Jeanson et al., 2015).

Whitening

Introduction

In BAT, the expansion of LDs within the depot will cause a shift in characteristics where the depot will acquire a WAT-like phenotype (Shimizu and Walsh, 2015). This shift in phenotype is termed "whitening" where the BAT depot will lose vascularity, its oxidative capacity and increase the storage of lipids (Shimizu and Walsh, 2015). The mechanism of BAT whitening is not completely understood; however, the histological and protein changes have been previously noted (Shimizu and Walsh, 2015). When BAT undergoes whitening, the depot itself becomes larger and contains less mitochondria giving it a light brown appearance, in addition to histological studies confirming these changes with increased adipocyte size (Cedikova et al., 2016; Shimizu and Walsh, 2015). The whitening of BAT is thought to be associated with the loss of VEGF and UCP1 protein expression and β3AR signaling. All three of these factors lead to a less vascularized depot with diminished thermogenesis capabilities and increased mitochondrial dysfunction (Shimizu and Walsh, 2015).

The increase in adipocyte dysfunction through hypertrophy may be involved in diseases including cancer, thrombosis, polycystic ovarian syndrome and other metabolic diseases in ways scientists never thought possible (Deng et al., 2020). While the exact cellular mechanism by which whitening of BAT occurs is not fully known, more research into how metabolic diseases like obesity and diabetes contribute to a physiological change in the depot should be investigated to facilitate therapeutic options to reverse this phenomenon.

Whitening, Adipose Tissue Inflammation, Insulin Resistance and Endoplasmic Reticulum Stress

The connections between inflammation and IR have been reviewed by Chen et al. (2015) however, how this links with AT beiging will be discussed below (Chen et al., 2015). In periods of inflammation stress, the pro-inflammatory cytokines will increase within the tissue (Chen et al., 2015). These cytokines, such as TNFα, can stimulate lipolysis to occur within the LD, and in turn increase the amount of FFA that accumulates within the cell (Chen et al., 2015). These excess FFA will bind to TLR4 in the adipocyte and initiate the ER stress pathways c-Jun N-terminal kinase (JNK) and NFkB to then increase the pro-inflammatory cytokines within the tissue (Chen et al., 2015). When these two pathways are initiated, they will phosphorylate through serine/threonine phosphorylation the IRS-1 and IRS-2, blocking insulin signalling (Chen et al., 2015). This IR is further enhanced by the increased IL-6 concentration within the stressed cell, which initiates the Janus kinases- signal transducer and activator of transcription (JAK/STAT) signalling pathway that will increase suppressor of cytokine signaling 3 (SOCS3) and affect the expression of GLUT4 that can be translocated to the cell membrane (Chen et al., 2015).

Stress

Glucocorticoids (GCs)

Defined as "*steroid hormones that play key roles in metabolic adaptations during stress in order to maintain plasma glucose levels*" GCs required for normal physiological function (Lee et al., 2018). GCs are a class of steroid hormones produced in the adrenal cortex that regulate many body processes during stress including energy and glucose metabolism, and the inflammatory response (Akalestou et al., 2020; Di Dalmazi et al., 2012; Harvey et al., 2018; Ramage et al., 2016). These molecules are regulated by the HPA axis and will exert their effects on body tissues through specific glucocorticoid receptors (GRs) (Di Dalmazi et al., 2012). At normal levels, these hormones will provide anti-inflammatory effects and allow for cells to use stored TAG as energy and stimulate glucose production (Harvey et al., 2018). These hormones will allow the body to utilize stored energy to handle stress and inhibit cellular functions that promote storage (Harvey et al., 2018).

In situations of chronic stress, the GCs can contribute to many metabolic disorders including IR, and dyslipidemia (M.J. Lee et al., 2014; Lee et al., 2018). The exact mechanism for GC-induced IR in AT is not clear, however, GCs have been shown to suppress insulin-stimulated glucose uptake in adipocytes and therefore contributes to whole-body glucose and insulin homeostasis (Lee et al., 2018).

In the acute state, GCs have been known to stimulate lipolysis in AT to release FFA and glycerol that can be used for energy during times of fasting (Lee et al., 2018). In the chronic release of GCs or exogenous administration of GCs, there have been conflicting effects reported

for lipid metabolism in this tissue (Lee et al., 2018). Cushing's syndrome patients have chronically elevated cortisol levels and will exhibit central visceral obesity but lipodystrophy in the scWAT (M.J. Lee et al., 2014; Lee et al., 2018). Whereas exogenous GCs have been shown to promote AT dysfunction and lipid accumulation. Many rodent models have shown the negative effect GCs can have on thermogenesis and the overall metabolism (Cassano et al., 2012; Do, 2019; Harvey et al., 2018; Karatsoreos et al., 2010; M.J. Lee et al., 2014; Lee et al., 2018; Legeza et al., 2017; Luijten et al., 2019b, 2019a; Veyrat-Durebex et al., 2012; Vienberg and Björnholm, 2014). Lee et al. (2018) have reviewed studies in an attempt to understand the mechanism for how adipocytes play a role in the GC stress response, with many factors including the GR, the AT depot, and the physiological status of the organism all playing a role in how the adipocyte will function in response to GC excess (Lee et al., 2018). The complex nature of stress hormones and their role in AT metabolism needs to be better understood for researchers to determine the role this physiological response plays in disease.

The Hypothalamus Pituitary Adrenal Axis (HPA Axis) and Adipose Tissue

In periods of stress, tissues such as AT will increase their metabolic and energy demands in order for the body to deal with the stress (Peckett et al., 2011). In the short term, catecholamines will render their effects, however, the long-term effects of stress are facilitated through GCs (Peckett et al., 2011). Catecholamines will quickly render their effects in the tissue by binding to ARs, whereas GCs will need to bind to specific GRs in order for their effects to be rendered long term (Peckett et al., 2011). In AT, 11β-hydroxysteroid dehydrogenase type 1 (11β -HSD1), will activate the inactive GCs cortisone to cortisol in humans. In rodents, 11β-

hydroxysteroid dehydrogenase to converts the inactive GCs to corticosterone (Akalestou et al., 2020; Di Dalmazi et al., 2012; Lee et al., 2018; Vienberg and Björnholm, 2014). This enzyme is key in controlling the local effects of GCs in AT directly and its effects of this on the entire body (Akalestou et al., 2020; Lee et al., 2018).

In situations of stress, the body will respond by activating the HPA Axis to release chemical messengers that will allow the body to respond. The HPA axis is a regulatory system that connects the endocrine hormone system with the central nervous system (Kudielka and Kirschbaum, 2005). The stress response system will increase physiological functioning of the organism in order to combat the stressful situation and bring it back to homeostasis once the stress is gone (Akalestou et al., 2020; Di Dalmazi et al., 2012; Kudielka and Kirschbaum, 2005). The pathway for the HPA axis is as follows (McEwen, 2007; Oakley and Cidlowski, 2013):

1. The hypothalamus in the brain will sense the stress via the autonomic nervous system and sensory receptors in the form of impulses. As a response to these signals, the hypothalamus will secrete corticotropin-releasing hormone (CRH) that will bind to the anterior pituitary gland.
2. The pituitary gland will then release adrenocorticotropic hormone (ACTH) that will bind to the adrenal gland.
3. The adrenal cortex will then secrete GCs that will circulate in the blood, normally bound to transcortin and travel to GC-sensitive tissues.

Once the GCs reach their target tissue, the GCs will move freely from the bloodstream through the cell membranes due to their lipophilic structure (Luijten et al., 2019a; Oakley and Cidlowski, 2013). Figure 4 depicts this signaling pathway within BAT. Once in the cytosol, the GCs

will become activated by the 11β-HSD1 enzyme that has been upregulated in response to the excess GCs (Di Dalmazi et al., 2012; Doig et al., 2017; Woo et al., 2019). The 11β-HSD1 enzyme will interconvert cortisone to cortisol (humans) and dehydroxycorticosterone to corticosterone (rodents) (Di Dalmazi et al., 2012). Most predominantly found in AT and the liver, this enzyme will amplify the action GCs can have on the body (Di Dalmazi et al., 2012). The counter enzyme for 11β-HSD1 is 11β-HSD2, which will inactivate GCs and reduce the effects of cortisol/corticosterone (Di Dalmazi et al., 2012; Veyrat-Durebex et al., 2012). 11β-HSD2 is predominantly found in the kidneys and will lower the amount of active GCs circulating in the body (Di Dalmazi et al., 2012; Doig et al., 2017). 11β-HSD1 will negatively impact the expression of BAT and mitochondrial biogenesis genes, such as *Ucp1* and affect thermogenesis in the tissue (Doig et al., 2017; Liu et al., 2013; Woo et al., 2019). Some researchers have reported that excess levels of the 11β-HSD1 enzyme will promote BAT dysfunction through increased lipid accumulation and inhibition of NST within the depot (Campbell et al., 2011; Doig et al., 2017; Liu et al., 2013). Legeza et al. (2017) conducted a review and noted that many metabolic diseases associated with AT expressing increased amounts of this 11β-HSD1 enzyme (Legeza et al., 2017). In obesity, the activation of GCs at the AT depot itself has been shown to be increased, due to the elevation in the 11β-HSD1 enzyme within the depot (Legeza et al., 2017). Once activated, the GCs can bind to the GR where it will undergo a conformational change and be actively transported to the nucleus (Oakley and Cidlowski, 2013). Once in the nucleus, the GR will bind to the GC response element (GRE) and allow for the transcription of target genes to be expressed (Luijten et al., 2019a; Oakley and Cidlowski, 2013; Peckett et al., 2011; Poggioli et al., 2013). The genomic effects of GCs take longer to transpire into physiological effects, which is

why GCs take longer to show alterations in metabolism compared to catecholamines (Peckett et al., 2011).

In periods of high stress, the HPA axis will secrete more GCs in the blood that will have profound effects on the body, especially in AT. With respect to NST, the excess GCs will result in decreased transcription and activation of the β3AR and UCP1, inhibiting this pathway in the brown adipocyte (Luijten et al., 2019a; Reddy et al., 2014). It will also affect lipid homeostasis and storage by activating the transcription of TAG synthesis genes in addition to decreasing the regulation of LD proteins further supporting lipid storage (Doig et al., 2017; Reddy et al., 2014). Lipid transport proteins will be upregulated further expanding the storage of lipids by amplifying FATPs such as CD36. GCs released will render their effects in a delayed fashion where catecholamines will provide immediate support to combat the stress, and GCs will allow the body to handle the stress over the long term, but this means they have the possibility of more damaging effects.

Adipose Tissue Metabolism of Glucocorticoids

While the main focus of this thesis is GCs due to their strong effects on metabolism, it is important to note that there is another type of corticosteroid that affects salt and water balance called mineralocorticoids (MC) (McKay and Cidlowski, 2003). MCs exert their effects through mineralocorticoid receptors (MR) which are found primarily in the kidneys and large intestines (Taves et al., 2011). The major MC, aldosterone, rises in response to low blood volume or sodium concentrations and stimulates the renin-angiotensin-aldosterone system (RAAS) to release more MCs from the adrenal gland to regulate the body's mineral ion concentration by causing sodium

absorption and reabsorption of water (Jia et al., 2017; Taves et al., 2011). AT has been found to synthesize aldosterone which can activate MRs within the AT depot and lead to increases in WAT, enhanced LDs, oxidative stress, pro-inflammatory states, adipocyte autophagy and inhibition of UCP1 (Jia et al., 2017). While aldosterone directly activates MRs, cortisol can also activate this receptor and induce its effects within AT (Jia et al., 2017). Once activated, MR will induce adipogenesis through the mammalian target of rapamycin (mTOR) and activate PPARγ and CEBP signaling (Jia et al., 2017). In BAT and beige AT, the activation of MR is not completely known, however, beiging of ingWAT has been shown with MR agonists which provide clues into its role as an inhibitor of NST (Armani et al., 2014; Jia et al., 2017).

The effects of GCs will mainly be facilitated by the GR within adipocytes, encoded by the *Nr3c1* gene, as this intracellular receptor will influence the metabolic status of the organism (Lee et al., 2018) (Akalestou et al., 2020; Shen et al., 2017). This receptor remains localized in the cytosol with the heat shock protein 90 (hsp90)-containing chaperone complex until hormones bind to it (Lee et al., 2018). Once GCs diffuse through the cellular membrane and bind to the GR-hsp90-containing complex, the GR can move to the nucleus where it can dissociate from the hsp90-containing chaperone complex and bind to the GRE in order to render its effects on transcriptional control on many genes (Lee et al., 2018). Some of these genes code for key enzymes for glucose and lipid metabolism including hormone-sensitive lipase (*Lipe*), *Atgl*, and monoglyceride lipase (*Mgll)* (Akalestou et al., 2020; Lee et al., 2018). Shen et al. (2017) demonstrated the importance of the adipocyte GR in lipolysis and mediating the metabolic effects of exogenous steroids by using adipocyte-specific GR knockout (AGRKO) mice (Shen et al., 2017). Their study illustrated that dexamethasone administration for 2 months promoted

metabolic dysfunction and "whitened" BAT in control mice, however, the effects were mitigated in KO mice (Shen et al., 2017). High levels of these GCs present at the AT level have been associated with obesity, even with circulating levels of the GCs not elevated, adding a different dimension to the unknown effects these hormones play in disease (Akalestou et al., 2020). Akalestou et al. (2020) note studies where GCs induce adiposity and IR, however the exact role GCs play in metabolic diseases still remains to be discovered (Akalestou et al., 2020). Peckett et al. (2011) reviewed numerous in vitro effects on adipocytes in terms of their effects on lipolysis, however, there are still many questions that need to be answered including how GCs function in different AT depots and how excess GCs truly lead to AT accumulation (Peckett et al., 2011). Below, potential connections between GCs signaling and BAT and beige AT are discussed.

In periods of high stress, the HPA axis will increase the release of GCs, which will travel in the bloodstream bound to transcortin to various tissues (Luijten et al., 2019a). GCs are able to move freely from the bloodstream to cell membranes due to their lipophilic structure (Luijten et al., 2019a). Once in the cytosol, the GCs will become activated by 11β-HSD1 enzyme, which is upregulated in periods of GC excess (Doig et al., 2017). GCs can bind to both the GRs and MRs in excess stress, both of which culminate with binding with the GRE (Macfarlane et al., 2008; Reddy et al., 2014; van den Beukel et al., 2015). Transcriptionally, inhibition of PPARγ and NFkB will lead to the decrease in *Ucp1* transcription within the tissue, an increase in FFA uptake and TAG synthesis genes in addition to decreased lipolysis (Luijten et al., 2019a; Poggioli et al., 2013). All of these changes within the adipocyte will increase the LD size and intracellular stress leading to a pro-inflammatory response (Hotamisligil, 2006). This pathway has been investigated by Hotamisligil (2006) where overexpression of TNFα resulted in obesity, leading to the first link

between obesity, diabetes, and chronic inflammation (Hotamisligil, 2006). In the NST pathway, the GRE will decrease *Ucp1* transcription and activation in addition to lowering the transcription of the β3AR receptor itself, further inhibiting the NST pathway (Luijten et al., 2019a; Reddy et al., 2014). Lipid homeostasis genes will be affected through increased transcription of the genes required for TAG synthesis, CD36, and lipid storage (Doig et al., 2017). These lipid storage genes will be transcribed and then made into proteins by ribosomes that will allow for lipids to accumulate in the LD (Reddy et al., 2014). LD protein genes, such as PLIN1, will be downregulated further inhibiting lipolysis and promoting lipid storage, and with more lipid transport proteins made, FFAs can be transported into the cell through proteins, such as CD36, and be stored in the LD. 11β-HSD1 can also directly affect BAT thermogenesis, independently of GC excess, by decreasing the expression of BAT genes (such as Ucp1) (Doig et al., 2017; Liu et al., 2013). 11β-HSD1 will induce BAT dysfunction by increasing lipid accumulation in the adipocyte and by inhibiting NST (Campbell et al., 2011; Doig et al., 2017; Liu et al., 2013).

AT will metabolize GC through the enzyme 11β-HSD1, which will convert inactive 11β-ketoglucorticoid metabolites to hormonally active versions of these metabolites within the AT depot and increase their local concentration (Kershaw and Flier, 2004). This will not drastically alter the systemic GC concentration within the body, but it will affect the tissue regulation which is implicated in conditions including obesity, T2D, dyslipidemia and hypertension (Kershaw and Flier, 2004; Ramage et al., 2016).

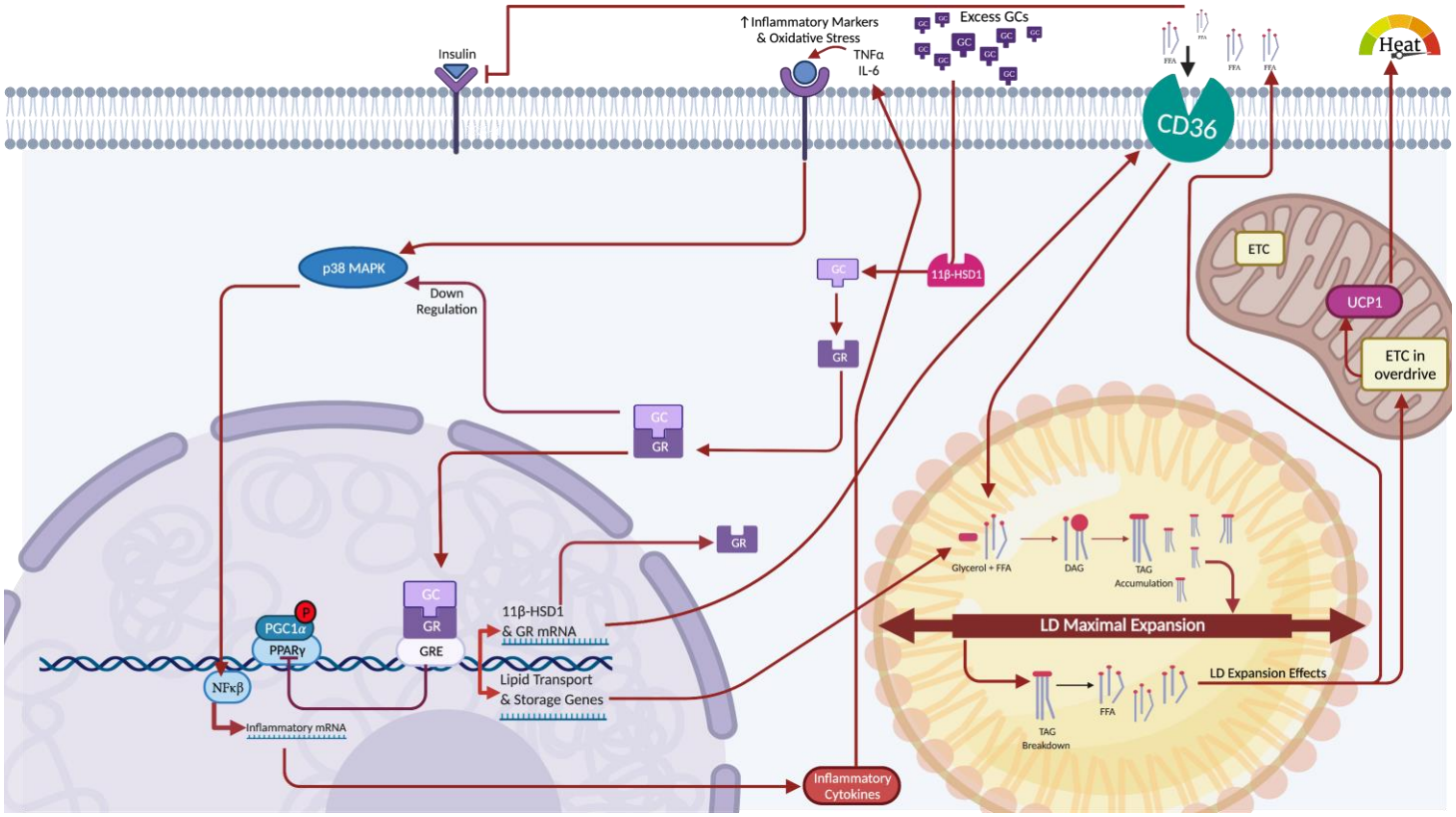

Figure 4: Excess glucocorticoid signaling in BAT.

In the event of excess glucocorticoids (GC), the GCs will travel through the cell membrane and become activated by 11β-hydroxysteroid dehydrogenase type 1 (11β-HSD1). Once active, GCs will bind to the Glucocorticoid receptor (GR) where it will travel to the nucleus and bind to the glucocorticoid response element (GRE). Once bound inside the nucleus, the GRE will inhibit mitochondrial biogenesis gene transcription and instead initiate the transcription of inflammatory marker nuclear factor kappa-light-chain-enhancer of activated B cells (NFκβ) and initiate the production of inflammatory cytokines. These inflammatory cytokines, including tumour necrosis factor α (TNFα) and interleukin 6 (IL-6) will increase in concentration and further potentiate the inflammatory response. The GRE will also increase the transcription of 11β-HSD1 mRNA and other lipid transport/storage genes to increase the lipid storage capacity of the lipid droplet (LD). The expansion of the lipid droplet (LD) and its inflammatory response will increase the amount of circulating free fatty acids (FFA) which will put the electron transport chain (ETC) into overdrive causing an increase in uncoupling protein 1 (UCP1) and production of heat. Excess FFAs will use fatty acid transport protein cluster of differentiation 36 (CD36) to enter the cell and travel to the LD. Once in the LD, FFA will combine with glycerol to make diacylglycerol (DAG) and subsequently triacylglycerol (TAG), further increasing the lipids stored in the LD.

Effects of Glucocorticoid Excess

Mouse Models of Glucocorticoid Excess

Rodent studies have yielded strong evidence for excess and chronic GCs to inhibit BAT thermogenesis and suppress UCP1 expression (Ramage et al., 2016). The physiological response of excess GCs and the effect this has on AT has been examined using chronic doses of corticosterone to determine their effects on insulin sensitivity, behaviour, and metabolic syndrome, just to name a few, all with varying exposure times. This dissertation will focus on studies administering corticosterone via drinking water in order to minimize external stress to the animals and more closely mimic the kinetics of clinical GCs (Gasparini et al., 2016). Tamashiro et al. (2011) review the connection between chronic stress, metabolism and metabolic syndrome with the conclusion that drinking water is useful in evaluating the contributions GCs may have on metabolic processes (Tamashiro et al., 2011). A comparative study was conducted on the effectiveness of corticosterone delivery from either drinking water or pellet implantation (Gasparini et al., 2016). This study used CD1 Swiss mice at doses of 25, 50, 75, and 100µg/ml in drinking water and found that these doses resulted in consistent diurnal exposure patterns that closely mimic clinical GC therapy (Gasparini et al., 2016). Additionally, drinking water administration decreases the operative stress in animals that is easily adjustable and non-invasive when compared to weekly pellet implantation (Gasparini et al., 2016). The dose of 50µg/ml in drinking water was determined to be an effective dose that induced pronounced obesity and visceral fat accumulation, IR, and arrest of musculoskeletal growth (Gasparini et al., 2016). This dose also closely mimicked the metabolic changes induced by pellet implantation that was administered at a dose of 1.5mg per week (Gasparini et al., 2016).

However, other studies investigating metabolic syndrome in mice report the higher corticosterone doses of 75 and 100μg/ml in the drinking water to more closely resemble the disease (Karatsoreos et al., 2010; van Donkelaar et al., 2014). Below, we will summarize some of the notable studies investigating ingWAT (the WAT depot with the most likelihood to beige) and BAT with chronic exposure to GCs.

Cassano et al. (2012) reported the effects of chronic oral corticosterone in mice. This study used doses of 25, 50, and 100μg/ml delivered to mice in their drinking water for four weeks, in order to investigate the true effects each dose has on anatomical, hematological (namely white blood cells) and biochemical features in mice (Cassano et al., 2012). Cassano et al. (2012) found that GCs induce histological changes in brown adipocytes, with corticosterone treated adipocytes increase in size (Cassano et al., 2012). This change in adipocyte size is thought to shift the thermogenic response and energy output within these corticosterone treated animals (Cassano et al., 2012). The in vivo analysis found glucose intolerance, hypercortisolemia, hyperinsulinemia, hyperleptinemia, and elevated plasma TAGs in the 100μg/ml treated mice, yielding metabolic syndrome (Cassano et al., 2012). This phenotype and metabolic changes were not observed with bolus doses of corticosterone, further illustrating drinking water delivery as one of the best approaches (Cassano et al., 2012). The dose of 100μg/ml was also used to investigate the physiological and endocrine response to chronic corticosterone in C57BL/6J male mice by Karastoreos et al. (2010) (Karatsoreos et al., 2010). This study was able to also show the drastic alterations that occur in the body in response to excess GCs. They found increased food consumption, decreased locomotor activity, elevated plasma TAG, leptin, and insulin levels, in addition to impaired glucose tolerance (Karatsoreos et al.,

2010). The rapid increase in weight gain and the metabolic alterations that occurred with it were described as the changes that occur in patients with metabolic syndrome, hypercortisolemia and stress-related obesity (Karatsoreos et al., 2010). They also noted that the 25μg/ml dose of corticosterone did not alter the physiology or phenotype in some measures (Karatsoreos et al., 2010). Do (2019) used the 100μg/ml corticosterone dose in drinking water to male C57BL/6J mice for up to eight weeks to determine the interactions between GCs and AT in the development and metabolic syndrome (Do, 2019). This study found that four weeks of treatment induced significant changes in weight gain that was not related to food consumption, although water intake in these mice was doubled during the course of treatment (Do, 2019). Corticosterone treated mice (100μg/ml) displayed dyslipidemia with increased plasma TAG, cholesterol, and FFA levels in addition to increased AT mass in scWAT, gonadal WAT, perirenal WAT, and BAT (Do, 2019). At the cellular level, adipocytes from corticosterone treated mice increased in size, most likely due to increased FFA uptake and decreased lipolysis (Do, 2019).

Van Donkelaar et al. (2014) also used chronic doses of corticosterone (100μg/ml) delivered to male mice, however, they administered the GC treatment for 12 weeks. Similar to previous studies, they also reported increased weight gain in corticosterone treated mice, and that these mice were more IR (determined through HOMA-IR) than control mice (van Donkelaar et al., 2014). This study also noted that the C57BL/6NCrl mice treated with corticosterone displayed a depressive-like behaviour (van Donkelaar et al., 2014). Wray et al. (2019) administered 75μg/ml corticosterone in drinking water to C57BL/6J mice for up to four weeks and reported that a four-week treatment induced hyperphagia, increased weight gain and fat pad mass, although the circulating insulin levels were increased, the plasma glucose

concentrations were not altered (Wray et al., 2019). Kinlen et al. (2017) investigated the effects chronic corticosterone treatment on metabolism and skeletal development in male C57BL6/N mice using doses of 25µg/ml and 100µg/ml (Kinlein et al., 2017). The adolescent mice (62 days old) displayed blunted growth rates, increased adiposity, increased body fat mass, enhanced glucose clearance and decreased bone density (Kinlein et al., 2017). The study noted that these findings are consistent with the clinical presentation of early-onset Cushing's disease (Kinlein et al., 2017). This study indicated the differences in glucose metabolism with chronic exposure to stress in two different life stages; adolescent mice display enhanced glucose clearance, a large reduction in bone density, and adult mice show impaired glucose clearance with chronic exposure to GCs (Kinlein et al., 2017). The researchers note that adolescent mice are more resilient to defects in glucose handling because glucose tolerance is maintained during corticosterone treatment, even though the plasma insulin levels in adolescent mice are higher than adult mice treated with high doses of CORT, this illustrates that increased insulin amounts were required to elicit the same effect (Kinlein et al., 2017). Luijten et al. (2019) treated male C57BL/6J mice with 50µg/ml in their drinking water for two weeks and reported that the UCP1 protein expression was much lower under thermoneutral conditions in corticosterone treated mice (Luijten et al., 2019a). Corticosterone treatment for two weeks was found to alter the AT histology independent of the downregulation of UCP1, with tissue weights increasing with bodyweight for corticosterone treatment (Luijten et al., 2019a). BAT has been reported to gain a whiteish appearance and show reduced protein expression levels of UCP1 in conditions like obesity, diabetes, or even chronic warm acclimation (Peng et al., 2015). Diabetes also compromised the BAT insulin-mediated glucose uptake in the depot (Peng et al., 2015).

Diabetes and other disorders have even shown increased susceptibility to stressors which can have metabolic consequences (Tamashiro et al., 2011). Sefton et al. (2019) noted that there may be a species-specific response to GCs and exactly how GCs effect BAT activity remains to be understood (Sefton et al., 2019). The clinical and pathological etiologies of metabolic syndrome are produced when mice are exposed to corticosterone in their drinking water for 4 weeks with weight gain, increased plasma insulin levels, glucose intolerance and dyslipidemia, validating this methodology for studying the disease.

Human Models of Glucocorticoid Excess

There is a paucity of research in human models with GC excess with respect to AT, especially BAT. Obesity has been used as a substitute for GC excess in many cases where BAT activity and prevalence has been reduced in these patients. Alcala et al. (2019) conducted a comprehensive review of the different mechanisms that are at play when obesity causes impairment in BAT (Alcala et al., 2017). One notable study was conducted on young patients with obesity exposed to ICE which caused an increase in BAT activity (Hanssen et al., 2015). This study notes the many factors including genes, transcription factors, proteins, oxidative and ER stress, adipokines, and micro RNAs that are implicated when BAT becomes obese (Alcala et al., 2017), however, there are still many questions regarding the signaling processes and possible therapeutic potential of targeting each factor in the fight against obesity when high levels of GCs are present (M.J. Lee et al., 2014).

Connecting the β3AR and Stress Studies in Mice

Connections Between Beiging, Stress and Metabolism: Known Interactions in Mice

Most studies to date show that chronic levels of GCs suppress BAT activation in rodents and cause metabolic phenotypes similar to metabolic syndromes like obesity and T2D (Ramage et al., 2016; van den Beukel et al., 2015). The direct effects of excess stress on the beiging process and metabolism have not been well established in the literature. Two studies conducted by van den Beukel et al. (2014) and (2015) are of note in drawing connections between these three processes (van den Beukel et al., 2015, 2014). One study in C57BL/6J mice exposed to cold temperatures for 24 hours indicated that the HPA axis activity was increased in this timeframe as corticosterone concentrations were 2-folds higher than controls, illustrating that the CE itself induced stress to the animal and acute treatment with GCs can lead to increased BAT activity (van den Beukel et al., 2014). The enhanced HPA axis activity in this study was accompanied by an increased expression of both *Ucp1* and *Pgc1α* genes in ingWAT suggests that signaling involved in initiating the beiging process is underway (van den Beukel et al., 2014). The effects of GCs on AT have been loosely observed in beiging studies (Ramage et al., 2016; van den Beukel et al., 2015). However, combining chronic stress with CE as a means to mediate the effects of excess GCs has only been employed by van den Beukel et al. (2015) (van den Beukel et al., 2015). This study illustrated that chronic corticosterone administration in mice caused elevated plasma TAG levels and lipogeneic gene expressions, both of which were immediately normalized following CE (van den Beukel et al., 2015). The beiging of ingWAT induced by CE was reduced by

corticosterone (van den Beukel et al., 2015). This study further illustrates the need for further research into the effects of stress on AT and whole-body metabolism in order to determine novel CE approaches to combat metabolic disorders associated with chronic GC levels. Chronic GC treatment has been found to suppress BAT activity in humans and mice, which contributes to increased WAT growth, hyperglycemia, and reduced insulin tolerance (Luijten et al., 2019a). With this understanding, we need to better investigate if the capacity for BAT/ beige AT activation is lowered by stress, in order to be able to mitigate the metabolic dysfunction that results from excess GCs.

Other interactions with the beiging and stress pathways have been shown in adipocytes in both inflammatory and reactive oxygen species (ROS) signaling. Pro-inflammatory marker TNFα harnesses the ability to suppress the expression of many proteins that are required for insulin-stimulated glucose uptake in adipocytes including the insulin receptor, IRS-1 and GLUT4 (Cawthorn and Sethi, 2008). While ROS have been shown to play crucial roles in BAT metabolism through the p38MAPK pathway and NST gene *Ucp1* expression within brown adipocytes (Ro et al., 2014). Obesity therapies using antioxidants have shown controversial results in both mice and human studies (Brandão et al., 2021; Ro et al., 2014). Ro et al. (2014) were able to showcase the vital role ROS plays in the activation of *Ucp1* which controls the metabolism and function of BAT (Ro et al., 2014). Antioxidants such as catalase, superoxide dismutase, peroxiredoxins and sestrins will scavenge the ROS molecules and prevent them from building up within the cellular environment (Ro et al., 2014). Ro et al. (2014) have shown that overexpression of the sestrin antioxidant actually interfered with *Ucp1* gene expression through the p38MAPK pathway in BAT (Ro et al., 2014). With dysregulated gene expression, the balance

of ROS to mediate the metabolic state of BAT cannot be ignored (Ro et al., 2014). The signaling depicted in Figure 5 illustrates the interactions that may be occurring in BAT when GCs are in excess, inhibiting β3AR signaling*, Ucp1* transcription and lipolysis activities while promoting LD expansion and the GC response. Further research into how these pathways directly interact with each other will allow for the exact mechanism to be uncovered.

The effects of GCs on AT have been loosely observed in beiging studies in conjunction with lipid metabolism (Ramage et al., 2016; van den Beukel et al., 2015). These studies illustrate that GCs in chronic levels will suppress BAT activation in rodents and cause metabolic phenotypes similar to metabolic syndromes like obesity and T2D (Ramage et al., 2016; van den Beukel et al., 2015). However, combining chronic stress with CE as a means to mediate the effects of excess GCs has only been employed by van den Beukel et al. (2015). This study illustrated that corticosterone in mice administered chronically via pellet implantation can elevate plasma TAG levels and lipogenic gene expression, both of which are normalized by CE (van den Beukel et al., 2015). The beiging of ingWAT in this study was reduced by corticosterone but corrected partially by CE (van den Beukel et al., 2015). This study illustrates the need for further research into the effects of stress on AT and whole-body metabolism to determine a more methodical approach to combatting metabolic disorders associated with chronic GC levels.

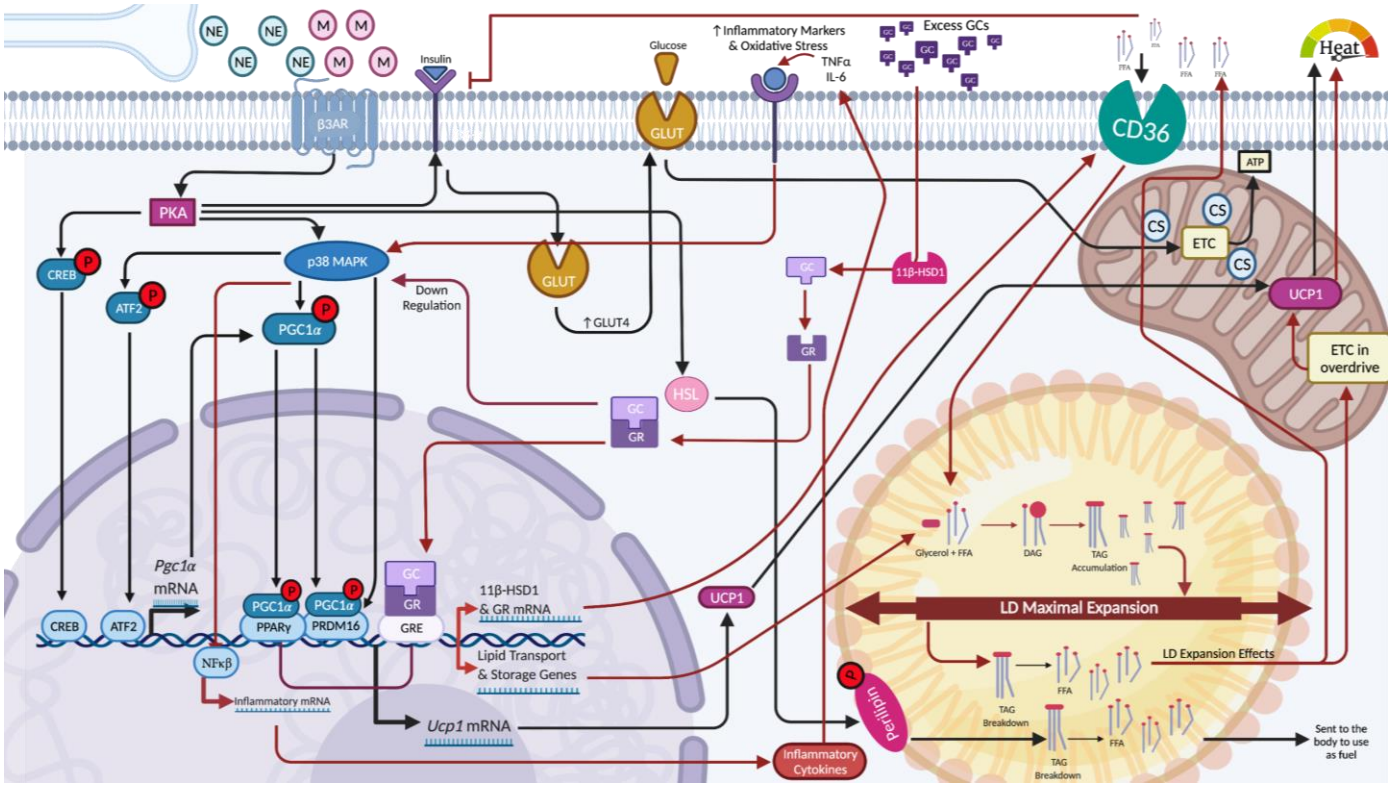

Figure 5: Potential interaction between β3AR and glucocorticoid excess in BAT.

Chronic exposure to GC excess (red arrows) and activation of the β3-adrenergic receptor (β3AR) pathway (black arrows) may result in the potential interactions. Excess glucocorticoids (GC) will become activated by 11β-hydroxysteroid dehydrogenase type 1 (11β-HSD1). Once active, GCs will bind to the Glucocorticoid receptor (GR) where it will travel to the nucleus and bind to the glucocorticoid response element (GRE). Once bound inside the nucleus, the GRE will inhibit mitochondrial biogenesis gene transcription including peroxisome proliferator-activated receptor γ (PPARγ) and PR domain zinc finger 16 (PRDM16) and instead initiate the transcription of inflammatory marker nuclear factor kappa-light-chain-enhancer of activated B cells (NFκβ) and initiate the production of inflammatory cytokines. These inflammatory cytokines, including tumour necrosis factor α (TNFα) and interleukin 6 (IL-6) will increase in concentration and further potentiate the inflammatory response. The GRE will also increase the transcription of 11β-HSD1 mRNA and other lipid transport/storage genes to increase the lipid storage capacity of the lipid droplet (LD). Excess FFAs will use fatty acid transport protein cluster of differentiation 36 (CD36) to enter the cell and travel to the LD. Once in the LD, FFA will combine with glycerol to make diacylglycerol (DAG) and subsequently triacylglycerol (TAG), further increasing the lipids stored in the LD. The expansion of the LD in its inflammatory response to excess GC will increase the amount of circulating free fatty acids (FFA) which may put the electron transport chain (ETC) into overdrive causing an increase in uncoupling protein 1 (UCP1) and production of heat. UCP1 will already be active in the mitochondria (containing citrate synthase (CS)) from β3AR activation, and it can further uncouple the ETC and produce heat. While protein kinase A (PKA) will also activate hormone sensitive lipase (HSL) which will then phosphorylate perilipin

allowing for the breakdown of stored triglycerides (TAG) to occur in the LD. The effect of excess GC on perilipin is unknown, however, the storage capacity of the LD will be increased from the GCs and result in an unknown interaction. The β3AR, activated by either mirabegron (M) or Norepinephrine (NE), will PKA which will then phosphorylate the cAMP response element binding protein (CREB) or activate protein p38 mitogen-activated protein kinase (p38MAPK). Active p38MAPK will subsequently phosphorylate activating transcription Factor 2 (ATF2) or peroxisome proliferator-activator receptor-gamma coactivator-1α (PGC1α). Inflammatory cytokines may inhibit this activation of p38MAPK for mitochondrial biogenesis and instead potentiate the inflammatory cascade. Phosphorylated CREB, ATF2, or PGC1α will enter the nucleus and bind to subsequent transcription factors allowing for the translation of proteins UCP1 and PGC1α. When insulin binds to the insulin receptor, a series of reactions will allow for translocation of glucose transporter 4 (GLUT4) to the cell membrane allowing for increased amounts of glucose to enter the cell in order to be used to make ATP in the mitochondria. However, the excess FFA from the GCs may inhibit this insulin-mediated glucose uptake to occur.

Unknowns, Directions for Future Research, and Implications for Metabolic Health

There is a need to understand how stress can affect more than just lipid metabolism of AT and investigate the activation of BAT. We need to see if the capacity for BAT adaptation is lowered by stress in order to be better positioned to combat metabolic dysfunction and its negative effects of stress. Luijten et al. (2019) note that GCs channel energy from food into lipid storage through a currently unexplained pathway and the unknowns listed in this dissertation further illustrate the adaptions undertaken by BAT and WAT depots and potential methods to mitigate the effects of chronic GCs.

References

Ahmad, B., Serpell, C.J., Fong, I.L., Wong, E.H., 2020. Molecular Mechanisms of Adipogenesis: The Anti-adipogenic Role of AMP-Activated Protein Kinase. Front. Mol. Biosci. 7, 76. https://doi.org/10.3389/fmolb.2020.00076

Akalestou, E., Genser, L., Rutter, G.A., 2020. Glucocorticoid Metabolism in Obesity and Following Weight Loss. Front. Endocrinol. 11, 59. https://doi.org/10.3389/fendo.2020.00059

Alcala, M., Calderon-Dominguez, M., Bustos, E., Ramos, P., Casals, N., Sera, D., Viana, M., Herrero, L., 2017. Increased inflammation, oxidative stress and mitochondrial respiration in brown adipose tissue from obese mice. Scientific Reports 7. https://doi.org/10.1038/s41598-017-16463-6

Armani, A., Cinti, F., Marzolla, V., Morgan, J., Cranston, G.A., Antelmi, A., Carpinelli, G., Canese, R., Pagotto, U., Quarta, C., Malorni, W., Matarrese, P., Marconi, M., Fabbri, A., Rosano, G., Cinti, S., Young, M.J., Caprio, M., 2014. Mineralocorticoid receptor antagonism induces browning of white adipose tissue through impairment of autophagy and prevents adipocyte dysfunction in high-fat-diet-fed mice. FASEB j. 28, 3745–3757. https://doi.org/10.1096/fj.13-245415

Bartlet, A., Heeren, J., 2013. Adipose Tissue Browning and Metabolic Health. Nature Reviews Endocrinology 10, 24–26. https://doi.org/doi:10.1038/nrendo.2013.204

Baskin, A.S., Linderman, J.D., Brychta, R.J., McGehee, S., Anflick-Chames, E., Cero, C., Johnson, J.W., O'Mara, A.E., Fletcher, L.A., Leitner, B.P., Duckworth, C.J., Huang, S., Cai, H., Garraffo, H.M., Millo, C.M., Dieckmann, W., Tolstikov, V., Chen, E.Y., Gao, F., Narain, N.R., Kiebish, M.A., Walter, P.J., Herscovitch, P., Chen, K.Y., Cypess, A.M., 2018. Regulation of Human Adipose Tissue Activation, Gallbladder Size, and Bile Acid Metabolism by a β3-Adrenergic Receptor Agonist. Diabetes 67, 2113–2125. https://doi.org/10.2337/db18-0462

Beaudry, J.L., Kaur, K.D., Varin, E.M., Baggio, L.L., Cao, X., Mulvihill, E.E., Stern, J.H., Campbell, J.E., Scherer, P.E., Drucker, D.J., 2019. The brown adipose tissue glucagon receptor is functional but not essential for control of energy homeostasis in mice. Molecular Metabolism 22, 37–48. https://doi.org/10.1016/j.molmet.2019.01.011

Bel, J.S., Tai, T.C., Khaper, N., Lees, S.J., 2021. Mirabegron: The most promising adipose tissue beiging agent. Physiol Rep 9. https://doi.org/10.14814/phy2.14779

Berry, D.C., Jiang, Y., Arpke, R.W., Close, E.L., Uchida, A., Reading, D., Berglund, E.D., Kyba, M., Graff, J.M., 2017. Cellular Aging Contributes to Failure of Cold-Induced Beige Adipocyte Formation in Old Mice and Humans. Cell Metabolism 25, 166–181. https://doi.org/10.1016/j.cmet.2016.10.023

Berry, D.C., Stenesen, D., Zeve, D., Graff, J.M., 2013. The developmental origins of adipose tissue. Development 140, 3939–3949. https://doi.org/10.1242/dev.080549

Blondin, D.P., Labbé, S.M., Tingelstad, H.C., Noll, C., Kunach, M., Phoenix, S., Guérin, B., Turcotte, É.E., Carpentier, A.C., Richard, D., Haman, F., 2014. Increased Brown Adipose Tissue Oxidative Capacity in Cold-Acclimated Humans. The Journal of Clinical Endocrinology & Metabolism 99, E438–E446. https://doi.org/10.1210/jc.2013-3901

Boström, P., Wu, J., Jedrychowski, M.P., Korde, A., Ye, L., Lo, J.C., Rasbach, K.A., Boström, E.A., Choi, J.H., Long, J.Z., Kajimura, S., Zingaretti, M.C., Vind, B.F., Tu, H., Cinti, S., Højlund, K., Gygi, S.P., Spiegelman, B.M., 2012. A PGC1-α-dependent myokine that drives brown-fat-like development of white fat and thermogenesis. Nature 481, 463–468. https://doi.org/10.1038/nature10777

Brandão, B.B., Poojari, A., Rabiee, A., 2021. Thermogenic Fat: Development, Physiological Function, and Therapeutic Potential. IJMS 22, 5906. https://doi.org/10.3390/ijms22115906

Brasaemle, D.L., 2007. Thematic review series: Adipocyte Biology. The perilipin family of structural lipid droplet proteins: stabilization of lipid droplets and control of lipolysis. Journal of Lipid Research 48, 2547–2559. https://doi.org/10.1194/jlr.R700014-JLR200

Brestoff, J.R., Artis, D., 2015. Immune Regulation of Metabolic Homeostasis in Health and Disease. Cell 161, 146–160. https://doi.org/10.1016/j.cell.2015.02.022

Calmasini, F.B., de Oliveira, M.G., Alexandre, E.C., da Silva, F.H., da Silva, C.P.V., Candido, T.Z., Antunes, E., Mónica, F.Z., 2017. Long-term treatment with the beta-3 adrenoceptor agonist, mirabegron ameliorates detrusor overactivity and restores cyclic adenosine monophosphate (cAMP) levels in obese mice. Neurourology and Urodynamics 36, 1511–1518. https://doi.org/10.1002/nau.23171

Cameron, R.B., Beeson, C.C., Schnellmann, R.G., 2016. Development of Therapeutics That Induce Mitochondrial Biogenesis for the Treatment of Acute and Chronic Degenerative Diseases. J. Med. Chem. 59, 10411–10434. https://doi.org/10.1021/acs.jmedchem.6b00669

Campbell, J.E., Peckett, A.J., D'souza, A.M., Hawke, T.J., Riddell, M.C., 2011. Adipogenic and lipolytic effects of chronic glucocorticoid exposure. American Journal of Physiology-Cell Physiology 300, C198–C209. https://doi.org/10.1152/ajpcell.00045.2010

Cao, W., Daniel, K.W., Robidoux, J., Puigserver, P., Medvedev, A.V., Bai, X., Floering, L.M., Spiegelman, B.M., Collins, S., 2004. p38 Mitogen-Activated Protein Kinase Is the Central Regulator of Cyclic AMP-Dependent Transcription of the Brown Fat Uncoupling Protein 1 Gene. Mol Cell Biol 24, 3057–3067. https://doi.org/10.1128/MCB.24.7.3057-3067.2004

Cassano, A.E., White, J.R., Penraat, K.A., Wilson, C.D., Rasmussen, S., Karatsoreos, I.N., 2012. Anatomic, Hematologic, and Biochemical Features of C57BL/6NCrl Mice Maintained on Chronic Oral Corticosterone. Comparative Medicine by the American Association for Laboratory Animal Science 62, 348–360.

Cawthorn, W.P., Sethi, J.K., 2008. TNF-α and adipocyte biology. FEBS Letters 582, 117–131. https://doi.org/10.1016/j.febslet.2007.11.051

Cedikova, M., Kripnerová, M., Dvorakova, J., Pitule, P., Grundmanova, M., Babuska, V., Mullerova, D., Kuncova, J., 2016. Mitochondria in White, Brown, and Beige Adipocytes. Stem Cells International 2016, 1–11. https://doi.org/10.1155/2016/6067349

Chait, A., den Hartigh, L.J., 2020. Adipose Tissue Distribution, Inflammation and Its Metabolic Consequences, Including Diabetes and Cardiovascular Disease. Front. Cardiovasc. Med. 7, 22. https://doi.org/10.3389/fcvm.2020.00022

Chen, K.Y., Brychta, R.J., Linderman, J.D., Smith, S., Courville, A., Dieckmann, W., Herscovitch, P., Millo, C.M., Remaley, A., Lee, P., Celi, F.S., 2013. Brown Fat Activation Mediates Cold-Induced Thermogenesis in Adult Humans in Response to a Mild Decrease in Ambient Temperature. The Journal of Clinical Endocrinology & Metabolism 98, E1218–E1223. https://doi.org/10.1210/jc.2012-4213

Chen, K.Y., Cypess, A.M., Laughlin, M.R., Haft, C.R., Hu, H.H., Bredella, M.A., Enerbäck, S., Kinahan, P.E., Lichtenbelt, W. van M., Lin, F.I., Sunderland, J.J., Virtanen, K.A., Wahl, R.L., 2016. Brown Adipose Reporting Criteria in Imaging STudies (BARCIST 1.0): Recommendations for Standardized FDG-PET/CT Experiments in Humans. Cell Metabolism 24, 210–222. https://doi.org/10.1016/j.cmet.2016.07.014

Chen, L., Chen, R., Wang, H., Liang, F., 2015. Mechanisms Linking Inflammation to Insulin Resistance. International Journal of Endocrinology 2015, 1–9. https://doi.org/10.1155/2015/508409

Chevalier, C., Stojanović, O., Colin, D.J., Suarez-Zamorano, N., Tarallo, V., Veyrat-Durebex, C., Rigo, D., Fabbiano, S., Stevanović, A., Hagemann, S., Montet, X., Seimbille, Y., Zamboni, N., Hapfelmeier, S., Trajkovski, M., 2015. Gut Microbiota Orchestrates Energy Homeostasis during Cold. Cell 163, 1360–1374. https://doi.org/10.1016/j.cell.2015.11.004

Chondronikola, M., Volpi, E., Børsheim, E., Porter, C., Annamalai, P., Enerbäck, S., Lidell, M.E., Saraf, M.K., Labbe, S.M., Hurren, N.M., Yfanti, C., Chao, T., Andersen, C.R., Cesani, F., Hawkins, H., Sidossis, L.S., 2014. Brown Adipose Tissue Improves Whole-Body Glucose Homeostasis and Insulin Sensitivity in Humans. Diabetes 63, 4089–4099. https://doi.org/10.2337/db14-0746

Cinti, S., 2005. The adipose organ. Prostaglandins, Leukotrienes and Essential Fatty Acids 73, 9–15. https://doi.org/10.1016/j.plefa.2005.04.010

Cline, D.L., Short, L.I., Forster, M.A.M., Gray, S.L., 2019. Adipose Tissue Expression of PACAP, VIP, and Their Receptors in Response to Cold Stress. J Mol Neurosci 68, 427–438. https://doi.org/10.1007/s12031-018-1099-x

Collins, S., 2011. β-adrenoceptor signaling networks in adipocytes for recruiting stored fat and energy expenditure. Front. Endocrin. 2. https://doi.org/10.3389/fendo.2011.00102

Cypess, A.M., Weiner, L.S., Roberts-Toler, C., Elía, E.F., Kessler, S.H., Kahn, P.A., English, J., Chatman, K., Trauger, S.A., Doria, A., Kolodny, G.M., 2015. Activation of Human Brown Adipose Tissue by a β3-Adrenergic Receptor Agonist. Cell Metabolism 21, 33–38. https://doi.org/10.1016/j.cmet.2014.12.009

Cypess, A.M., Williams, G., Goldfine, A.B., Tseng, Y.-H., Kolodny, G.M., 2009. Identification and Importance of Brown Adipose Tissue in Adult Humans. The New England Journal of Medicine 9.

Czech, M.P., 2020. Mechanisms of insulin resistance related to white, beige, and brown adipocytes. Molecular Metabolism 34, 27–42. https://doi.org/10.1016/j.molmet.2019.12.014

Darlington, G.J., Ross, S.E., MacDougald, O.A., 1998. The Role of C/EBP Genes in Adipocyte Differentiation. Journal of Biological Chemistry 273, 30057–30060. https://doi.org/10.1074/jbc.273.46.30057

De Matteis, R., Lucertini, F., Guescini, M., Polidori, E., Zeppa, S., Stocchi, V., Cinti, S., Cuppini, R., 2013. Exercise as a new physiological stimulus for brown adipose tissue activity. Nutrition, Metabolism and Cardiovascular Diseases 23, 582–590. https://doi.org/10.1016/j.numecd.2012.01.013

Defour, M., Dijk, W., Ruppert, P., Nascimento, E.B.M., Schrauwen, P., Kersten, S., 2018. The Peroxisome Proliferator-Activated Receptor α is dispensable for cold-induced adipose tissue browning in mice. Molecular Metabolism 10, 39–54. https://doi.org/10.1016/j.molmet.2018.01.023

Deng, J., Guo, Y., Yuan, F., Chen, S., Yin, H., Jiang, X., Jiao, F., Wang, F., Ji, H., Hu, G., Ying, H., Chen, Y., Zhai, Q., Xiao, F., Guo, F., 2020. Autophagy inhibition prevents glucocorticoid-increased adiposity via suppressing BAT whitening. Autophagy 16, 451–465. https://doi.org/10.1080/15548627.2019.1628537

Di Dalmazi, G., Pagotto, U., Pasquali, R., Vicennati, V., 2012. Glucocorticoids and Type 2 Diabetes: From Physiology to Pathology. Journal of Nutrition and Metabolism 2012, 1–9. https://doi.org/10.1155/2012/525093

Do, T.T.H., 2019. Glucocorticoid-induced insulin resistance is related to macrophage visceral adipose tissue infiltration. Journal of Steroid Biochemistry and Molecular Biology 13.

Doig, C.L., Fletcher, R.S., Morgan, S.A., McCabe, E.L., Larner, D.P., Tomlinson, J.W., Stewart, P.M., Philp, A., Lavery, G.G., 2017. 11β-HSD1 Modulates the Set Point of Brown Adipose Tissue Response to Glucocorticoids in Male Mice. Endocrinology 158, 1964–1976. https://doi.org/10.1210/en.2016-1722

Dominy, J.E., Puigserver, P., 2013. Mitochondrial Biogenesis through Activation of Nuclear Signaling Proteins. Cold Spring Harbor Perspectives in Biology 5, a015008–a015008. https://doi.org/10.1101/cshperspect.a015008

Evans, W.J., Morley, J.E., Argilés, J., Bales, C., Baracos, V., Guttridge, D., Jatoi, A., Kalantar-Zadeh, K., Lochs, H., Mantovani, G., Marks, D., Mitch, W.E., Muscaritoli, M., Najand, A., Ponikowski, P., Rossi Fanelli, F., Schambelan, M., Schols, A., Schuster, M., Thomas, D., Wolfe, R., Anker, S.D., 2008. Cachexia: A new definition. Clinical Nutrition 27, 793–799. https://doi.org/10.1016/j.clnu.2008.06.013

Fernández-Verdejo, R., Marlatt, K.L., Ravussin, E., Galgani, J.E., 2019. Contribution of brown adipose tissue to human energy metabolism. Molecular Aspects of Medicine 68, 82–89. https://doi.org/10.1016/j.mam.2019.07.003

Finlin, B.S., Memetimin, H., Confides, A.L., Kasza, I., Zhu, B., Vekaria, H.J., Harfmann, B., Jones, K.A., Johnson, Z.R., Westgate, P.M., Alexander, C.M., Sullivan, P.G., Dupont-Versteegden, E.E., Kern, P.A., 2018. Human adipose beiging in response to cold and mirabegron. JCI Insight 3, e121510. https://doi.org/10.1172/jci.insight.121510

Flachs, P., Adamcova, K., Zouhar, P., Marques, C., Janovska, P., Viegas, I., Jones, J.G., Bardova, K., Svobodova, M., Hansikova, J., Kuda, O., Rossmeisl, M., Liisberg, U., Borkowska, A.G., Kristiansen, K., Madsen, L., Kopecky, J., 2017. Induction of lipogenesis in white fat during cold exposure in mice: link to lean phenotype. Int J Obes 41, 372–380. https://doi.org/10.1038/ijo.2016.228

Foster, M.T., Softic, S., Caldwell, J., Kohli, R., deKloet, A.D., Seeley, R.J., 2013. Subcutaneous adipose tissue transplantation in diet-induced obese mice attenuates metabolic dysregulation while removal exacerbates it. Physiol Rep 1. https://doi.org/10.1002/phy2.15

Gasparini, S.J., Weber, M.-C., Henneicke, H., Kim, S., Hong, Z., Seibel, M.J., 2016. Continuous corticosterone delivery via the drinking water or pellet implantation: A comparative study in mice. Steroids 116, 76–82.

Ghazarian, M., Luck, H., Revelo, X.S., Winer, S., Winer, D.A., 2015. Immunopathology of adipose tissue during metabolic syndrome. TJPATH. https://doi.org/10.5146/tjpath.2015.01323
Giralt, M., Villarroya, F., 2013. White, Brown, Beige/Brite: Different Adipose Cells for Different Functions? Endocrinology 154, 2992–3000. https://doi.org/10.1210/en.2013-1403
Gong, J., Sun, Z., Li, P., 2009. CIDE proteins and metabolic disorders. Current Opinion in Lipidology 20, 121–126. https://doi.org/10.1097/MOL.0b013e328328d0bb
Greenberg, A.S., Coleman, R.A., Kraemer, F.B., McManaman, J.L., Obin, M.S., Puri, V., Yan, Q.-W., Miyoshi, H., Mashek, D.G., 2011. The role of lipid droplets in metabolic disease in rodents and humans. J. Clin. Invest. 121, 2102–2110. https://doi.org/10.1172/JCI46069
Guilherme, A., Henriques, F., Bedard, A.H., Czech, M.P., 2019. Molecular pathways linking adipose innervation to insulin action in obesity and diabetes mellitus. Nat Rev Endocrinol 15, 207–225. https://doi.org/10.1038/s41574-019-0165-y
Hanssen, M.J.W., Hoeks, J., Brans, B., van der Lans, A.A.J.J., Schaart, G., van den Driessche, J.J., Jörgensen, J.A., Boekschoten, M.V., Hesselink, M.K.C., Havekes, B., Kersten, S., Mottaghy, F.M., van Marken Lichtenbelt, W.D., Schrauwen, P., 2015. Short-term cold acclimation improves insulin sensitivity in patients with type 2 diabetes mellitus. Nat Med 21, 863–865. https://doi.org/10.1038/nm.3891
Hao, L., Scott, S., Abbasi, M., Zu, Y., Khan, M.S.H., Yang, Y., Wu, D., Zhao, L., Wang, S., 2019. Beneficial Metabolic Effects of Mirabegron In Vitro and in High-Fat Diet-Induced Obese Mice. J Pharmacol Exp Ther 369, 419–427. https://doi.org/10.1124/jpet.118.255778
Harvey, I., Stephenson, E.J., Redd, J.R., Tran, Q.T., Hochberg, I., Qi, N., Bridges, D., 2018. Glucocorticoid-Induced Metabolic Disturbances Are Exacerbated in Obese Male Mice. Endocrinology 159, 2275–2287. https://doi.org/10.1210/en.2018-00147
Heeren, J., Scheja, L., 2018. Brown adipose tissue and lipid metabolism: Current Opinion in Lipidology 29, 180–185. https://doi.org/10.1097/MOL.0000000000000504
Hotamisligil, G.S., 2006. Inflammation and metabolic disorders. Nature 444, 860–867. https://doi.org/10.1038/nature05485
Huang, Z., Zhong, L., Lee, J.T.H., Zhang, J., Wu, D., Geng, L., Wang, Y., Wong, C.-M., Xu, A., 2017. The FGF21-CCL11 Axis Mediates Beiging of White Adipose Tissues by Coupling Sympathetic Nervous System to Type 2 Immunity. Cell Metabolism 26, 493-508.e4. https://doi.org/10.1016/j.cmet.2017.08.003
Hui, X., Gu, P., Zhang, J., Nie, T., Pan, Y., Wu, D., Feng, T., Zhong, C., Wang, Y., Lam, K.S.L., Xu, A., 2015. Adiponectin Enhances Cold-Induced Browning of Subcutaneous Adipose Tissue via Promoting M2 Macrophage Proliferation. Cell Metabolism 22, 279–290. https://doi.org/10.1016/j.cmet.2015.06.004
Imai, J., Katagiri, H., Yamada, T., Ishigaki, Y., Ogihara, T., Uno, K., Hasegawa, Y., Gao, J., Ishihara, H., Sasano, H., Oka, Y., 2006. Cold Exposure Suppresses Serum Adiponectin Levels through Sympathetic Nerve Activation in Mice*. Obesity 14, 1132–1141. https://doi.org/10.1038/oby.2006.130
Jamaluddin, M.S., Weakley, S.M., Yao, Q., Chen, C., 2012. Resistin: functional roles and therapeutic considerations for cardiovascular disease: Resistin and cardiovascular disease. British Journal of Pharmacology 165, 622–632. https://doi.org/10.1111/j.1476-5381.2011.01369.x
Jarc, E., Petan, T., 2020. A twist of FATe: Lipid droplets and inflammatory lipid mediators. Biochimie 169, 69–87. https://doi.org/10.1016/j.biochi.2019.11.016

Jeanson, Y., Carrière, A., Casteilla, L., 2015. A New Role for Browning as a Redox and Stress Adaptive Mechanism? Front. Endocrinol. 6. https://doi.org/10.3389/fendo.2015.00158
Jia, G., Aroor, A.R., Sowers, J.R., 2017. The role of mineralocorticoid receptor signaling in the cross-talk between adipose tissue and the vascular wall. Cardiovascular Research 113, 1055–1063. https://doi.org/10.1093/cvr/cvx097
Jornayvaz, F.R., Shulman, G.I., 2010. Regulation of mitochondrial biogenesis. Essays in Biochemistry 47, 69–84. https://doi.org/10.1042/bse0470069
Kahn, C. R, Wang, G., Lee, K.Y., 2019. Altered adipose tissue and adipocyte function in the pathogenesis of metabolic syndrome. Journal of Clinical Investigation 129, 3990–4000. https://doi.org/10.1172/JCI129187
Kahn, C Ronald, Wang, G., Lee, K.Y., 2019. Altered adipose tissue and adipocyte function in the pathogenesis of metabolic syndrome. The Journal of Clinical Investigation 129, 12.
Karatsoreos, I.N., Bhagat, S.M., Bowles, N.P., Weil, Z.M., Pfaff, D.W., McEwen, B.S., 2010. Endocrine and Physiological Changes in Response to Chronic Corticosterone: A Potential Model of the Metabolic Syndrome in Mouse. Endocrinology 151, 2117–2127. https://doi.org/10.1210/en.2009-1436
Kataru, R.P., Park, H.J., Baik, J.E., Li, C., Shin, J., Mehrara, B.J., 2020. Regulation of Lymphatic Function in Obesity. Front. Physiol. 11, 459. https://doi.org/10.3389/fphys.2020.00459
Kershaw, E.E., Flier, J.S., 2004. Adipose Tissue as an Endocrine Organ. The Journal of Clinical Endocrinology & Metabolism 89, 2548–2556. https://doi.org/10.1210/jc.2004-0395
Kiefer, F.W., 2016. Browning and thermogenic programing of adipose tissue. Best Practice & Research Clinical Endocrinology & Metabolism 30, 479–485. https://doi.org/10.1016/j.beem.2016.09.003
Kinlein, S.A., Shahanoor, Z., Romeo, R.D., Karatsoreos, I.N., 2017. Chronic Corticosterone Treatment During Adolescence Has Significant Effects on Metabolism and Skeletal Development in Male C57BL6/N Mice. Endocrinology 158, 2239–2254.
Konige, M., Wang, H., Sztalryd, C., 2014. Role of adipose specific lipid droplet proteins in maintaining whole body energy homeostasis. Biochimica et Biophysica Acta (BBA) - Molecular Basis of Disease 1842, 393–401. https://doi.org/10.1016/j.bbadis.2013.05.007
Kotzbeck, P., Giordano, A., Mondini, E., Murano, I., Severi, I., Venema, W., Cecchini, M.P., Kershaw, E.E., Barbatelli, G., Haemmerle, G., Zechner, R., Cinti, S., 2018. Brown adipose tissue whitening leads to brown adipocyte death and adipose tissue inflammation. Journal of Lipid Research 59, 784–794. https://doi.org/10.1194/jlr.M079665
Kudielka, B.M., Kirschbaum, C., 2005. Sex differences in HPA axis responses to stress: a review. Biological Psychology 69, 113–132. https://doi.org/10.1016/j.biopsycho.2004.11.009
Lee, M.J., Pramyothin, P., Karastergiou, K., Fried, S.K., 2014. Deconstructing the roles of glucocorticoids in adipose tissue biology and the development of central obesity. Biochimica et Biophysica Acta (BBA) - Molecular Basis of Disease 1842, 473–481. https://doi.org/10.1016/j.bbadis.2013.05.029
Lee, M.J., Wu, Y., Fried, S.K., 2012. A Modified Protocol to Maximize Differentiation of Human Preadipocytes and Improve Metabolic Phenotypes. Obesity 20, 2334–2340. https://doi.org/10.1038/oby.2012.116
Lee, R.A., Harris, C.A., Wang, J.-C., 2018. Glucocorticoid Receptor and Adipocyte Biology 21.

Lee, Y.H., Jung, Y.-S., Choi, D., 2014a. Recent advance in brown adipose physiology and its therapeutic potential. Exp Mol Med 46, e78–e78. https://doi.org/10.1038/emm.2013.163
Lee, Y.H., Mottillo, E.P., Granneman, J.G., 2014b. Adipose tissue plasticity from WAT to BAT and in between. Biochimica et Biophysica Acta (BBA) - Molecular Basis of Disease 1842, 358–369. https://doi.org/10.1016/j.bbadis.2013.05.011
Legeza, B., Marcolongo, P., Gamberucci, A., Varga, V., Bánhegyi, G., Benedetti, A., Odermatt, A., 2017. Fructose, Glucocorticoids and Adipose Tissue: Implications for the Metabolic Syndrome. Nutrients 9, 426. https://doi.org/10.3390/nu9050426
Leiria, L.O., Tseng, Y.-H., 2020. Lipidomics of brown and white adipose tissue: Implications for energy metabolism. Biochimica et Biophysica Acta (BBA) - Molecular and Cell Biology of Lipids 1865, 158788. https://doi.org/10.1016/j.bbalip.2020.158788
Leitner, B.P., Huang, S., Brychta, R.J., Duckworth, C.J., Baskin, A.S., McGehee, S., Tal, I., Dieckmann, W., Gupta, G., Kolodny, G.M., Pacak, K., Herscovitch, P., Cypess, A.M., Chen, K.Y., 2017. Mapping of human brown adipose tissue in lean and obese young men. Proc Natl Acad Sci USA 114, 8649–8654. https://doi.org/10.1073/pnas.1705287114
Liu, J., Kong, X., Wang, L., Qi, H., Di, W., Zhang, X., Wu, L., Chen, X., Yu, J., Zha, J., Lv, S., Zhang, A., Cheng, P., Hu, M., Li, Yujie, Bi, J., Li, Yan, Hu, F., Zhong, Y., Xu, Y., Ding, G., 2013. Essential roles of 11β-HSD1 in regulating brown adipocyte function. Journal of Molecular Endocrinology 50, 103–113. https://doi.org/10.1530/JME-12-0099
Liu, X., Wang, S., You, Y., Meng, M., Zheng, Z., Dong, M., Lin, J., Zhao, Q., Zhang, C., Yuan, X., Hu, T., Liu, L., Huang, Y., Zhang, L., Wang, D., Zhan, J., Jong Lee, H., Speakman, J.R., Jin, W., 2015. Brown Adipose Tissue Transplantation Reverses Obesity in Ob/Ob Mice. Endocrinology 156, 2461–2469. https://doi.org/10.1210/en.2014-1598
Lowe, C.E., O'Rahilly, S., Rochford, J.J., 2011. Adipogenesis at a glance. Journal of Cell Science 124, 2681–2686. https://doi.org/10.1242/jcs.079699
Lowell, B.B., Spiegelman, B.M., 2000. Towards a molecular understanding of adaptive thermogenesis. Nature 404, 652–660. https://doi.org/10.1038/35007527
Lu, X., Solmonson, A., Lodi, A., Nowinski, S.M., Sentandreu, E., Riley, C.L., Mills, E.M., Tiziani, S., 2017. The early metabolomic response of adipose tissue during acute cold exposure in mice. Scientific Reports 7, 3455. https://doi.org/10.1038/s41598-017-03108-x
Luijten, I.H.N., Brooks, K., Boulet, N., Shabalina, I.G., Jaiprakash, A., Carlsson, B., Fischer, A.W., Cannon, B., Nedergaard, J., 2019a. Glucocorticoid-Induced Obesity Develops Independently of UCP1. Cell Reports 27, 1686-1698.e5. https://doi.org/10.1016/j.celrep.2019.04.041
Luijten, I.H.N., Cannon, B., Nedergaard, J., 2019b. Glucocorticoids and Brown Adipose Tissue: Do glucocorticoids really inhibit thermogenesis? Molecular Aspects of Medicine 68, 42–59. https://doi.org/10.1016/j.mam.2019.07.002
Luo, L., Liu, M., 2016. Adipose tissue in control of metabolism. Journal of Endocrinology 231, R77–R99. https://doi.org/10.1530/JOE-16-0211
Macfarlane, D.P., Forbes, S., Walker, B.R., 2008. Glucocorticoids and fatty acid metabolism in humans: fuelling fat redistribution in the metabolic syndrome. Journal of Endocrinology 197, 189–204. https://doi.org/10.1677/JOE-08-0054
Marlatt, K.L., Ravussin, E., 2017. Brown Adipose Tissue: an Update on Recent Findings. Curr Obes Rep 6, 389–396. https://doi.org/10.1007/s13679-017-0283-6

Mauer, J., Chaurasia, B., Goldau, J., Vogt, M.C., Ruud, J., Nguyen, K.D., Theurich, S., Hausen, A.C., Schmitz, J., Brönneke, H.S., Estevez, E., Allen, T.L., Mesaros, A., Partridge, L., Febbraio, M.A., Chawla, A., Wunderlich, F.T., Brüning, J.C., 2014. Signaling by IL-6 promotes alternative activation of macrophages to limit endotoxemia and obesity-associated resistance to insulin. Nat Immunol 15, 423–430. https://doi.org/10.1038/ni.2865

Maximus, P.S., Al Achkar, Z., Hamid, P.F., Hasnain, S.S., Peralta, C.A., 2020. Adipocytokines: Are they the Theory of Everything? Cytokine 133, 155144. https://doi.org/10.1016/j.cyto.2020.155144

McEwen, B.S., 2007. Physiology and Neurobiology of Stress and Adaptation: Central Role of the Brain. Physiological Reviews 87, 873–904. https://doi.org/10.1152/physrev.00041.2006

McKay, L., Cidlowski, J., 2003. Physiologic and Pharmacologic Effects of Corticosteroids, 6th edition. ed, Holland-Frei Cancer Medicine. BC Decker, Hamilton, ON.

Mraz, M., Haluzik, M., 2014. The role of adipose tissue immune cells in obesity and low-grade inflammation. Journal of Endocrinology 222, R113–R127. https://doi.org/10.1530/JOE-14-0283

Münzberg, H., Floyd, E., Chang, J.S., 2021. Sympathetic Innervation of White Adipose Tissue: to Beige or Not to Beige? Physiology 36, 246–255. https://doi.org/10.1152/physiol.00038.2020

Nettebrock, N.T., Bohnert, M., 2020. Born this way – Biogenesis of lipid droplets from specialized ER subdomains. Biochimica et Biophysica Acta (BBA) - Molecular and Cell Biology of Lipids 1865, 158448. https://doi.org/10.1016/j.bbalip.2019.04.008

Nguyen, K.D., Qiu, Y., Cui, X., Goh, Y.P.S., Mwangi, J., David, T., Mukundan, L., Brombacher, F., Locksley, R.M., Chawla, A., 2011. Alternatively activated macrophages produce catecholamines to sustain adaptive thermogenesis. Nature 480, 104–108. https://doi.org/10.1038/nature10653

Nishimoto, Y., Tamori, Y., 2017. CIDE Family-Mediated Unique Lipid Droplet Morphology in White Adipose Tissue and Brown Adipose Tissue Determines the Adipocyte Energy Metabolism. J Atheroscler Thromb 24, 989–998. https://doi.org/10.5551/jat.RV17011

Oakley, R.H., Cidlowski, J.A., 2013. The biology of the glucocorticoid receptor: New signaling mechanisms in health and disease. Journal of Allergy and Clinical Immunology 132, 1033–1044. https://doi.org/10.1016/j.jaci.2013.09.007

Okamatsu-Ogura, Y., Fukano, K., Tsubota, A., Uozumi, A., Terao, A., Kimura, K., Saito, M., 2013. Thermogenic Ability of Uncoupling Protein 1 in Beige Adipocytes in Mice. PLoS ONE 8, e84229. https://doi.org/10.1371/journal.pone.0084229

Okla, M., Wang, W., Kang, I., Pashaj, A., Carr, T., Chung, S., 2015. Activation of Toll-like Receptor 4 (TLR4) Attenuates Adaptive Thermogenesis via Endoplasmic Reticulum Stress. Journal of Biological Chemistry 290, 26476–26490. https://doi.org/10.1074/jbc.M115.677724

O'Mara, A.E., Johnson, J.W., Linderman, J.D., Brychta, R.J., McGehee, S., Fletcher, L.A., Fink, Y.A., Kapuria, D., Cassimatis, T.M., Kelsey, N., Cero, C., Sater, Z.A., Piccinini, F., Baskin, A.S., Leitner, B.P., Cai, H., Millo, C.M., Dieckmann, W., Walter, M., Javitt, N.B., Rotman, Y., Walter, P.J., Ader, M., Bergman, R.N., Herscovitch, P., Chen, K.Y., Cypess, A.M., 2020. Chronic mirabegron treatment increases human brown fat, HDL cholesterol, and insulin sensitivity. Journal of Clinical Investigation 130, 2209–2219. https://doi.org/10.1172/JCI131126

Park, A.J., Battaglino, R.A., Nguyen, N.M.H., Morse, L.R., 2018. Associations between lean mass and leptin in men with chronic spinal cord injury: Results from the FRASCI-muscle study. PLoS ONE 13, e0198969. https://doi.org/10.1371/journal.pone.0198969

Peckett, A.J., Wright, D.C., Riddell, M.C., 2011. The effects of glucocorticoids on adipose tissue lipid metabolism. Metabolism 60, 1500–1510. https://doi.org/10.1016/j.metabol.2011.06.012

Peng, X.-R., Gennemark, P., O'Mahony, G., Bartesaghi, S., 2015. Unlock the Thermogenic Potential of Adipose Tissue: Pharmacological Modulation and Implications for Treatment of Diabetes and Obesity. Front. Endocrinol. 6. https://doi.org/10.3389/fendo.2015.00174

Peres Valgas da Silva, C., Hernández-Saavedra, D., White, J., Stanford, K., 2019. Cold and Exercise: Therapeutic Tools to Activate Brown Adipose Tissue and Combat Obesity. Biology 8, 9. https://doi.org/10.3390/biology8010009

Poggioli, R., Ueta, C.B., e Drigo, R.A., Castillo, M., Fonseca, T.L., Bianco, A.C., 2013. Dexamethasone reduces energy expenditure and increases susceptibility to diet-induced obesity in mice. Obesity n/a-n/a. https://doi.org/10.1002/oby.20338

Porter, C., Hardee, J.P., Herndon, D.N., Suman, O.E., 2015. The Role of Exercise in the Rehabilitation of Patients with Severe Burns. Exercise and Sport Sciences Reviews 43, 34–40. https://doi.org/10.1249/JES.0000000000000029

Presby, D.M., Jackman, M.R., Rudolph, M.C., Sherk, V.D., Foright, R.M., Houck, J.A., Johnson, G.C., Orlicky, D.J., Melanson, E.L., Higgins, J.A., MacLean, P.S., 2019. Compensation for cold-induced thermogenesis during weight loss maintenance and regain. American Journal of Physiology-Endocrinology and Metabolism 316, E977–E986. https://doi.org/10.1152/ajpendo.00543.2018

Qiu, Y., Nguyen, K.D., Odegaard, J.I., Cui, X., Tian, X., Locksley, R.M., Palmiter, R.D., Chawla, A., 2014. Eosinophils and Type 2 Cytokine Signaling in Macrophages Orchestrate Development of Functional Beige Fat. Cell 157, 1292–1308. https://doi.org/10.1016/j.cell.2014.03.066

Ramage, L.E., Akyol, M., Fletcher, A.M., Forsythe, J., Nixon, M., Carter, R.N., van Beek, E.J.R., Morton, N.M., Walker, B.R., Stimson, R.H., 2016. Glucocorticoids Acutely Increase Brown Adipose Tissue Activity in Humans, Revealing Species-Specific Differences in UCP-1 Regulation. Cell Metabolism 24, 130–141. https://doi.org/10.1016/j.cmet.2016.06.011

Ramos, S.V., Turnbull, P.C., MacPherson, R.E.K., 2016. Adipose tissue depot specific differences of PLIN protein content in endurance trained rats. Adipocyte 5, 212–223. https://doi.org/10.1080/21623945.2016.1157672

Ravussin, Y., Xiao, C., Gavrilova, O., Reitman, M.L., 2014. Effect of Intermittent Cold Exposure on Brown Fat Activation, Obesity, and Energy Homeostasis in Mice. PLoS ONE 9, e85876. https://doi.org/10.1371/journal.pone.0085876

Reddy, N.L., Tan, B.K., Barber, T.M., Randeva, H.S., 2014. Brown adipose tissue: endocrine determinants of function and therapeutic manipulation as a novel treatment strategy for obesity. BMC Obes 1, 13. https://doi.org/10.1186/s40608-014-0013-5

Ro, S.-H., Nam, M., Jang, I., Park, H.-W., Park, H., Semple, I.A., Kim, M., Kim, J.S., Park, H., Einat, P., Damari, G., Golikov, M., Feinstein, E., Lee, J.H., 2014. Sestrin2 inhibits uncoupling protein 1 expression through suppressing reactive oxygen species. Proceedings of the National Academy of Sciences 111, 7849–7854. https://doi.org/10.1073/pnas.1401787111

Roberts-Toler, C., O'Neill, B.T., Cypess, A.M., 2015. Diet-induced obesity causes insulin resistance in mouse brown adipose tissue: DIO Causes BAT Insulin Resistance. Obesity 23, 1765–1770. https://doi.org/10.1002/oby.21134

Rogero, M., Calder, P., 2018. Obesity, Inflammation, Toll-Like Receptor 4 and Fatty Acids. Nutrients 10, 432. https://doi.org/10.3390/nu10040432

Rosen, E.D., Hsu, C.-H., Wang, X., Sakai, S., Freeman, M.W., Gonzalez, F.J., Spiegelman, B.M., 2002. C/EBP␣ induces adipogenesis through PPAR␥: a unified pathway 6.

Rutkowski, J.M., Stern, J.H., Scherer, P.E., 2015. The cell biology of fat expansion. Journal of Cell Biology 208, 501–512. https://doi.org/10.1083/jcb.201409063

Saito, M., Okamatsu-Ogura, Y., Matsushita, M., Watanabe, K., Yoneshiro, T., Nio-Kobayashi, J., Iwanaga, T., Miyagawa, M., Kameya, T., Nakada, K., Kawai, Y., Tsujisaki, M., 2009. High Incidence of Metabolically Active Brown Adipose Tissue in Healthy Adult Humans: Effects of Cold Exposure and Adiposity. Diabetes 58, 1526–1531. https://doi.org/10.2337/db09-0530

Salum, K.C.R., Rolando, J. de M., Zembrzuski, V.M., Carneiro, J.R.I., Mello, C.B., Maya-Monteiro, C.M., Bozza, P.T., Kohlrausch, F.B., da Fonseca, A.C.P., 2021. When Leptin Is Not There: A Review of What Nonsyndromic Monogenic Obesity Cases Tell Us and the Benefits of Exogenous Leptin. Front. Endocrinol. 12, 722441. https://doi.org/10.3389/fendo.2021.722441

Sanchez-Gurmaches, J., Hung, C.-M., Guertin, D.A., 2016. Emerging Complexities in Adipocyte Origins and Identity. Trends in Cell Biology 26, 313–326. https://doi.org/10.1016/j.tcb.2016.01.004

Saraf, M.K., Herndon, D.N., Porter, C., Toliver-Kinsky, T., Radhakrishnan, R., Chao, T., Chondronikola, M., Sidossis, L.S., 2016. Morphological Changes in Subcutaneous White Adipose Tissue After Severe Burn Injury: Journal of Burn Care & Research 37, e96–e103. https://doi.org/10.1097/BCR.0000000000000292

Sarvas, J.L., Otis, J.S., Khaper, N., Lees, S.J., 2015. Voluntary physical activity prevents insulin resistance in a tissue specific manner. Physiol Rep 3, e12277. https://doi.org/10.14814/phy2.12277

Schena, G., Caplan, M.J., 2019. Everything You Always Wanted to Know about β3-AR * (* But Were Afraid to Ask). Cells 8, 357. https://doi.org/10.3390/cells8040357

Schulz, T.J., Tseng, Y.-H., 2013. Brown adipose tissue: development, metabolism and beyond. Biochemical Journal 453, 167–178. https://doi.org/10.1042/BJ20130457

Sefton, C., Davies, A., Allen, T.-J., Wray, J.R., Shoop, R., Adamson, A., Humphreys, N., Coll, A.P., White, A., Harno, E., 2019. Metabolic Abnormalities of Chronic High-Dose Glucocorticoids Are Not Mediated by Hypothalamic AgRP in Male Mice. Endocrinology 160, 964–978. https://doi.org/10.1210/en.2019-00018

Shan, T., Liang, X., Bi, P., Zhang, P., Liu, W., Kuang, S., 2013. Distinct populations of adipogenic and myogenic Myf5-lineage progenitors in white adipose tissues. Journal of Lipid Research 54, 2214–2224. https://doi.org/10.1194/jlr.M038711

Shao, M., Wang, Q.A., Song, A., Vishvanath, L., Busbuso, N.C., Scherer, P.E., Gupta, R.K., 2019. Cellular Origins of Beige Fat Cells Revisited. Diabetes 68, 1874–1885. https://doi.org/10.2337/db19-0308

Shen, Y., Roh, H.C., Kumari, M., Rosen, E.D., 2017. Adipocyte glucocorticoid receptor is important in lipolysis and insulin resistance due to exogenous steroids, but not insulin resistance caused by high fat feeding. Molecular Metabolism 6, 1150–1160. https://doi.org/10.1016/j.molmet.2017.06.013

Shimizu, I., Walsh, K., 2015. The Whitening of Brown Fat and Its Implications for Weight Management in Obesity. Curr Obes Rep 4, 224–229. https://doi.org/10.1007/s13679-015-0157-8

Sidossis, L.S., Porter, C., Saraf, M.K., Børsheim, E., Radhakrishnan, R.S., Chao, T., Ali, A., Chondronikola, M., Mlcak, R., Finnerty, C.C., Hawkins, H.K., Toliver-Kinsky, T., Herndon, D.N., 2015. Browning of Subcutaneous White Adipose Tissue in Humans after Severe Adrenergic Stress. Cell Metabolism 22, 219–227. https://doi.org/10.1016/j.cmet.2015.06.022

Simonds, S.E., Cowley, M.A., Enriori, P.J., 2012. Leptin increasing sympathetic nerve outflow in obesity: A cure for obesity or a potential contributor to metabolic syndrome? Adipocyte 1, 177–181. https://doi.org/10.4161/adip.20690

Smith, R.E., Horwitz, B.A., 1969. Brown fat and thermogenesis. 49, 96.

Song, N.-J., Chang, S.-H., Li, D.Y., Villanueva, C.J., Park, K.W., 2017. Induction of thermogenic adipocytes: molecular targets and thermogenic small molecules. Exp Mol Med 49, e353–e353. https://doi.org/10.1038/emm.2017.70

Stanford, K.I., Goodyear, L.J., 2013. The therapeutic potential of brown adipose tissue. Hepatobiliary surgery and nutrition 2, 286–288.

Stanford, K.I., Middelbeek, R.J.W., Townsend, K.L., An, D., Nygaard, E.B., Hitchcox, K.M., Markan, K.R., Nakano, K., Hirshman, M.F., Tseng, Y.-H., Goodyear, L.J., 2013. Brown adipose tissue regulates glucose homeostasis and insulin sensitivity. J. Clin. Invest. 123, 215–223. https://doi.org/10.1172/JCI62308

Sui, W., Li, H., Yang, Y., Jing, X., Xue, F., Cheng, J., Dong, M., Zhang, M., Pan, H., Chen, Y., Zhang, Yunjian, Zhou, Q., Shi, W., Wang, X., Zhang, H., Zhang, C., Zhang, Yun, Cao, Y., 2019. Bladder drug mirabegron exacerbates atherosclerosis through activation of brown fat-mediated lipolysis. Proc Natl Acad Sci USA 116, 10937–10942. https://doi.org/10.1073/pnas.1901655116

Tamashiro, K.L., Sakai, R.R., Shively, C.A., Karatsoreos, I.N., Reagan, L.P., 2011. Chronic stress, metabolism, and metabolic syndrome. Stress 14, 468–474. https://doi.org/10.3109/10253890.2011.606341

Tansey, J., Sztalryd, C., Hlavin, E., Kimmel, A., Londos, C., 2004. The Central Role of Perilipin A in Lipid Metabolism and Adipocyte Lipolysis. IUBMB Life (International Union of Biochemistry and Molecular Biology: Life) 56, 379–385. https://doi.org/10.1080/15216540400009968

Taves, M.D., Gomez-Sanchez, C.E., Soma, K.K., 2011. Extra-adrenal glucocorticoids and mineralocorticoids: evidence for local synthesis, regulation, and function. American Journal of Physiology-Endocrinology and Metabolism 301, E11–E24. https://doi.org/10.1152/ajpendo.00100.2011

Trayhurn, P., 2017. Origins and early development of the concept that brown adipose tissue thermogenesis is linked to energy balance and obesity. Biochimie 134, 62–70. https://doi.org/10.1016/j.biochi.2016.09.007

van den Beukel, J.C., Boon, M.R., Steenbergen, J., Rensen, P.C.N., Meijer, O.C., Themmen, A.P.N., Grefhorst, A., 2015. Cold Exposure Partially Corrects Disturbances in Lipid Metabolism in a Male Mouse Model of Glucocorticoid Excess. Endocrinology 156, 4115–4128. https://doi.org/10.1210/en.2015-1092

van den Beukel, J.C., Grefhorst, A., Quarta, C., Steenbergen, J., Mastroberardino, P.G., Lombès, M., Delhanty, P.J., Mazza, R., Pagotto, U., Lely, A.J., Themmen, A.P.N., 2014. Direct activating effects of adrenocorticotropic hormone (ACTH) on brown adipose tissue are attenuated by corticosterone. FASEB j. 28, 4857–4867. https://doi.org/10.1096/fj.14-254839

van Donkelaar, E.L., Vaessen, K.R.D., Pawluski, J.L., Sierksma, A.S., Blokland, A., Cañete, R., Steinbusch, H.W.M., 2014. Long-Term Corticosterone Exposure Decreases Insulin Sensitivity and Induces Depressive-Like Behaviour in the C57BL/6NCrl Mouse. PLoS ONE 9, e106960. https://doi.org/10.1371/journal.pone.0106960

Veyrat-Durebex, C., Deblon, N., Caillon, A., Andrew, R., Altirriba, J., Odermatt, A., Rohner-Jeanrenaud, F., 2012. Central Glucocorticoid Administration Promotes Weight Gain and Increased 11β-Hydroxysteroid Dehydrogenase Type 1 Expression in White Adipose Tissue. PLoS ONE 7, e34002. https://doi.org/10.1371/journal.pone.0034002

Vienberg, S.G., Björnholm, M., 2014. Chronic glucocorticoid treatment increases *de novo* lipogenesis in visceral adipose tissue. Acta Physiol 211, 257–259. https://doi.org/10.1111/apha.12283

Villarroya, F., Cereijo, R., Gavaldà-Navarro, A., Villarroya, J., Giralt, M., 2018. Inflammation of brown/beige adipose tissues in obesity and metabolic disease. J Intern Med 284, 492–504. https://doi.org/10.1111/joim.12803

Virtanen, K.A., Lidell, M.E., Orava, J., Heglind, M., Westergren, R., Niemi, T., Taittonen, M., Laine, J., Savisto, N.-J., Enerbäck, S., Nuutila, P., 2009. Functional Brown Adipose Tissue in Healthy Adults. N Engl J Med 360, 1518–1525. https://doi.org/10.1056/NEJMoa0808949

Virtue, S., Vidal-Puig, A., 2013. Assessment of brown adipose tissue function. Front. Physiol. 4. https://doi.org/10.3389/fphys.2013.00128

Wang, L., Pydi, S.P., Cui, Y., Zhu, L., Meister, J., Gavrilova, O., Berdeaux, R., Fortin, J.-P., Bence, K.K., Vernochet, C., Wess, J., 2019. Selective activation of Gs signaling in adipocytes causes striking metabolic improvements in mice. Molecular Metabolism 27, 83–91. https://doi.org/10.1016/j.molmet.2019.06.018

Wang, T.-Y., Liu, C., Wang, A., Sun, Q., 2015. Intermittent cold exposure improves glucose homeostasis associated with brown and white adipose tissues in mice. Life Sciences 139, 153–159. https://doi.org/10.1016/j.lfs.2015.07.030

Warner, A., Mittag, J., 2016. Breaking BAT: can browning create a better white? Journal of Endocrinology 228, R19–R29. https://doi.org/10.1530/JOE-15-0408

Weidlich, D., Honecker, J., Gmach, O., Wu, M., Burgkart, R., Ruschke, S., Franz, D., Menze, B.H., Skurk, T., Hauner, H., Kulozik, U., Karampinos, D.C., 2019. Measuring large lipid droplet sizes by probing restricted lipid diffusion effects with diffusion-weighted MRS at 3T. Magn Reson Med 81, 3427–3439. https://doi.org/10.1002/mrm.27651

Welte, M.A., 2009. Fat on the move: intracellular motion of lipid droplets. Biochemical Society Transactions 37, 991–996. https://doi.org/10.1042/BST0370991

Woo, C.-Y., Jang, J.E., Lee, S.E., Koh, E.H., Lee, K.-U., 2019. Mitochondrial Dysfunction in Adipocytes as a Primary Cause of Adipose Tissue Inflammation. Diabetes Metab J 43, 247. https://doi.org/10.4093/dmj.2018.0221

World Health Organization, 2022. Obesity and overweight.

Wray, J.R., Davies, A., Sefton, C., Allen, T.-J., Adamson, A., Chapman, P., Lam, B.Y.H., Yeo, G.S.H., Coll, A.P., Harno, E., White, A., 2019. Global transcriptomic analysis of the arcuate nucleus following chronic glucocorticoid treatment. Molecular Metabolism 26, 5–17. https://doi.org/10.1016/j.molmet.2019.05.008

Wu, J., Boström, P., Sparks, L.M., Ye, L., Choi, J.H., Giang, A.-H., Khandekar, M., Virtanen, K.A., Nuutila, P., Schaart, G., Huang, K., Tu, H., van Marken Lichtenbelt, W.D., Hoeks, J., Enerbäck, S., Schrauwen, P., Spiegelman, B.M., 2012. Beige Adipocytes Are a Distinct Type of Thermogenic Fat Cell in Mouse and Human. Cell 150, 366–376. https://doi.org/10.1016/j.cell.2012.05.016

Xu, S., Zhang, X., Liu, P., 2018. Lipid droplet proteins and metabolic diseases. Biochimica et Biophysica Acta (BBA) - Molecular Basis of Disease 1864, 1968–1983. https://doi.org/10.1016/j.bbadis.2017.07.019

Yoo, H. sun, Qiao, L., Bosco, C., Leong, L.-H., Lytle, N., Feng, G.-S., Chi, N.-W., Shao, J., 2014. Intermittent Cold Exposure Enhances Fat Accumulation in Mice. PLoS ONE 9, e96432. https://doi.org/10.1371/journal.pone.0096432

Yu, J., Zhang, S., Cui, L., Wang, W., Na, H., Zhu, X., Li, L., Xu, G., Yang, F., Christian, M., Liu, P., 2015. Lipid droplet remodeling and interaction with mitochondria in mouse brown adipose tissue during cold treatment. Biochimica et Biophysica Acta (BBA) - Molecular Cell Research 1853, 918–928. https://doi.org/10.1016/j.bbamcr.2015.01.020

Chapter 3: Experimental Design & Methods

Background

This study was completed in mice; the mouse research model is commonly used in order to study the physiological processes in mammals. Rodents are used in comparative medical research because of their shared genes (30,000 genes shared between mice, rats and humans) and similarities in terms of their physiology (Bryda, 2013). The C57BL/6 strain is the most widely used inbred strain of mice used in medical research and was the first to have their genome sequenced (Fontaine and Davis, 2016; Jackson Laboratory, 2021). This strain is greatly used in metabolic research as they are susceptible to diabetes and diet-induced obesity (Fontaine and Davis, 2016). Our study specifically used the C57BL/6NCrl mice from Charles River Laboratories.

Stress is defined as "*the real or perceived perturbation to an organism's physiological homeostasis or psychological well-being*" (National Research Council (US) Committee on Recognition and Alleviation of Distress in Laboratory Animals, 2008). As your body responds to this tension, it can take a toll on both your mental and physical health. While stress is a normal aspect of life, the impact of severe and/prolonged stress can have a negative impact on health. A better understanding of what prolonged and sustained stress does to the body's metabolic state is key for understanding whole-body health. For mice, there are known stressors that would lead to increased GCs, including poor housing conditions, physical pain, and even emotional/psychological distress (National Research Council (US) Committee on Recognition and Alleviation of Distress in Laboratory Animals, 2008). The effects of stress hormones (GCs) on the body have been documented in both the acute and chronic states (as previously discussed in the literature review). While the acute effects of glucocorticoids in adipose tissue have both anti-inflammatory and energy liberating effects, chronic GC exposure appears to have pro-

inflammatory effects and promote energy storage. The effect of chronic stress on BAT is not fully understood, therefore this study was designed to investigate a treatment group receiving high doses (100μg/ml) of oral corticosterone for four weeks. This dose has been found to model Cushing's disease, metabolic syndrome, and stress-related obesity (Fransson et al., 2013; Karatsoreos et al., 2010; Tamashiro et al., 2011; Uehara et al., 2020).

Specific WAT depots are prone to alter their phenotype to develop a higher amount of mitochondria and have more thermogenic potential as part of an adaptive response to environmental challenges, a phenomenon called beiging (Bartlet and Heeren, 2013). To investigate beiging and its implications on metabolism, a β3AR agonist that has shown promise in metabolic instances (summarized in the review by (Bel et al., 2021)) called mirabegron was also used. While the conventional method to beige AT is to subject rodents to cold temperatures, due to pragmatic and financial reasons, mirabegron was chosen instead.

The interaction between beiging and chronic exposure to stress hormones was previously examined by van den Beukel et al. (2015). They implanted mice with corticosterone pellets (50mg) and left them for 7 days before exposing the mice to cold temperatures for just 24 hours (van den Beukel et al., 2015). While this timeframe and dose of corticosterone delivery were significantly less than our study (7 days of corticosterone vs four weeks, and 24 hours of β3AR stimulation vs four weeks), the findings yielded promising results with CE correcting the increased plasma TAGs induced by corticosterone, normalizing the de novo lipogenic gene expression in the liver, and correcting the negative effect that corticosterone has on ingWAT beiging (van den Beukel et al., 2015). This was the only study to directly examine the interaction

between corticosterone and beiging, but further investigations were needed to fully understand the chronic effects and their implication in whole-body metabolism.

The goal of this study was to determine the effects of chronic corticosterone and how β3AR stimulation impacts AT. This will be investigated through two different animal studies. Animal study number 1 (AS1) was conducted first to verify if we could reproduce the effects of chronic corticosterone administration in mice, and which dose of mirabegron administered by Sui et al. (2019) would be the most optimal dose to achieve beiging in ingWAT (Sui et al., 2019). AS1 allowed for the effects of each treatment to be determined individually before investigating the combination of the two treatments in animal study number 2 (AS2). While studies using the high dose of corticosterone has been conducted by others (Cassano et al., 2012; Do et al., 2019; Karatsoreos et al., 2010; Kinlein et al., 2017; van Donkelaar et al., 2014), this short four week study allows for the AT-specific effects of each treatment to be investigated much closer than what has been reported previously. The hypothesis for AS1 is that the β3AR agonist mirabegron will promote AT beiging and metabolic health in mice.

AS2 was conducted after analysis of AS1 was completed. Similar measurements from AS1 were repeated in AS2 in order to investigate the effects of a combination treatment of corticosterone and mirabegron. Additional measurements including mitochondrial content and circulating leptin levels were added in order to dive deeper into the effects observed at the tissue level. The hypothesis for AS2 is that the negative effects of corticosterone induced alterations to AT will be mitigated by the β3AR agonist mirabegron.

The layout for the two animal studies are displayed below in Figure 6.

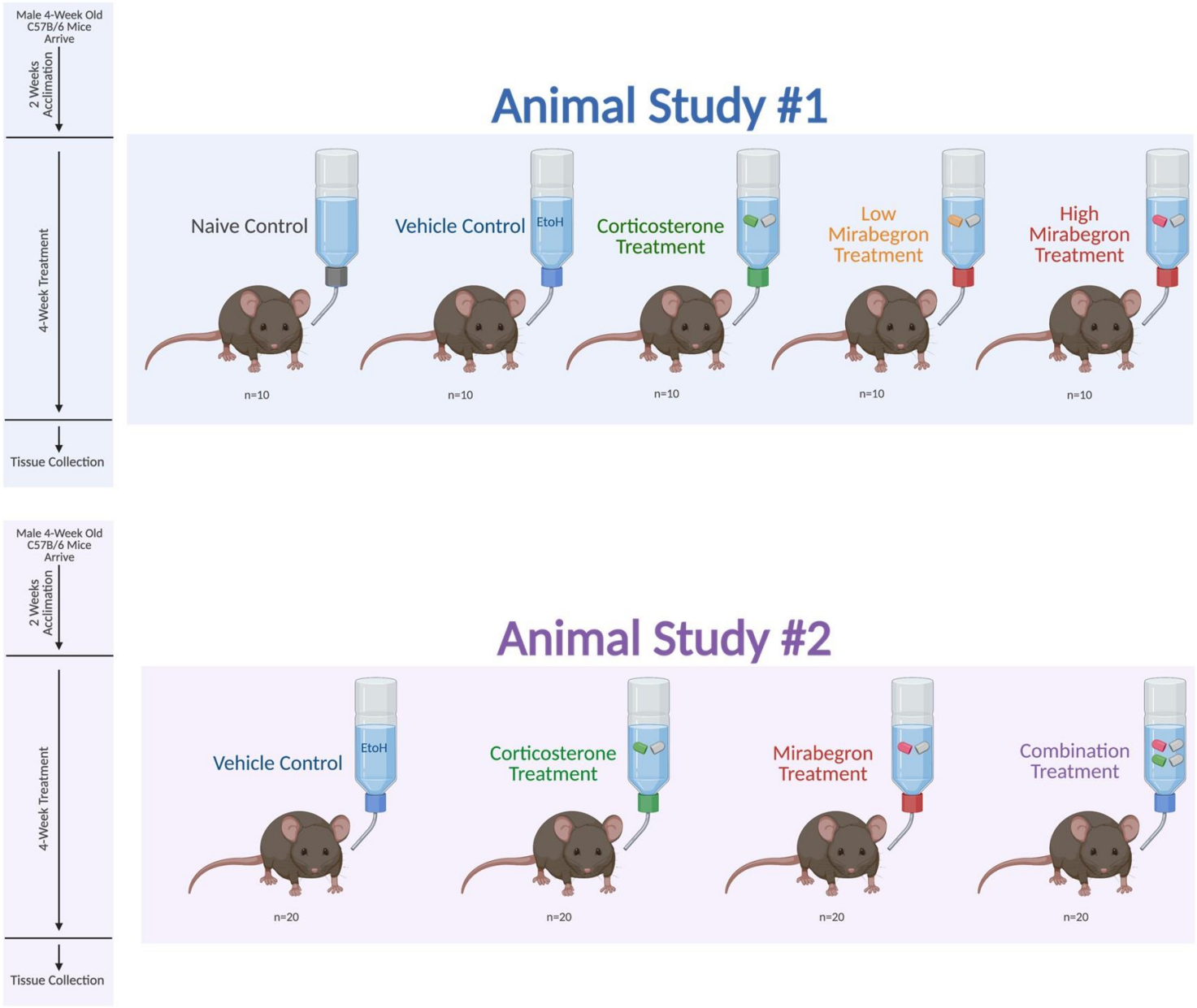

Figure 6: A visual representation of the experimental timelines and various treatment groups for the animal studies conducted in this dissertation.

Specific Aims

The specific aims of this project are as follows and displayed in Figure 7:

1. Establish how corticosterone or β3AR stimulation impact AT and UCP1 expression
    a. Visualize whitening and beiging phenotypes with histology
    b. Determine the protein expression of UCP1 with protein blotting techniques
2. Determine how oxidative stress, immune cell infiltration and leptin are influenced by corticosterone or β3AR stimulation
    a. Visualize immune cell infiltration with histology
    b. Measure lipid peroxidation marker 4-HNE with protein blotting techniques
    c. Determine plasma leptin concentrations
3. Investigate the effects of corticosterone or β3AR stimulation on whole-body insulin resistance
    a. Measure plasma glucose concentrations
    b. Measure plasma insulin concentrations
    c. Calculate the Homeostatic Model of Assessment for Insulin Resistance (HOMA-IR) for each mouse to determine insulin resistance (IR)
4. Examine mitochondrial content response to corticosterone and β3AR stimulation in both BAT and WAT
    a. Repeat all measurements from specific aims 1-3
    b. Measure mitochondrial content through protein blotting techniques

Specific Aims

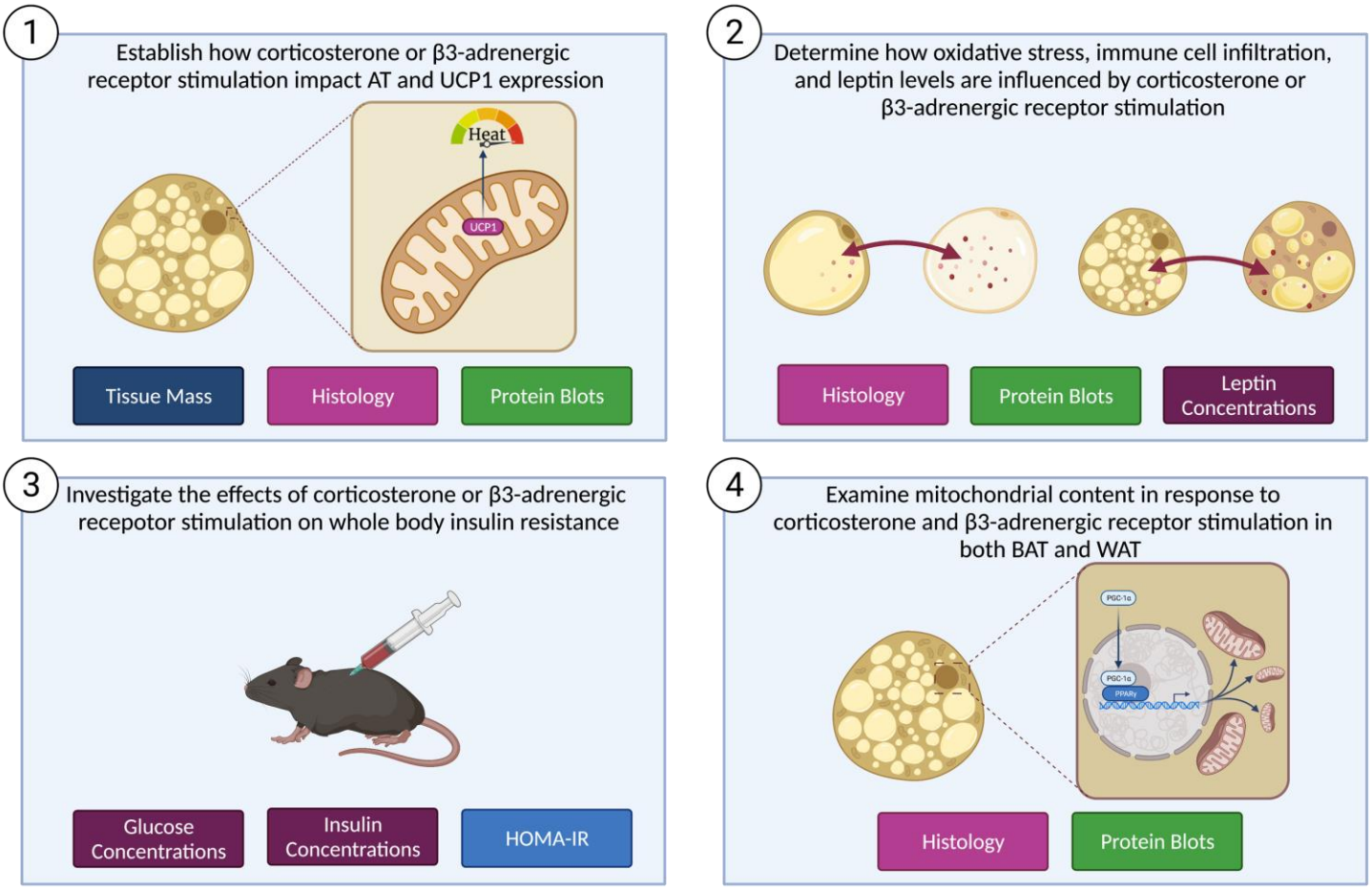

Figure 7: Illustration of the project-specific aims for this dissertation.

Animal Housing

Male mice were used for this study primarily to facilitate replication of literature findings with adipose tissue research and corticosterone treatment. Most studies using chronic corticosterone as a treatment conducted the experiments in male mice and the differences between the sexes are explained (Luine et al., 2017; Rincón-Cortés et al., 2019). While beiging experiments have been conducted with females, there appears to be some variability in the response to β3AR activation and the beiging response. Our β3AR agonist, mirabegron, has been used for the *in vivo* studies primarily with male mice. While human studies with mirabegron have been conducted in both males and females, we needed to verify that we can produce the same results as the literature with our treatments in order to successfully implement our combination treatment. Even though scientific research is widely criticized for only using predominantly the male sex, future studies can be designed to determine the effects in females.

All protocols were approved by the animal care committee at Lakehead University. Four-week-old male C57BL/6N mice were purchased from Charles River and allowed to acclimate for approximately 2 weeks prior to treatment. Mice were housed in groups consisting of 3-4 mice per cage at the Pre-Clinical Research facility and ear notched for identification purposes (SOP R-46-LUACF attached in appendix). Mice were housed at ambient temperatures (22-25˚C) on a 12:12 light-dark cycle with 40-70% humidity. Mice were fed ad libitum a standard chow diet for the duration of the experiment with free access to water.

Treatment Preparation and Administration

In AS1, mice were exposed to oral treatments (n=10/treatment) at target doses consisting either of corticosterone (500μg/day), mirabegron (0.024mg/day or 0.24mg/day), vehicle (<1% ethanol), or naïve control (autoclaved water). Mirabegron, a β3AR agonist known to increase BAT activity, was used as a positive control in order to compare the effects of corticosterone against changes observed in BAT under chronic activation. Mirabegron doses were selected based on a study by Sui et al. (2019) who reported BAT activation and WAT beiging under these conditions (Sui et al., 2019). The dose delivered in the water to achieve the target dose for corticosterone was 100μg/ml at the beginning of the treatment and lowered to 50μg/ml on day 20 of the study, and for the mirabegron low and high treatments were either 0.0048mg/ml or 0.048mg/ml respectively. The doses for mirabegron were used by Sui et al. (2019) who was able to show beiging and activating effects of this pharmacological compound, however they did not examine the metabolic effects of this compound with respect to whole body metabolism. The mirabegron high dose was approximately equivalent to the maximal mirabegron dose approved and administered in humans of 50mg/day (Nair and Jacob, 2016) (see appendix for dose calculations). All treatments were administered through a water bottle to each group (n=10/treatment) and mice were allowed to drink *ad libitum*. A power analysis was conducted in order to determine the minimum sample size required for each treatment (see appendix). Corticosterone was purchased from Sigma Aldrich (27840), mirabegron was purchased from Best of Chemical Sciences (B0084-182334) and 95% ethanol was purchased from Cedarlane (40120791-3).

The appropriate amount of either corticosterone or mirabegron powder was weighed using an analytical balance and stored in canonical tubes until use. Fresh solutions were prepared

using the appropriate amount of either corticosterone or mirabegron and ethanol every 3-4 days. Tubes were then placed in a 37°C bead bath for the treatment powders to dissolve into solution. Treatment solutions were added to autoclaved water to give a final concentration of 100μg/ml for corticosterone, or 0.0048mg/ml mirabegron or 0.048mg/ml mirabegron. Vehicle water was prepared in the manner with ethanol where the final concentration of ethanol in the bottle was <1%. Naïve control water bottles were prepared using autoclaved water. Treatments were administered to the mice through water bottles that were pre-weighed in order to track water consumption. The amount of water consumed was then divided by the number of mice in the cage for approximate water amount consumed per mouse. A summary of the experimental timeline is displayed below in Figure 8.

The estimated delivered doses of corticosterone and mirabegron were tracked throughout the experiment to ensure the animals received adequate treatment. The corticosterone-treated animals started to drink significantly more of the treatment water in the middle of the study, leading to the administered dose being greater than desired. This led to the corticosterone concentration in the treatment water being decreased to 50μg/ml in order for the animals to receive the targeted dose of 500μg per day, after which point the drinking water consumption stabilized. Two corticosterone mice perished during the course of the study, possibly due to corticosterone-induced complications, however, this was not tested. One vehicle mouse was removed from the study due to unrelated health complications.

AS2 was completed in a similar manner to AS1 with minor alterations. The number of mice used was doubled to n=20/treatment in order to have more tissues to conduct the appropriate analyses. The naïve control group was not repeated as it did not demonstrate significant

differences from the vehicle control group in AS1. One mirabegron dose (0.048mg/ml) was selected as little difference was observed between the low and high doses in AS1. With the knowledge from AS1 where the corticosterone treatment group began to consume more water and therefore received a higher dose than anticipated, the corticosterone dose was reduced to 75μg/ml to align with the target dose of 500μg/day per mouse. Lastly, a combination group was included where the same corticosterone and mirabegron doses used as individual treatments were both placed in this group's drinking water to examine the effects of the two treatments simultaneously. AS2 was therefore comprised of a vehicle treatment group (<1% ethanol), a corticosterone treatment group (75μg/ml), a mirabegron treatment group (0.048mg/ml), and a combination group. Three combination treatment mice perished during the study, and one vehicle mouse was euthanized due to unrelated health complications.

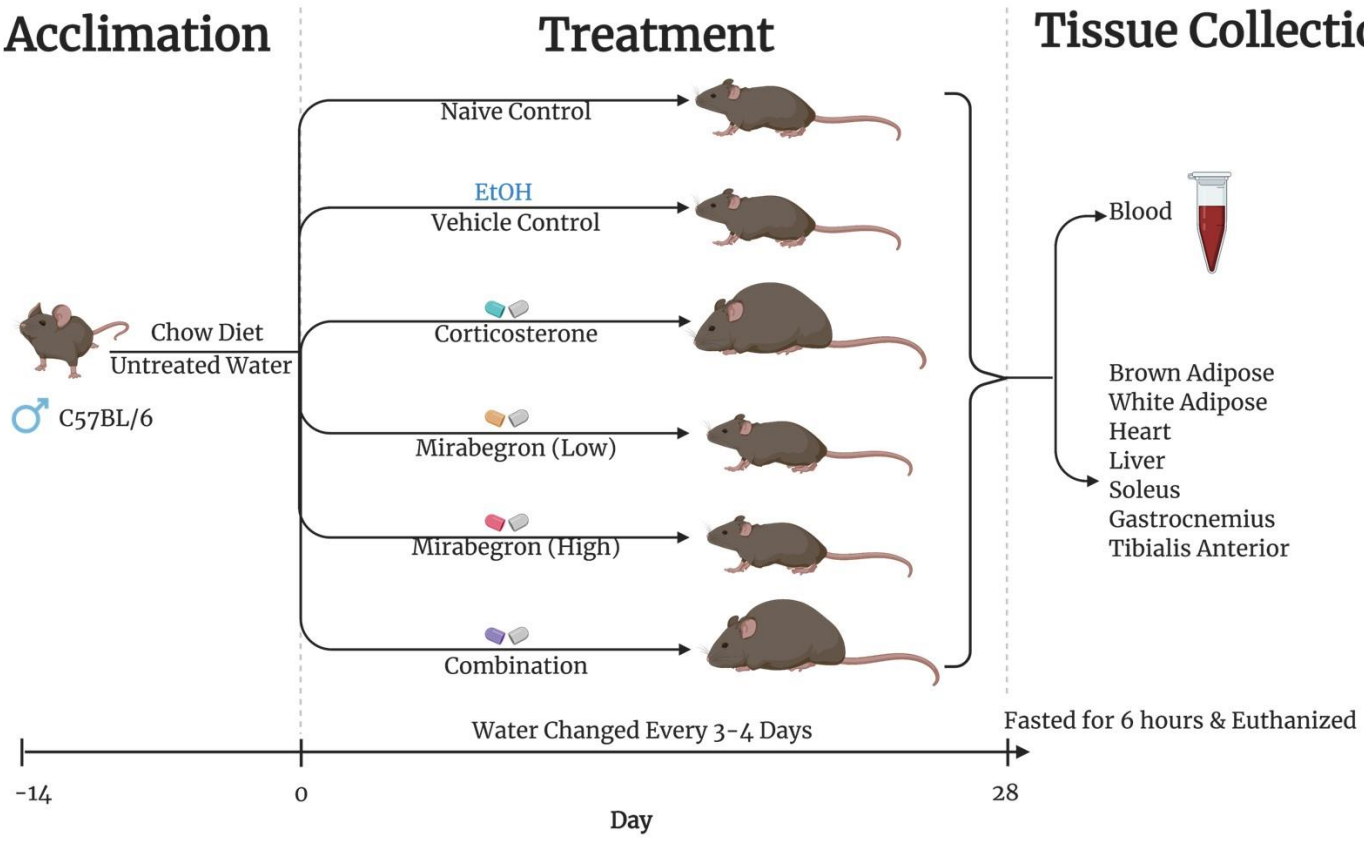

Figure 8: Schematic representation of the timeline of events for the animal studies.

Tissue Collection

After four weeks of exposure to mirabegron &/or corticosterone, animals were weighed and moved to a clean cage without food (containing water and enrichment) to fast for 4-6 hours (average=5h) prior to being euthanized for dissections. This is a standard procedure for performing metabolic tests of glucose homeostasis in mice (Ayala JE, et al). Animals were anesthetized with an inhalant anesthetic (isoflurane) (SOP R-18-LUACF attached in appendix) for tissue collection.

Once under the deep surgical plane of anesthesia, the blood was collected from every mouse through cardiac puncture (SOP R-9-LUACF attached in appendix) where it was combined with 0.5M EDTA (pH 8) to give a final mixture of 10% EDTA. Blood was mixed by inversion 10 times prior to being stored on ice for transportation back to the wet lab facility. Within 2 hours of collection, blood was centrifuged at 3,000xg for 10 minutes in order to remove plasma, which was stored at -30˚C until use in plasma assays (outlined below).

Tissue collection of the heart, iBAT, ingWAT, liver, and the gastrocnemius, tibialis anterior, and soleus skeletal muscles were dissected from the mouse within 10 minutes of cardiac puncture. Tissues were weighed using an analytical balance prior to being flash-frozen in liquid nitrogen and stored on dry ice before long-term storage at -80˚C. A schematic of the tissues retrieved for this study is displayed in Figure 9. This dissertation focuses on AT only, but other tissues were retrieved in order to fully utilize the animals and gain the most information about our treatments.

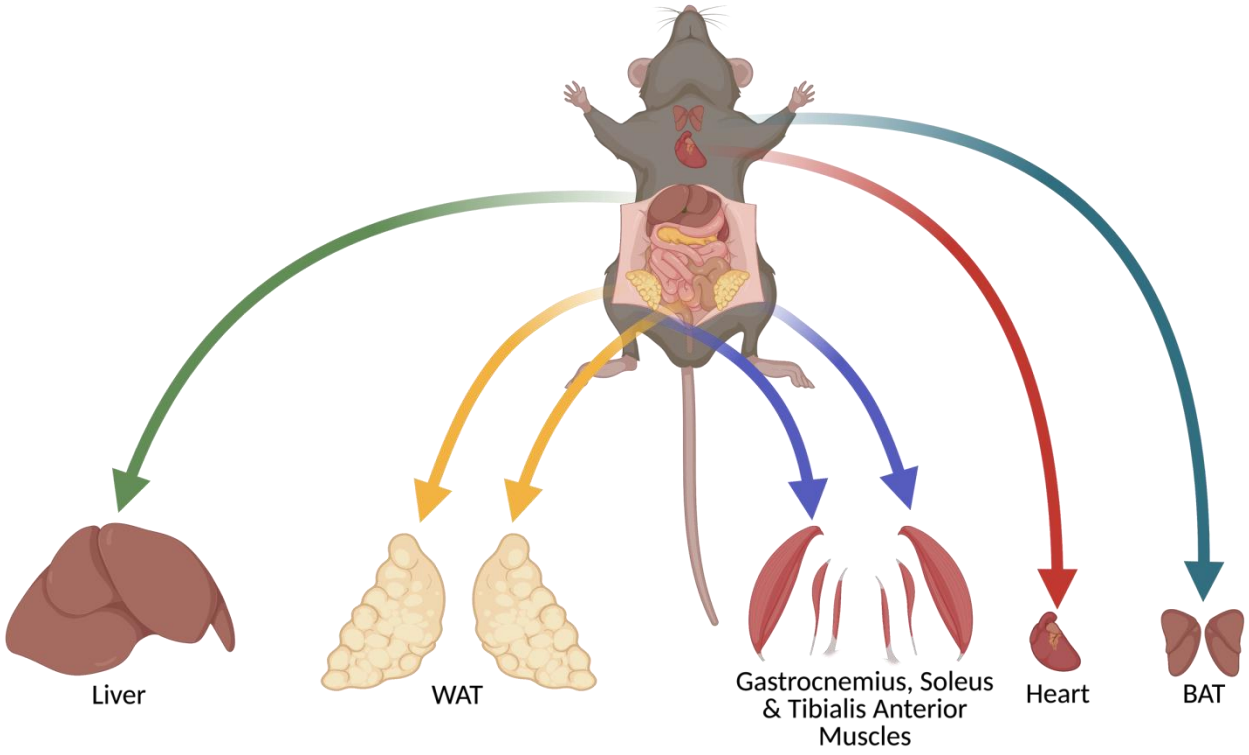

Figure 9: Illustration of the tissues retrieved from each mouse for further analysis.

In AS1, the BAT was cut in half in order for half of the tissue to be used for protein analysis and the other half to be stored in a cassette submerged in formalin for histological experiments. Likewise, one side of the ingWAT was stored for protein analysis and the other for histological experiments. In AS2, the number of animals in the study was doubled in order to obtain more tissue to conduct these analyses.

Plasma Assays

Plasma glucose, insulin and leptin levels were determined through commercially available kits. Glucose concentrations were determined with a colourimetric assay from Cayman Chemical (1000958) and insulin concentrations were determined with the Mouse Insulin ELISA kit from ALPCO (80-INSMS-E01) following the manufacturers' instructions. The Homeostatic Model of Assessment for Insulin Resistance (HOMA-IR) was determined for each mouse in the study using the formula: [Fasting Glucose x Fasting Insulin]/405. Plasma leptin concentrations were determined through the Mouse Plasma Leptin ELISA from R&D Systems (MOB00B) following the manufacturer's instructions.

Tissue Disruption and Lysis

Tissue lysis and protein collection were performed using a modified version of the Removal of Excess Lipids (RELi) protocol described by Martin et al. (2019) (Marin et al., 2019). Fresh RIPA buffer was prepared using 1M Tris (pH 8), 1.5M NaCl, 10% NP-40, 10% Sodium deoxycholate, 10% Sodium dodecyl sulfate (SDS) and distilled water and stored on ice prior to supplementing with protease inhibitor cocktail (Sigma P8240) (1:500) and phosphatase inhibitor cocktail (1:100) consisting of 1mM sodium orthovanadate (ab120386) and 25mM sodium fluoride (Thermo Scientific S299-100).

150mg of WAT was weighed on an analytical balance and kept on ice in a 2ml round bottom conical tube prior to the addition of 900μl RIPA buffer with inhibitors. A metal bead was

added to the tube in order for the samples to be disrupted and lysed at 20 Hz for 2 minutes (Qiagen Tissue Lyser 85210), chilled and re-lysed for a total of 3 times. BAT samples were aliquoted with the appropriate amount of RIPA buffer with inhibitors to give 300µl of buffer for every 50mg of AT (6:1 ratio) prior to the addition of a metal bead. BAT samples were lysed at 20 Hz for 2 minutes, chilled and re-lysed for a total of 4 times. The metal bead was removed, and samples were left on ice for 2 hours. The samples were centrifuged at 4˚C for 15 minutes at 20,000xg in order for the supernatant to be separated from the layer of lipids and transferred to a new tube. The process of centrifuging the supernatants was conducted three times in order to reduce the number of lipids in the sample. After the final collection of supernatant, the samples were used for protein quantification prior to being stored at -80˚C.

Protein Quantification

Protein quantification was conducted using the Pierce BCA Protein Assay (Thermo Fisher 23227). Samples were diluted 1:3 with 10% SDS and distilled water in order to be utilized in the assay. The manufacturer's instructions were followed using 10µl of each standard or diluted sample loaded into the plate, in triplicate or duplicate respectively, prior to the addition of 200µl of working reagent (prepared as outlined containing 50 reagent A:1 reagent B). The plate was mixed and incubated at 37˚C for 30 minutes prior to being cooled to room temperature for absorbance reading at 562nm with a BioTek Cytation 5 microplate reader using Gen5 software.

A standard curve was prepared from the protein assay and protein concentrations for each sample were determined. For western blots, samples were prepared at concentrations of 0.4µg/µl or 0.5µg/µl for WAT and BAT respectively. Samples were prepared using distilled water

and 4X reducing loading buffer containing 125mM Tris (pH 6.8),2% SDS, 0.01% bromophenol blue and 10% glycerol, and 0.1M DTT, which resulted in a final concentration of 1X. Prepared samples were vortexed prior to being heated at 100˚C for 5 minutes and stored at -80˚C for long-term storage.

Before separating the prepped samples using gel electrophoresis, a Pierce 660nm assay (Thermo Fisher 22660) was conducted in order to verify the concentration of each of the prepped samples. Briefly, 10µl of each standard or sample were loaded into a 96-well plate in either triplicate or duplicate respectively. Ionic detergent compatibility reagent (Thermo Fisher 22663) was added to 20ml of 660 Assay Reagent before adding 150µl to each well. The plate was mixed on a plate shaker for 1 minute before being incubated at room temperature for 5 minutes. The plate was then read at 660nm using the BioTek Cytation 5 microplate reader using Gen5 software. The concentrations determined from this 660 assay were then used to precisely load each sample with the corresponding volume to achieve the desired sample concentration in each blot.

Western Blotting

Prepared protein samples were thawed on ice and analyzed by separation with 10-15% separating and 4% stacking polyacrylamide gels and transferred to nitrocellulose or polyvinylidene fluoride (PVDF) membranes for western blotting. 5µl of BLUelf pre-stained protein ladder (FroggaBio) was added to the first lane of each gel, then a loading control sample, followed by samples from alternating treatment groups. Gels were run at 200V until the dye front ran off the gel. Gels were then transferred with 30V for 960 minutes to nitrocellulose

membranes or 0.2μm PVDF membranes were stained with Ponceau S to ensure equal loading, de-stained with 0.1M NaOH and quickly rinsed with 1X TBST before antibody detection. Membranes were blocked with either 5% milk or 5% BSA made with 1X TBST at room temperature for 1 hour on a Storvall Belly Dancer Shaker. Immunoblotting was performed using primary antibody solutions prepared in 5% milk at UCP1 (Abcam ab209483, 1:1000), or citrate synthase (Abcam ab129095, 1:100,000). Membranes were then placed on a rocker at 4˚C appropriate primary antibody solution overnight. Membranes were washed 3 times for 5 minutes with 1X TBST prior to being placed on a Storvall Belly Dancer Shaker in goat-anti-rabbit secondary antibody (Fisher Scientific PI31460) at 1:2500 for UCP-1 and 1:500,000 for citrate synthase prepared in 5% milk for 1 hour at room temperature. Membranes were then washed again with 1X TBST 3 times for 5 minutes prior to being detected with either SuperSignal (Thermo Scientific 34577) or enhanced chemiluminescence (ECL) solution, using the manufacturer's instructions. Membranes were imaged using a BioRad ChemiDoc Imager with auto exposures.

After detection of the antigen, the membranes blots were then stained with Coomassie R250 membrane stain following the protocol outlined in Current Protocols in Science-Electrophoresis 1.5.3. Briefly, stock Coomassie R250 staining solution was prepared with 2.4g of Coomassie Blue R250 powder (BioRad), 60ml of methanol and 12ml of acetic acid and mixed on a stir plate overnight. The membrane staining solution was prepared with 0.75ml of stock Coomassie R250 solution, 40ml of methanol, 7ml acetic acid and 52.25ml of distilled water (Goldman et al., 2016). The de-staining solution was prepared with 50ml of methanol, 7ml of

acetic acid, and 43ml of distilled water to create a 15% methanol/10% acetic acid v/v solution (Goldman et al., 2016). Before staining, the membranes were washed 3-5 times with distilled water before being covered with 15ml of the staining solution and being placed on a Storvall Belly Dancer Shaker for 5 minutes. The staining solution was then poured off before adding 10 volumes of the de-staining solution to the container. A Kimwipe was placed in the corner of the container to absorb some of the dye during the de-staining time of 10 minutes on a Storvall Belly Dancer Shaker. The de-staining step was then repeated for a second time. The membranes were then rinsed with distilled water and left to dry at room temperature. Once dry, the membranes were scanned and analyzed or the protein content within the entire lane. All blots were quantified using ImageJ software and loading controls were used to normalize each blot and were then normalized to the Coomassie or Ponceau S stain of the entire lane for that sample for accurate quantification of protein expression relative to protein loaded in the lane. In AS1, both western blots were transferred to nitrocellulose membranes and were stained with Ponceau S. In AS2, western blots were transferred to PVDF membranes and stained with both Ponceau S and with Coomassie blue stain. The switch to Coomassie blue and PVDF was undertaken in order to better stain for total protein.

Slot Blotting

Slot and dot blots have been used to detect proteins in adipose tissue previously and provide simple, sensitive and reproducible results (Milner et al., 1990). In order to quantify difficult to detect proteins in WAT and BAT due to limitations in the quantity of protein that could be loaded into the well of the SDS-PAGE, a slot blot was conducted instead of a western

blot. The slot blot apparatus was assembled with a nitrocellulose membrane as per the manufacturer's instructions. The nitrocellulose membrane was rinsed three times with PBS before the experiment. The protein concentrations determined through the BCA assay were used to load onto a nitrocellulose membrane into designated slots of the Bio-Dot SF apparatus (Bio-Rad 1706542) with a vacuum. For UCP1 40µg of protein was loaded and for 4-Hydroxyneonenal (4-HNE), 10µg was loaded, supplemented with PBS for a final volume of 200µl. The membrane was rinsed once more with PBS before the apparatus was disassembled. The membrane was then stained with Ponceau S to ensure equal loading, and an image was taken for later quantification. The membrane was de-stained with 0.1M NaOH before being rinsed with 1X TBST before being blocked in 5% milk made with 1X TBST at room temperature for 1 hour on a Storvall Belly Dancer Shaker. Immunoblotting was performed using primary antibody solutions prepared in 5% milk at UCP1 (Abcam ab209483, 1:1000), or 4-HNE (Abcam ab46545, 1:1000). Membranes were then placed on a rocker at 4˚C appropriate primary antibody solution overnight. Membranes were washed 3 times for 5 minutes with 1X TBST prior to being placed on a Storvall Belly Dancer Shaker in either goat-anti-rabbit secondary antibody (Fisher Scientific PI31460) at 1:2500 for UCP-1 or 1:1000 for 4-HNE prepared in 5% milk for 1 hour at room temperature. Membranes were then washed again 3 times for 5 minutes with 1X TBST prior to being detected with either SuperSignal (Thermo Scientific 34577) or ECL solution, using the manufacturer's instructions. All blots were quantified using ImageJ software and the Ponceau S stain image was used to normalize each blot.

Histological Staining and Analysis

Tissues used for histological staining were stored in 10% formalin upon collection and were shipped to Ontario Veterinary College at the University of Guelph for slide preparation. Tissues were processed under vacuum using a Shandon Excelsior Tissue Processor. Briefly, the samples were subjected to 70% isopropanol at 30°C for 45 min, 85% isopropanol at 30°C for 45 min, 90% isopropanol at 30°C for 45 min, 95% isopropanol at 30°C for 45 min, 100% isopropanol at 30°C for 45 min twice, Xylene at 30°C for 45 min three times, and Paraffin at 62°C for 45 min three times. Tissues were then embedded with TissuePrep (Fisher Scientific T565) and sectioned using a Leica RM255 into 5μm sections. Slides were stained with hematoxylin and eosin (H&E) in order for histological analysis of lipid droplet size to be conducted. Microscopic images of each BAT were taken at 10X magnification for three separate fields of view for each sample. Each of the three fields of view were quantified for lipid droplet area using Cell Profiler software as described (Berry et al., 2014). The analysis was completely automated to avoid any biased results. 1300-3500 lipid droplets were analyzed from each field of view in BAT and 80-210 lipid droplets were analyzed from each field of view in WAT. All fields of view are represented in the figure, but the statistical tests were conducted on averaged field of view per animal. Each of the average lipid droplet sizes from each field of view was then used for statistical analysis to compare each treatment. Each field of view was also scanned for the formation of CLS in order to detect any tissue level inflammatory changes.

Statistical Analysis

All statistical analyses were performed in GraphPad Prism software version 9.3.1. Means ± SD were calculated for all data sets and displayed in each figure. Data sets were analyzed using either one-way ANOVA or two-way ANOVA with Fisher's LSD test, where $p \leq 0.05$ was considered statistically significant. Histological analyses histograms were created using frequency distribution analyses in GraphPad Prism where bin centers were determined as relative frequency percentages. .

Graphical Software

All graphics were created using BioRender with a premium account and publishing rights.

References

Bartlet, A., Heeren, J., 2013. Adipose Tissue Browning and Metabolic Health. Nature Reviews Endocrinology 10, 24–26. https://doi.org/doi:10.1038/nrendo.2013.204

Bel, J.S., Tai, T.C., Khaper, N., Lees, S.J., 2021. Mirabegron: The most promising adipose tissue beiging agent. Physiol Rep 9. https://doi.org/10.14814/phy2.14779

Berry, R., Church, C., Gericke, M.T., Jeffery, E., Colman, L., Rodeheffer, M.S., 2014. Methods in Enzymology (MIE): Methods of Adipose Tissue Biology-: 30.

Bryda, E.C., 2013. The Mighty Mouse - The Impacts of Rodents on Advances in Biomedical Research. Science of Medicien 110, 207–211.

Cassano, A.E., White, J.R., Penraat, K.A., Wilson, C.D., Rasmussen, S., Karatsoreos, I.N., 2012. Anatomic, Hematologic, and Biochemical Features of C57BL/6NCrl Mice Maintained on Chronic Oral Corticosterone. Comparative Medicine by the American Association for Laboratory Animal Science 62, 348–360.

Do, T.T.H., Marie, G., Héloïse, D., Guillaume, D., Marthe, M., Bruno, F., Marion, B., 2019. Glucocorticoid-induced insulin resistance is related to macrophage visceral adipose tissue infiltration. The Journal of Steroid Biochemistry and Molecular Biology 185, 150–162. https://doi.org/10.1016/j.jsbmb.2018.08.010

Fontaine, D.A., Davis, D.B., 2016. Attention to Background Strain Is Essential for Metabolic Research: C57BL/6 and the International Knockout Mouse Consortium. Diabetes 65, 25–33. https://doi.org/10.2337/db15-0982

Fransson, L., Franzén, S., Rosengren, V., Wolbert, P., Sjöholm, Å., Ortsäter, H., 2013. β-cell adaptation in a mouse model of glucocorticoid-induced metabolic syndrome. Journal of Endocrinology 219, 231–241. https://doi.org/10.1530/JOE-13-0189

Goldman, A., Harper, S., Speicher, D.W., 2016. Detection of Proteins on Blot Membranes. Current Protocols in Protein Science 86. https://doi.org/10.1002/cpps.15

Jackson Laboratory, 2021. C57BL/6J.

Karatsoreos, I.N., Bhagat, S.M., Bowles, N.P., Weil, Z.M., Pfaff, D.W., McEwen, B.S., 2010. Endocrine and Physiological Changes in Response to Chronic Corticosterone: A Potential Model of the Metabolic Syndrome in Mouse. Endocrinology 151, 2117–2127. https://doi.org/10.1210/en.2009-1436

Kinlein, S.A., Shahanoor, Z., Romeo, R.D., Karatsoreos, I.N., 2017. Chronic Corticosterone Treatment During Adolescence Has Significant Effects on Metabolism and Skeletal Development in Male C57BL6/N Mice. Endocrinology 158, 2239–2254.

Lee, J., Moy, S., Meijer, J., Krauwinkel, W., Sawamoto, T., Kerbusch, V., Kowalski, D., Roy, M., Marion, A., Takusagawa, S., et al. (2013). Role of Cytochrome P450 Isoenzymes 3A and 2D6 in the In Vivo Metabolism of Mirabegron, a β3-Adrenoceptor Agonist. Clin Drug Investig *33*, 429–440. https://doi.org/10.1007/s40261-013-0084-y.

Luine, V., Gomez, J., Beck, K., Bowman, R., 2017. Sex differences in chronic stress effects on cognition in rodents. Pharmacology Biochemistry and Behavior 152, 13–19. https://doi.org/10.1016/j.pbb.2016.08.005

Marin, R.D., Crespo-Garcia, S., Wilson, A.M., Sapieha, P., 2019. RELi protocol: Optimization for protein extraction from white, brown and beige adipose tissues. MethodsX 918–928. https://doi.org/10.1016/j.mex.2019.04.010

Matoulková, P., Pávek, P., Malý, J., and Vlček, J. (2014). Cytochrome P450 enzyme regulation by glucocorticoids and consequences in terms of drug interaction. Expert Opinion on Drug Metabolism & Toxicology *10*, 425–435. https://doi.org/10.1517/17425255.2014.878703.

McLaughlin, K.L., Hagen, J.T., Coalson, H.S., Nelson, M.A.M., Kew, K.A., Wooten, A.R., and Fisher-Wellman, K.H. (2020). Novel approach to quantify mitochondrial content and intrinsic bioenergetic efficiency across organs. Sci Rep *10*, 17599. https://doi.org/10.1038/s41598-020-74718-1.

Milner, R.E., Géloën, A., Trayhurn, P., 1990. A dot immunobinding assay for the rapid quantification of uncoupling protein in brown adipose tissue mitochondria. Biochemical Society Transactions 18, 547–547. https://doi.org/10.1042/bst0180547

Mundell, L., Lindemann, R., and Douglas, J. (2017). Monitoring long-term oral corticosteroids. BMJ Open Qual *6*, e000209. https://doi.org/10.1136/bmjoq-2017-000209.

Nair, A., Jacob, S., 2016. A simple practice guide for dose conversion between animals and human. J Basic Clin Pharma 7, 27. https://doi.org/10.4103/0976-0105.177703

National Research Council (US) Committee on Recognition and Alleviation of Distress in Laboratory Animals, 2008. Recognition and Alleviation of Distress in Laboratory Animals. National Academies Press, Washington, D.C. https://doi.org/10.17226/11931

Rincón-Cortés, M., Herman, J.P., Lupien, S., Maguire, J., Shansky, R.M., 2019. Stress: Influence of sex, reproductive status and gender. Neurobiology of Stress 10, 100155. https://doi.org/10.1016/j.ynstr.2019.100155

Sui, W., Li, H., Yang, Y., Jing, X., Xue, F., Cheng, J., Dong, M., Zhang, M., Pan, H., Chen, Y., Zhang, Yunjian, Zhou, Q., Shi, W., Wang, X., Zhang, H., Zhang, C., Zhang, Yun, Cao, Y., 2019. Bladder drug mirabegron exacerbates atherosclerosis through activation of brown fat-mediated lipolysis. Proc Natl Acad Sci USA 116, 10937–10942. https://doi.org/10.1073/pnas.1901655116

Tamashiro, K.L., Sakai, R.R., Shively, C.A., Karatsoreos, I.N., Reagan, L.P., 2011. Chronic stress, metabolism, and metabolic syndrome. Stress 14, 468–474. https://doi.org/10.3109/10253890.2011.606341

Uehara, M., Yamazaki, H., Yoshikawa, N., Kuribara-Souta, A., Tanaka, H., 2020. Correlation among body composition and metabolic regulation in a male mouse model of Cushing's syndrome. Endocr J 67, 21–30. https://doi.org/10.1507/endocrj.EJ19-0205

UpToDate Inc (2022). Prednisone: Drug information. URL: https://www.uptodate.com/contents/prednisone-drug-information/print?topicRef=127454&source=see_link

van den Beukel, J.C., Boon, M.R., Steenbergen, J., Rensen, P.C.N., Meijer, O.C., Themmen, A.P.N., Grefhorst, A., 2015. Cold Exposure Partially Corrects Disturbances in Lipid Metabolism in a Male Mouse Model of Glucocorticoid Excess. Endocrinology 156, 4115–4128. https://doi.org/10.1210/en.2015-1092

van Donkelaar, E.L., Vaessen, K.R.D., Pawluski, J.L., Sierksma, A.S., Blokland, A., Cañete, R., Steinbusch, H.W.M., 2014. Long-Term Corticosterone Exposure Decreases Insulin Sensitivity and Induces Depressive-Like Behaviour in the C57BL/6NCrl Mouse. PLoS ONE 9, e106960. https://doi.org/10.1371/journal.pone.0106960

Williams, D.M. (2018). Clinical Pharmacology of Corticosteroids. Respir Care *63*, 655–670. https://doi.org/10.4187/respcare.06314.

Chapter 4: Results

Animal Study #1 (AS1)

Corticosterone treatment increased body weight

Throughout the experiment, corticosterone-treated mice illustrated significantly ($p \leq 0.05$) elevated body weights from day seven until the end of the treatment (Figure 10). The change in body weight from baseline was significantly ($p \leq 0.05$) elevated in the corticosterone group (Figure 11). The fasting body weight was also significantly ($p \leq 0.05$) increased in the corticosterone group (Figure 12).

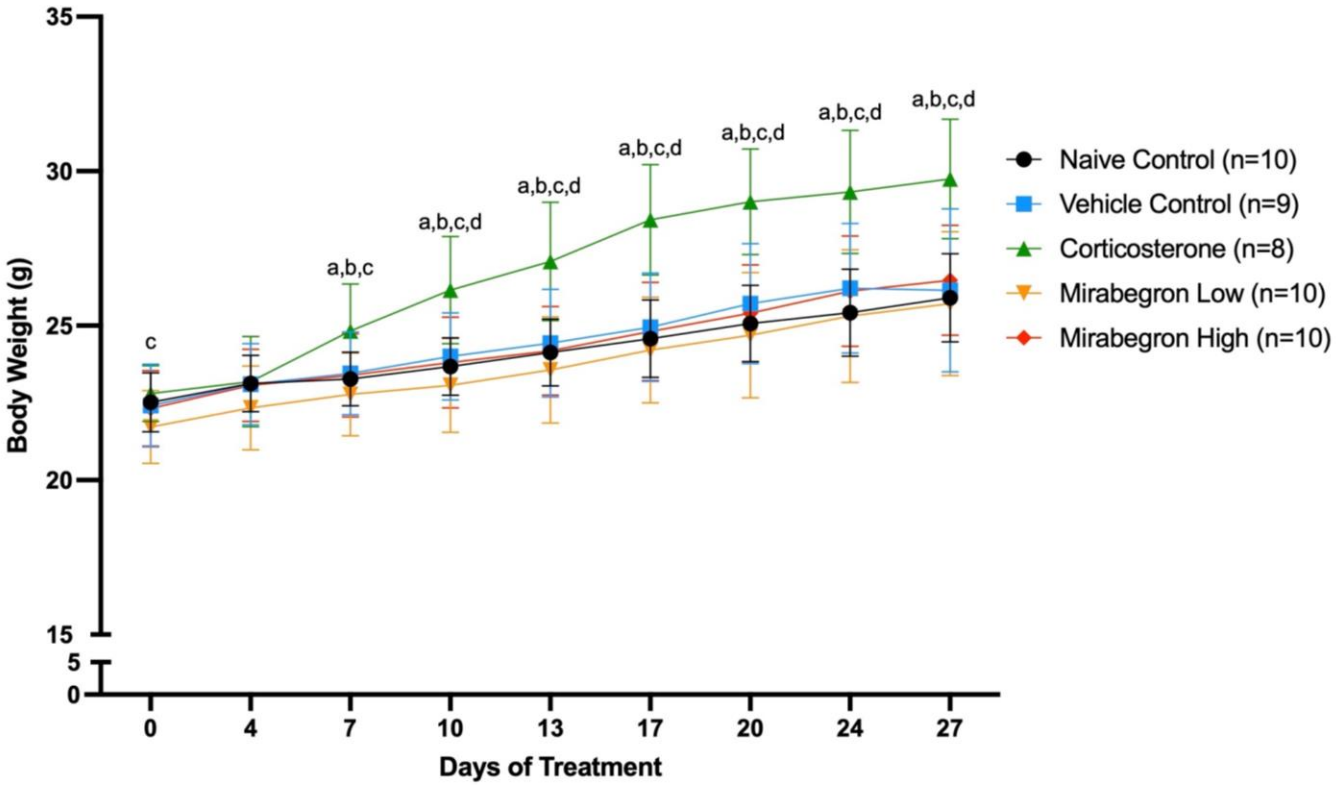

Figure 10: A Summary of the Body Weight Over the Course of Animal Study #1.

The corticosterone treated mice illustrated significantly ($p \leq 0.05$) increased body weights after seven days of treatment compared to all other treatment groups. (a) represents significantly different ($p \leq 0.05$) from naive control, (b) represents significantly different ($p \leq 0.05$) from vehicle control, (c) represents significantly different ($p \leq 0.05$) from mirabegron low treatment, (d) represents significantly different ($p \leq 0.05$) from mirabegron high treatment.

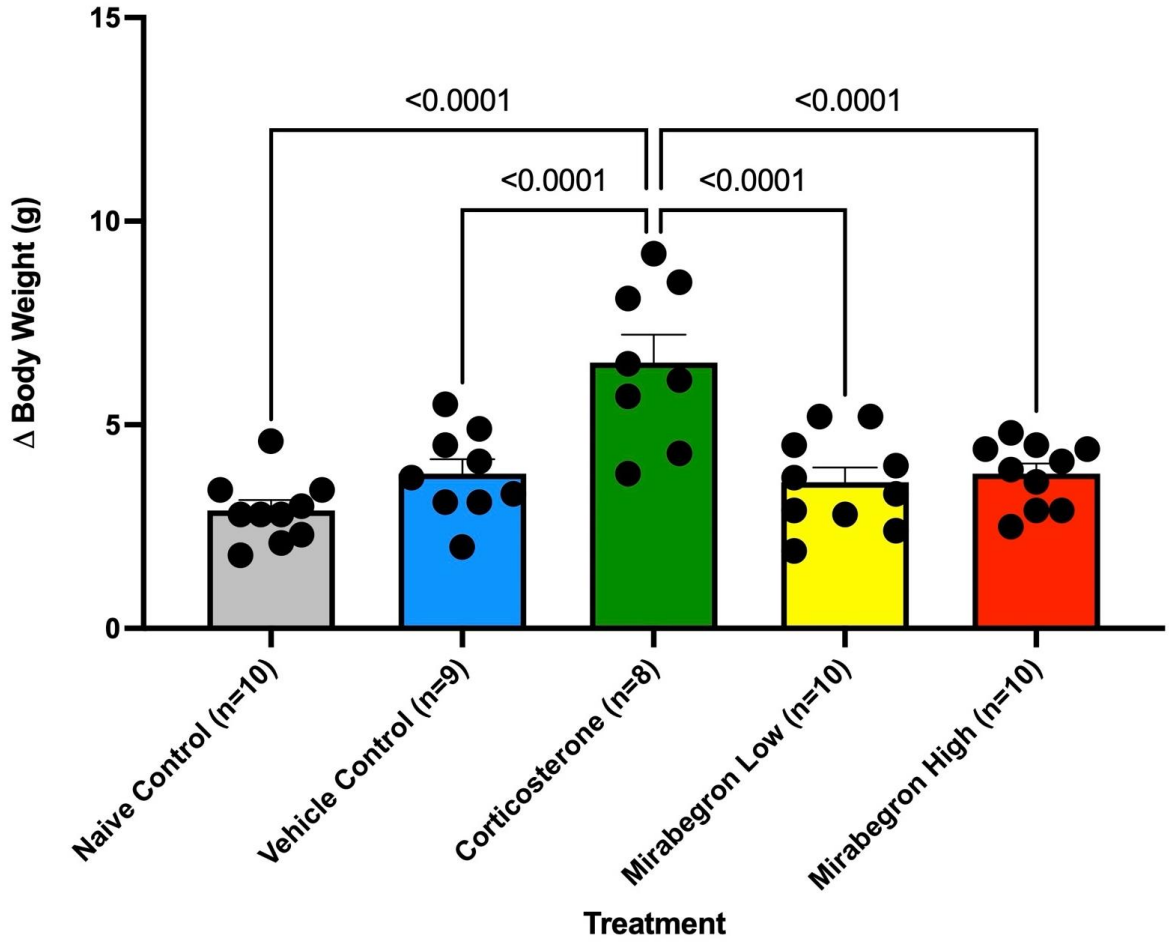

Figure 11: Overall Change in Body Weight After Animal Study #1.

The corticosterone mice also illustrated a significant ($p \leq 0.05$) increase in body weight gain from the start of the experiment.

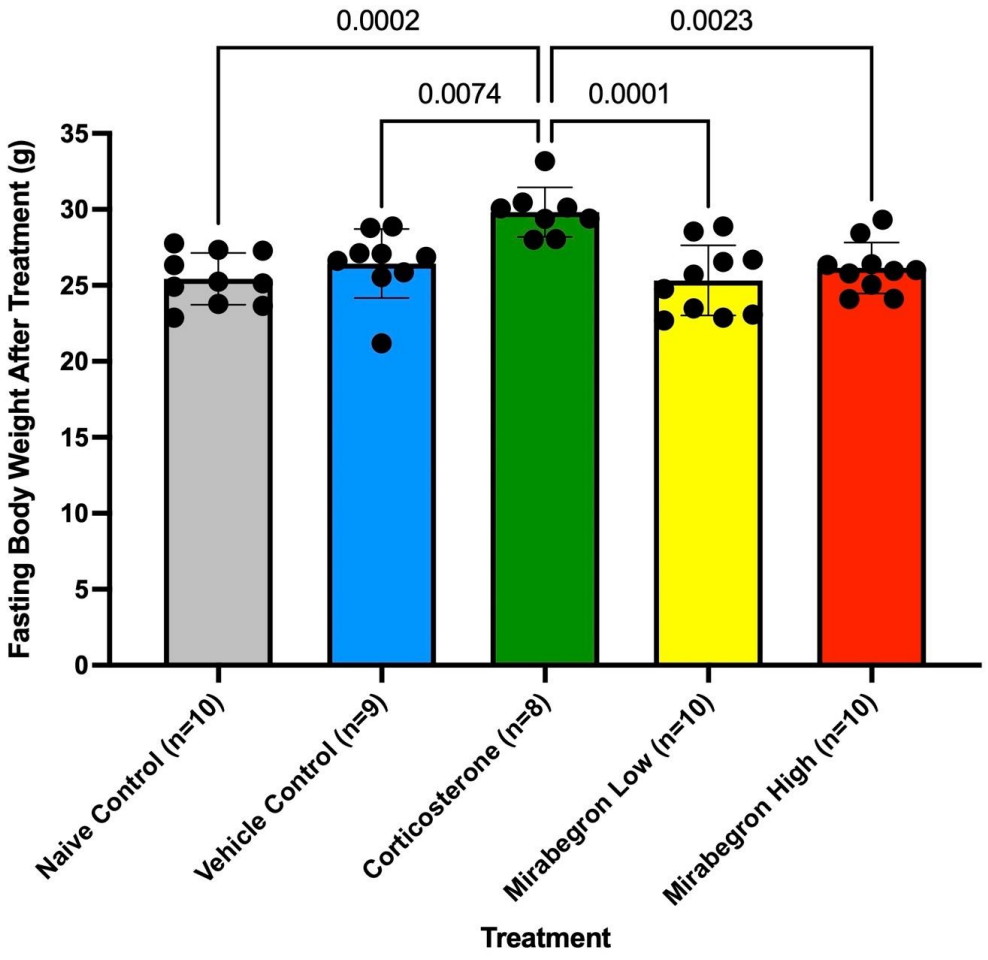

Figure 12: Fasting Body Weight in Animal Study #1.

At the time of euthanasia, the corticosterone mice weighted significantly ($p \leq 0.05$) more than all other treatment groups.

Corticosterone treatment altered mouse physical appearance and drinking water behaviour

Corticosterone-treated mice appeared to move less around the cage (although this was not measured). The physical appearance of the corticosterone-treated mice was also altered as they had oily-looking coats compared to the other treatment groups as evident in Figure 13. Drinking water behaviour was also altered with the corticosterone group drinking significantly ($p \leq 0.05$) more water than any other treatment group (Figure 14). This increase in drinking water began on day 4 of treatment and reached its maximum on day 19 of the study (Figure 15). At this maximum point, the corticosterone concentration was decreased in order to better match the target dose desired (Figure 15). The corticosterone concentration in the water was decreased to 50μg/ml from day 20 until the end of the study (indicated with an arrow) (Figure 16). At this lower dose, the drinking water behaviour became similar to the naïve and vehicle control mice in our study. The actual mirabegron doses administered were slightly below the target doses (Figure 17) (Figure 18).

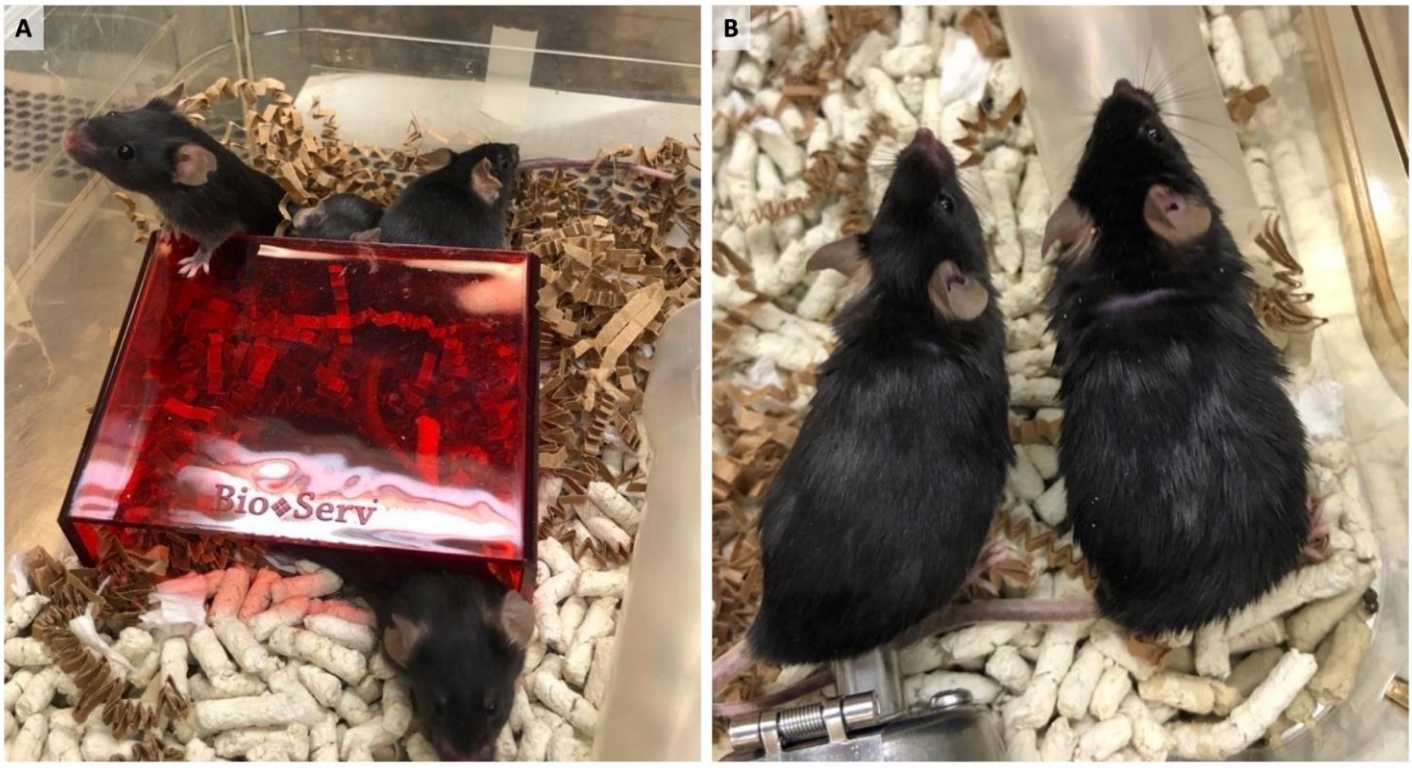

Figure 13: Photographs of the Mice in Animal Study #1.

A photograph of the high mirabegron (A) and corticosterone (B) treated mice. The oily coat and larger body size is apparent in the corticosterone group.

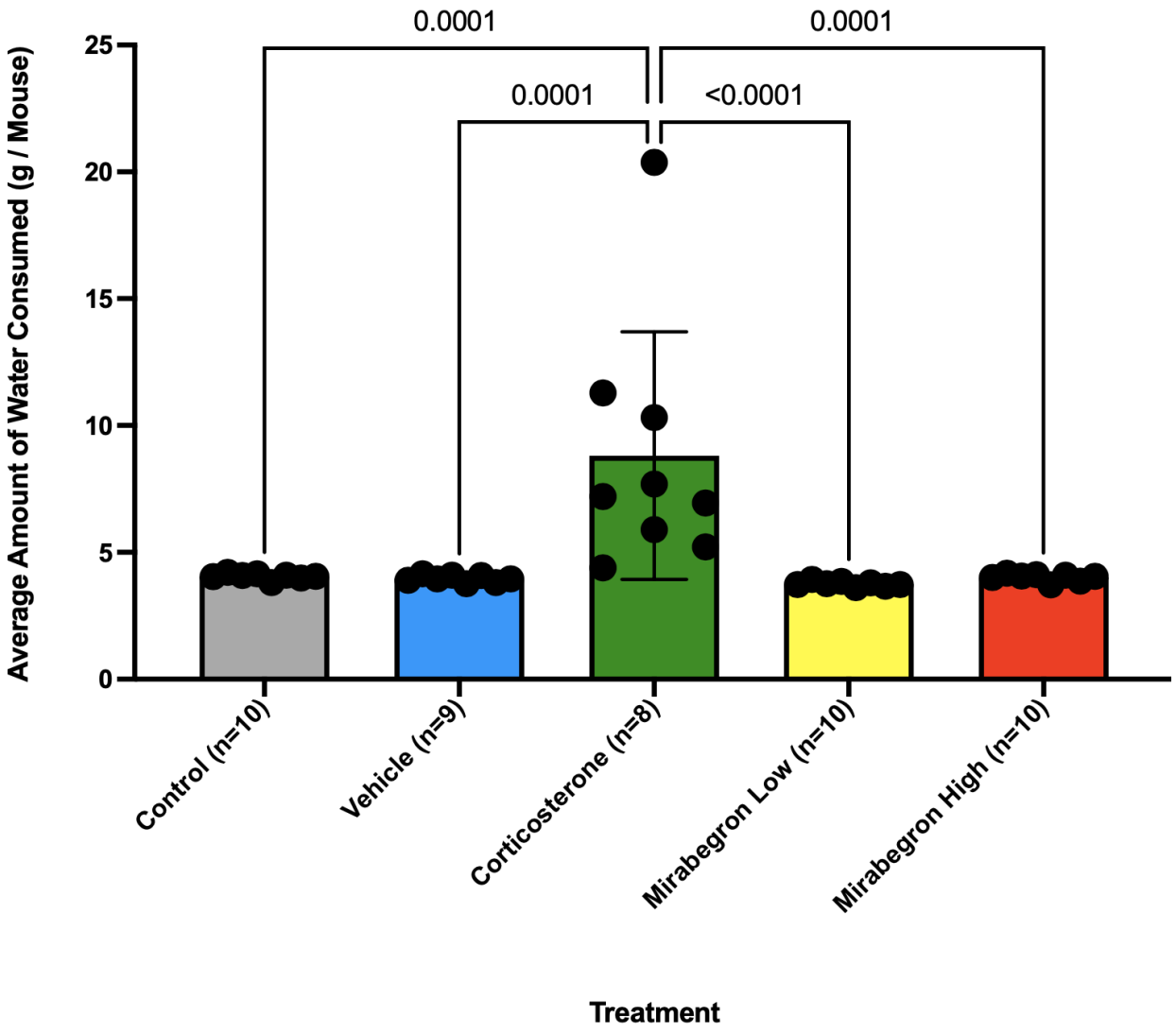

Figure 14: Average Drinking Water Consumption in Animal Study #1.

The corticosterone mice drank significantly ($p \leq 0.05$) more water than all other treatment groups.

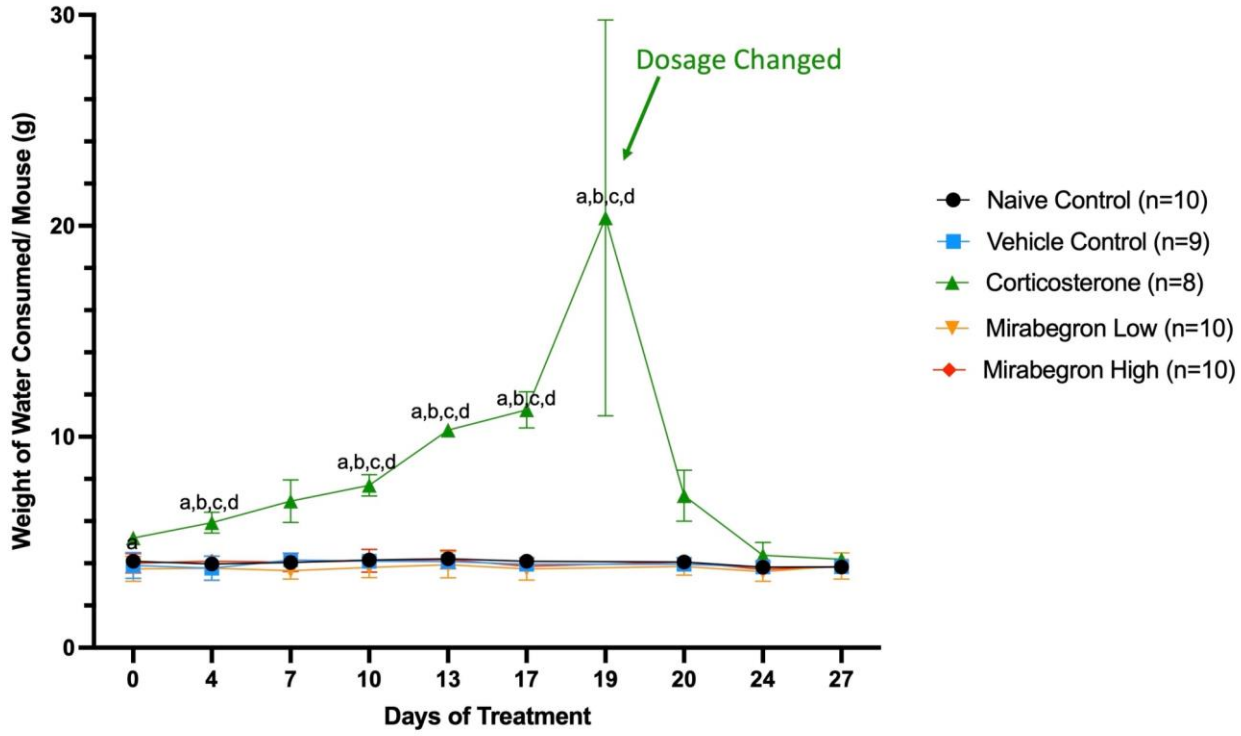

Figure 15: Drinking Water Consumption Throughout Animal Study #1.

Chronic corticosterone treatment resulted in mice drinking significantly ($p \leq 0.05$) more of the treatment water during the course of the experiment. The arrow indicates where the dose in the corticosterone water was lowered. (a) represents significantly ($p \leq 0.05$) different than the naïve control group on the day indicated, (b) represents significantly ($p \leq 0.05$) different from the vehicle control group on the day indicated, (c) represents significantly ($p \leq 0.05$) different from the mirabegron low treatment on the day indicated, and (d) represents significantly ($p \leq 0.05$) different from the mirabegron high treatment on the day indicated.

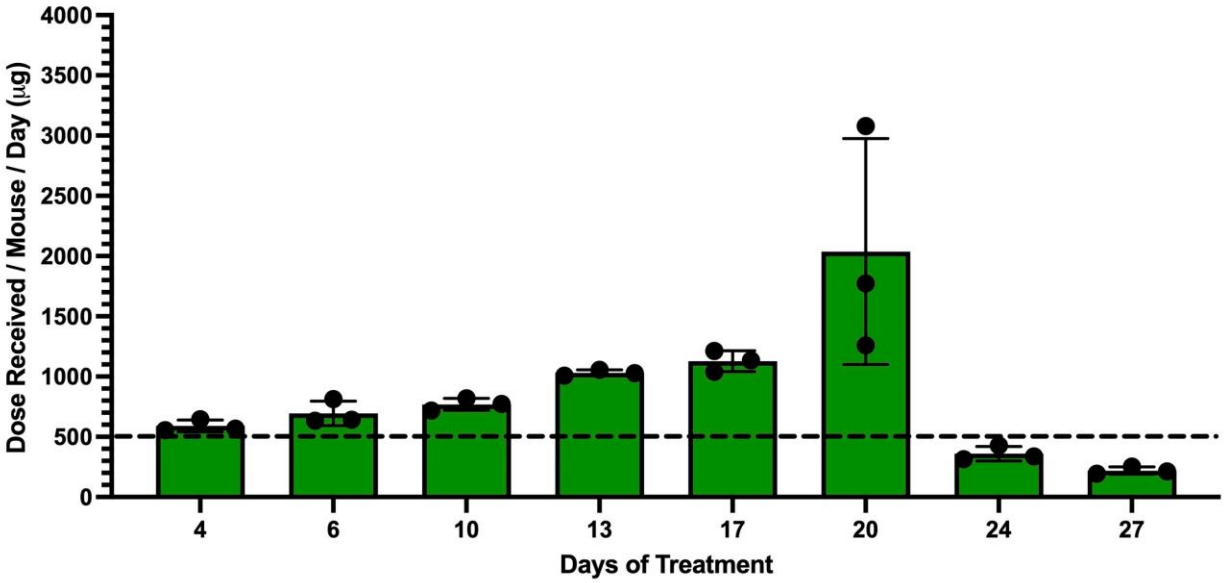

Figure 16: Administered and Target Dose for the Corticosterone Group for Animal Study #1.

The dose of corticosterone received per mouse per day during the course of the experiment. The 10 mice in this treatment were separated into 3 cages where the average dose received was calculated based on the water consumed for the cage and divided by the number of mice in that cage.The dashed line represents the desired dose to be delivered.

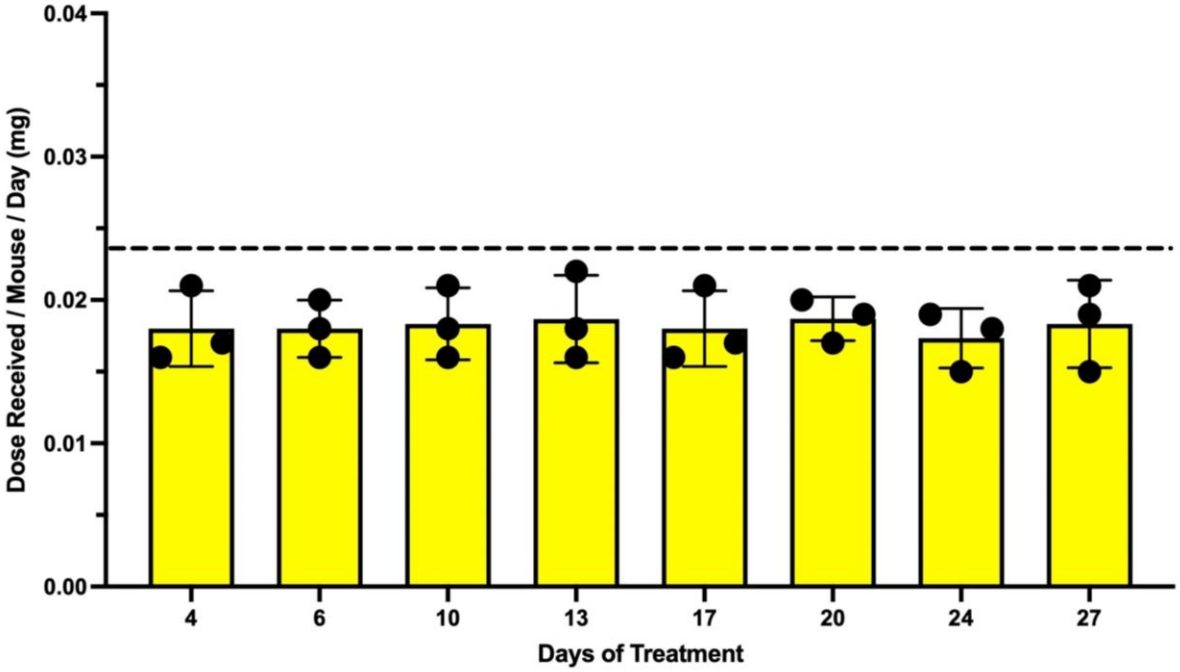

Figure 17: Administered and Target Dose for the Low Mirabegron Group for Animal Study #1.

The dose of the mirabegron that the low dose treatment group received per mouse per day during the course of the experiment. The 10 mice in this treatment were separated into 3 cages where the average dose received was calculated based on the water consumed for the cage and divided by the number of mice in that cage. The dashed line represents the desired dose to be delivered.

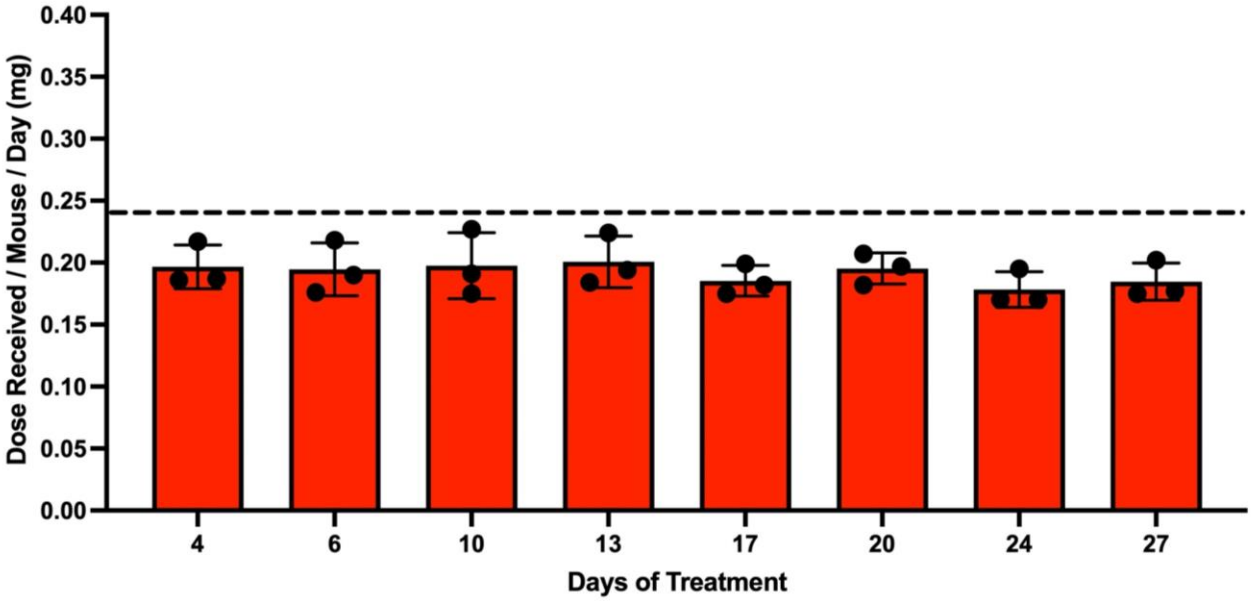

Figure 18: Administered and Target Dose for the High Mirabegron Group for Animal Study #1.

The dose of the mirabegron that the high dose treatment group received per mouse per day during the course of the experiment. The 10 mice in this treatment were separated into 3 cages where the average dose received was calculated based on the water consumed for the cage and divided by the number of mice in that cage. The dashed line represents the desired dose to be delivered.

Corticosterone and mirabegron treatments altered the tissue appearance, size, and morphology

The corticosterone-treated mice displayed observable phenotypical changes in the tissue with both WAT and BAT displaying a larger size in comparison to naïve and vehicle controls and both mirabegron treatments (Figure 19). The BAT also displayed a lighter brown colour in comparison to the controls. The high mirabegron treated mice had BAT that was subjectively a darker brown colour in comparison to the vehicle control (Figure 19), although, this was not quantified. Both the BAT weights (Figure 20A) and BAT weights relative to body weight (Figure 20B) were significantly ($p \leq 0.05$) heavier in the corticosterone-treated mice compared to all other treatment groups. Both the WAT weights (Figure 21A) and WAT weights relative to body weight (Figure 22B) were significantly ($p \leq 0.05$) heavier in the corticosterone-treated mice compared to all other treatment groups.

Histological examination of the BAT also reveals large differences between the corticosterone and other treatment groups (Figure 22). A significant ($p \leq 0.05$) increase in the mean lipid droplet (LD) area is apparent in the corticosterone-treated group (Figure 23A). The high mirabegron treatment was not significantly different from the naïve or vehicle controls and closely resembles them upon visual examination. The low mirabegron treatment had significantly ($p \leq 0.05$) larger lipid droplet areas than both the naïve and vehicle controls. The distribution of the LD areas reveals an increased frequency of larger LDs in the corticosterone treatment group (Figure 23B).

Histological examination of the WAT also reveals large differences between the corticosterone and other treatment groups (Figure 24). A significant ($p \leq 0.05$) increase in the

mean LD area is apparent in the LD distribution of the WAT depot when compared to all other treatments (Figure 25A). The distribution of the LD areas reveals an increased frequency of larger LDs in the corticosterone treatment group (Figure 25B).

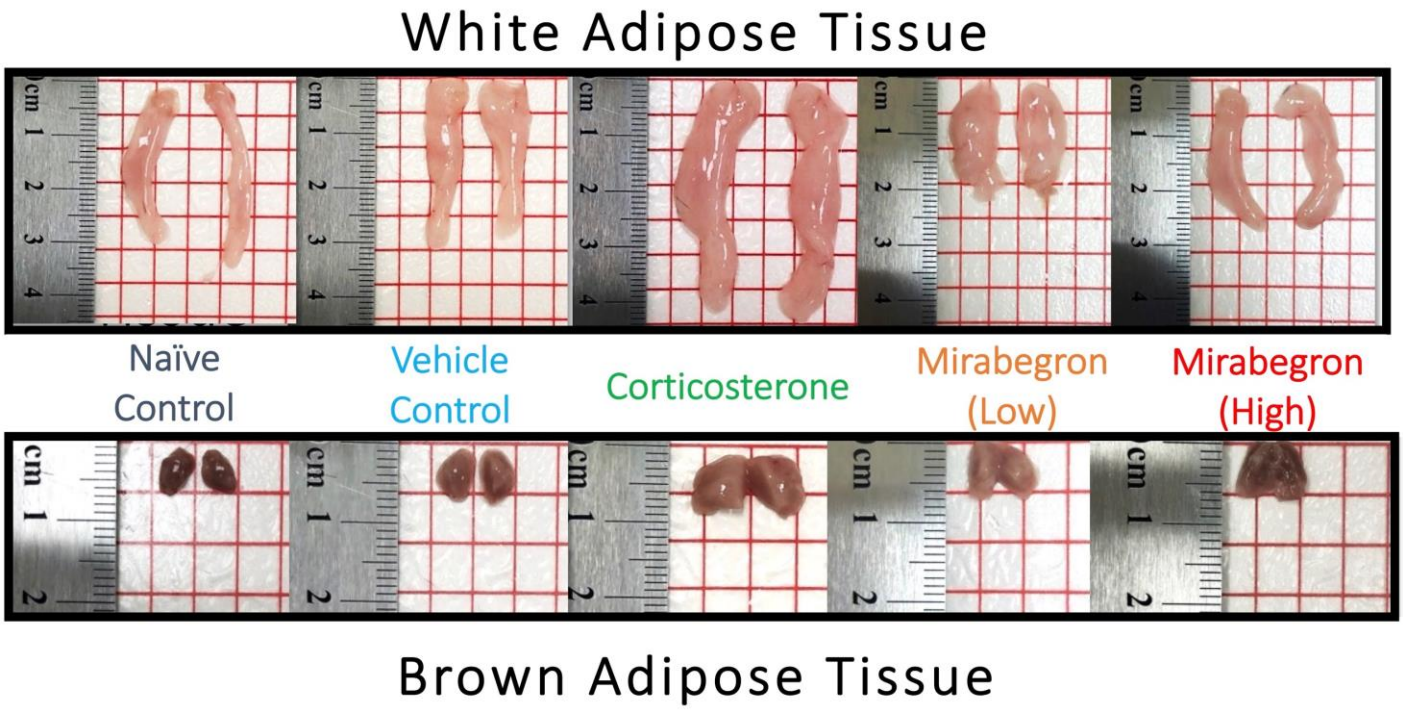

Figure 19: Adipose Tissue Visual Comparison for Animal Study #1.

A visual comparison of the inguinal white (top) and interscapular brown (bottom) AT depots from each of the treatment groups. The corticosterone treated mice exhibited much larger WAT and BAT compared to all other treatment groups. The grid represents 1/4 inch and the ruler illustrates the measurements of each tissue in centimeters.

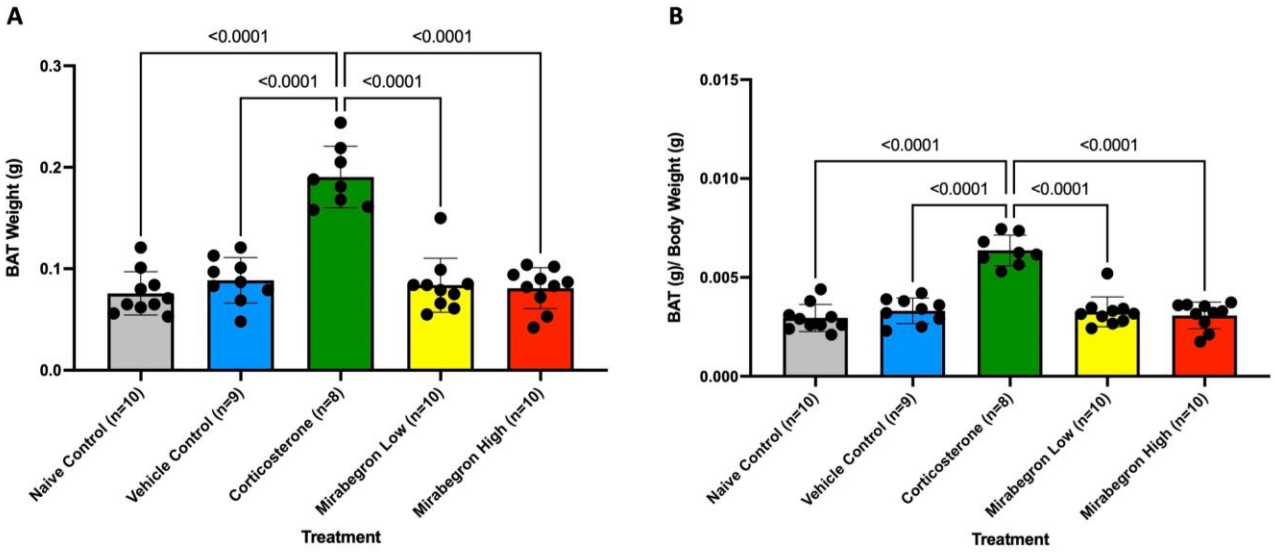

Figure 20: BAT Weights and Ratio for Animal Study #1.

Comparison of the BAT from each treatment displayed as absolute weight (A) and relative to body weight (B). The corticosterone treatment significantly ($p \leq 0.05$) increased BAT weights compared to the other treatment and control groups.

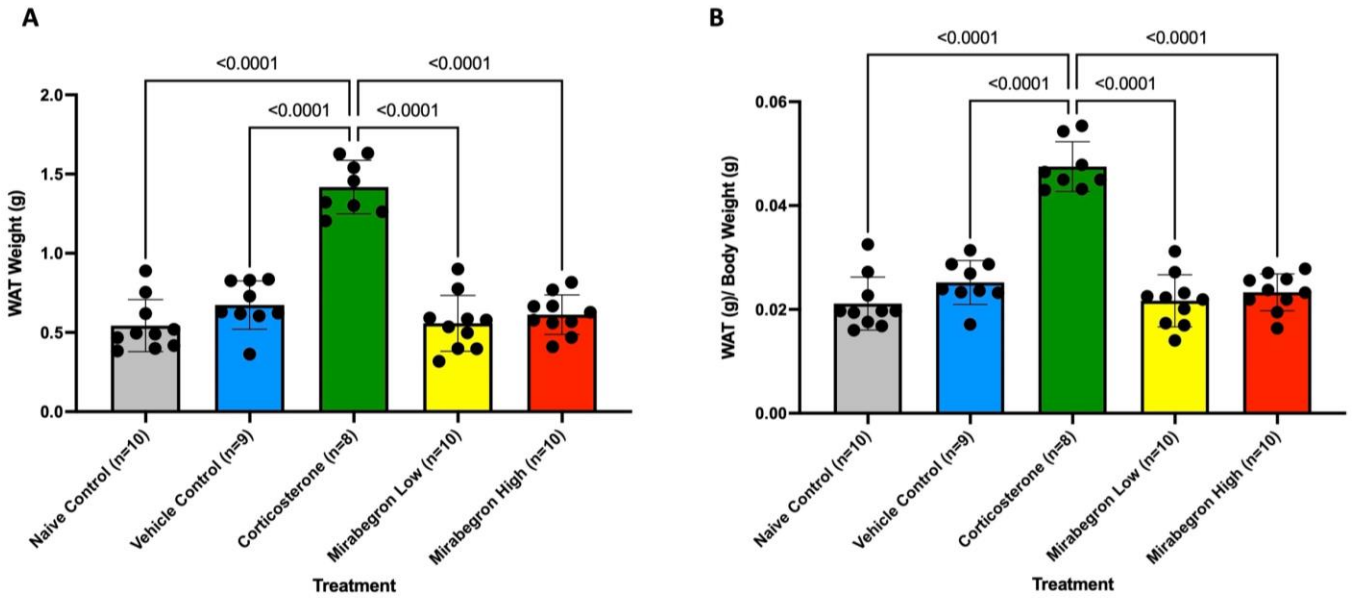

Figure 21: WAT Weights and Ratio for Animal Study #1.

Comparison of the inguinal WAT (ingWAT) from each treatment displayed as absolute weight (A) and relative to body weight (B). The corticosterone treatment significantly ($p \leq 0.05$) increased WAT weights compared to other treatment and control groups in this study.

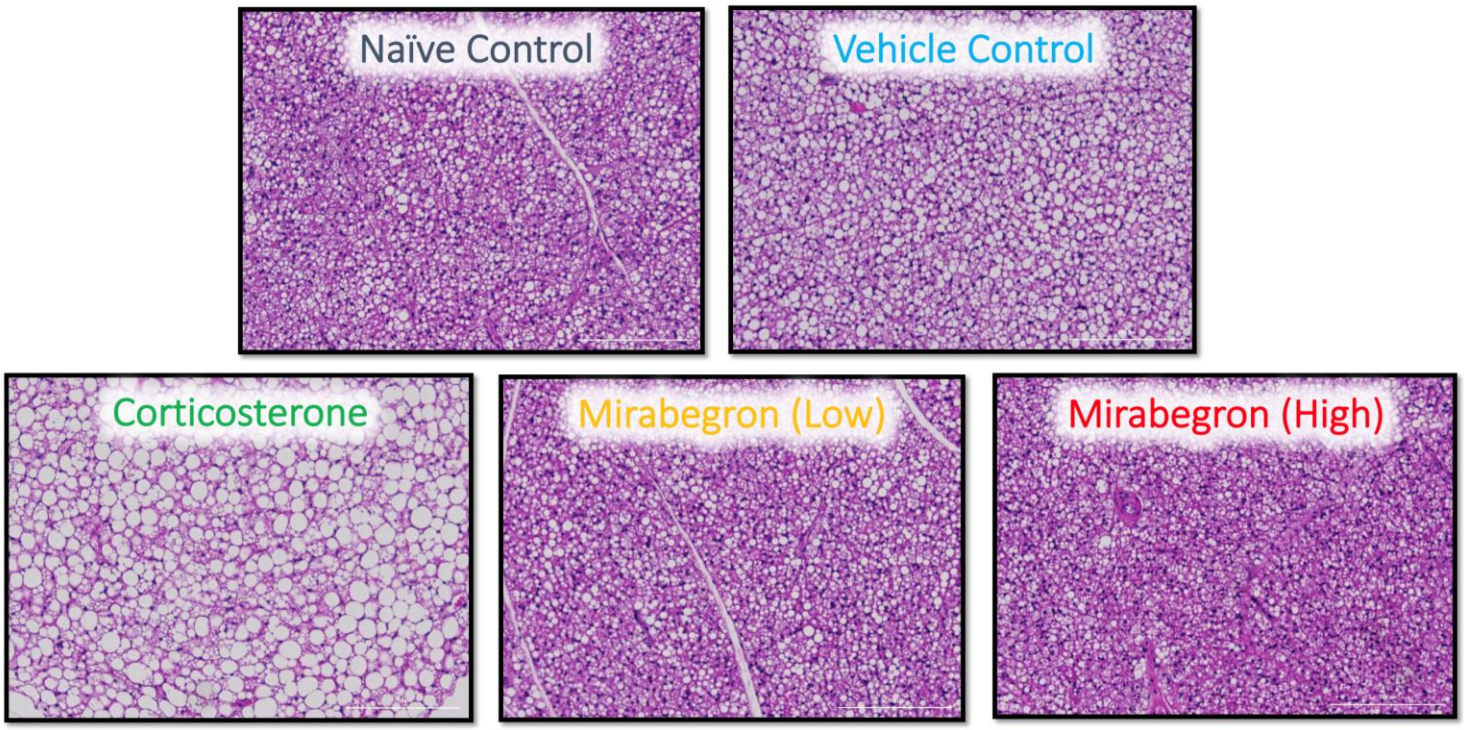

Figure 22: Representative BAT Histology from Animal Study #1.

Representative images of BAT at 10X magnification (H&E staining) from each treatment where the scalebar represents 200µm in the field of view. H&E staining allowed for lipid droplet size to be determined from each AT sample.

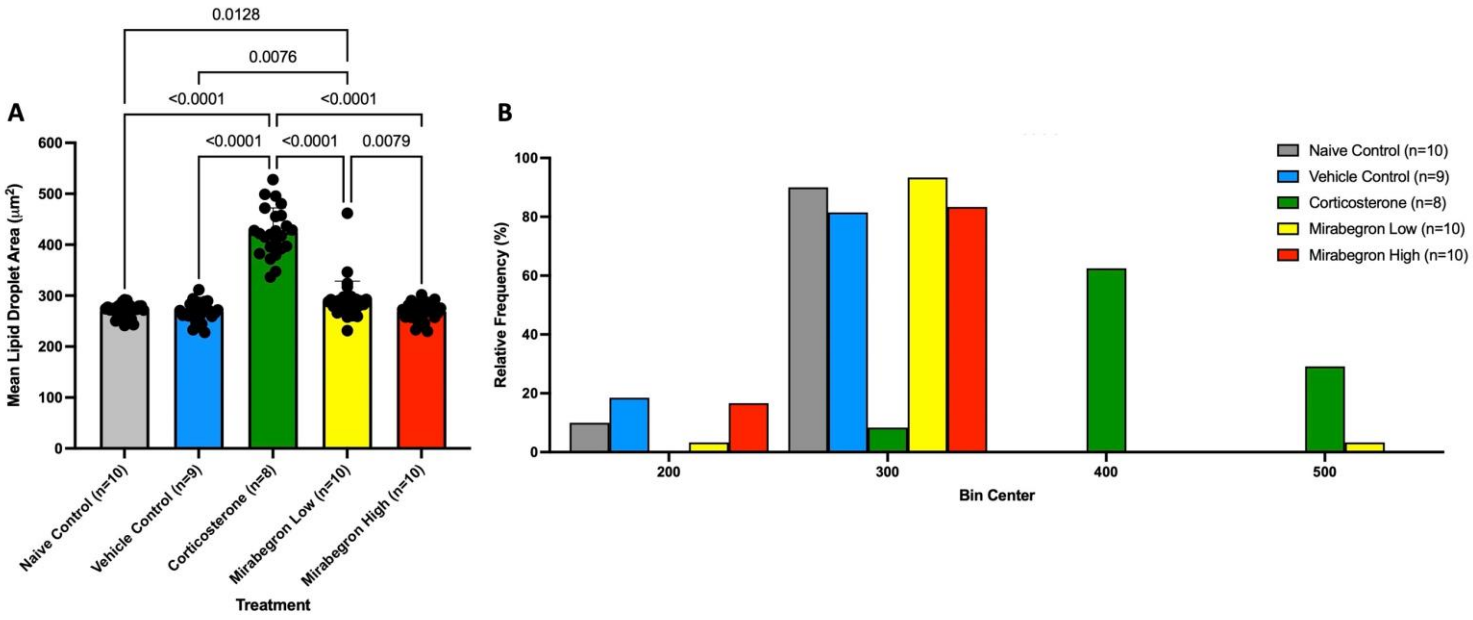

Figure 23: Comparison of BAT Lipid Droplet Area from Animal Study #1.

The mean lipid droplet area from three separate fields of view were determined through the automated programming in order to avoid any biases. Panel A illustrates the three average lipid droplet areas from each field of view for each sample from each treatment group and panel B illustrates the frequency distribution of the mean lipid droplet area (bin center). All fields of view are represented in the figure, but the statistical tests were conducted on averaged field of view per animal. Bin centers represented in this figure are BAT lipid droplet areas of: 150-250μm^2, 250-350μm^2, 350-450μm^2, and 450-550μm^2. The corticosterone treatment illustrates significantly ($p \leq 0.05$) larger lipid droplets than all other treatment groups (A). The corticosterone treatment has a greater percentage of lipid droplets (bin centers) that are larger in size than the other treatment groups (B).

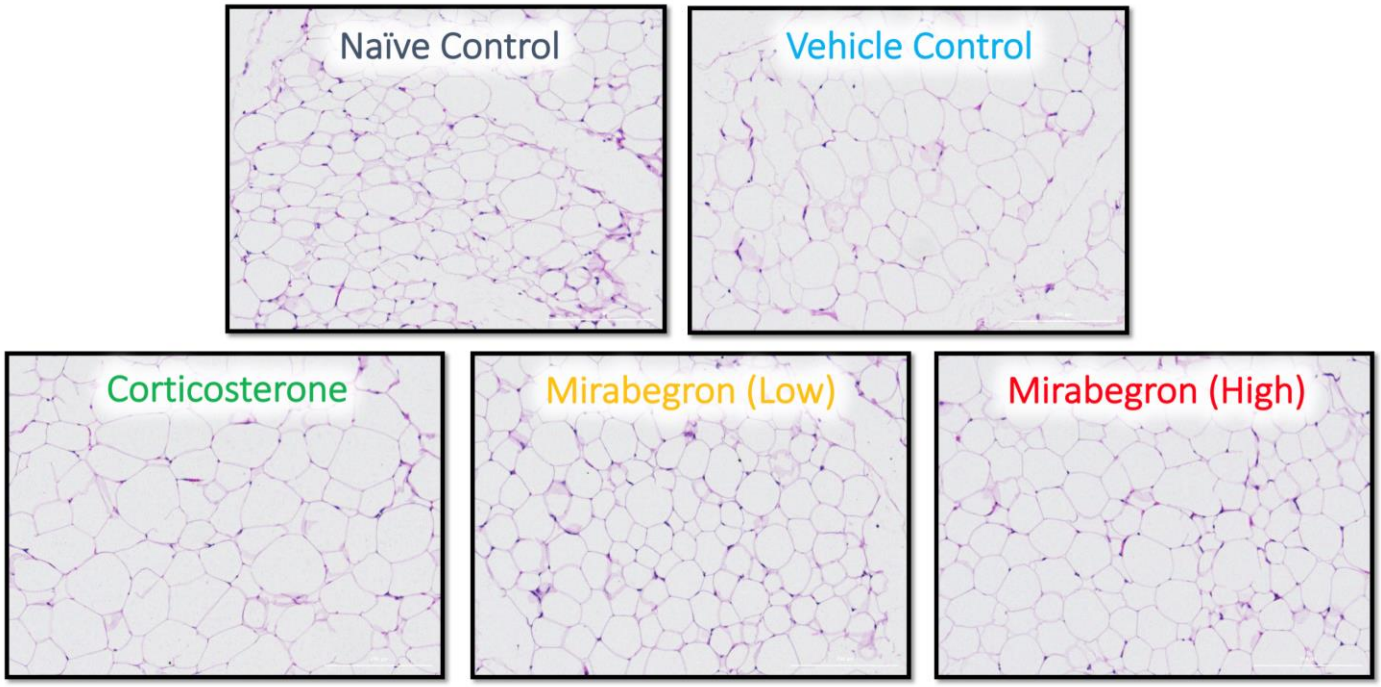

Figure 24: Representative WAT Histology from Animal Study #1.

Representative images of inguinal WAT (ingWAT) at 10X magnification (H&E staining) from each treatment where the scalebar represents 200µm in the field of view. H&E staining allowed for lipid droplet size to be determined from each AT sample.

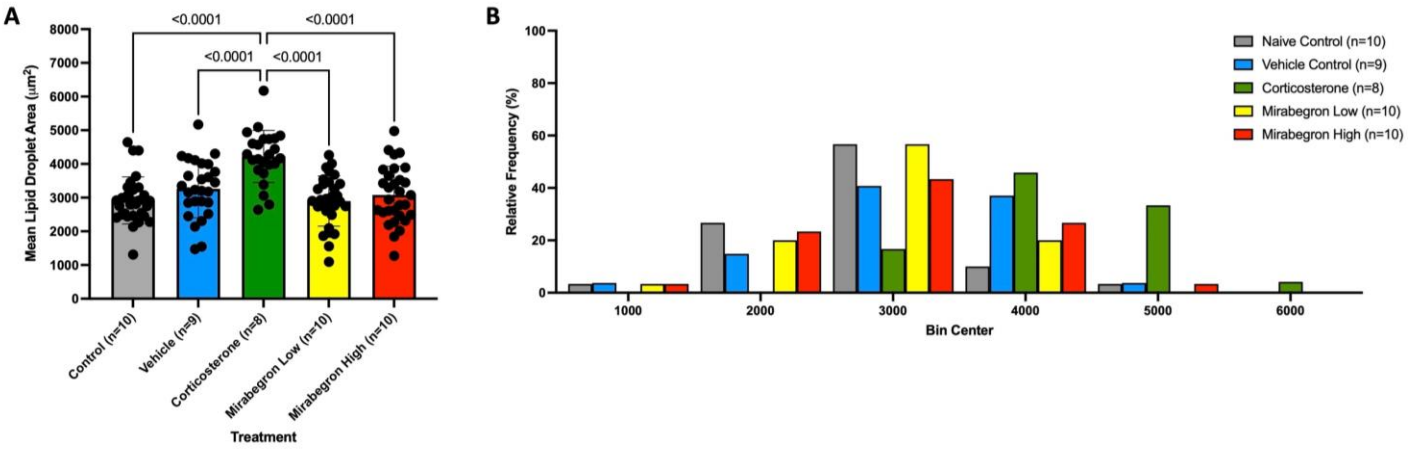

Figure 25: Comparison of WAT Lipid Droplet Area from Animal Study #1.

The mean lipid droplet area from three separate fields of view were determined through the automated programming in order to avoid any biases. Panel A illustrates the three average lipid droplet areas from each field of view for each sample from each treatment group and panel B illustrates the frequency distribution of the mean lipid droplet area (bin center). All fields of view are represented in the figure, but the statistical tests were conducted on averaged field of view per animal. Bin centers represented in this figure are WAT lipid droplet areas of: 1500-2500µm^2, 2500-3500µm^2, 3500-4500µm^2, and 4500-5500µm^2. The corticosterone treatment illustrates significantly ($p \leq 0.05$) larger lipid droplets than all other treatment groups (A). The corticosterone treatment has a greater percentage of lipid droplets (bin centers) that are larger in size than the other treatment groups (B).

Corticosterone and mirabegron treated mice display significantly elevated UCP1 expressions in BAT

Through western blot, the UCP1 expression was determined. The mirabegron treatments had significantly ($p \leq 0.05$) increased BAT UCP1 expression compared to both the naïve and vehicle controls (Figure 26). Surprisingly, the corticosterone-treated mice displayed UCP1 expression that was significantly ($p \leq 0.05$) higher with arbitrary units of 0.049 ± 0.016 when compared to the naïve (0.019 ± 0.012 a.u) and vehicle (0.017 ± 0.0107 a.u) controls, mirabegron low (0.034 ± 0.017 a.u), and mirabegron high (0.040 ± 0.007 a.u) treatments (Figure 26).

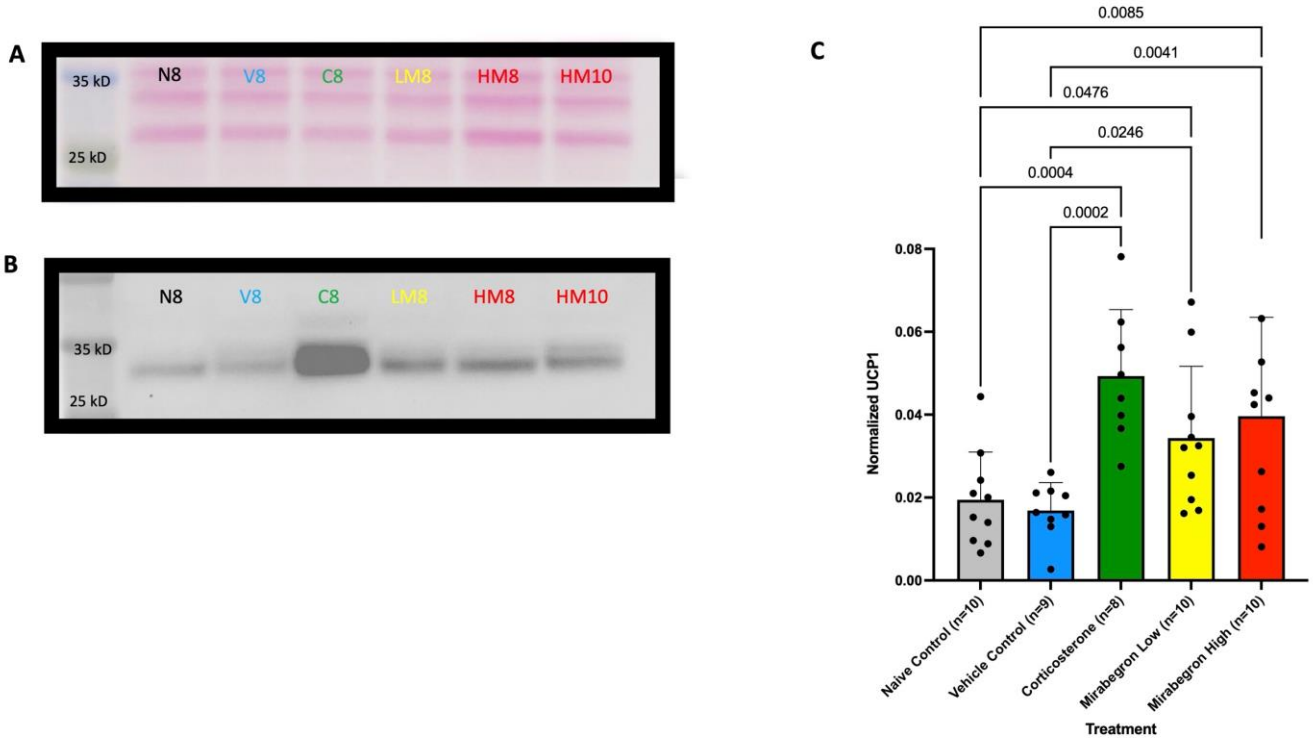

Figure 26: BAT UCP1 Protein Expression Following Animal Study #1.

A representative image of the ponceau S stain (panel A), protein expression of UCP1 (panel B), and normalized protein expressions (panel C) in BAT. Samples were separated on a 12% SDS-PAGE gel with 15µg of protein loaded into each lane. Western blot lane labels represent naïve control sample (N), vehicle control sample (V), corticosterone sample (C), low mirabegron sample (LM) and high mirabegron sample (HM). Samples were expressed relative to the loading control loaded onto each membrane. The corticosterone group had a significant ($p \leq 0.05$) increase in the amount of UCP1 expressed in the BAT of each of the treatment groups compared to the naïve and vehicle control groups. Both mirabegron groups also had significantly ($p \leq 0.05$) increased amounts of UCP1 expressed in the BAT compared to the naïve and vehicle controls.

WAT UCP1 expression was significantly reduced in the corticosterone treated mice

WAT UCP1 expression was determined through slot blots. Based on the protein concentration obtained from the WAT samples in this study, slot blots were performed in order to detect UCP1 within this AT depot. Slot blots allowed for 40µg of protein to be loaded onto the membrane. The corticosterone treatment resulted in a significantly ($p \leq 0.05$) reduced expression of UCP1 within the tissue compared to both mirabegron treatments and naïve control groups (Figure 27). Surprisingly, the naïve and vehicle controls displayed different UCP1 expressions. The naïve control group illustrated similar UCP1 expression, compared to the mirabegron treatments (Figure 27). However, both the low and high mirabegron treatment resulted in significantly ($p \leq 0.05$) increased UCP1 expression, compared to the vehicle control group.

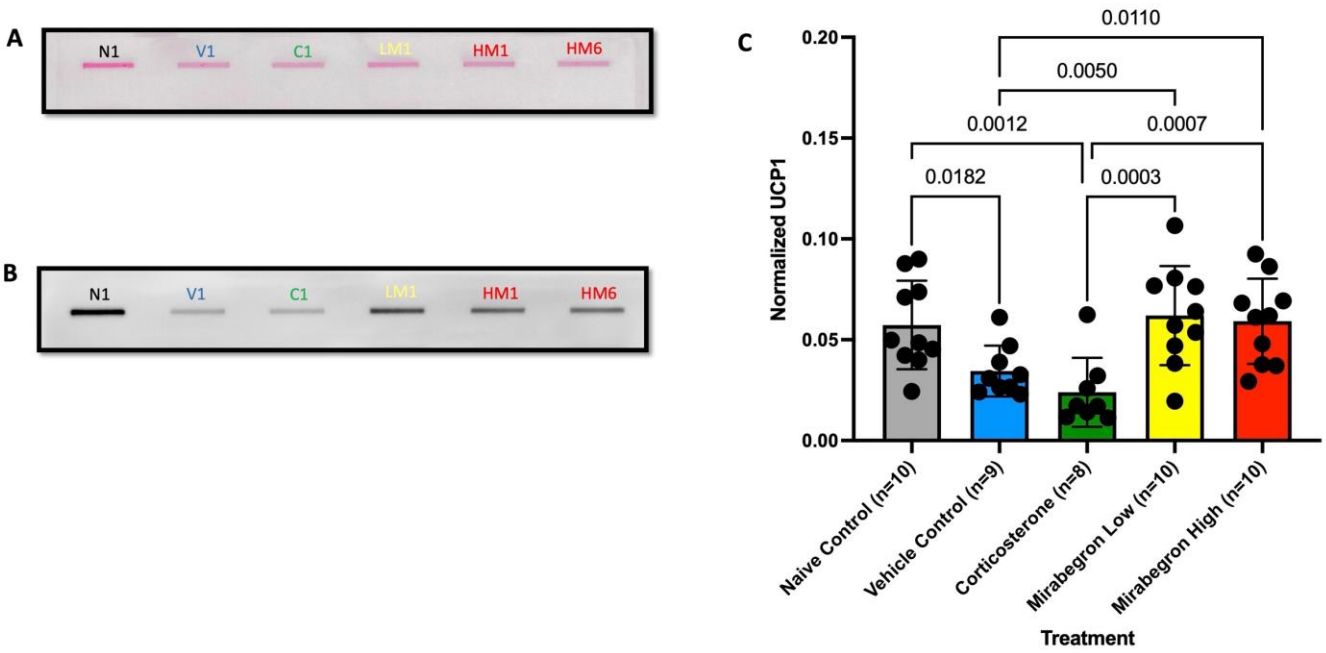

Figure 27: WAT UCP1 Protein Expression Following Animal Study #1.

A representative image of the ponceau S stain (panel A), protein expression of UCP1 (panel B), and normalized protein expressions (panel C). 40µg of protein loaded into each lane of the slot blot. Slot bot lane labels represent naïve control sample (N), vehicle control sample (V), corticosterone sample (C), low mirabegron sample (LM) and high mirabegron sample (HM). Slot blots were normalized back to the ponceau S stain for each sample. The corticosterone group had a significant ($p \leq 0.05$) decrease in the amount of UCP1 expressed in each WAT when compared to the naïve control, and mirabegron groups.

Mitochondrial content was unchanged

Citrate synthase was measured as a surrogate marker for mitochondrial content for each of the AT depots. Citrate synthase activity does not reflect mitochondrial content across all mouse tissues, especially in BAT and liver (McLaughlin et al., 2020). The activity of citrate synthase has only been validated as a marker for mitochondrial content in mouse skeletal muscle (McLaughlin et al., 2020). While citrate synthase protein is an accepted marker, it cannot be considered the gold standard for measuring mitochondrial content; however, the extensive measurements required to confirm mitochondrial content are beyond the scope of this study. Citrate synthase activity and protein expression were evaluated in omental AT from patients with obesity or who were diabetic (Christe et al., 2013). The activity and protein expression of citrate synthase were increased in patients with obesity, however only the protein amount increases in diabetic patients, and activity of citrate synthase remains unchanged (Christe et al., 2013). This increase in citrate synthase protein was deemed part of a compensatory mechanism whereby diabetes impairs this protein and its abilities (Christe et al., 2013). Therefore, protein measurements of citrate synthase are important when examining mitochondrial content and its influence on metabolic disease. Citrate synthase expression was not altered by the treatments in this study for either the BAT (Figure 28) or WAT (Figure 29), indicating there wasn't a difference in mitochondrial content. In order to determine if UCP1 normalized to mitochondrial content was altered with the treatments, a ratio was determined for the relative protein expression from each mouse in the study. When comparing the relative protein expression of UCP1 to citrate synthase in the BAT, there was a significant ($p \leq 0.05$) increase in the level of UCP1

in both the corticosterone and the high mirabegron treatment groups (Figure 30A). The WAT displayed opposite effects with corticosterone-treated mice displaying significantly ($p \leq 0.05$) less UCP1 relative to citrate synthase (Figure 30B) than the controls. The high mirabegron treatment was not significantly different from the naïve or vehicle controls (Figure 30B) while the UCP1 relative to citrate synthase in the low mirabegron group was higher, compared to the vehicle control group (Figure 30B).

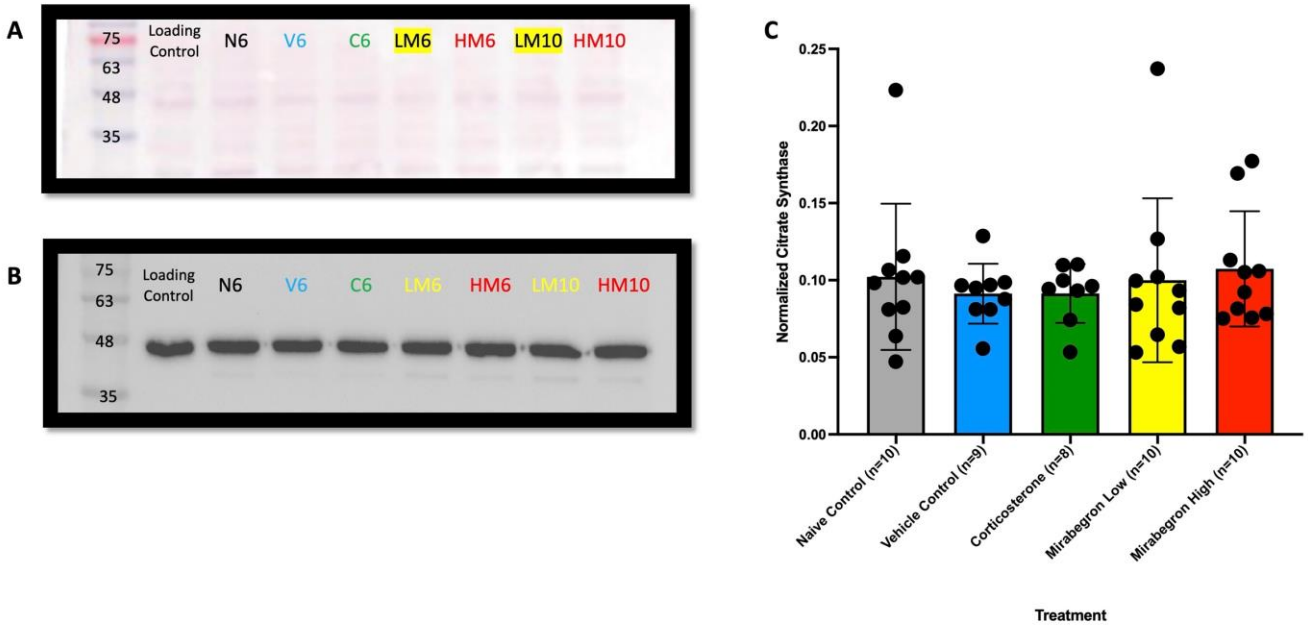

Figure 28: BAT Citrate Synthase Protein Expression Following Animal Study #1.

A representative image of the ponceau S stain (panel A), protein expression of citrate synthase (panel B), and normalized protein expressions (panel C) in BAT. Samples were separated on a 12% SDS-PAGE gel with 10µg of protein loaded into each lane. Western blot lane labels represent naïve control sample (N), vehicle control sample (V), corticosterone sample (C), low mirabegron sample (LM) and high mirabegron sample (HM). Samples were expressed relative to the loading control loaded onto each membrane.

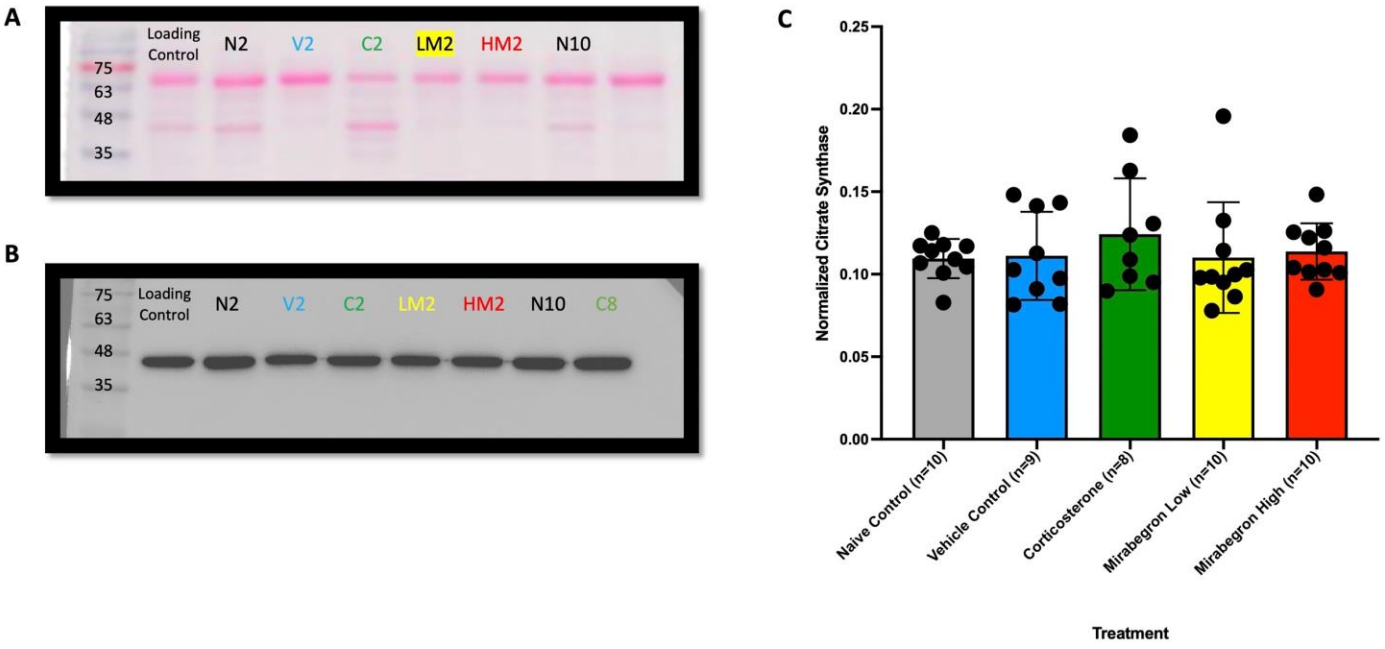

Figure 29: WAT Citrate Synthase Protein Expression Following Animal Study #1.

A representative image of the ponceau S stain (panel A), protein expression of citrate synthase (panel B), and normalized protein expressions (panel C) in WAT. Samples were separated on a 12% SDS-PAGE gel with 10µg of protein loaded into each lane. Western blot lane labels represent naïve control sample (N), vehicle control sample (V), corticosterone sample (C), low mirabegron sample (LM) and high mirabegron sample (HM). Samples were expressed relative to the loading control loaded onto each membrane.

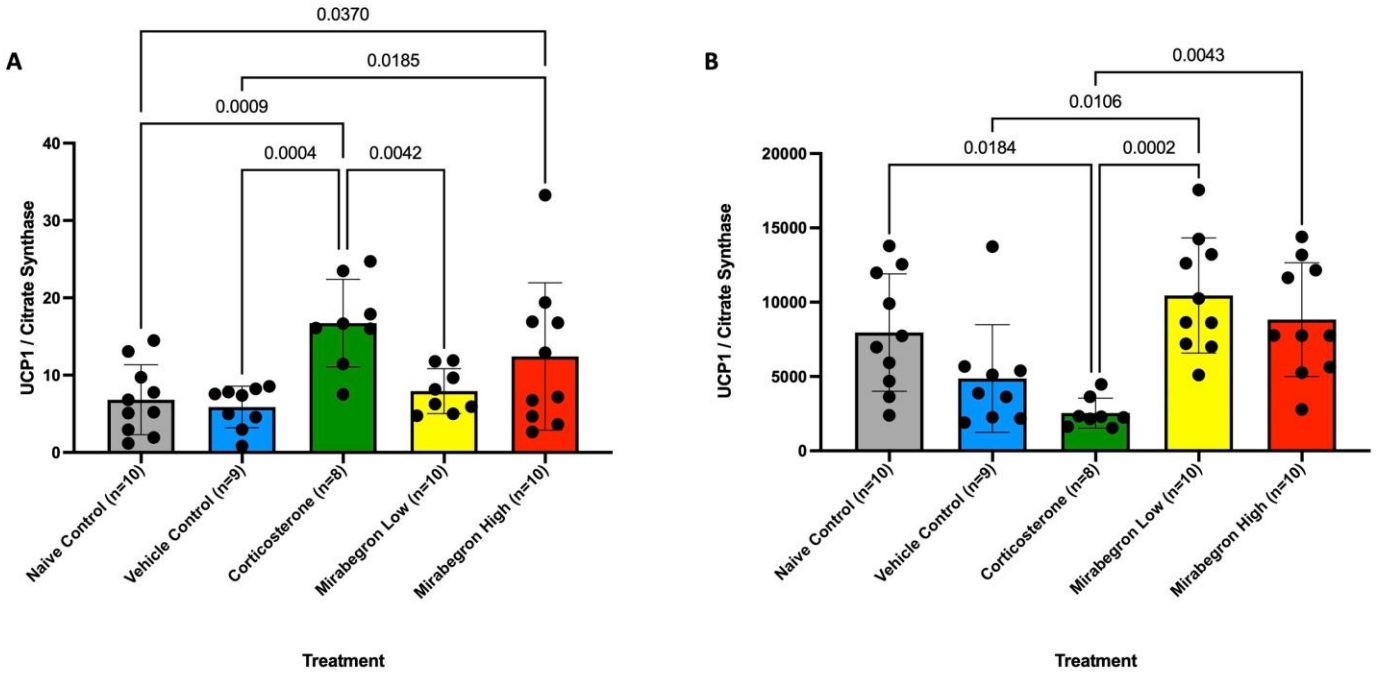

Figure 30: The Ratio of Uncoupling Relative to Mitochondrial Content in Animal Study #1.

The relative ratio of UCP1 to citrate synthase in each of the treatment groups for BAT (A) and WAT (B). (A) The corticosterone group illustrated significantly ($p \leq 0.05$) more UCP1/citrate synthase than the naïve control, vehicle control, and low mirabegron treatments in the BAT. The high mirabegron treatment also displayed significantly ($p \leq 0.05$) more UCP1/citrate synthase than the naïve and vehicle controls in the BAT. (B) The WAT illustrated significantly ($p \leq 0.05$) more UCP1/citrate synthase in the naïve control and with both mirabegron treatments. The corticosterone group had significantly less UCP1/citrate synthase than the naïve control and mirabegron treatments.

Lipid peroxidation marker 4-HNE was not affected by the treatments

Increased oxidative stress is associated with obesity and metabolic syndrome (Masschelin et al., 2020). With this study's focus on AT, how lipids are oxidized was of particular interest in each AT depot. As a measure of lipid peroxidation, 4-HNE was measured with slot blots. Slot blots were used for both tissues in order to concentrate all protein adducts into a singular band and allow for direct analysis. Only 5-10μg of protein were loaded for BAT and WAT respectively due to the sensitivity of this measurement. Both BAT and WAT were analyzed by slot blots for the amount of lipid peroxidation within each tissue. Surprisingly, both the BAT (Figure 31) and WAT (Figure 32) were unaffected by the corticosterone and mirabegron treatments. Upon observation of the blots, it appeared as though the samples with high 4-HNE protein adduct formation in the BAT, were also elevated in the WAT, regardless of the treatment group the sample originated from. A Pearson correlation analysis was then performed and revealed a moderate positive correlation (coefficient of 0.6422) (Figure 33) illustrating this observed relationship.

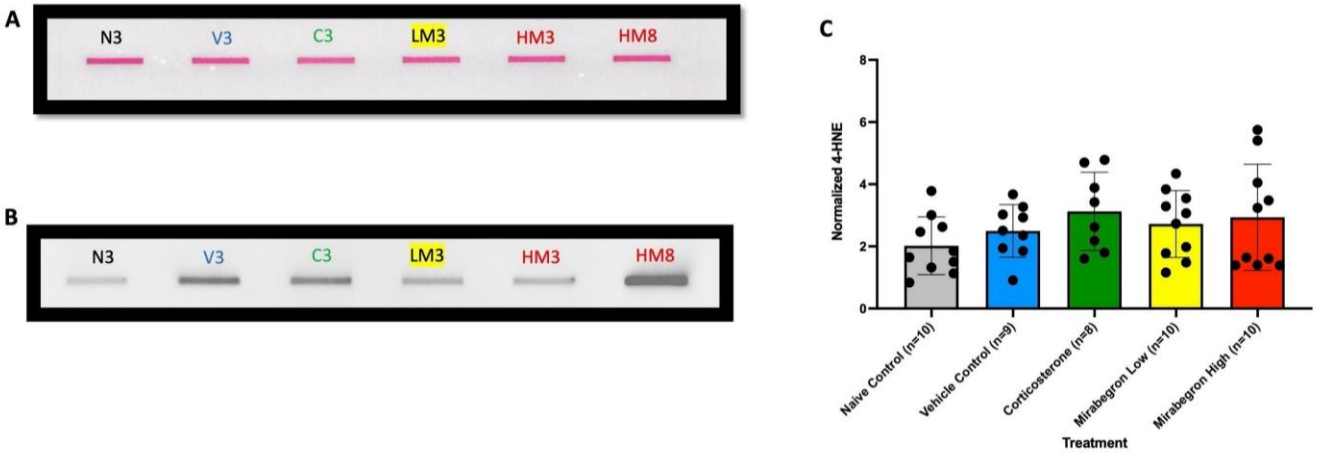

Figure 31: BAT Protein Adducts of 4-HNE Following Animal Study #1.

A representative image of the ponceau S stain (panel A), protein adduct formation of 4-HNE (panel B), and normalized protein adduct formation (panel C). 5µg of BAT protein loaded into each lane of the slot blot. Lane labels represent naïve control sample (N), vehicle control sample (V), corticosterone sample (C), low mirabegron sample (LM) and high mirabegron sample (HM). Slot blots were normalized back to the ponceau S stain for each sample.

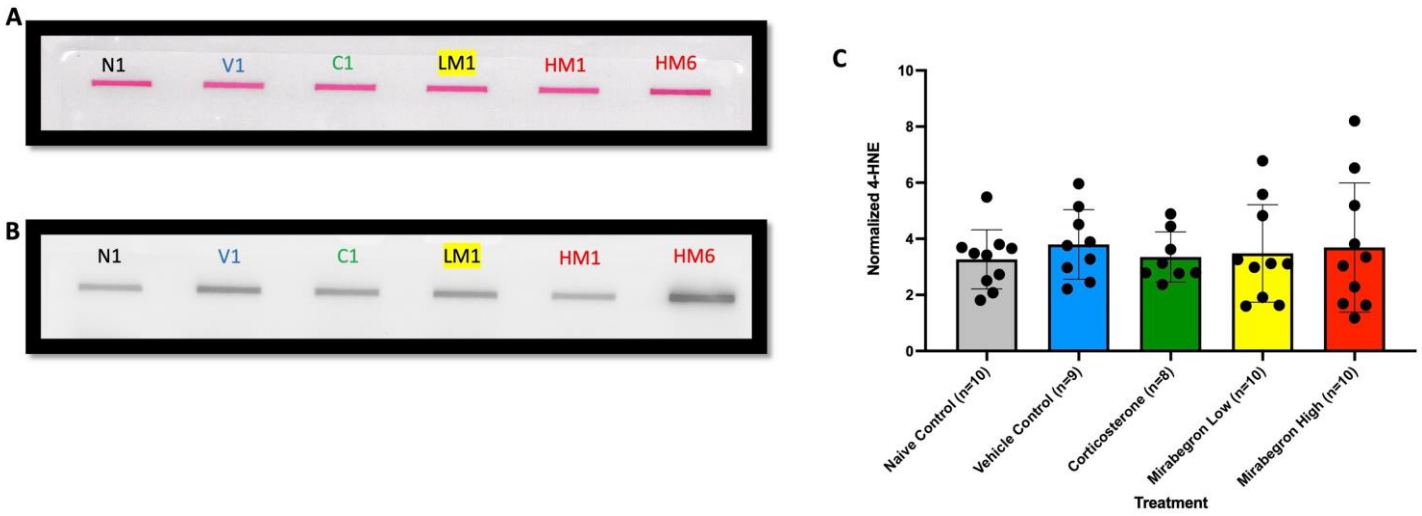

Figure 32: WAT Protein Adducts of 4-HNE Following Animal Study #1.

A representative image of the ponceau S stain (panel A), protein adduct formation of 4-HNE (panel B), and normalized protein adduct formation (panel C). 10µg of WAT protein loaded into each lane of the slot blot. Lane labels represent naïve control sample (N), vehicle control sample (V), corticosterone sample (C), low mirabegron sample (LM) and high mirabegron sample (HM). Slot blots were normalized back to the ponceau S stain for each sample.

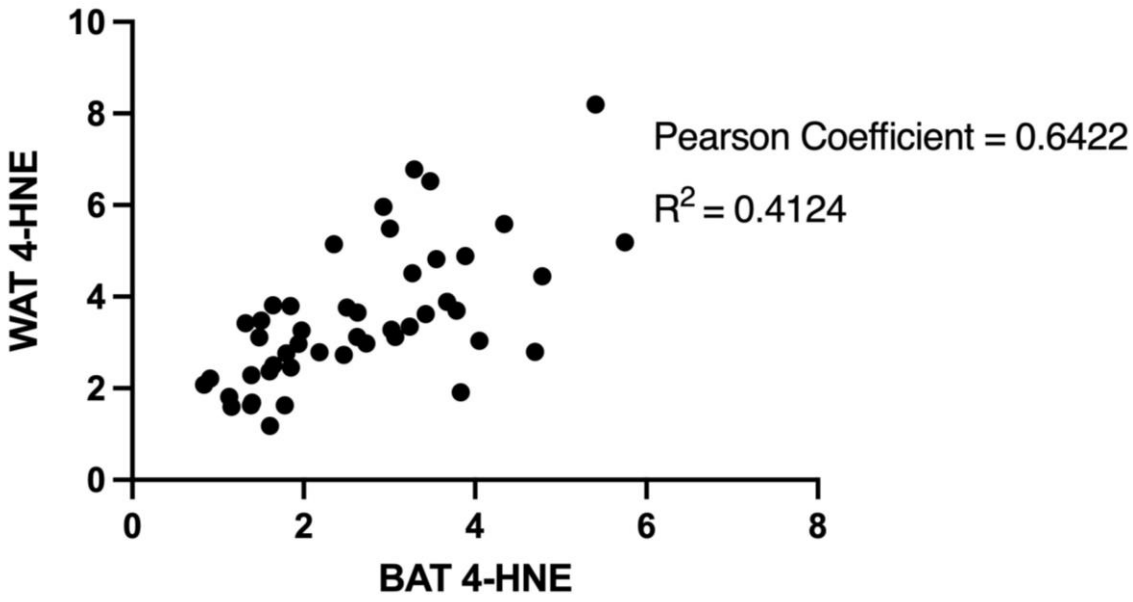

Figure 33: The Correlation Between the BAT and WAT Levels of 4-HNE from Animal Study #1.

The Pearson coefficient (0.6422) shows a moderate positive correlation.

Corticosterone treatment increases fasting plasma insulin levels and insulin resistance

Using commercially available assays, the plasma from each mouse was analyzed for their fasting glucose and insulin concentrations. The HOMA-IR values were then computed to determine the level of insulin resistance under each treatment. The fasting glucose concentrations were not different between treatment groups (Figure 34A). However, the corticosterone group illustrated significantly ($p \leq 0.05$) elevated fasting insulin (Figure 34B) and HOMA-IR values (Figure 34C).

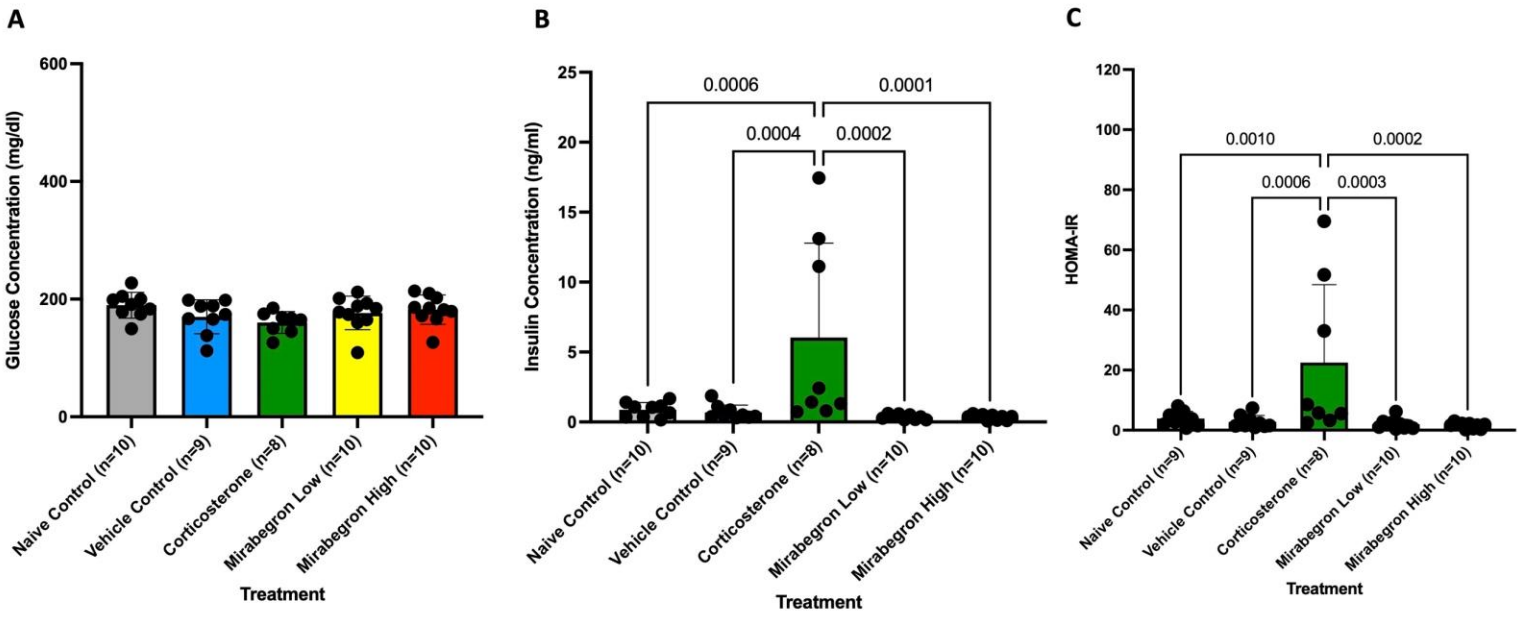

Figure 34: Animal Study #1 Plasma Measurements.

Plasma glucose (A) and insulin (B) measurements, and (C) HOMA-IR for each treatment. The corticosterone group illustrated significantly ($p \leq 0.05$) elevated insulin concentrations and insulin resistance (HOMA-IR) compared to all other treatment groups.

Animal Study #2 (AS2)

Corticosterone and combination treatments increased body weight

Throughout the experiment, corticosterone-treated mice illustrated significantly ($p \leq 0.05$) elevated body weights from day 14 until the end of the treatment (Figure 35). The combination treatment also resulted in significantly ($p \leq 0.05$) increased body weights when compared to the vehicle control and mirabegron treatment (Figure 35). The change in body weight from baseline was significantly ($p \leq 0.05$) elevated in the corticosterone and combination treatment groups (Figure 36). The fasting body weight was also significantly ($p \leq 0.05$) increased in the corticosterone and combination treatment groups (Figure 37).

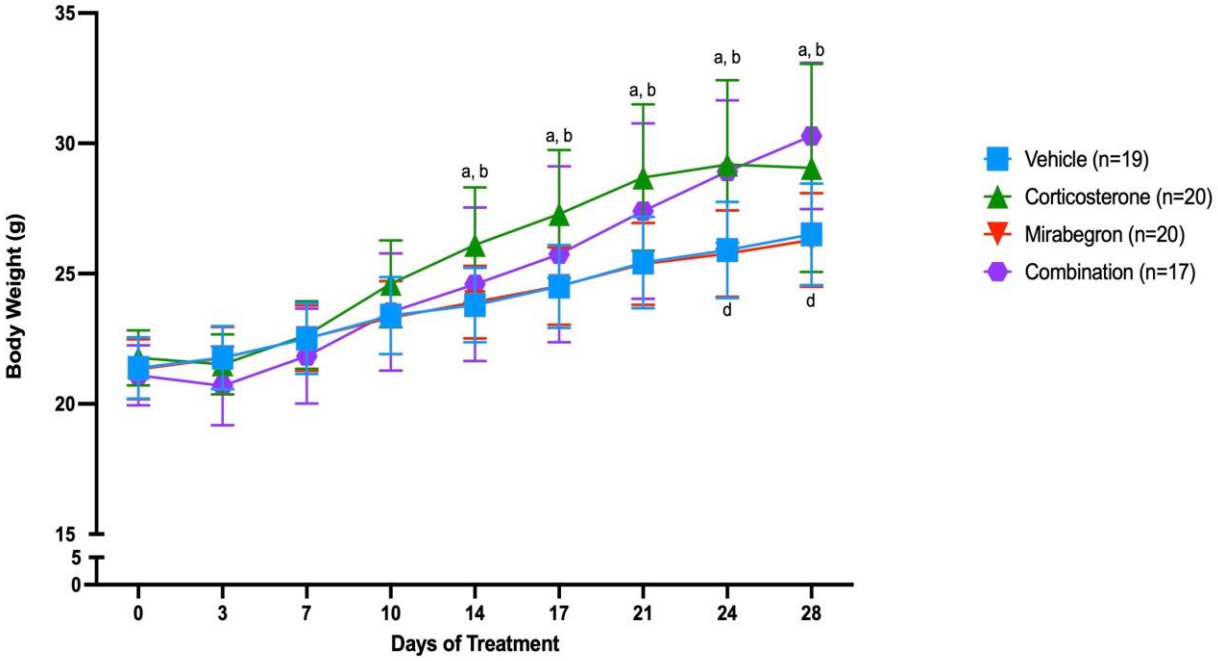

Figure 35: A Summary of the Body Weight over the course of Animal Study #2.

The body weight of the corticosterone treated mice increased significantly ($p \leq 0.05$) after 14 days of treatment compared to all other treatment groups. (a) represents significantly different ($p \leq 0.05$) from vehicle control on the day indicated, (b) represents significantly different ($p \leq 0.05$) from mirabegron treatment on the day indicated, (c) represents significantly different ($p \leq 0.05$) from the corticosterone treatment on the day indicated, (d) represents significantly different ($p \leq 0.05$) from combination treatment on the day indicated.

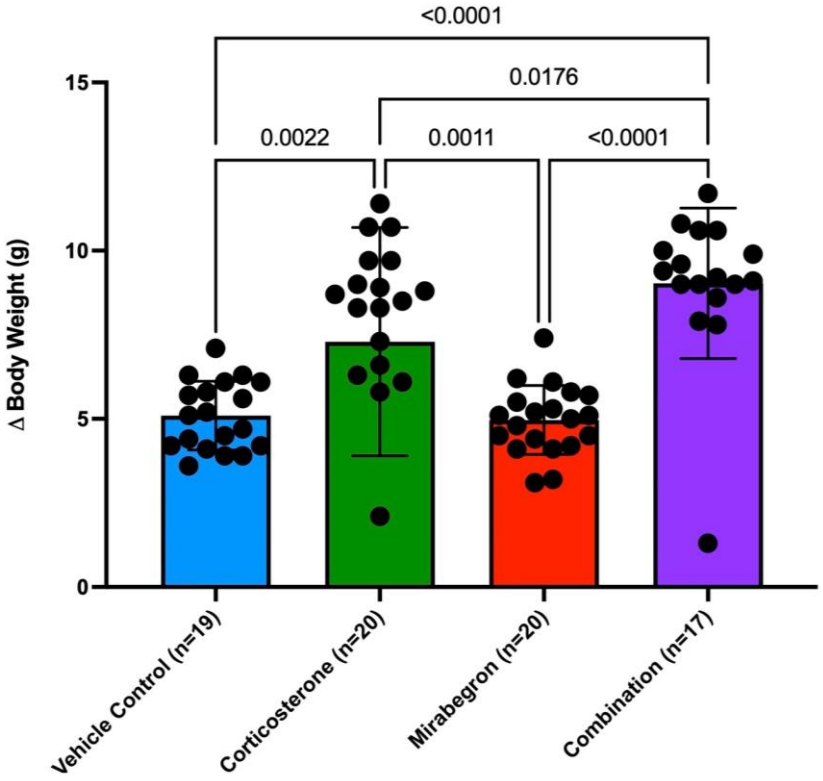

Figure 36: Overall Change in Body Weight after Animal Study #2.

The corticosterone mice illustrated a significant ($p \leq 0.05$) increase in weight gain from the start of the experiment. The combination treatment weighed significantly ($p \leq 0.05$) more than all other treatment groups.

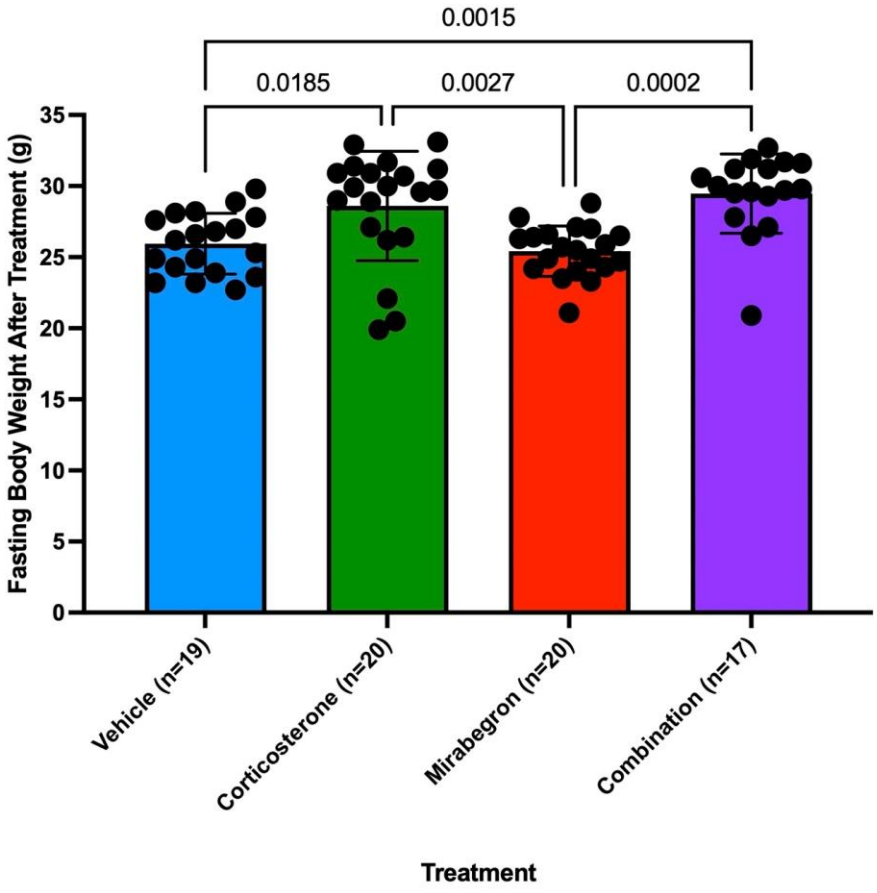

Figure 37: Fasting Body Weight in Animal Study #2.

At the time of euthanasia, the corticosterone and combination mice weighed significantly ($p \leq 0.05$) more than the mirabegron and vehicle control treatment groups.

Corticosterone and combination treatment mice had altered mouse physical appearance and drinking water behaviour

In addition to the significant ($p \leq 0.05$) increase in body mass in the corticosterone and combination treatments, these mice also appeared to move less around the cage (although this was not measured). The physical appearances of the corticosterone and combination mice were altered as they had oily-looking coats compared to the other treatment groups as evident in Figure 38. Their drinking water behaviour was altered with the corticosterone and combination groups where they drank significantly ($p \leq 0.05$) more water than the vehicle control or mirabegron treatment (Figure 39). With the information gained from AS1, the effects of corticosterone-induced water consumption were anticipated. In an attempt to balance these effects of corticosterone, the dose was lowered to 75μg/ml, allowing for the target dose of 500μg/mouse/day to be achieved (Figure 40). The actual mirabegron dose administered was also at the target dose (Figure 41). The delivered doses of corticosterone and mirabegron were also on target for the combination treatment (Figure 42).

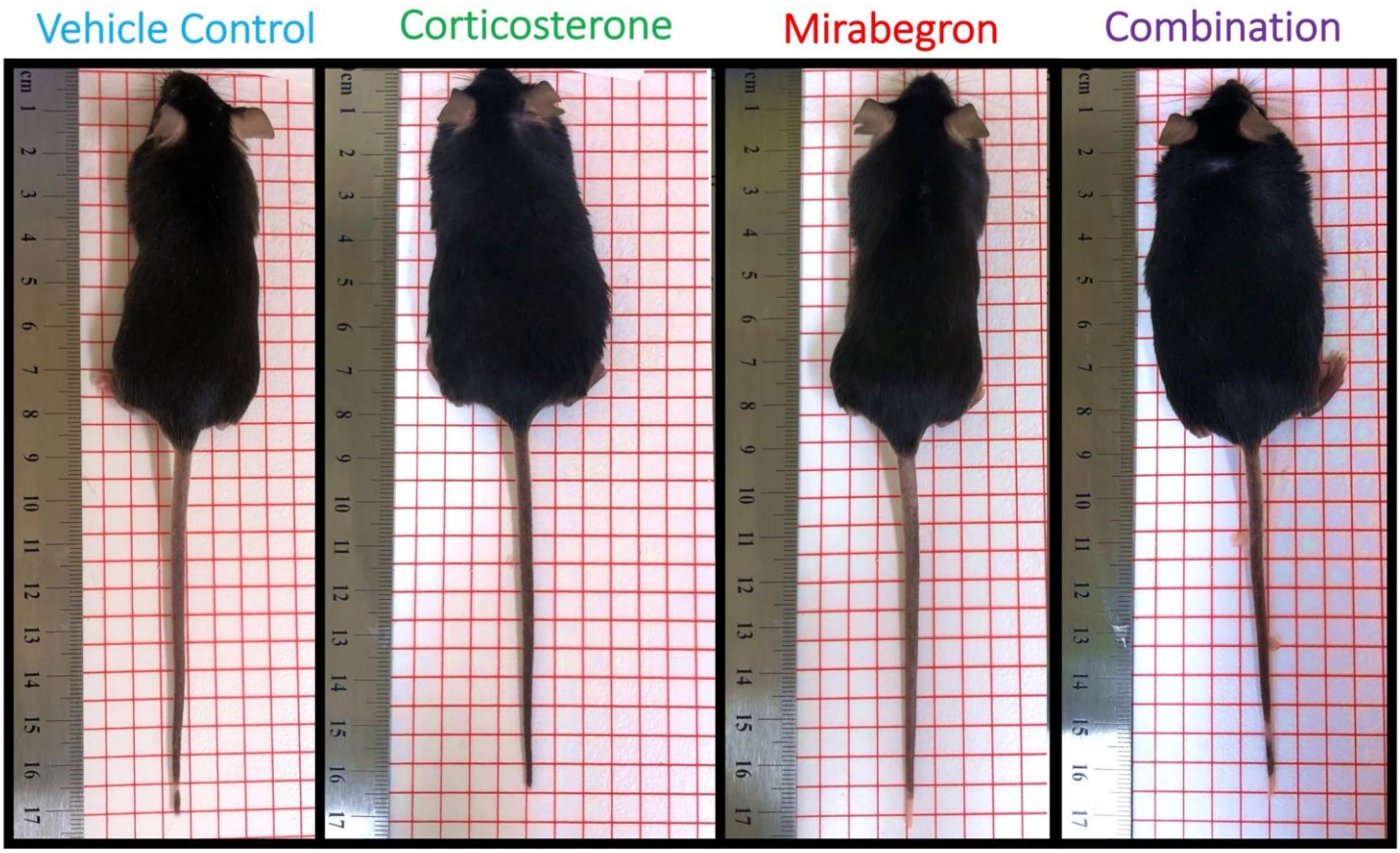

Figure 38: A Photograph of a Representative Mouse from Each Treatment in Animal Study #2.

The grid represents 1/4 inch and the ruler illustrates the measurements of each mouse in centimeters. The corticosterone and combination treatment groups resulted in an observable increase body size and width compared to the mirabegron and vehicle control groups.

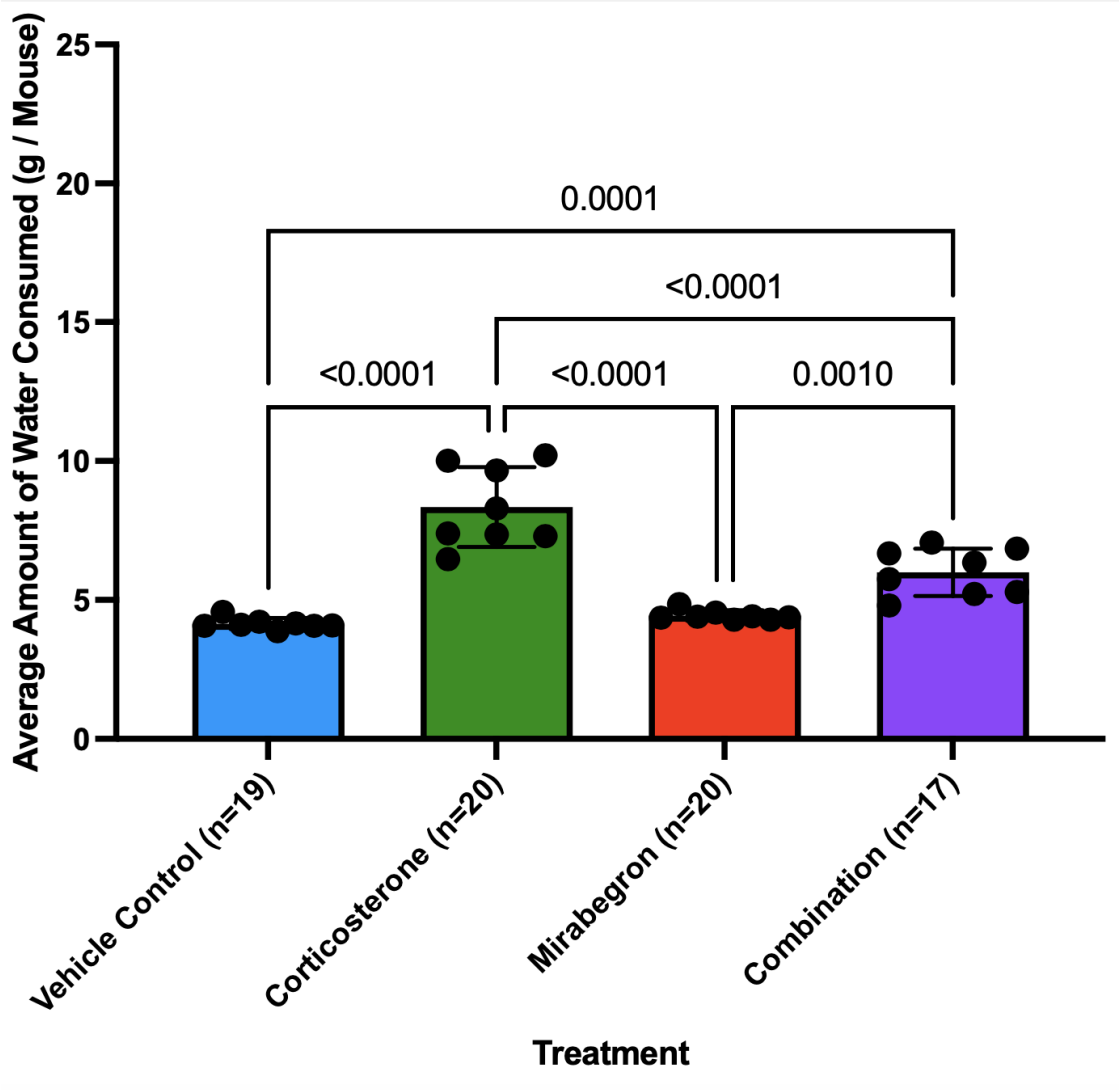

Figure 39: Average Water Consumption in Animal Study #2.

The corticosterone mice drank significantly ($p \leq 0.05$) more water than all other treatment groups. The combination treatment drank significantly ($p \leq 0.05$) more water than the vehicle control and mirabegron treatment.

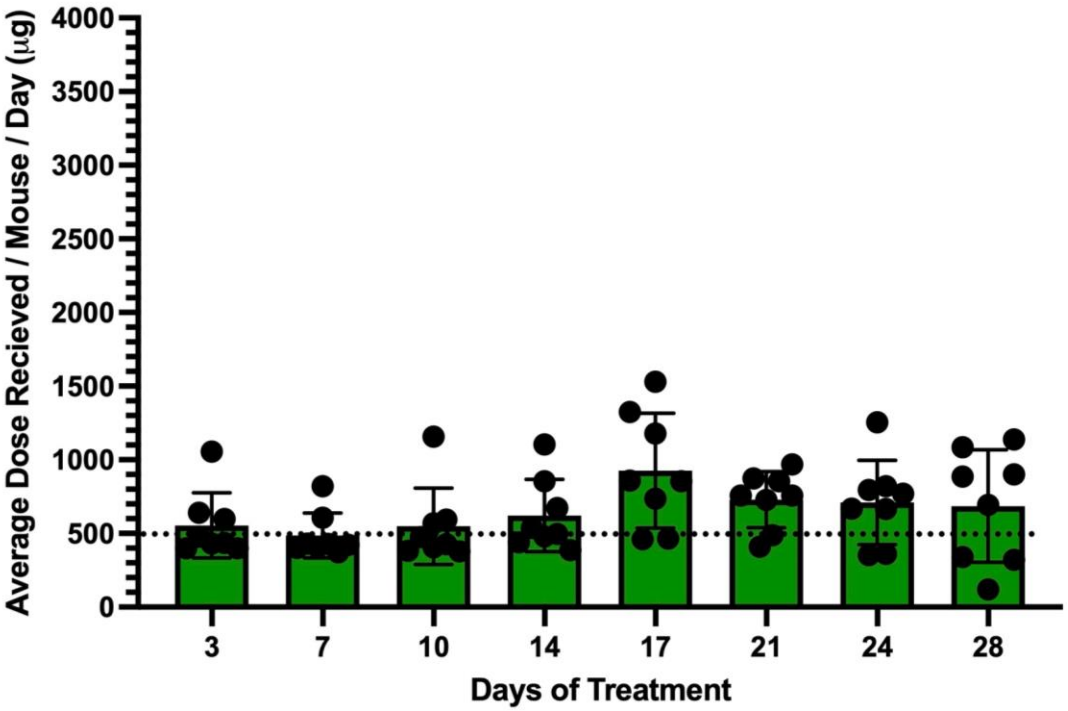

Figure 40: Administered and Target Dose for the Corticosterone Group in Animal Study #2.

The dose of corticosterone received per mouse per day during the course of the experiment. The 20 mice in this treatment were separated into 8 cages where the average dose received was calculated based on the water consumed for the cage and divided by the number of mice in that cage. The dotted line represents the desired dose to be delivered.

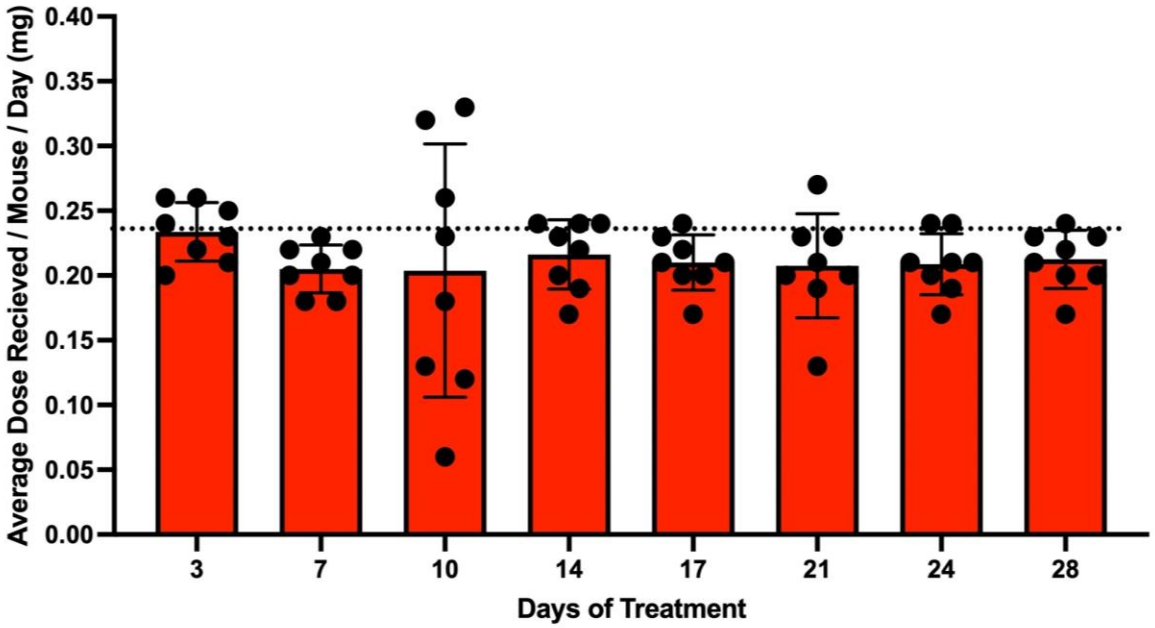

Figure 41: Administered and Target Dose for the Mirabegron Group in Animal Study #2.

The dose of the mirabegron that the treatment group received per mouse per day during the course of the experiment. The 20 mice in this treatment were separated into 8 cages where the average dose received was calculated based on the water consumed for the cage and divided by the number of mice in that cage. The dotted line represents the desired dose to be delivered.

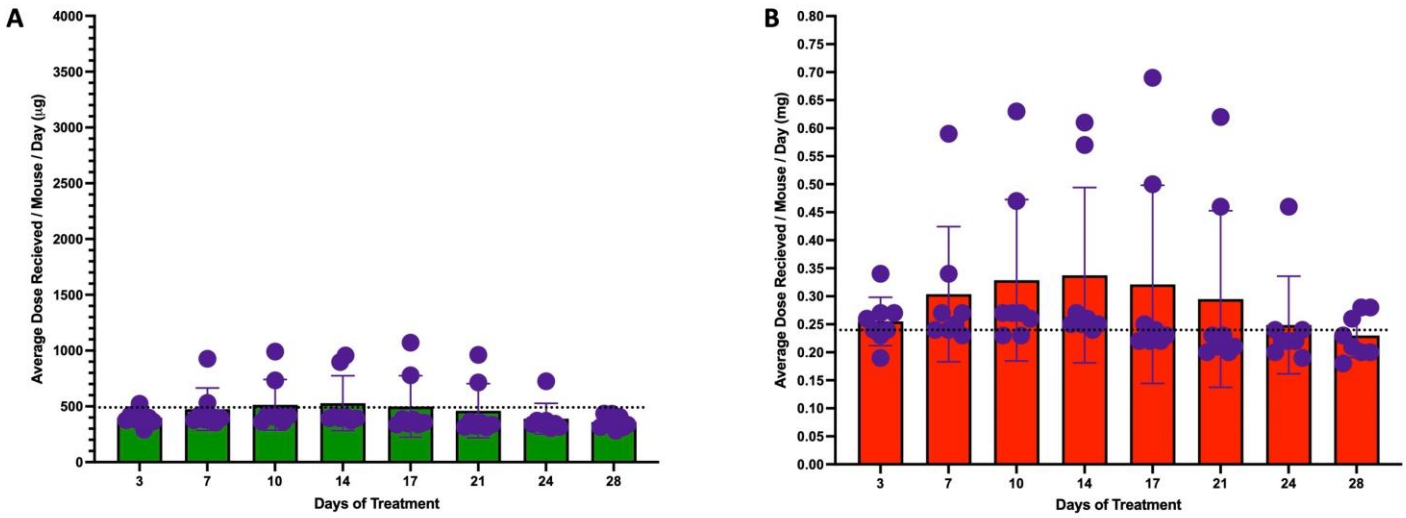

Figure 42: Administered and Target Dose for the Combination Group in Animal Study #2.

The dose of the corticosterone (A) and mirabegron (B) that the combination treatment group received per mouse per day during the course of the experiment. The 20 mice in this treatment were separated into 8 cages where the average dose received was calculated based on the water consumed for the cage and divided by the number of mice in that cage. The dotted lines represent the desired dose to be delivered.

Corticosterone and combination treatments altered the tissue appearance, size, and morphology

The corticosterone and combination-treated mice displayed observable phenotypical changes at the tissue level with both WAT and BAT displaying a larger size in comparison to the vehicle control and mirabegron treatment (Figure 43). The BAT in both the corticosterone and combination treatments subjectively displayed a lighter brown colour in comparison to the vehicle control, although, this colour difference was not quantified. Both the BAT weights (Figure 44A) and BAT weights relative to body weight (Figure 44B) were significantly ($p \leq 0.05$) heavier in the corticosterone and combination-treated mice compared to the mirabegron treatment and vehicle control groups. Both the WAT weights (Figure 45A) and WAT weights relative to body weight (Figure 45B) were significantly ($p \leq 0.05$) heavier in the corticosterone and combination-treated mice compared to both the mirabegron treatment and vehicle control groups.

Histological examination of the BAT also revealed differences between the treatment groups (Figure 46). A significant ($p \leq 0.05$) increase in the mean LD area was apparent in both the corticosterone and combination-treated groups (Figure 47A). The LD distribution of the corticosterone and combination groups illustrated more LDs being of larger size than those of the mirabegron or vehicle treatments (Figure 47B). The mirabegron treatment LDs were significantly ($p \leq 0.05$) larger than the vehicle control LDs, but displayed significantly ($p \leq 0.05$) smaller LDs than both the corticosterone and combination treatments. Histological examination of the WAT also revealed differences between treatment groups (Figure 48). A significant ($p \leq 0.05$) increase in the mean LD area was apparent for both the corticosterone and combination treatment groups (Figure 49A). The distribution of the LD areas revealed an

increased frequency of larger LDs in both the corticosterone and combination treatment group (Figure 49B).

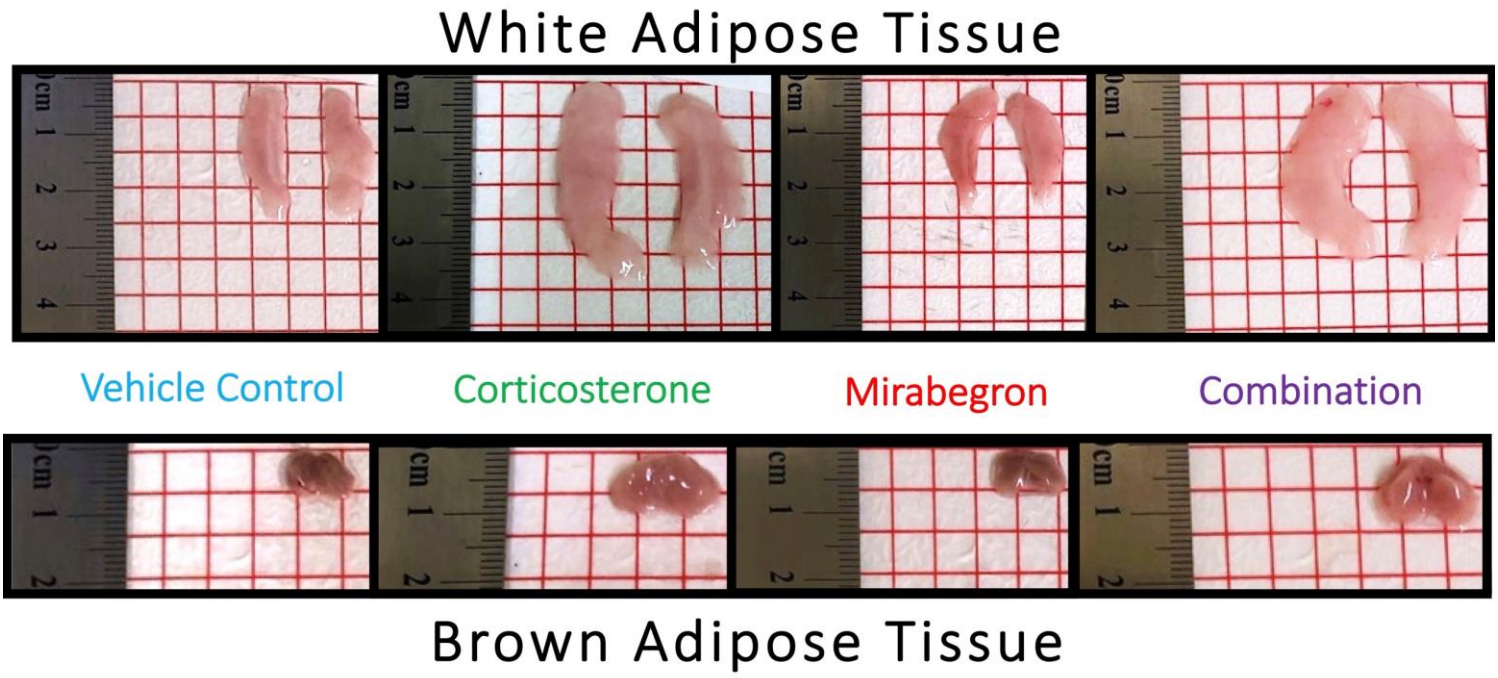

Figure 43: Adipose Tissue Visual Comparison for Animal Study #2.

A visual comparison of the inguinal white (top) and interscapular brown (bottom) AT depots from each of the treatment groups. The corticosterone and combination treated mice exhibited much larger WAT and BAT compared to the mirabegron and vehicle control groups. The grid represents 1/4 inch and the ruler illustrates the measurements of each tissue in centimeters.

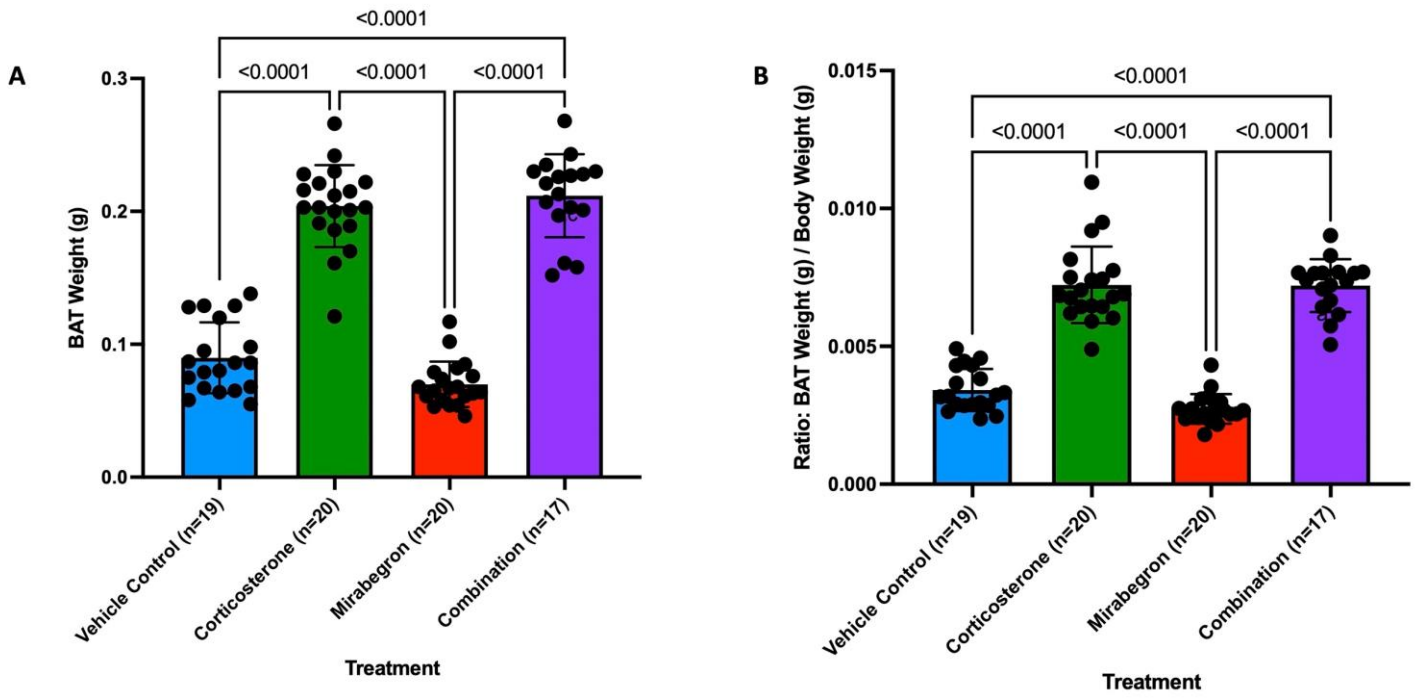

Figure 44: BAT Weights and Ratio for Animal Study #2.

Comparison of the BAT from each treatment displayed as absolute weight (A) and relative to body weight (B). The corticosterone and combination treatment groups had significantly ($p \leq 0.05$) heavier BATs compared to all other treatments in this study.

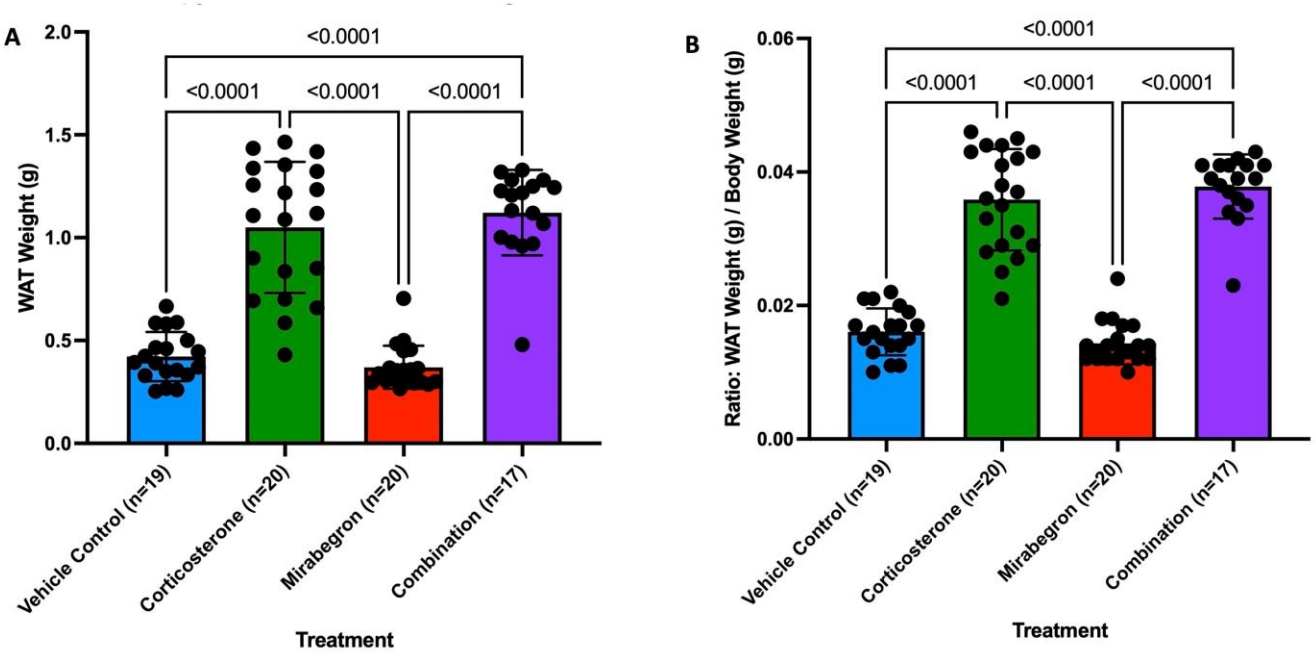

Figure 45: WAT Weights and Ratio for Animal Study #2.

Comparison of the inguinal WAT (ingWAT) from each treatment displayed as absolute weight (A) and relative to body weight (B). The corticosterone and combination treatment groups had significantly ($p \leq 0.05$) heavier WATs compared to all other treatments in this study.

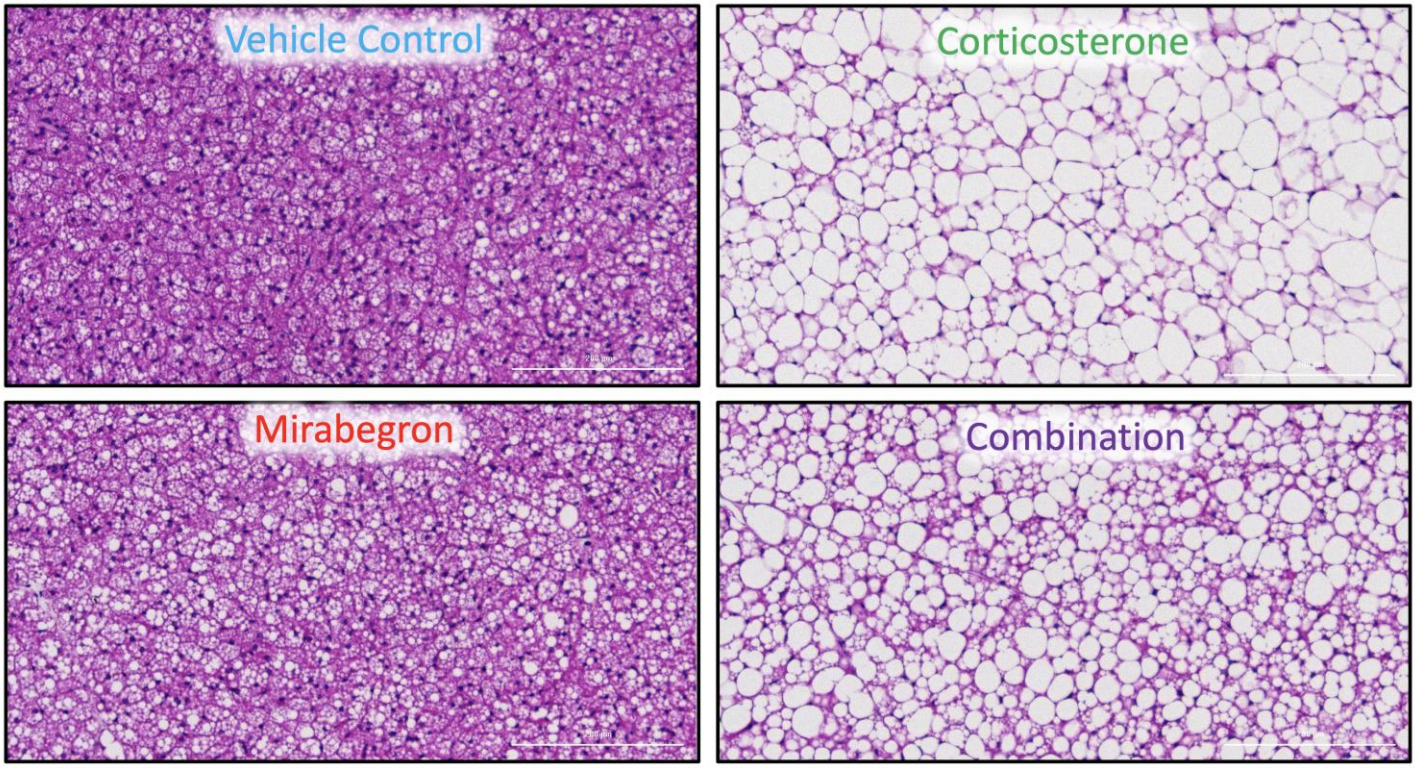

Figure 46: Representative BAT Histology from Animal Study #2.

Representative images of BAT at 10X magnification (H&E staining) from each treatment where the scalebar represents 200µm in the field of view. H&E staining allowed for lipid droplet size to be determined from each AT sample.

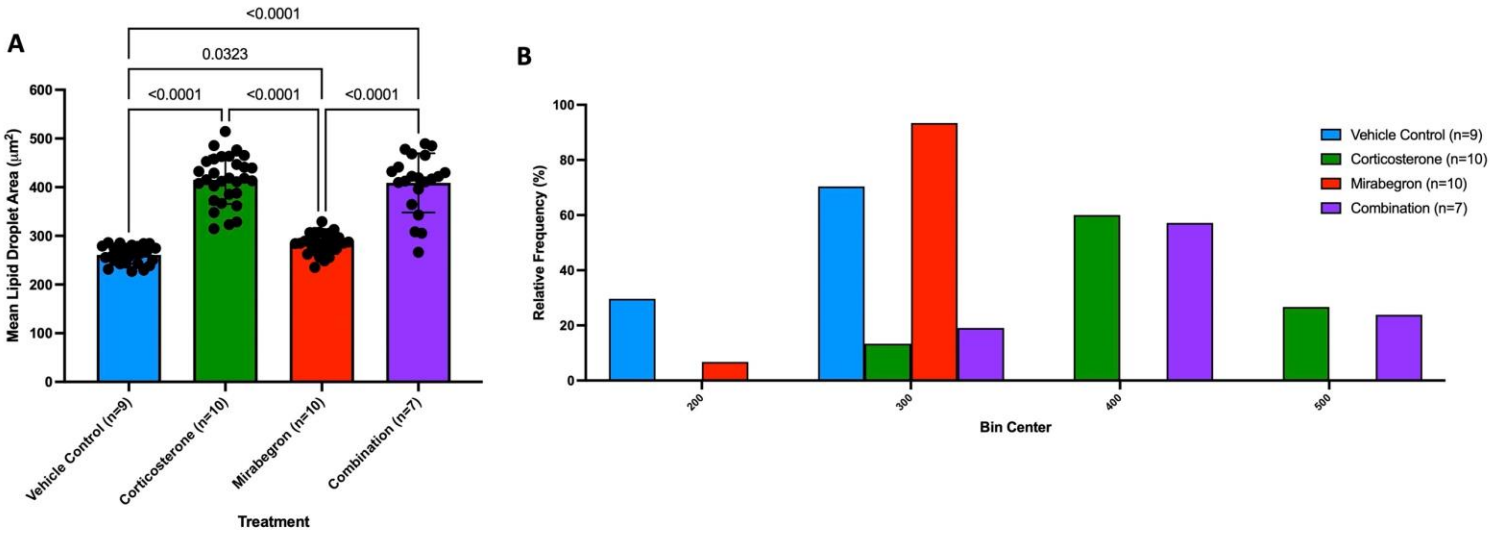

Figure 47: Comparison of BAT Lipid Droplet Area from Animal Study #2.

The mean lipid droplet area from three separate fields of view were determined through the automated programming in order to avoid any biases. Panel A illustrates the three average lipid droplet areas from each field of view for each sample from each treatment group and panel B illustrates the frequency distribution of the mean lipid droplet area (bin center). All fields of view are represented in the figure, but the statistical tests were conducted on averaged field of view per animal. Bin centers represented in this figure are BAT lipid droplet areas of: 150-250μm^2, 250-350μm^2, 350-450μm^2, and 450-550μm^2. The corticosterone treatment illustrates significantly ($p \leq 0.05$) larger lipid droplets than all other treatment groups (A). The corticosterone and combination treatments had a greater percentage of lipid droplets (bin centers) that are larger in size than the other treatment groups (B). Mirabegron treatment resulted in significantly ($p \leq 0.05$) larger lipid droplet areas than the vehicle control, however, both were smaller in area than the corticosterone and combination treatments.

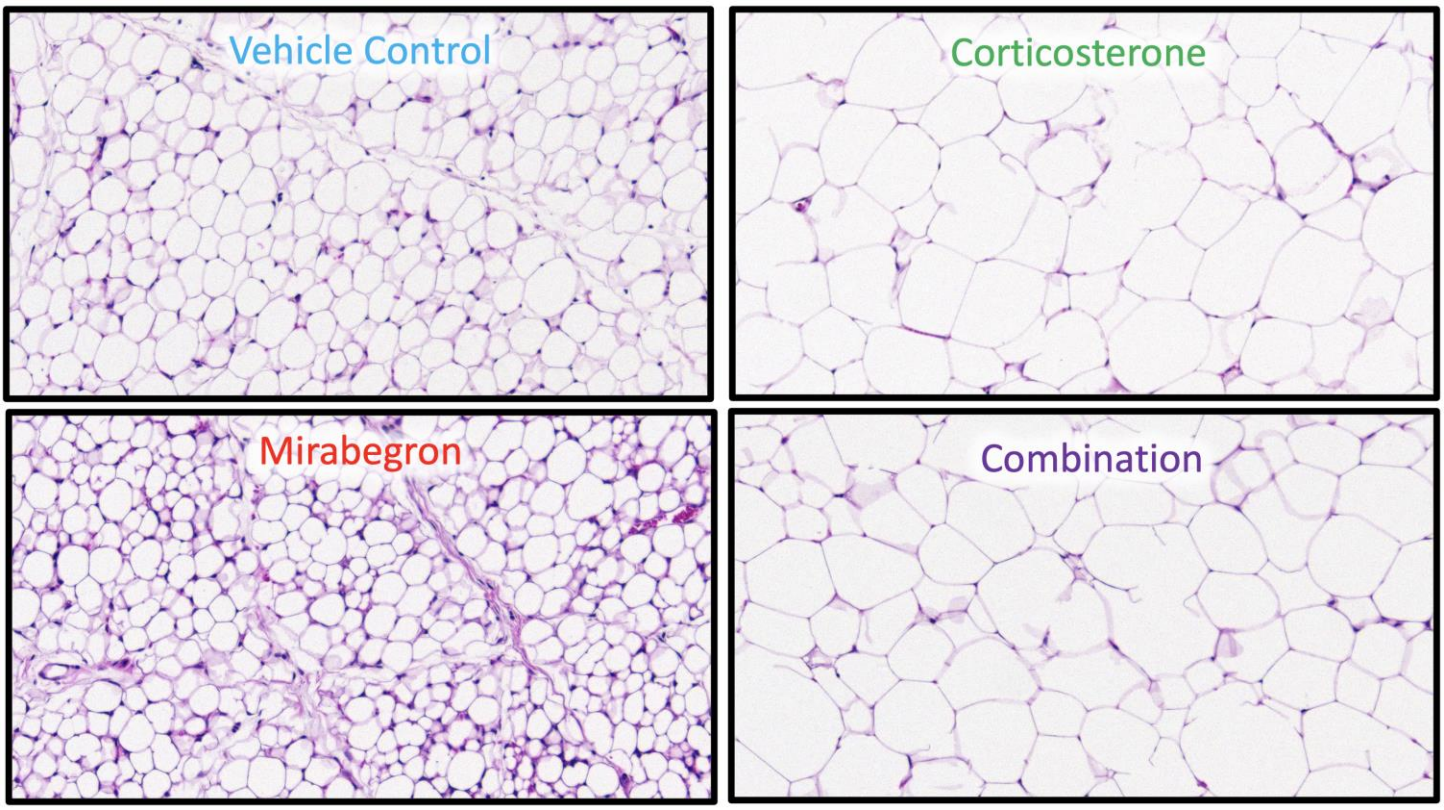

Figure 48: Representative WAT Histology from Animal Study #2.

Representative images of inguinal WAT (ingWAT) at 10X magnification (H&E staining) from each treatment where the scalebar represents 200µm in the field of view. H&E staining allowed for lipid droplet size to be determined from each AT sample.

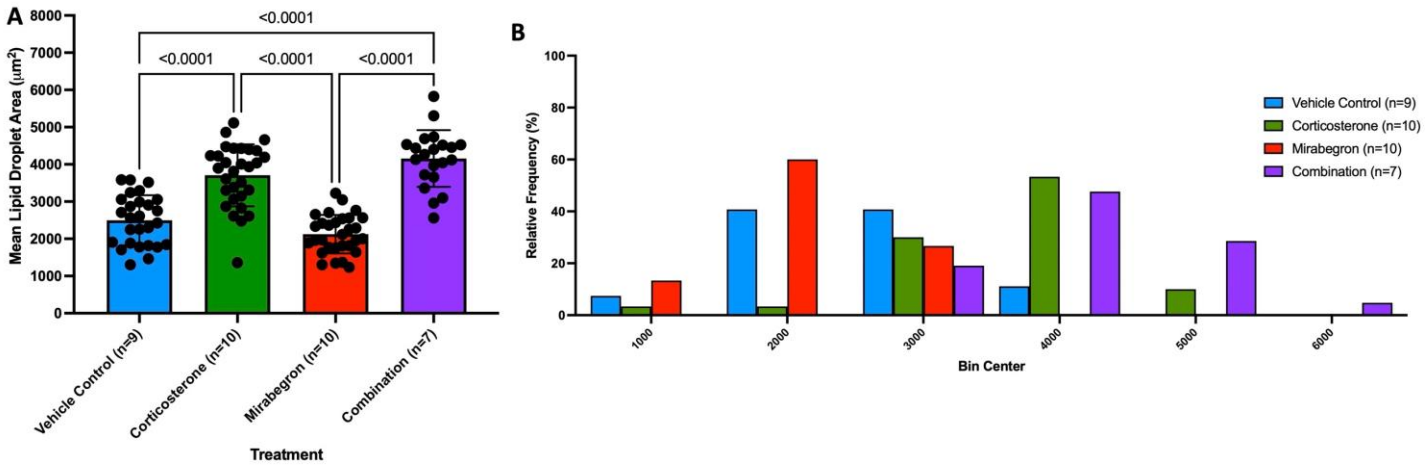

Figure 49: Comparison of WAT Lipid Droplet Area from Animal Study #2.

The mean lipid droplet area from three separate fields of view were determined through the automated programming in order to avoid any biases. Panel A illustrates the three average lipid droplet areas from each field of view for each sample from each treatment group and panel B illustrates the frequency distribution of the mean lipid droplet area (bin center). All fields of view are represented in the figure, but the statistical tests were conducted on averaged field of view per animal. Bin centers represented in this figure are lipid droplet areas of: 1500-2500µm^2, 2500-3500µm^2, 3500-4500µm^2, and 4500-5500µm^2. The corticosterone and combination treatments illustrated significantly ($p \leq 0.05$) larger lipid droplets than all other treatment groups (A). The corticosterone and combination treatments had a greater percentage of lipid droplets (bin centers) that are larger in size than the other treatment groups (B).

Corticosterone and mirabegron treated mice did not display altered UCP1 expressions in BAT

Through western blot, the UCP1 expression was determined. Unlike animal study #1, none of the treatments displayed elevated UCP1 expressions (Figure 50).

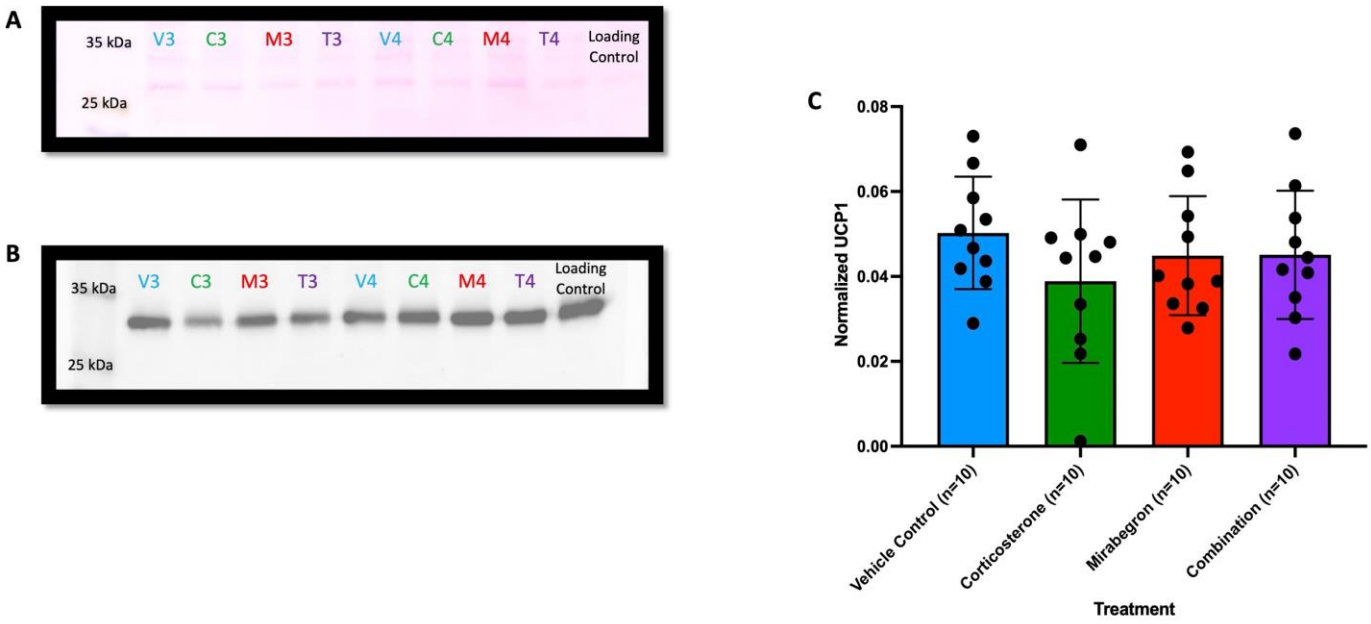

Figure 50: BAT UCP1 Protein Expression Following Animal Study #2.

A representative image of the ponceau S stain (panel A), protein expression of UCP1 (panel B), and normalized protein expressions (panel C) in BAT. Samples were separated on a 12% SDS-PAGE gel with 15µg of protein loaded into each lane. Western blot lane labels represent vehicle control sample (V), corticosterone sample (C), mirabegron sample (M), and combination sample (T). Samples were expressed relative to the loading control loaded onto each membrane. All treatment groups were not significantly different from each other in terms of their UCP1 protein expression.

WAT UCP1 expression was significantly reduced in the corticosterone treated mice

WAT UCP1 expression was determined through slot blots. The corticosterone treatment significantly ($p \leq 0.05$) reduced the expression of UCP1 within the tissue compared to both the mirabegron and vehicle treatments (Figure 51). Surprisingly, vehicle control displayed significantly ($p \leq 0.05$) increased UCP1 expressions compared to the mirabegron treatment (Figure 51).

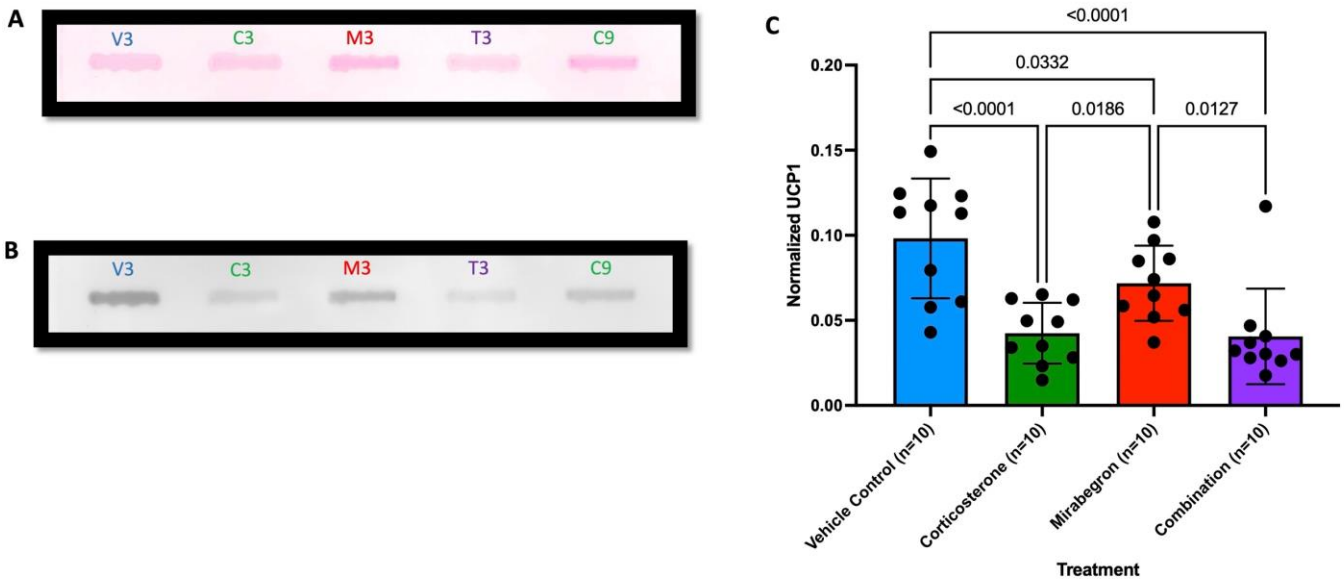

Figure 51: WAT UCP1 Protein Expression Following Animal Study #2.

A representative image of the ponceau S stain (panel A), protein expression of UCP1 (panel B), and normalized protein expressions (panel C). 40µg of protein loaded into each lane of the slot blot. Slot bot lane labels represent vehicle control sample (V), corticosterone sample (C), mirabegron sample (M), and combination sample (T). Slot blots were normalized back to the ponceau S stain for each sample. The corticosterone and combination groups had significantly ($p \leq 0.05$) less UCP1 expressed in each WAT when compared to the vehicle control and mirabegron groups.

The corticosterone and combination-treated mice had less of the mitochondrial content per gram of tissue

Citrate synthase was measured as a surrogate marker for mitochondrial content for each of the AT depots. Citrate synthase expression was not altered by the treatments in this study for both the BAT (Figure 52) and WAT (Figure 53). When comparing the relative protein expression of UCP1 to citrate synthase in the BAT, there were no differences between the treatments (Figure 54A). In the WAT, the vehicle-treated mice displayed significantly ($p \leq 0.05$) more UCP1 relative to citrate synthase (Figure 54B) than the controls.

To further understand if the mitochondrial content was altered in each depot, we related the protein expression back to the mass of each AT (Figure 55). When the protein expression was equated to the mass of the tissue per gram of AT, the corticosterone and combination treatments resulted in significantly ($p \leq 0.05$) fewer mitochondria in that depot compared to the vehicle control and mirabegron treatment in both BAT and WAT.

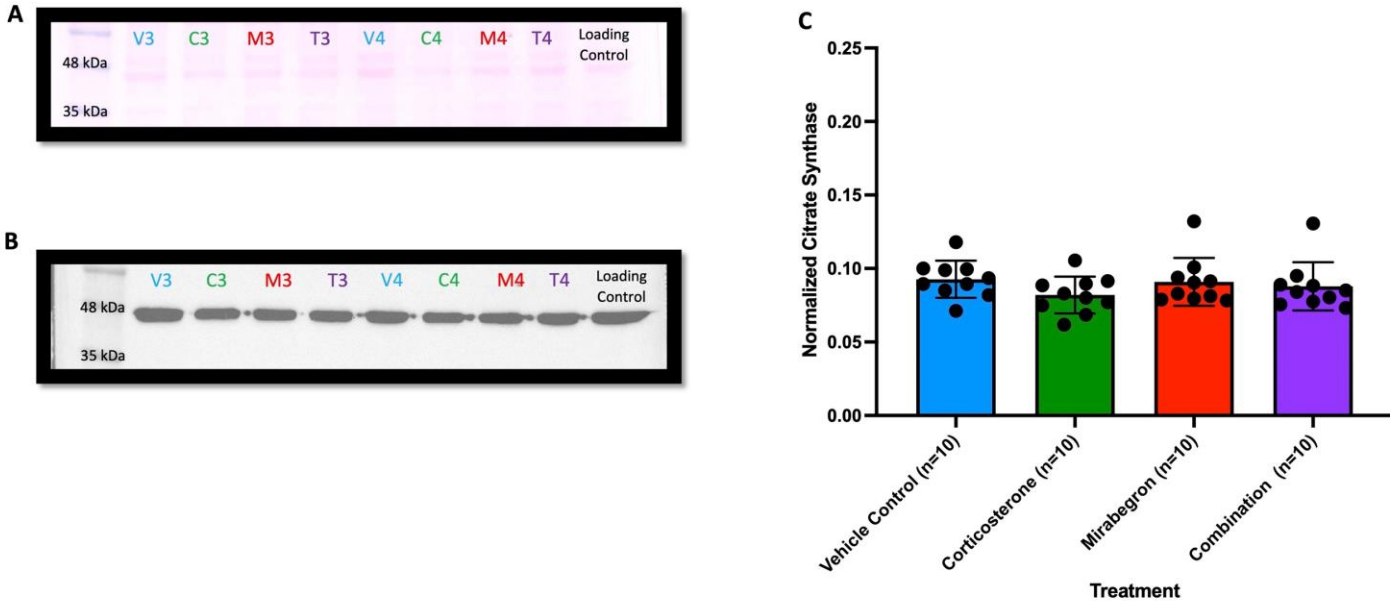

Figure 52: BAT Citrate Synthase Protein Expression Following Animal Study #2.

A representative image of the ponceau S stain (panel A), protein expression of citrate synthase (panel B), and normalized protein expressions (panel C) in BAT. Samples were separated on a 12% SDS-PAGE gel with 10µg of protein loaded into each lane. Western blot lane labels represent vehicle control sample (V), corticosterone sample (C), mirabegron sample (M), and combination sample (T). Samples were expressed relative to the loading control loaded onto each membrane.

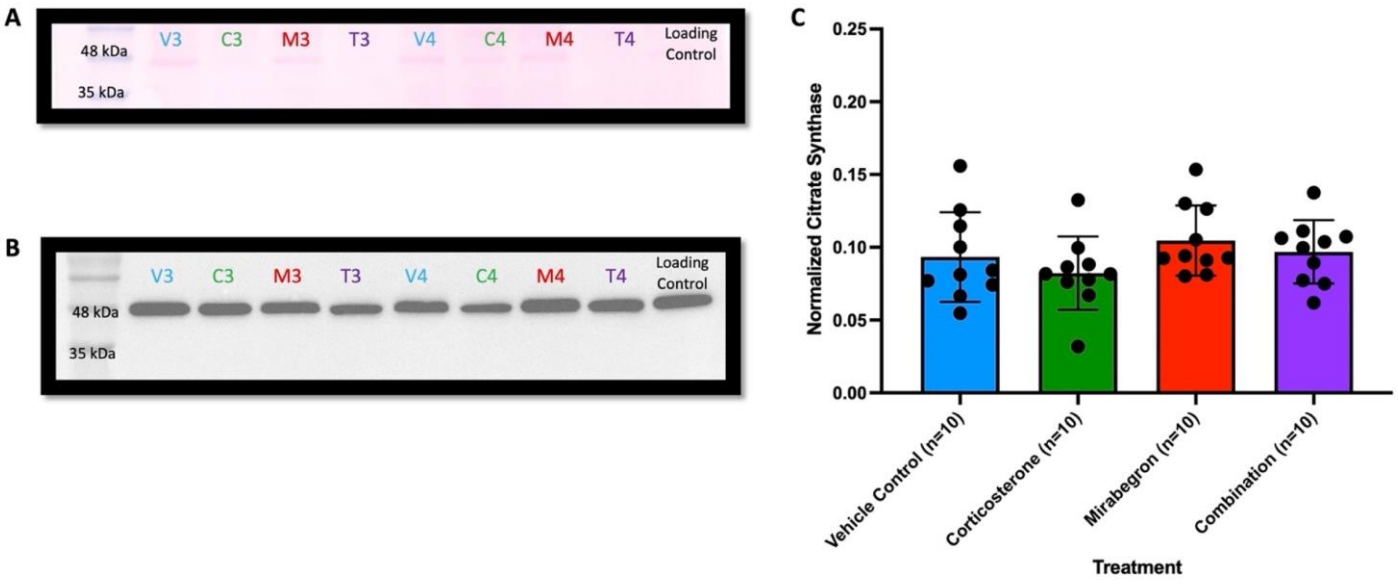

Figure 53: WAT Citrate Synthase Protein Expression Following Animal Study #2.

A representative image of the ponceau S stain (panel A), protein expression of citrate synthase (panel B), and normalized protein expressions (panel C) in WAT. Samples were separated on a 12% SDS-PAGE gel with 10µg of protein loaded into each lane. Western blot lane labels represent vehicle control sample (V), corticosterone sample (C), mirabegron sample (M), and combination sample (T). Samples were expressed relative to the loading control loaded onto each membrane.

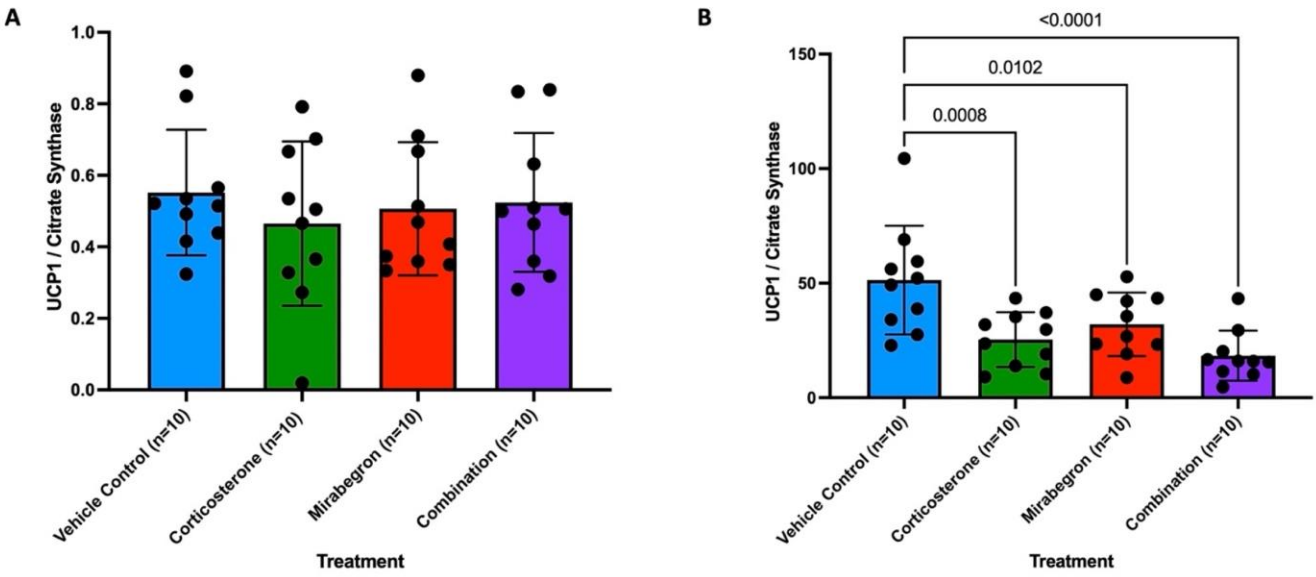

Figure 54: The Ratio of Uncoupling Relative to Mitochondrial Content in Animal Study #2.

The relative ratio of UCP1 to citrate synthase in each of the treatment groups for BAT (A) and WAT (B). (A) There was no difference in the ratio between treatment groups in the BAT. (B) The WAT illustrated significantly ($p \leq 0.05$) more UCP1/citrate synthase in the vehicle control than all other treatment groups.

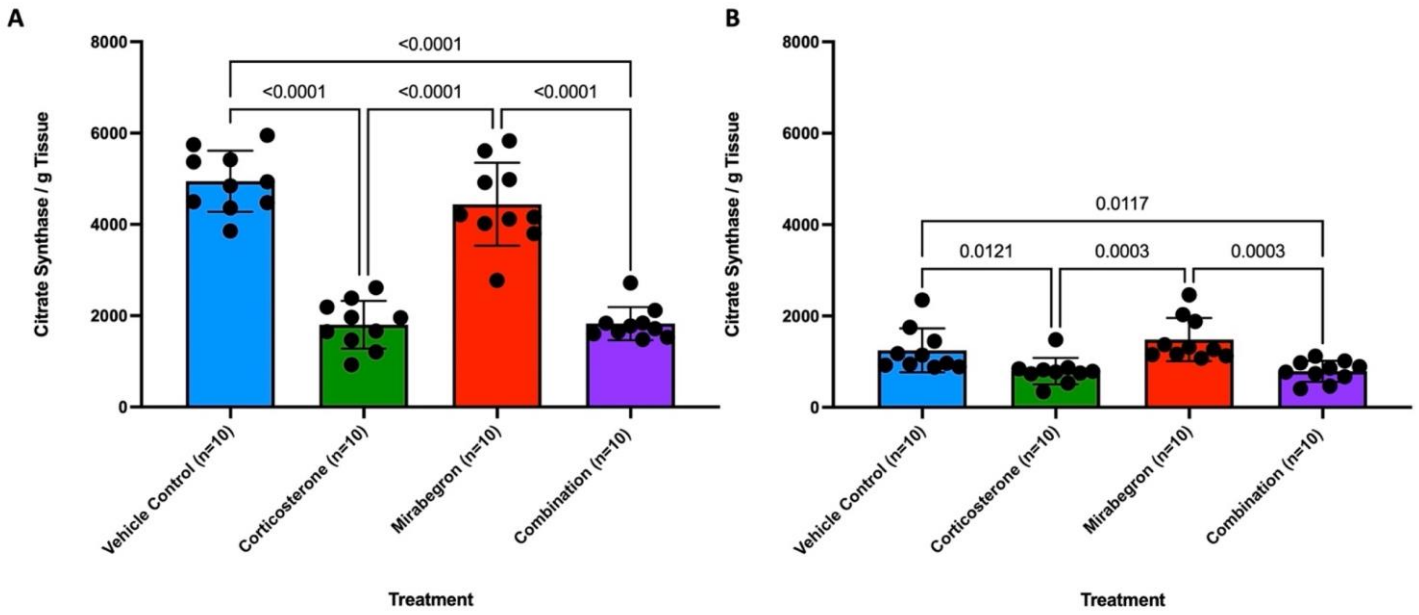

Figure 55: Mitochondrial Content per Gram of Tissue in Animal Study #2.

The relative ratio of citrate synthase per gram of tissue in each of the treatment groups for BAT (A) and WAT (B). (A) The mitochondrial content per gram of tissue was significantly ($p \leq 0.05$) less in the corticosterone and combination treatments compared to the mirabegron treatment and vehicle control groups in both BAT (A) and WAT (B).

Lipid peroxidation marker 4-HNE was not affected by the treatments but was correlated

Both BAT and WAT were analyzed by slot blots for the amount of lipid peroxidation within each tissue. Surprisingly, both the BAT (Figure 56) and WAT (Figure 57) were unaffected by the corticosterone, mirabegron, and combination treatments. Upon observation of the blots, it appeared as though the samples with high 4-HNE expressions in the BAT, were also elevated in the WAT, regardless of the treatment group the sample originated from. A Pearson correlation analysis was then performed and revealed a moderate positive correlation (coefficient of 0.6397) (Figure 58) illustrating this observed relationship.

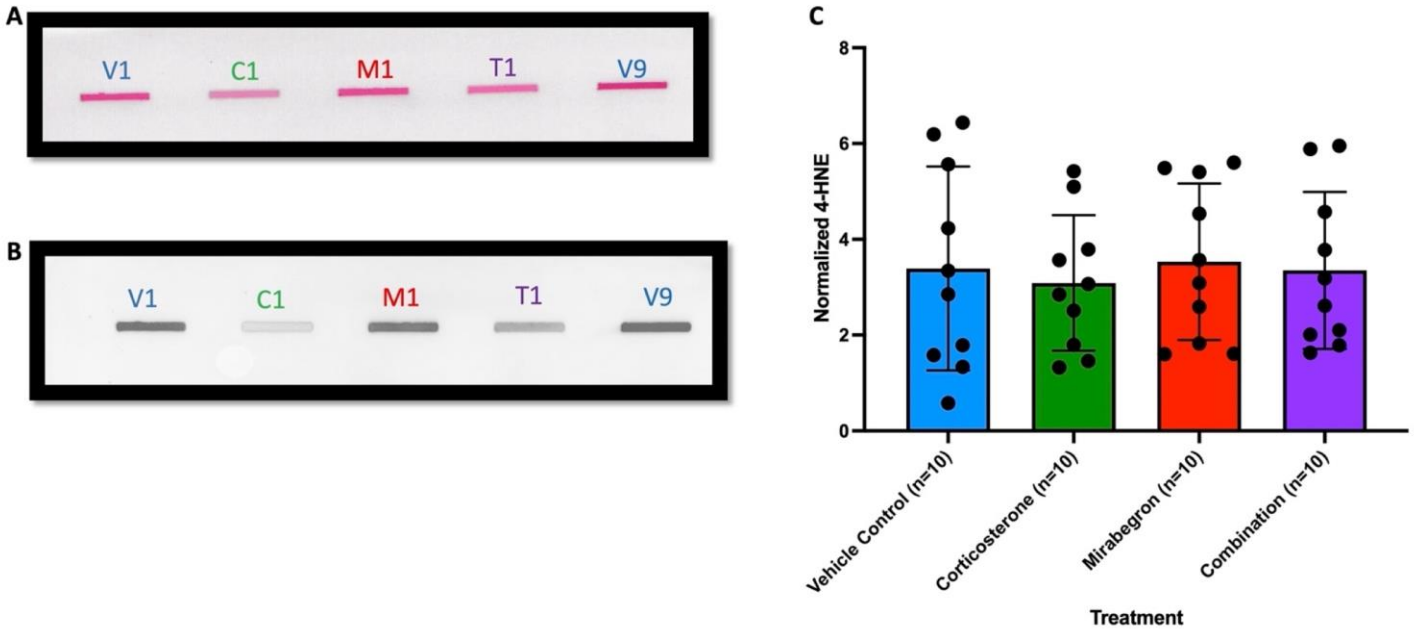

Figure 56: BAT Protein Adducts of 4-HNE Following Animal Study #2.

A representative image of the ponceau S stain (panel A), protein adduct formation of 4-HNE (panel B), and normalized protein adduct formation (panel C). 5µg of BAT protein loaded into each lane of the slot blot. Lane labels represent vehicle control sample (V), corticosterone sample (C), mirabegron sample (M), and combination sample (T). Slot blots were normalized back to the ponceau S stain for each sample.

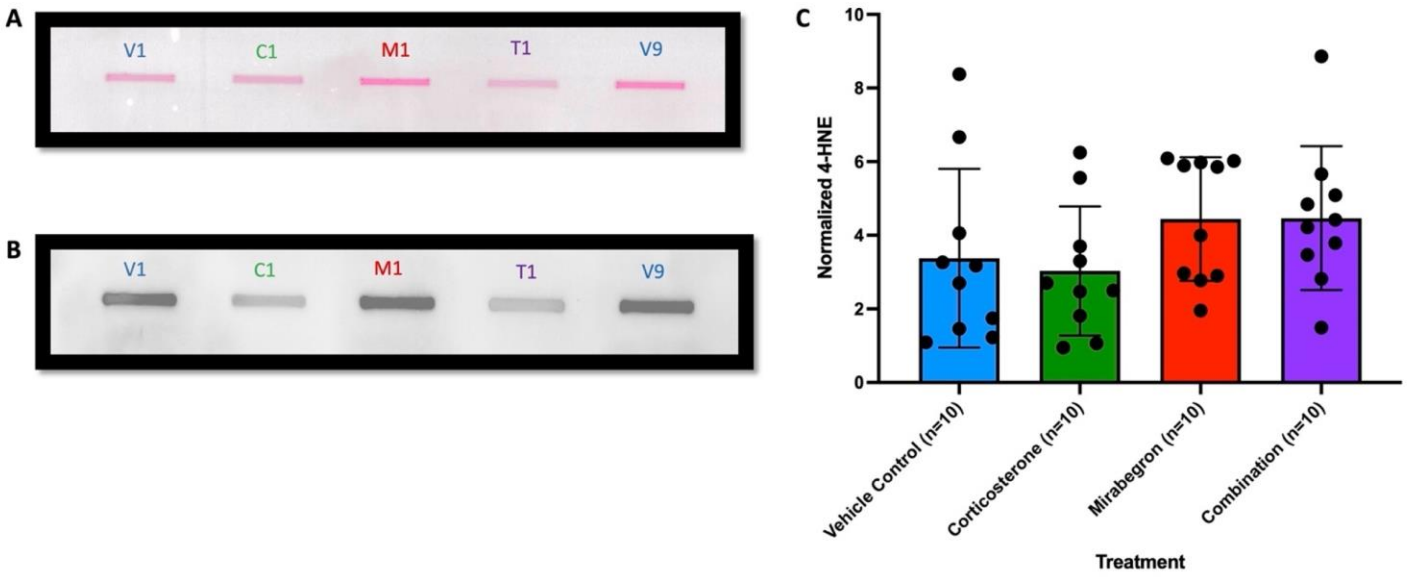

Figure 57: WAT Protein Adducts of 4-HNE Following Animal Study #2.

A representative image of the ponceau S stain (panel A), protein adduct formation of 4-HNE (panel B), and normalized protein adduct formation (panel C). 10µg of WAT protein loaded into each lane of the slot blot. Lane labels represent vehicle control sample (V), corticosterone sample (C), mirabegron sample (M), and combination sample (T). Slot blots were normalized back to the ponceau S stain for each sample.

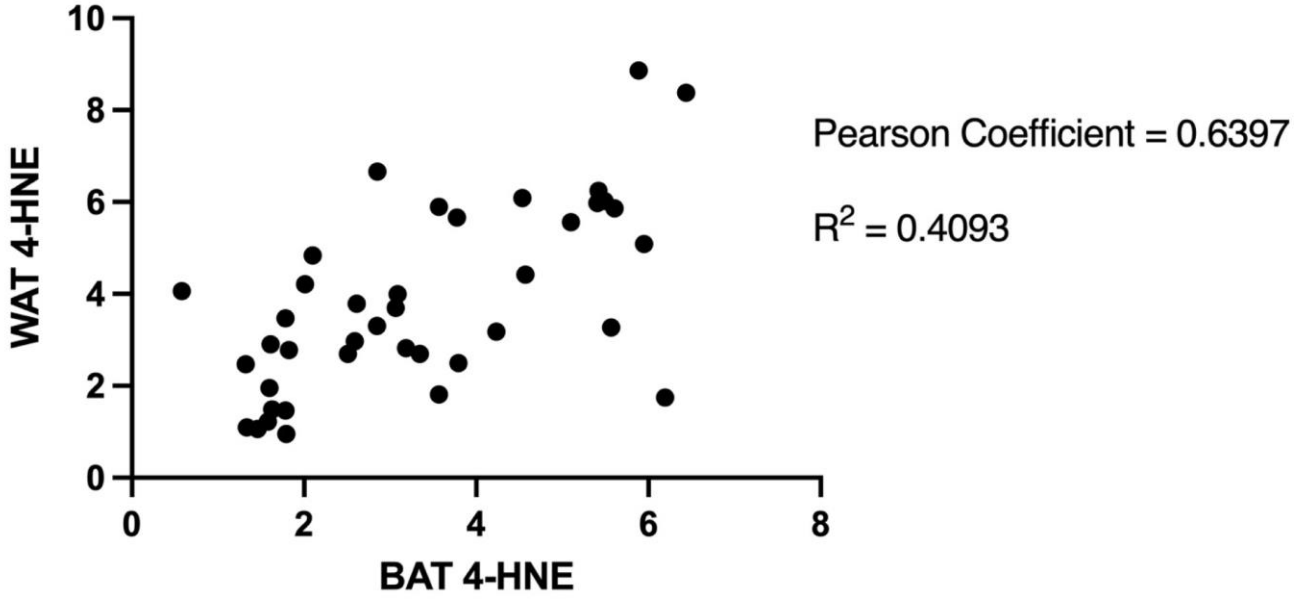

Figure 58: The Correlation between the BAT and WAT levels of 4-HNE in Animal Study #2.

The Pearson coefficient (0.6397) shows a moderate positive correlation.

Corticosterone treatment increased fasting plasma insulin and leptin levels and caused insulin resistance

Through commercially available assays, the plasma from each mouse was analyzed for their fasting glucose, insulin and leptin concentrations. The HOMA-IR values were then calculated to determine the level of insulin resistance under each treatment. The fasting glucose concentrations were not different between treatment groups (Figure 59A). However, the corticosterone and combination treatment groups illustrated significantly ($p \leq 0.05$) elevated fasting insulin (Figure 59B) and HOMA-IR values (Figure 59C). The plasma leptin concentrations were also determined in this study. The corticosterone and combination treatments also had significantly ($p \leq 0.05$) elevated fasting plasma leptin levels (Figure 60).

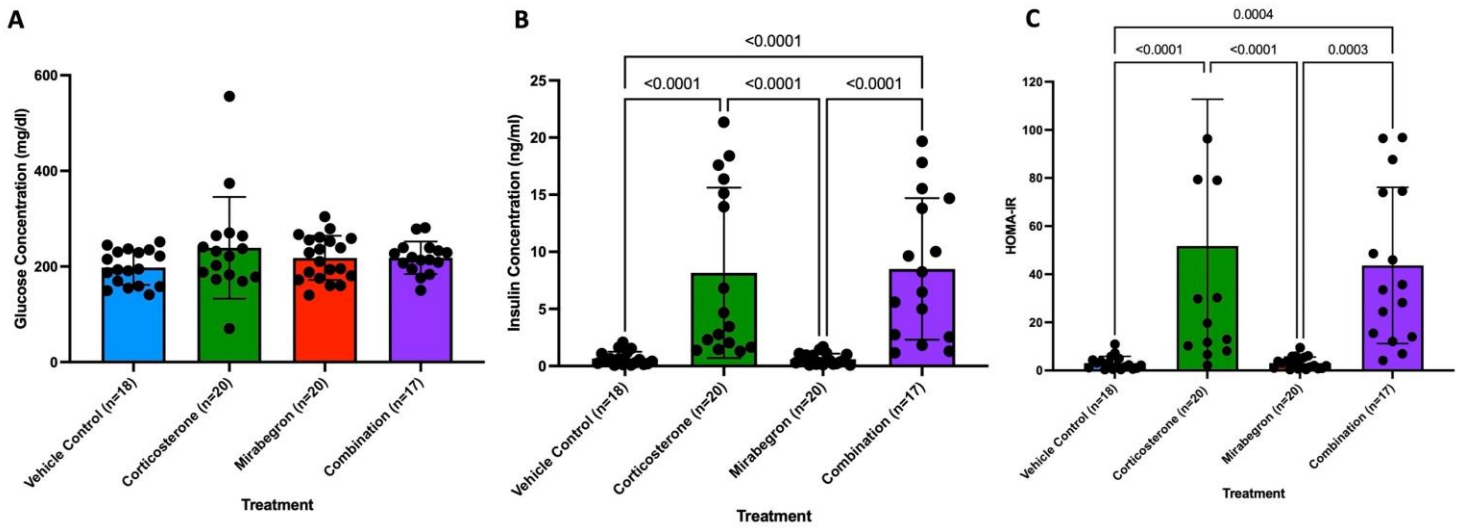

Figure 59: Animal Study #2 Plasma Measurements.

Plasma glucose (A) and insulin (B) measurements, and (C) HOMA-IR for each treatment. The corticosterone and combination groups illustrated significantly ($p \leq 0.05$) elevated insulin concentrations and insulin resistance (HOMA-IR) compared to the mirabegron and vehicle control groups.

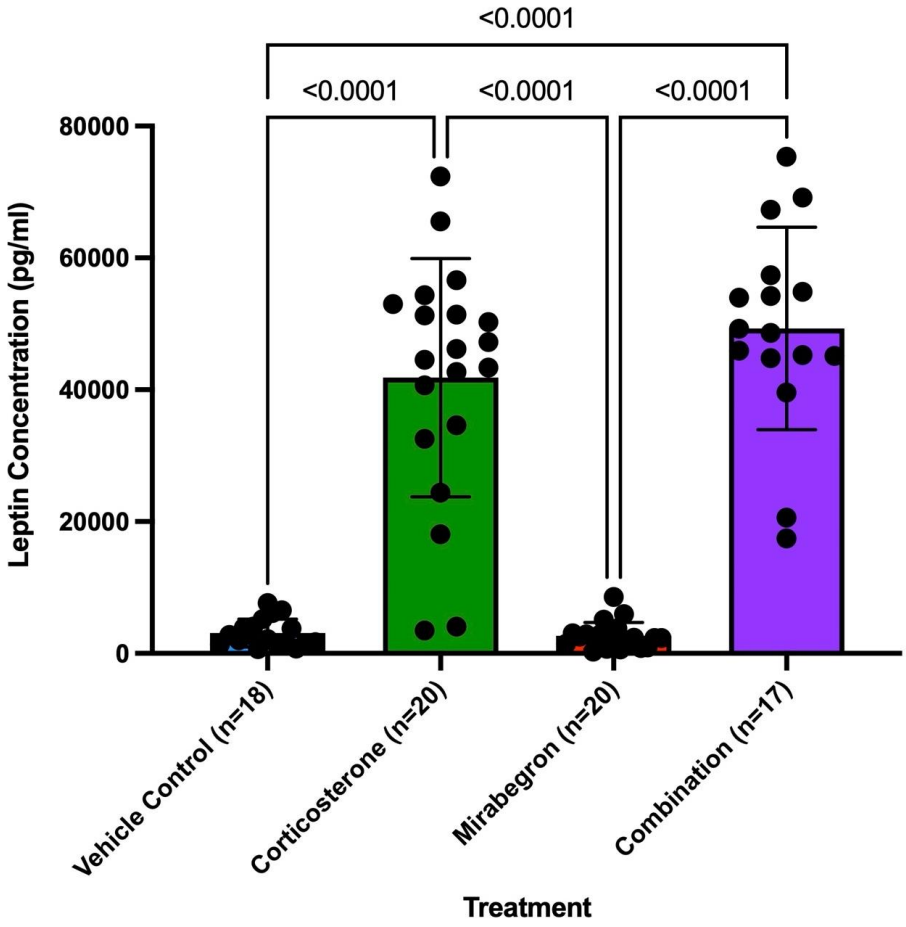

Figure 60: Plasma Leptin Concentrations for Animal Study #2.

The corticosterone and combination groups illustrated significantly ($p \leq 0.05$) elevated leptin concentrations compared to the mirabegron and vehicle control groups.

Animal Study #1 and #2 had notable differences

In order to determine if there were environmental or seasonal differences between the two animal studies, several comparisons were conducted. AS1 was conducted in the winter (from the end of January to the beginning of March) and AS2 was conducted in the spring/summer (from the beginning of May through June), so seasonal effects may play a role in the results. The temperature and humidity were logged daily (96 measurements per 24-hour period) and tracked throughout each experiment. Upon comparison, AS1 had a significantly ($p \leq 0.05$) higher temperature (Figure 61) and significantly ($p \leq 0.05$) lower level of humidity than AS2 (Figure 62). The final body weights were directly analyzed with similar treatments being directly compared to each other (Figure 63). There were no statistical differences found at the bodyweight levels. Both BAT and WAT weights and ratios relative to body weight were also compared between studies. While the BAT weights were not different alone, relative to body weight, the ratio in the second animal study was significantly ($p \leq 0.05$) higher for the corticosterone group compared to AS1 (Figure64). The WAT weights and ratios relative to body weight were significantly ($p \leq 0.05$) lower in AS2 than AS1 (Figure 65). When directly comparing the relative protein expressions for UCP1 in BAT of the vehicle controls from both animal studies on the same blot, AS2 had significantly ($p \leq 0.05$) more UCP1 in their BAT than AS1 (Figure 66).

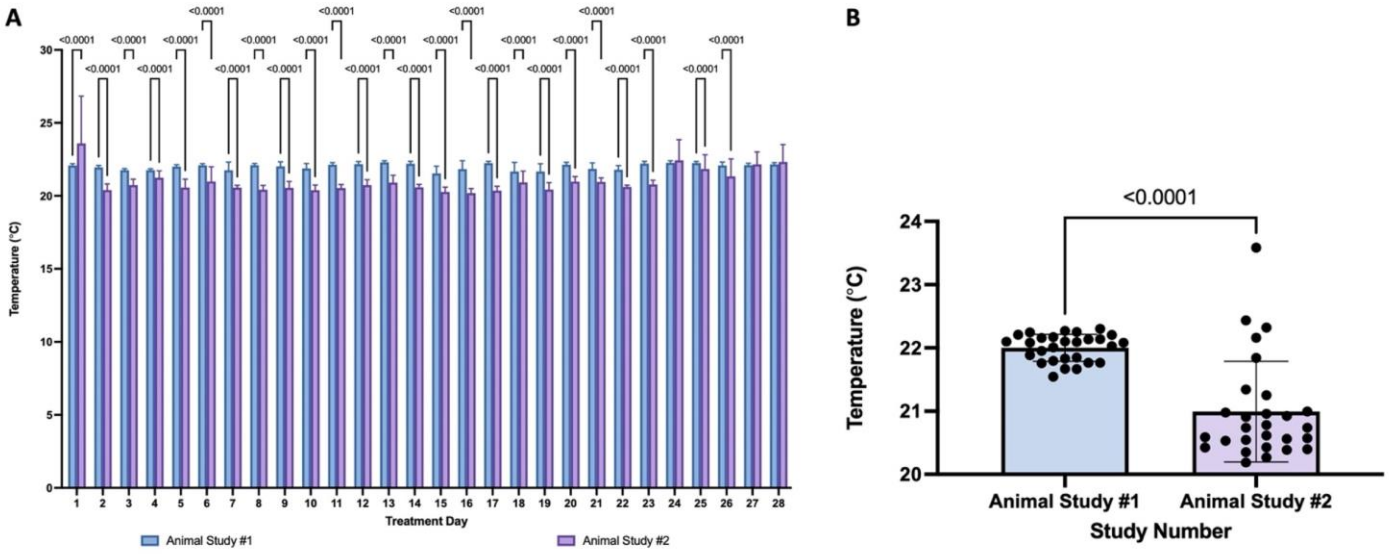

Figure 61: Room Temperature Comparisons Between Animal Studies.

A comparison of the room temperature between animal studies #1 and #2 per day (A) and as an average (B). Animal study #1 displayed a significantly ($p \leq 0.05$) higher room temperature than animal study #2 from treatment day 2-26 (A) and overall (B).

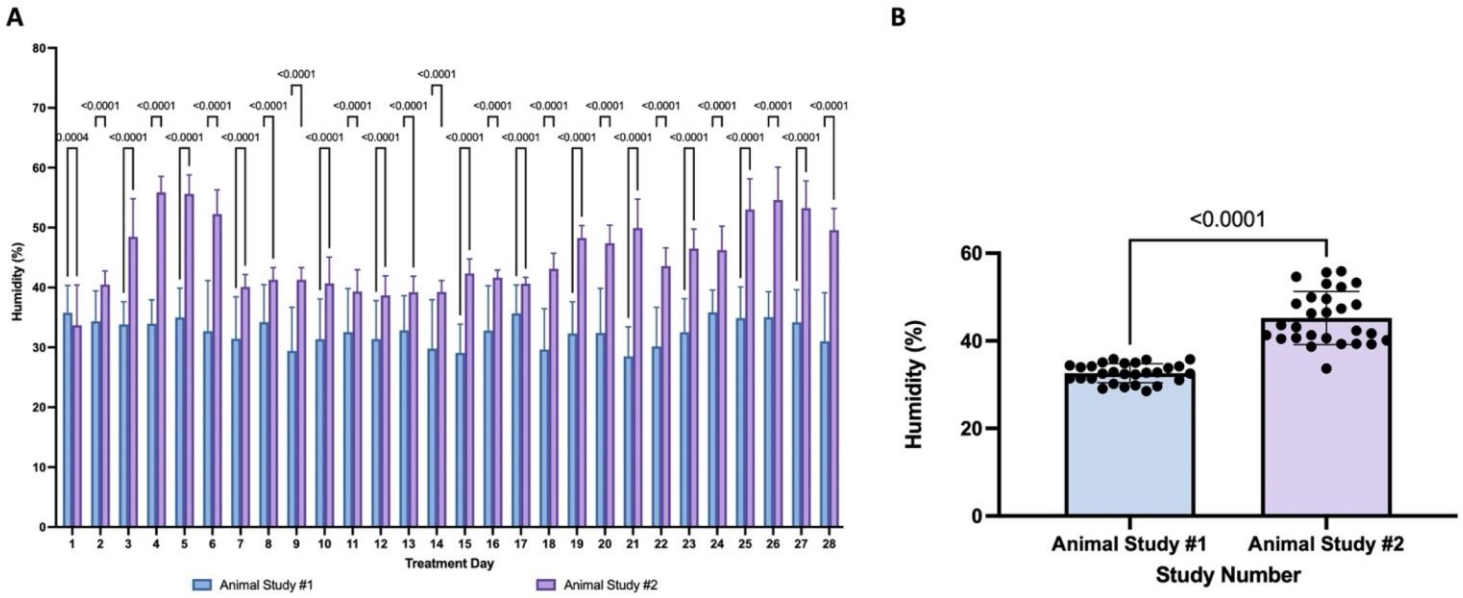

Figure 62: Comparisons Between Animal Studies.

A comparison of the room humidity between animal studies #1 and #2 per day (A) and as an average (B). Animal study #2 displayed a significantly ($p \leq 0.05$) higher level of humidity than animal study #1 from treatment day 2-28 (A) and overall (B).

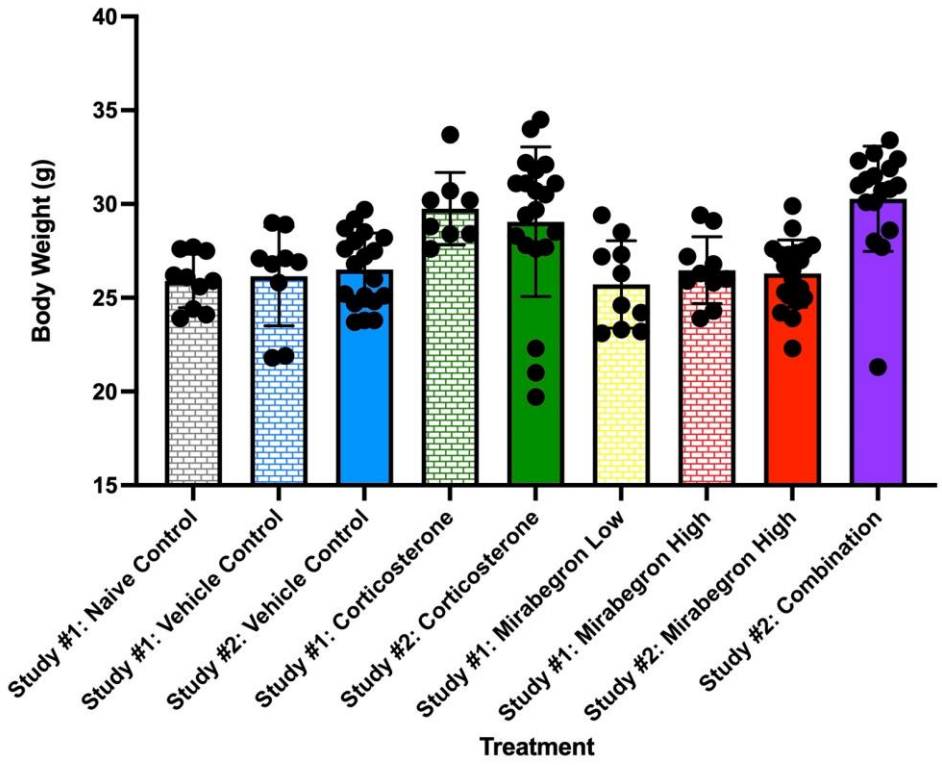

Figure 63: A Comparison of the Body Weights Between Animal Studies #1 and #2.

There were no differences observed between similar treatments between the two studies. All statistical analyses comparing between animal studies were performed in GraphPad Prism where data sets of the same treatment group were compared using a one-way ANOVA with Fisher's LSD test, with $p \leq 0.05$ considered statistically significant.

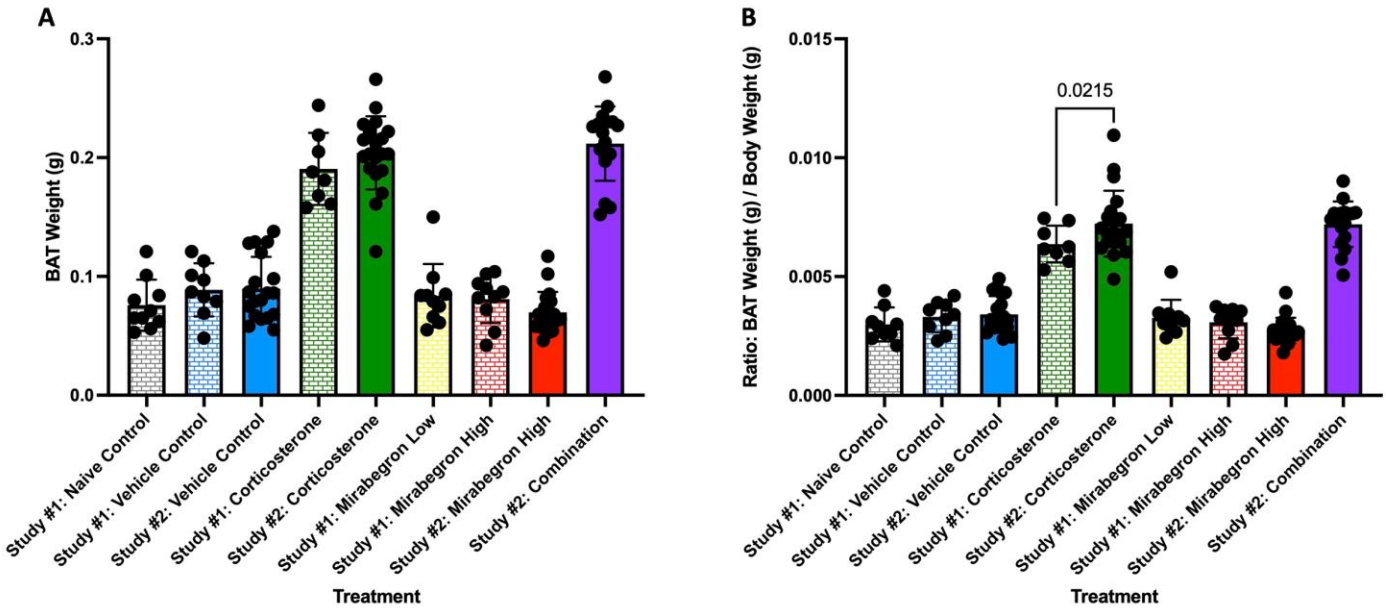

Figure 64: BAT Weight Comparisons Between Animal Studies.

A comparison of the BAT weights (A) and ratio to body weight (B) between animal studies #1 and #2. All statistical analyses comparing between animal studies were performed in GraphPad Prism where data sets of the same treatment group were compared using a one-way ANOVA with Fisher's LSD test, with $p \leq 0.05$ considered statistically significant. There were no differences observed between similar treatments between the two studies for BAT weights (A). The only observed difference in the ratio relative to body weight was found between the corticosterone treatments where animal study #2 is significantly ($p \leq 0.05$) greater when compared to animal study #1.

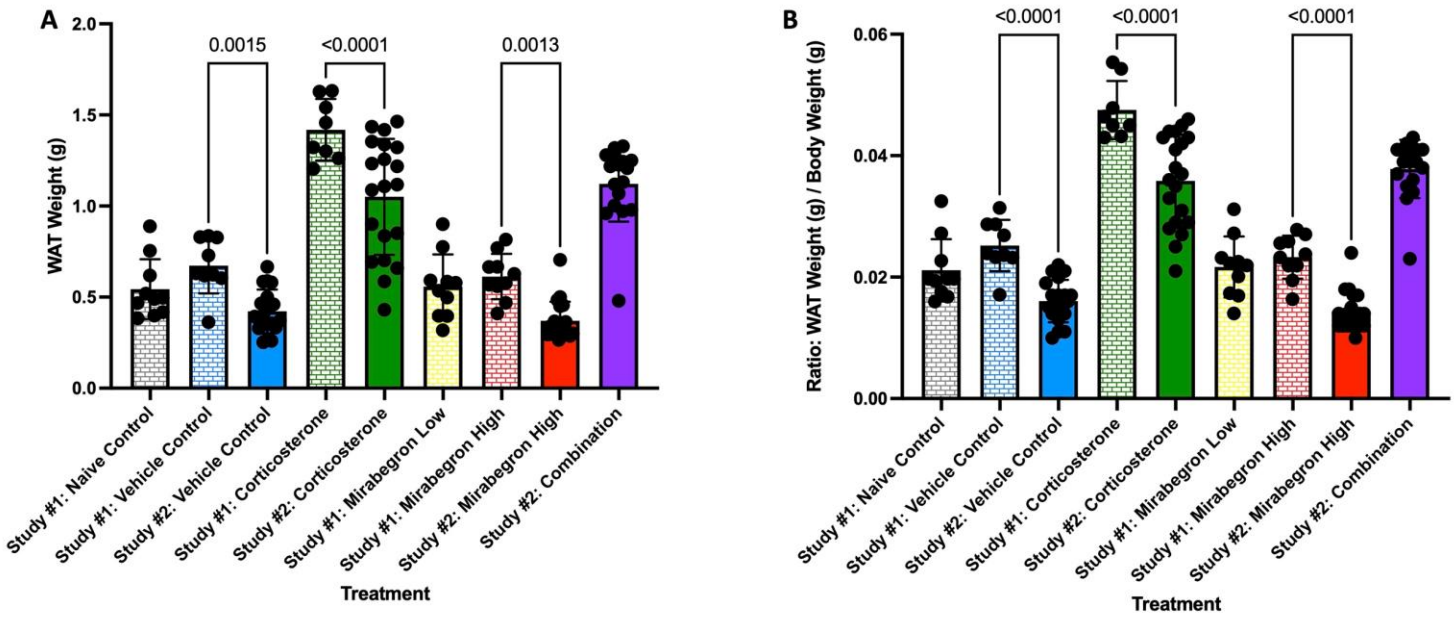

Figure 65: WAT Weight Comparisons Between Animal Studies.

A comparison of the WAT weights (A) and ratio to body weight (B) between animal studies #1 and #2. All statistical analyses comparing between animal studies were performed in GraphPad Prism where data sets of the same treatment group were compared using a one-way ANOVA with Fisher's LSD test, with $p \leq 0.05$ considered statistically significant. Animal study #2 had significantly ($p \leq 0.05$) lower WAT weights (A) and ratios relative to body weight (B) than animal study #1 for all repeated treatments.

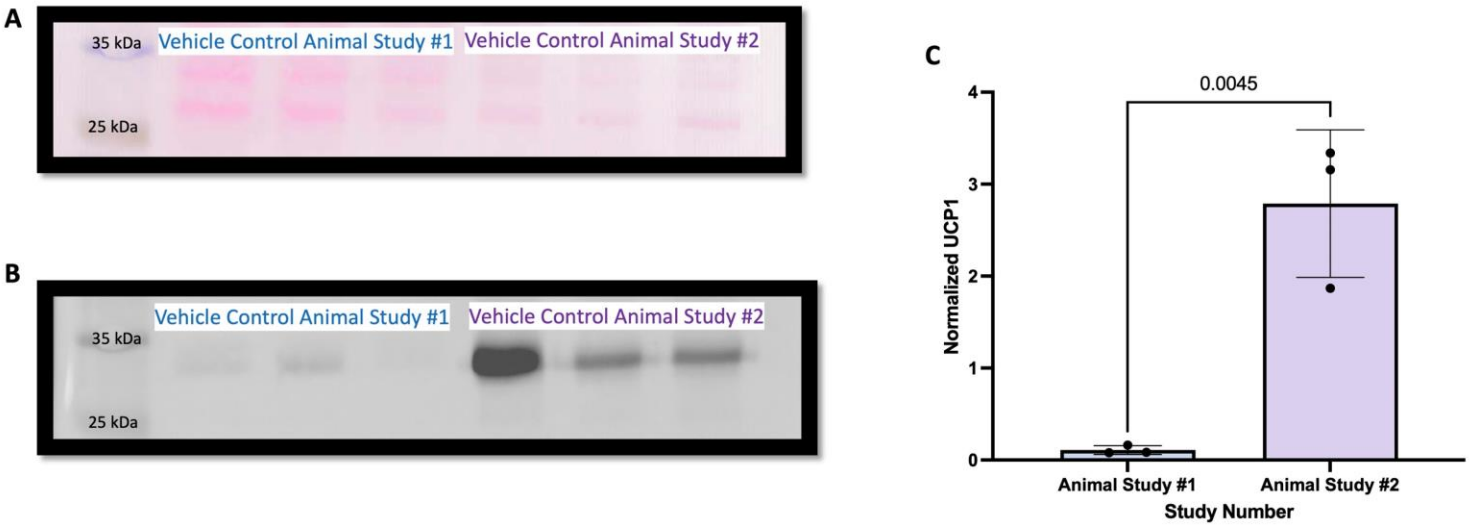

Figure 66: A Comparison of BAT UCP1 Protein Expressions from Animal Studies #1 and #2.

A representative image of ponceau S stain (A), the protein expression of UCP1 (B), and normalized protein expressions (C). Animal study #2 vehicle treated mice had significantly ($p \leq 0.05$) more UCP1 compared to animal study #1.

References

Berry, R., Church, C., Gericke, M.T., Jeffery, E., Colman, L., Rodeheffer, M.S., 2014. Methods in Enzymology (MIE): Methods of Adipose Tissue Biology-: 30.

Christe, M., Hirzel, E., Lindinger, A., Kern, B., von Flüe, M., Peterli, R., Peters, T., Eberle, A. N., & Lindinger, P. W. (2013). Obesity Affects Mitochondrial Citrate Synthase in Human Omental Adipose Tissue. *ISRN Obesity*, *2013*, 1–8. https://doi.org/10.1155/2013/826027

Masschelin, P. M., Cox, A. R., Chernis, N., & Hartig, S. M. (2020). The Impact of Oxidative Stress on Adipose Tissue Energy Balance. *Frontiers in Physiology*, *10*, 1638. https://doi.org/10.3389/fphys.2019.01638

McLaughlin, K.L., Hagen, J.T., Coalson, H.S., Nelson, M.A.M., Kew, K.A., Wooten, A.R., and Fisher-Wellman, K.H. (2020). Novel approach to quantify mitochondrial content and intrinsic bioenergetic efficiency across organs. Sci Rep *10*, 17599. https://doi.org/10.1038/s41598-020-74718-1.

Chapter 5: Discussion

Animal Study #1 (AS1)

In order to examine how corticosterone and β3AR stimulation affects the metabolic dysfunction of AT, we conducted two sets of animal studies. In AS1, we exposed young male mice to either chronic levels of corticosterone or mirabegron, a β3AR agonist, in their drinking water for four weeks. All of the treatments were administered in drinking water in order to be the least invasive, mitigate excess stress to the animals, and allow for the diurnal rhythm of corticosterone to be maintained (Cassano et al., 2012; Gasparini et al., 2016; Karatsoreos et al., 2010; van Donkelaar et al., 2014). Administration of corticosterone via drinking water has been used in several studies and is a model for metabolic syndrome, chronic stress-induced T2D, hypercortisolemia, dyslipidemia, obesity and Cushing's Syndrome (Cassano et al., 2012; Do, 2019; Karatsoreos et al., 2010; van Donkelaar et al., 2014). This model has also been described by Gasparini et al. (2016) to mimic clinical GC therapy and was the first study to directly compare corticosterone administration models *in vivo*. Gasparini et al. (2016) directly compared corticosterone administered via drinking water to the pellet implantation method. Their results further validated the use of drinking water to expose mice to excess GCs. It is also important to note that corticosterone administration through drinking water also allows for the effects of long-term stress to be studied in a rapid and safe manner (Cassano et al., 2012; Gasparini et al., 2016; Karatsoreos et al., 2010; van Donkelaar et al., 2014).

We hypothesized that mirabegron would promote AT beiging, reduce oxidative stress, and reduce insulin sensitivity. To investigate our hypothesis, we had three specific aims for this animal study:

1) Establish how corticosterone or β3AR stimulation impact AT and UCP1 expression
2) Determine how oxidative stress and immune cell infiltration are influenced by either corticosterone or β3AR stimulation
3) Investigate the effects of corticosterone or β3AR stimulation on whole-body insulin resistance

Specific Aim #1: Establish how corticosterone or β3AR stimulation impacts adipose tissue and UCP1 expression

As described in the literature review, beiging is the process where brown-like adipocytes are activated within the WAT depots to display increased levels of mitochondrial biogenesis, UCP1, induce the release of FFAs, and initiate thermogenesis, all of which can improve whole-body metabolism (Chait & den Hartigh, 2020; Heeren & Scheja, 2018; Jeanson et al., 2015). Conversely, whitening is the opposite process where brown adipocytes expand to the point of becoming hypertrophic, store more TAGs, display decreased UCP1 protein expression, and are less thermochemically active (Bartlet & Heeren, 2013). Both beiging and whitening were investigated via four-week treatments with either mirabegron or corticosterone, respectively. The corticosterone-treated mice gained significantly ($p \leq 0.05$) more weight after seven days of treatment (Figure 10). They had a larger change in body weight than any other treatment group

($p \leq 0.05$) (Figure 11). The fasting bodyweight of the corticosterone-treated mice was also statistically significantly ($p \leq 0.05$) higher than all other treatment groups (Figure 12). This increase in body weight in the corticosterone-treated mice compared to controls is in agreement with other studies (Do , 2019; Karatsoreos et al., 2010; Kinlein et al., 2017; van Donkelaar et al., 2014). Although Hao et al. (2019) showed reductions in body weight when mirabegron was administered to HFD induced obese mice, we did not observe any differences between the mirabegron treatments or the controls (Figure 12) (Hao et al., 2019). As previously reviewed in the literature, it appears that mirabegron offers more benefits with weight loss when an individual is already obese (Bel et al., 2021). An interesting observation we found that others haven't mentioned is that treatment with chronic corticosterone altered the coat of the mice to become oily in appearance (Figure 13). Although we did not directly measure home cage locomotion, these corticosterone-treated mice also appeared less active than the other treatment groups. This decreased movement has been previously described in corticosterone-treated mice by others (Cassano et al., 2012; Do , 2019; Karatsoreos et al., 2010; van Donkelaar et al., 2014).

Most previous studies using corticosterone in drinking water have not reported significant increases in the volume of water consumed. In this study the corticosterone-treated mice drank significantly ($p \leq 0.05$) more water than any of the naïve or vehicle controls and both mirabegron treatments (Figure 14). This increased consumption of drinking water began on day 4 and escalated from days 10 through 19, where it reached a maximum. While this did alter the dose of the treatment they received (Figure 15), it was corrected after day 19 of the experiment. Once lowered to a dosage of 50μg/ml, the drinking behaviour became similar to naïve and

vehicle controls (Figure 15). However, the final eight days resulted in a slightly lower dose than what was targeted (Figure 16). Both doses of mirabegron were slightly below what was targeted as well (Figure 17) (Figure 18). Studies conducted previously using the same dose, delivery mode, and housing temperatures did not widely report this increased water intake or the dose of corticosterone consumed by the mice (Karatsoreos et al., 2010; van Donkelaar et al., 2014). Only a handful of studies have reported a significant increase in water intake at this dose and housing temperature, but none of these previous studies reported the magnitude of this water consumption (which is directly related to the dose of corticosterone received) (Cassano et al., 2012; Do, 2019; Kinlein et al., 2017). Cassano et al. (2012) and Kinlein et al. (2017) reported this increase began from 14 days of exposure, which was much later into the treatment compared to what we observed in our study (Cassano et al., 2012; Do, 2019; Kinlein et al., 2017). Plasma corticosterone levels were reported by two of these studies to be sustained at supralocal levels, greater than 400ng/ml, at the beginning of the light cycle in adolescent mice; however, none of these studies have reported the actual dose of corticosterone the animals received based on the water consumption (Do, 2019; Kinlein et al., 2017). One study conducted at thermoneutral conditions (30°C) reported increased water intake in the corticosterone-treated mice (Luijten, Brooks, et al., 2019). With corticosterone-treated mice illustrating such an increase in drinking water volume, future studies should alter the dose administered accordingly and include either intermediate or dose-corrections to account for this increased water consumption. The water consumption and dose of the treatment should also be reported in future studies to ensure reproducibility and accuracy in interpreting results. We adjusted the dose the corticosterone treated mice received in their drinking water in AS2 of this dissertation.

In the present study, images of the ingWAT and BAT were taken to visually compare the AT from each treatment (Figure 19). One can visually observe the larger size and subjectively lighter colour in the BAT of the corticosterone-treated mice compared to the controls (Figure 19). Colour differences were not quantified and it is unclear if this observable difference affects metabolic activity. This is indicative of whitening in this tissue. The BAT weights and BAT weight to bodyweight ratios of the corticosterone-treated mice were significantly ($p \leq 0.05$) increased compared to all other treatments (Figure 20). In contrast, chronic BAT activation with mirabegron did not alter BAT mass. BAT activation with mirabegron was previously illustrated in a human study by O'Mara et al. (2020) where they gave healthy women mirabegron (100mg/day) for four weeks (this dose is 4X higher than the approved dose of 50mg per day) (O'Mara et al., 2020). They found that this dose of mirabegron increased the metabolic activity of BAT. They then measured BAT activity with ^{18}F-FDG PET/CT and found that at this high dose, mirabegron increased the metabolic activity (O'Mara et al., 2020). Cypess et al. (2015) also observed BAT activation through ^{18}F-FDG PET/CTwith mirabegron administration in humans at a dose of (200mg/day) (Cypess et al., 2015). ^{18}F-FDG PET/CT imaging with administration of mirabegron in mice has only been investigated by Sui et al. (2019) where they used the same doses and for a similar duration as our study to visually show mice also have increased ^{18}F-FDG uptake in the BAT of both mirabegron high and low doses compared to their vehicle (Sui et al., 2019). Visually, the high mirabegron treatment in our study appears to have resulted in a darker colour of the BAT (Figure 19), although, this was not quantified. The ingWAT of the corticosterone mice is visually larger in size than the controls and mirabegron treatments (Figure 19). The WAT weights and WAT weight to bodyweight ratio of the corticosterone-treated mice

were also significantly ($p \leq 0.05$) increased in comparison to all other treatments (Figure 21). Increased body weight is a hallmark of GC excess and illustrates the body's metabolic shift under these conditions. Other groups have also reported increased gonadal WAT and overall WAT under chronic corticosterone treatment (Gasparini et al., 2016; Karatsoreos et al., 2010), with one study specifically reporting an increase in BAT weight under these standard housing and corticosterone treatment conditions for two-weeks (Luijten, Brooks, et al., 2019). Do (2019) conducted a similar study but treated mice for eight weeks. They reported increased body and BAT mass that remained significant throughout eight weeks of corticosterone exposure (Do et al., 2019). This illustrates that our model of exposure to chronic levels of GCs reveals the same AT mass trend as studies of extended duration. Atrophy of the thymus and adrenal glands under this dosage of corticosterone has also been reported (Cassano et al., 2012; Do, 2019; Karatsoreos et al., 2010), whereas corticosterone treatment has also led to decreased spleen mass (Do, 2019) and increased liver size (Cassano et al., 2012).

Histological examinations were conducted on both the BAT and WAT depots in this study to investigate changes in tissue morphology. After four weeks of corticosterone treatment, the average LD area in the BAT was significantly ($p \leq 0.05$) increased compared to both the naïve and vehicle control groups and both mirabegron treatments (Figure 22) (Figure 23). This increased LD area was not the result of chronic activation of the β3AR pathway as the mirabegron treated groups did not alter the LD size. This larger LD area is representative of the BAT undergoing "whitening," where it is shifting its phenotype to store lipids. This is visually observed by the increased percentage of LDs of larger areas in the frequency distribution chart (Figure 23B). This adipocyte expansion has been found under both standard and thermoneutral housing conditions

in corticosterone treated mouse and rat models (Cassano et al., 2012; Luijten, Brooks, et al., 2019; Mousovich-Neto et al., 2019). Luijten, Brooks, et al. (2019b) directly compared the BAT adipocyte/LD size of mice exposed to chronic corticosterone treatments housed both at thermoneutrality and standard housing temperatures. They found that corticosterone treatment increased LD area regardless of room temperature (Luijten, Brooks, et al., 2019). Similar findings were observed in this study in the WAT depot of the corticosterone-treated mice, where they display significantly ($p \leq 0.05$) larger LDs compared to all other treatments (Figure 24) (Figure 25). This adipocyte expansion is further evidence that chronic storage occurs within the WAT depot under this chronic corticosterone treatment. This histological shift further exemplifies the whole-body response changing under GC excess.

Linking GCs and BAT thermogenesis has been previously conducted in healthy lean men, where acute administration of prednisone acutely increased BAT ^{18}F-FDG uptake upon mild CE accompanied by an increase in UCP1 protein expression in the BAT (Ramage et al., 2016). However, a double-blind study with men and women exposed to prednisone and subsequent CEs revealed that the GC suppressed BAT activity after only one week (Thuzar et al., 2018). Our study extends upon the findings with prednisone and CE by using corticosterone and mirabegron. Mirabegron administration is a more feasible option than CE for implementing a BAT activation protocol in humans for both logistical reasons and patient comfort. The link between activation of UCP1 and GCs brings up further questions into how UCP1 is precisely expressed when most rodent studies report decreased UCP1 expression with excess GCs.

It has been suggested that GCs result in BAT gaining a “pseudo-atrophy” state where it will exhibit extensive lipid storage capabilities but can also sustain some of its thermogenic

capacity (Luijten, Cannon, et al., 2019). This is a deviation from the conventional understanding that GCs will induce excess lipid accumulation in BAT, and the obese state will significantly lower the tissue's thermogenic capacity (Beaupere et al., 2021; Lee et al., 2014; Luijten, Cannon, et al., 2019; Reddy et al., 2014). Western blot analysis of BAT revealed that the chronic corticosterone treatment significantly ($p \leq 0.05$) increased UCP1 protein expression (Figure 26). In the BAT, this chronic GC treatment displayed even higher UCP1 protein levels than the mirabegron treatments, which directly target the β3AR receptor (Figure 26). In the WAT, slot blot analysis revealed the opposite effects where chronic corticosterone treatment resulted in significantly ($p \leq 0.05$) decreased UCP1 protein expressions compared to the mirabegron treatment groups (Figure 27). The naïve and vehicle controls displayed significantly ($p \leq 0.05$) different UCP1 protein expressions in WAT (Figure 27). While this difference was not expected because the ethanol concentration in the water was so low. The best control group is the vehicle control as this allows for the identification of any treatment effects while also accounting for any effects of the vehicle itself. In order to determine if the mitochondrial content of these AT depots was altered, thereby giving this unexpected result in the BAT, we also measured citrate synthase protein levels as a biomarker for mitochondrial content (Larsen et al., 2012). However, the amount of this protein was not different between sample groups in either tissue (Figure 28) (Figure 29). This represents an interesting finding that mitochondrial content may not change even though BAT UCP1 expression increased in corticosterone and both mirabegron treatments. A clinical trial investigating male omental AT reported variations in citrate synthase protein expression (Christe et al., 2013). In comparison to the nonobese patients, lower citrate synthase protein levels were reported in the patients with obesity and higher protein levels in diabetic patients (Christe et al.,

2013). When comparing the ratios of UCP1 to citrate synthase, Figure 30 illustrates that the corticosterone-treated mice have significantly ($p \leq 0.05$) higher relative UCP1 levels than both naïve and vehicle control groups and the low mirabegron treatment in the BAT. The high mirabegron treatment also displays significantly ($p \leq 0.05$) higher relative UCP1 than the control groups in the BAT (Figure 30). The increased relative UCP1 level in the BAT of the mirabegron high treatment was not an unexpected finding as this β3AR agonist functions to increase the BAT activation in this manner. However, the increased level of UCP1 to citrate synthase in the corticosterone-treated mice is a novel finding. In the WAT, the corticosterone-treated mice have significantly ($p \leq 0.05$) less UCP1 levels than both mirabegron treatments (Figure 30). The increased relative UCP1 level in the WAT of the mirabegron high treatment would suggest that beiging is occurring in this tissue; however, with the naïve control not being different from the mirabegron treatments, this conclusion cannot be supported.

As noted earlier, the relationship observed in the BAT of this study is a deviation from the conventional understanding that GCs will induce lipid accumulation in BAT, and this obese state will lower the tissue's thermogenic capacity which has been reviewed elsewhere (Beaupere et al., 2021; Lee et al., 2014; Luijten, Cannon, et al., 2019; Reddy et al., 2014). However, a further examination into obesity models reveals a plausible explanation. A study conducted at thermoneutrality (30°C) for a 12-week treatment of 50μg/ml corticosterone in drinking water also studied the effects of GC-induced obesity and its impacts on UCP1 (Luijten, Brooks, et al., 2019). Their treatment also caused severe obesity. However, UCP1 expression was only decreased under thermoneutral conditions, not under standard housing temperatures (Luijten, Brooks, et al., 2019). Luijten, Brooks, et al. (2019) further raised the question of how GCs

channel food energy into lipid storage, as they also found GC-induced obesity in UCP1 KO mice (Luijten, Brooks, et al., 2019). These researchers also discuss a unique concept related to examining UCP1 protein levels and conclusions about its effect on physiological significance. They concluded that the UCP1 expression should be reported as UCP1 per BAT protein, as this will represent physiological significance when it comes to the thermogenic capacity (Luijten, Brooks, et al., 2019). When comparing total protein levels from BAT of corticosterone-treated mice, Luijten, Brooks, et al. (2019) observed a decrease in the total amount of protein extracted when mice were housed at thermoneutrality (Luijten, Brooks, et al., 2019). Luijten, Brooks, et al. (2019) investigated the effects corticosterone had on UCP1 and reported that brown adipocytes isolated from corticosterone-treated mice responded with increased oxygen consumption to an artificial uncoupler, indicating that their result of lower norepinephrine-induced oxygen consumption was not the result of decreased respiratory chain capacity (Luijten, Brooks, et al., 2019). Moreover, corticosterone-treated mice at standard housing conditions had a reduction in their underlying metabolism accompanied by increased food intake, both of which contributed to their obese state (Luijten, Brooks, et al., 2019). Under standard housing conditions, they found no effect on total BAT UCP1, or total thermogenic capacity, even though corticosterone treatment induced obesity in these mice (Luijten, Brooks, et al., 2019). Luijten, Brooks, et al. (2019) also concluded that the total amount of BAT UCP1 protein at thermoneutrality was not influenced by the corticosterone induced AT expansion (Luijten, Brooks, et al., 2019). Although the AT mass increased from week two until the end of treatment (week 12) in their study, their body mass was stabilized in the obese state and the effects on

UCP1 protein levels were not maintained as they too normalized in the BAT (Luijten, Brooks, et al., 2019).

Although the GR is essential for signalling in the body, a recent study utilizing dexamethasone (a synthetic GC) has reported that it affects body weight, and glucose homeostasis in BAT (Glantschnig et al., 2019). AT specific deletion of GR has also been studied *in vivo* in response to dexamethasone treatment, where glucose tolerance and insulin sensitivity were unaffected by the GC treatment (Bose et al., 2016). The same study also examined the effect of GR in the liver and found that without liver GRs, fat mass and glycogen content was diminished, illustrating a possible role of the liver GR in the development of metabolic diseases (Bose et al., 2016). While another study that examined AT-specific KO of GR reported that AT function was altered during a HFD, but its expansion was not influenced by the presence or absence of GR (Desarzens & Faresse, 2016). These studies further add complexity to our current understanding of GC-induced metabolic disease and illustrate how it needs to be studied further. Our findings with increased UCP1 expression under chronic corticosterone treatment additionally show how BAT is altered under GC treatment. The exact mechanisms of AT adaptation may involve GR related signalling and potentially other signaling pathways. pathways likely to involve the GR. However, studies involving a HFD and obesity may aid in our understanding.

A study conducted by Winn et al. (2017) further adds validity to the observation of increased UCP1 under stressful situations such as HFD (Winn et al., 2017). They used female mice either with or without UCP1 (KO) to understand their susceptibility to BAT whitening under Western or control diets (Winn et al., 2017). Whitening occurred in both mice (either with or

without UCP1) under a Western diet; however, the whitening effects (increased fasting insulin, decreased glucose tolerance, increased adipocyte area, and increased macrophage infiltration) were amplified in mice without UCP1 (Winn et al., 2017). Therefore, UCP1 may be critical in any attempt to mitigate BAT whitening. Diet-induced thermogenesis (DIT) has been found to increase UCP1 under an obesogenic diet (containing high amounts of fat) (von Essen et al., 2017). However, von Essen et al. (2017) report that the total amount of UCP1 protein at thermoneutrality is dependent on the total BAT content itself. When diet induced thermogenesis (DIT) occurs, the more UCP1 present in BAT may limit obesity development during the HFD exposure, but it will not prevent obesity (von Essen et al., 2017). Alcala et al. (2017) conducted studies on HFD obese mice specifically to investigate BAT and WAT dysfunction. This study notably reported increased UCP1 protein expression without altering the mitochondrial content of BAT (Alcala et al., 2017). This increased UCP1 protein content was not reflected in the mRNA levels of BAT (Alcala et al., 2017). Both HFD and GCs induce obesity, IR, increased AT mass, increased protein catabolism and hyperphagia (Cummins et al., 2014; Karatsoreos et al., 2010; Licholai et al., 2018; Rose & Herzig, 2013; Sefton et al., 2019). HFDs will result in a lower respiratory exchange ratio (RER) indicating the use of fats as fuel instead of carbohydrates (Cummins et al., 2014). RER measurements have not been previously reported with corticosterone-induced obese mice (Sefton et al., 2019).

The obese BAT also illustrated higher reactive oxygen species (ROS) levels and enhanced mitochondrial respiration (2X as much as lean BAT), illustrating that this tissue responds to obesity differently from what was conventionally understood (Alcala et al., 2017). The initial increase in inflammation, endoplasmic reticulum (ER) stress and generation of ROS was not high

enough to completely alter the fuel burning capacity of the tissue (Alcala et al., 2017). Alcala et al. (2017) hypothesized that the increased UCP1 protein content arises from the accumulation of protons in the intermembrane space being pushed back into the mitochondrial matrix and from the FFAs activating the protein itself, further promoting its fuel-burning capabilities (Alcala et al., 2017). Findings from a recent study involving patients with obesity found an increase in *Ucp1* mRNA expression in the visceral AT in conjunction with increased resting energy expenditure (REE) (Bettini et al., 2019). The authors of this study conclude that the increase in *Ucp1* could represent a potential mechanism to prevent further weight gain in these patients with obesity (Bettini et al., 2019). The idea that increased uncoupling can result from the tissue increasing its energy-burning ability in order to respond to inflammation, ER stress or ROS could help explain why we found increased UCP1 expression under chronic corticosterone treatment in BAT. As UCP1 was higher in the corticosterone-treated group compared to the mirabegron treated mice, it is likely that the corticosterone treatment influences UCP1 in some manner. Moreover, in the GR-KO studies mentioned above (Bose et al., 2016; Desarzens & Faresse, 2016) it was demonstrated that AT expansion was not impacted by the presence or absence of the GR, suggesting that this signalling pathway may not be involved in the increased uncoupling at all.

Specific Aim #2: Determine how oxidative stress and immune cell infiltration is influenced by corticosterone or under β3AR stimulation

Inflamed adipocytes and the associated recruitment of macrophages that form CLSs are an important tissue level response in T2D, obesity, and metabolic syndrome (Kotzbeck et al., 2018; Murano et al., 2008; Wu & Ballantyne, 2020). Analysis of the histological sections was

conducted for both BAT and WAT to look for the formation of CLS, a hallmark of AT inflammation. While no CLS were found in either BAT or WAT, an investigation into the level of lipid peroxidation was conducted. Lipid peroxidation is a marker of altered lipid metabolism in response to oxidative damage and is increased in models of metabolic syndrome, obesity and diabetes (Choromańska et al., 2020; Dham et al., 2021; Furukawa et al., 2004; Manna & Jain, 2015). Obesity-linked inflammation is currently very poorly understood since the location and types of AT involved will vary in their response (Wu & Ballantyne, 2020). AT dysfunction can increase immune cell infiltration where dead or dying adipocytes signal macrophages to clear the cellular debris from the tissue (Kotzbeck et al., 2018; Wu & Ballantyne, 2020). During the development of obesity, inflammation and its associated M1 type inflammatory cells will increase in the AT depot; however, the depot dictates how early the inflammatory changes will occur (Wu & Ballantyne, 2020). In visceral AT, a HFD can induce these changes in as little as three days (Wu & Ballantyne, 2020). ScWAT is much slower to respond, maybe in part due to their increased potential to expand their LDs compared to visceral or brown adipocytes (Kotzbeck et al., 2018; Wu & Ballantyne, 2020).

Models of obesity and increased lipid deposition in BAT show that there is the potential for inflammation in the tissue. However, a great deal is currently still unknown when it comes to AT inflammation and the markers for determining the degree of tissue dysfunction.

Although CLSs were not observed in either AT depot studied in this investigation, the expression of oxidative stress-induced lipid peroxidation was determined. 4-Hydroxynoneal (4-HNE) is one of the most bioactive lipid molecules produced from oxidative stress that can interact with proteins and phospholipids (Dham et al., 2021; Manna & Jain, 2015; Zhong & Yin,

2015). Excessive accumulation of 4-HNE is associated with a host of diseases ranging from diabetes and cancer and can affect virtually every organ system in the body (Dham et al., 2021; Manna & Jain, 2015; Zhong & Yin, 2015). AT and 4-HNE have been linked metabolically with increased levels of 4-HNE being associated with decreased insulin sensitivity and poor metabolic health (Dham et al., 2021; Elrayess et al., 2017; Masschelin et al., 2020). The mitochondria are a major site for ROS production and are also important for forming 4-HNE (Zhong & Yin, 2015). With the relationship between mitochondria dysfunction and oxidative stress, it is crucial to investigate this in connection with chronic stress and AT further. Multiple studies have discussed obese rodents and patients exhibiting higher concentrations of lipids, 4-HNE, and ROS (Choromańska et al., 2020; Dham et al., 2021; Jaganjac et al., 2017; Manna & Jain, 2015; Marín-Royo et al., 2019; Petrick et al., 2020). In this study, we examined the protein adduct formation of 4-HNE in both BAT and WAT (Figure 31) (Figure 32). Unexpectedly, no differences between the treatment groups were observed when it came to the formation of 4-HNE adducts in these tissues. With apparent observable differences in LD area and tissue size, one might expect that dysfunction was occurring within the AT depots of these mice. The lack of change in treatment-dependent 4-HNE levels can be partially explained by the short duration of our study which may not have been sufficient time to elicit a protein change at the tissue level. Studies involving obese rodents reporting inflammation are usually greater than seven weeks in duration, and many of them only measure the RNA or plasma level of inflammatory/ stress markers, not changes in the protein level at the tissue. While we found no significant increase in the level of lipid peroxidation in either tissue, we did note a moderate positive correlation (coefficient=0.6422) between BAT and WAT depots (Figure 33). This correlation illustrates that

the increased level of lipid peroxidation in one AT depot is associated with increased 4-HNE levels in other AT depots. This is an interesting relationship that has not been previously reported by others to our knowledge.

Specific Aim #3: Investigate the effects of corticosterone or β3AR stimulation on whole-body insulin resistance

Impaired glucose clearance is a key component of metabolic syndromes and was described in chronic corticosterone-treated animals in as little as four-weeks (when performing a glucose tolerance test) (Karatsoreos et al., 2010; Kinlein et al., 2017). While our study did not measure oral glucose tolerance, we did not observe any significant alterations in fasting plasma glucose concentrations between the corticosterone group and to the other treatments (Figure AS1-Plasma A). Other studies with corticosterone treatment administered via drinking water reported increased glucose concentrations in corticosterone-treated mice. However, this increase was found to occur after five weeks of treatment which may account for why we did not observe this trend in our study (Burke et al., 2017; Cassano et al., 2012). Kinlein et al. (2017) compared the effects of corticosterone treatments in adolescent (3 weeks) and adult (>8 weeks) mice and found that age played a large role in glucose metabolism, with adolescent mice illustrating enhanced glucose clearance (Kinlein et al., 2017). Given the different results in glucose metabolism between adult (62 days old) and adolescent (22 days old) mice, there may be an age effect in addition to chronic corticosterone treatment on the glucose metabolism that cannot be ignored (Kinlein et al., 2017).

Fasting insulin concentrations were significantly ($p \leq 0.05$) greater in the corticosterone-treated mice compared to controls and mirabegron-treated groups in this study (Figure AS1-Plasma B). GC-induced IR has been reported in corticosterone-treated mice at this dose and housing temperature (Gasparini et al., 2016; Karatsoreos et al., 2010; Kinlein et al., 2017; van Donkelaar et al., 2014). Using the Homeostatic Model of Assessment for Insulin Resistance (HOMA-IR), we determined that corticosterone treatment for four weeks results in severe IR (Figure AS1-Plamsa C). Other researchers have also noted that this level of IR remains, even when corticosterone treatment lasts for 12-weeks (van Donkelaar et al., 2014). Burke et al. (2017) concluded that the development of IR is reciprocally related to body composition. This alteration in insulin sensitivity with corticosterone exposure has also been linked to increased expressions of genes promoting glucose metabolism (Burke et al., 2017) and protein breakdown in the muscle (Burke et al., 2017; Kinlein et al., 2017). It is important to note that both mirabegron treatments did not result in altered glucose or insulin levels compared to the controls (Figure 34). To our knowledge, this is the first *in vivo* study to examine mirabegron's effects on glucose and insulin levels at this physiologically relevant dose.

Karatsoresos et al. (2010) reported elevated plasma leptin and insulin levels under corticosterone treatment, and these two measurements correlated with one another, although these measurements were conducted on animals who were in the fed state. Considering the link between leptin resistance and WAT, they also demonstrated that increased plasma leptin, increased amounts of WAT, and increased hyperphagia was associated with leptin resistance (Karatsoreos et al., 2010). Due to leptin's origin in the adipocytes, there is a logical connection between leptin resistance and increased WAT (Karatsoreos et al., 2010). Chronic treatment with

corticosterone was found to be equivalent to those found in diet-induced obese (DIO) mice, connecting the importance of leptin and obesity to AT (Karatsoreos et al., 2010). The exact mechanism of GC-induced changes on leptin and insulin remains unclear, but more studies are beginning to hint at these answers. This will be further discussed later in the dissertation.

Summary and Conclusions from Animal Study #1

We were able to successfully stimulate the β3AR pathway with mirabegron, as evidenced by the increased UCP1 protein expression in BAT ($p \leq 0.05$) compared to the control groups. It is important to note that this β3AR stimulation did not affect fasting glucose or insulin levels, tissue or body mass, or oxidative stress markers, findings that have not been previously reported. To our knowledge, this is the first study to report significantly ($p \leq 0.05$) increased UCP1 protein expression accompanying a whitened phenotype in BAT under chronic treatment with corticosterone in just four weeks. Previous studies with GC treatments in both rodents and humans report decreased BAT activation, decreased UCP1 mRNA and protein levels, in combination with whitened BAT and whole-body IR (Poggioli et al., 2013; Ramage et al., 2016; Strack et al., 1995; Thuzar et al., 2018; van den Beukel et al., 2015).

In combination with the findings reported by Alcala et al. (2017) of obese BAT displaying enhanced mitochondrial respiration, we illustrate that chronic exposure to corticosterone induces IR, increased whole-body and BAT mass, increased LD area and increased UCP1 protein expression, while the mitochondrial content of the tissue remains unchanged. This increased uncoupling potential could be a compensatory mechanism being undertaken by the tissue for excess caloric intake as lipid storage increases dramatically. As illustrated by our study, BAT and

WAT will display different physiological outcomes when it comes to lipid overload conditions. Kotzbeck et al. (2018) also reported differences between these two tissues and describe how BAT has a greater likelihood of death under lipid overload than the expandable WAT cells, which may contribute to obesity-induced inflammation (Kotzbeck et al., 2018). We also illustrate that the level of lipid peroxidation found in one AT depot can be an indicator for other AT depots throughout the body. With no increase in BAT or WAT formation of 4-HNE adducts at the tissue level, it further supports our hypothesis that a compensatory mechanism may be at play in order to deal with the excess lipids being stored. Increased UCP1 protein expression has been widely regarded as a beiging phenotype accompanied by improved glucose and insulin sensitivities. However, the same level of increased UCP1 protein expression found in a whitened BAT requires further investigations into this alternative uncoupling pathway. Future studies investigating excess GCs and BAT uncoupling potential is fundamental to our understanding of this tissue and could provide future targets to explore when treating metabolic diseases.

Animal Study #2 (AS2)

In order to further examine how corticosterone affects the β3AR stimulation and metabolic dysfunction of AT, AS2 examined if these two treatments would directly interact at the whole-body level. Mirabegron was formulated to be an extended release tablet for oral administration in humans that will be absorbed through the oral controlled absorption system (Eltink et al., 2012). All evidence thus far explains that mirabegron is absorbed through the intestinal and/or the liver (Eltink et al., 2012). The absorption of mirabegron increases with larger doses and the drug becomes more bioavailable at these increased concentrations (likely though intestinal efflux transporter P-glycoprotein) (Eltink et al., 2012). Oral GCs, such as corticosterone, are absorbed systemically, with the liver and upper intestine being the major sites of absorption (Mundell et al., 2017; Williams, 2018). The liver is the major site of activation and deactivation of these compounds (Williams, 2018). GCs are known to regulate the enzyme cytochrome P450 both directly and through cross talk, both of which can affect how different pharmacological compounds are metabolized (Matoulková et al., 2014). Mirabegron has been investigated for its ability to interact with cytochrome P450 directly, and the results indicate that mirabegron is not considered a substrate for this molecule *in vivo* (Lee et al., 2013). While both are absorbed in the liver and intestine when taken orally, the lack of interaction between cytochrome P450 found with mirabegron indicates that there is likely not a mechanistic effect exhibited by mirabegron on corticosterone directly. Further studies need to be done to fully examine drug-to-drug interactions with GCs and mirabegron, however, the current understanding both in the scientific and medical community is that these two compounds will not adversely interact in patients/ *in vivo* (UpToDate Inc, 2022).

The interaction of these two pathways has only previously been explored by van den Beukel et al. (2014) and (2015), both of which were short-term studies (van den Beukel et al., 2014, 2015). Their 2014 study directly examined the effects of 24 hours of CE on young male mice (van den Beukel et al., 2014). They observed almost a two-fold increase in plasma adrenocorticotropic releasing hormone and fecal corticosterone excretion levels, concluding that adrenocorticotropic hormone plays a role in the beiging process and corticosterone opposes this effect (van den Beukel et al., 2014). In a follow up study, they implanted mice with a corticosterone pellet (50mg) for one week before CE for 24 hours (van den Beukel et al., 2015). After this short treatment, elevated plasma TAG and lipogenic genes were normalized by CE (van den Beukel et al., 2015). The beiging of ingWAT that was reduced by corticosterone was also partially corrected with CE (van den Beukel et al., 2015). This study exemplified the use of the β3AR pathway in mitigating the effects of chronic stress and its influence on AT. In AS2 of this dissertation, young male mice were exposed to either chronic corticosterone or mirabegron or a combination of both treatments together in their drinking water for four weeks. We hypothesized that the negative effects of corticosterone-induced alterations to AT would be mitigated by the β3AR agonist mirabegron. In order to examine the combination of the two treatments, similar outcome measurements to AS1 were applied to AS2 in order to compare the effects of the combination treatment to either corticosterone or mirabegron individually. To investigate our hypothesis, we had one specific aim for this animal study that would allow for the beiging and whitening processes to be explored when they are administered in combination.

Specific aim for animal study #2:

4) Examine how mitochondrial content is impacted in the presence of the combination of corticosterone and β3-adrenergic stimulation

Mirabegron does not induce adipose tissue beiging when in combination with corticosterone

Similar to AS1, the corticosterone mice weighed significantly ($p \leq 0.05$) more than the mirabegron and vehicle treatments (Figure 35). The increased weight gain began on day 14 of the study, seven days later than AS1. This delay in increased bodyweight is likely due to an improved delivery of the corticosterone to better match the target dose. As mentioned previously, the corticosterone concentration in the drinking water was lowered to more accurately achieve the target dose given this treatment group's increased drinking water consumption. A direct comparison of the average dose received per mouse per day and how closely this dose matched the target is displayed in Table 1. AS1 displays huge spikes in the dose received until week three where the dose was over 400% of what was desired. The corticosterone group in AS1 had an overall average dose 171% of the target, whereas the corticosterone group in AS2 was 132% of what was targeted (Table 1). The combination treatment experienced 91% of the corticosterone dose and 123% of the mirabegron dose desired (Table 1) (Table 2). An increase in weight gain during week two of corticosterone treatment was also found by Cassano et al. (2012), whereby 14 days into the treatment, weight gain became significantly different (Cassano et al., 2012). An increase in weight gain was also

significant for the combination treatment; however, this was only during the latter half of the experiment (Figure 35). The overall change in body weight was significantly ($p \leq 0.05$) higher in the corticosterone and combination treatment groups compared to the mirabegron treatment and vehicle control (Figure 36). This same trend was also observed for the fasting body weight, with the corticosterone and combination treatments being significantly ($p \leq 0.05$) greater than the mirabegron or vehicle groups (Figure 37). However, mirabegron is reported to be ineffective in regulating body weight gain of a healthy individual and is only effective for weight loss in the condition of obesity (O'Mara et al., 2020).

The corticosterone mice appeared to move less around the cage and had oily-looking coats than the mirabegron treatment or vehicle control (Figure 38). The combination-treated mice also displayed this oily appearance and had less home cage locomotion (Figure 38). This oily appearance may be related to the stress response in the sebaceous glands (Y. Chen & Lyga, 2014). The consumption of drinking water was again significantly ($p \leq 0.05$) increased in the corticosterone group (Figure 39); however, the target dose was better achieved (Figure 40). The corticosterone treatment in AS2 achieved on average 132% of the target dose, which is more on target than the corticosterone group in AS1 with at average dose received 171% of the target (Table 1). The mirabegron treatment group received consistent dose delivered per mouse per day (Figure 41) with the average dose being 88% of what was targeted (Table 2). The combination treatment mice also drank significantly ($p \leq 0.05$) more water than the mirabegron and vehicle groups (Figure 39). However, the average doses of corticosterone and mirabegron were closely matched with the targeted doses of 91% and 123% respectively in our combination treatment (Figure 42) (Table 1) (Table 2).

The BAT of the corticosterone and combination treatment groups visually appeared larger and less brown in colour than the vehicle control or mirabegron treatment (Figure 43), although this was not quantified. This larger size is accompanied by significantly ($p \leq 0.05$) increased BAT weights and in relation to body weight for both the corticosterone and combination treatments (Figure 44). The WAT also visually appears larger in corticosterone and combination treatments (Figure 43). These pictures are again supported by significantly ($p \leq 0.05$) larger WAT weights and in relation to body weight for the corticosterone and combination treatment groups (Figure 45). Histologically, the LD area for both corticosterone and combination treatments were significantly ($p \leq 0.05$) increased relative to the vehicle and mirabegron treatment for both the BAT and the WAT (Figure 46) (Figure 47) (Figure 48) (Figure 49).

In obese individuals (Baskin et al., 2018; K. Y. Chen et al., 2020; Finlin et al., 2020) or rodents (Hao et al., 2019; O'Mara et al., 2020) mirabegron has been found to increase AT lipolysis, lower LD area, and contribute to improved whole-body metabolism. While these studies use different parameters than our investigation, we anticipated the mechanisms to be similar. In our study, the BAT and WAT depots appear not to have been affected by having mirabegron in the combination treatment as the LD areas were not significantly different. With the corticosterone response being so strong, it is possible that mirabegron is not enough to elicit an effect to oppose the negative effects of the GC when administered simultaneously.

The effects of GCs on AT have been reviewed by others (Chait & den Hartigh, 2020; Peckett et al., 2011); however, it is crucial to understand what we know about the link between

stress and AT dysfunction. AT was described by Peckett et al. (2011) to be largely influenced by GCs due to an increased amount of 11β-HSD1 enzyme within both BAT and WAT depots. It has been hypothesized that modest increases in the activity of 11β-HSD1 can result in hyperphagia and visceral obesity (Liu et al., 2013; Masuzaki et al., 2001; Peckett et al., 2011). In fact, increases in the expression of this enzyme in BAT can decrease the functionality of this depot through reductions in BAT specific genes (Liu et al., 2013). GCs in acute settings increase lipolysis to liberate stored TAG in the LD and break it down into FFA and glycerol. This breakdown can be achieved through a variety of pathways, including the β3AR pathway, and allows the energy demands of the mammal to be fulfilled. While increased lipolysis and smaller LD size are part of the beiging process and can be achieved with acute doses of GCs, excess GCs follow a completely different response. Unlike acute GCs, chronic excess GCs promote AT expansion, weight gain, hypertension, and increased risk for T2D (Peckett et al., 2011; Pivonello et al., 2020). This phenotype is clinically seen in patients with Cushing's syndrome or patients on exogenous GC treatment (Peckett et al., 2011; Pivonello et al., 2020; Sharma et al., 2015). Since GCs render their effects on other hormones and influence the entire body, the direct and indirect effects are difficult to decipher (Peckett et al., 2011).

Connections between the effects of stress and AT are still being investigated, but a notable study involving rats, the hypothalamus-pituitary-thyroid (HPT) axis and BAT is worth mentioning. The effects of repeated chronic stress in rats were investigated by Castillo-Campos et al. (2021) for their relationship to the HPT axis and its effect on BATs response to CE (Castillo-Campos et al., 2021). They found chronic stress, either repeated restraint stress or chronic variable stress, blunts BATs ability to respond to CE (Castillo-Campos et al., 2021). Both types of

stress reduced food intake which corresponded to decreased body weight and decreased both BAT and WAT masses (Castillo-Campos et al., 2021). They concluded that the long-term effects of stress on adrenergic and hormonal signalling are likely more responsible for HPT dysfunction (Castillo-Campos et al., 2021). This connection between the HPT axis and chronic stress can likely be extrapolated to the HPA axis and the β3AR pathway and its interaction with chronic stress. Future work into examining these pathways directly will be vital for furthering our understanding of GCs and their effects on AT dysfunction that can result in obesity and metabolic syndrome.

While chronic stress can cause AT dysfunction, mirabegron may be able to counter this effect. Obese individuals who are administered mirabegron show reduced AT dysfunction, (Finlin et al., 2020) and in rodents, DIO mice administered mirabegron have reduced WAT weights (Hao et al., 2019). Therefore, we anticipated that mirabegron would reduce the negative effects of corticosterone and the protein expression of UCP1 to be strongly impacted. In AS2, the protein expression of UCP1 in BAT was the same amongst all treatments (Figure 50). Unlike AS1, neither corticosterone nor mirabegron resulted in increased UCP1. The difference between the two studies could be partially explained by the corticosterone dose being achieved, with AS2 being on closer to the target for the full duration. However, a further look into the differences between these two studies will be examined later in the discussion. In AS2 WAT, slot blot analysis revealed that the corticosterone and combination treatments resulted in a significant ($p \leq 0.05$) decrease in UCP1 protein expression compared to the mirabegron treatment groups (Figure 51). Surprisingly, the vehicle control in this study displayed significantly ($p \leq 0.05$) higher UCP1 in the WAT compared to all other treatment groups (Figure 51). In order to determine if the

mitochondrial content of these AT depots was altered, we also measured citrate synthase protein levels in each sample as it is a biomarker for mitochondrial content (Larsen et al., 2012). However, the amount of this protein was not different between sample groups in either tissue (Figure 52) (Figure 53).

When comparing the ratios of UCP1 to citrate synthase (Figure 54A), there is no difference found between the treatments in the BAT. In the WAT, the ratio reveals that the vehicle control is significantly ($p \leq 0.05$) higher UCP1 expressions than all other treatment groups (Figure 54B). The increase in UCP1 expression in the WAT of the vehicle control was a surprising result. This illustrated that the mirabegron treatment did not result in beiging, and in fact, the vehicle shows more beiging than the β3AR agonist. These results demonstrate that mirabegron does not have the desired effect of reducing weight or increasing beiging in the setting of elevated GCs.

A study conducted by Poggioli et al. (2013) examined the effects of exposure to the synthetic GC dexamethasone on the AT of mice fed a HFD (Poggioli et al., 2013). These mice also received an injection of a β3AR agonist, CL316,243, where the pre- and post-injection oxygen consumption were determined, and later the *Ucp1* mRNA expressions were also measured. The dexamethasone treatment increased body fat under both the chow diet and HFD (Poggioli et al., 2013). The dexamethasone-HFD treated mice had exacerbated fatty liver disease compared to those fed a HFD (Poggioli et al., 2013). The oxygen consumption rate was greatly suppressed in the dexamethasone-HFD treated mice, even with the β3AR agonist (Poggioli et al., 2013). The BAT expression of *Ucp1* in the dexamethasone-HFD treated mice was also significantly decreased in the dexamethasone-HFD treated mice (Poggioli et al., 2013). This study illustrated the strong

effects GCs can have on an animal's body weight, oxygen consumption and BAT *Ucp1* mRNA levels, each of which are exacerbated in cases of obesity or animals fed a HFD. Interestingly, a β3AR agonist could not rescue the animals' EE when treated with dexamethasone and a HFD. The long-term treatment with GCs results in what appears to be un-rescuable effects in BAT, even with a β3AR agonist. While Cassano et al. (2012) studied the effects of corticosterone administration in mice and found that many of the undesirable effects can be reversed when the GC is withdrawn for two weeks (Cassano et al., 2012), the continuation of these GCs appears to be "untouchable" with β3AR agonists. The β3AR agonist treatment in Poggioli et al.'s (2013) study was acute, but the lack of response further illustrates the strong effect GCs have on the body. Given the effects of the activated β3AR pathway noted above in short-term *in vivo* studies (van den Beukel et al., 2014, 2015), we expected the combination treatment to have reduced body and AT weights compared to that of the corticosterone treatment. However, since there was no reduction in body weight, nor a lower amount of body weight gained in the combination treatment group, the two treatments clearly do not directly oppose each other. Hao et al. (2019) induced obesity with a HFD for six weeks prior to administering mirabegron (via ALZET osmotic pump) at a dose of (2mg/kg/day) to C57BL/6J mice for three weeks (Hao et al., 2019). They found that mirabegron reduced the body weight gain and WAT weights (Hao et al., 2019). The reduced body weight gain and WAT weights were also associated with improved glucose tolerance and insulin sensitivity after two and three weeks of mirabegron treatment (Hao et al., 2019). The mirabegron reduction in body weight and WAT mass were less than HFD and vehicle but still significantly higher than the chow fed mice in their study (Hao et al., 2019). However, they did not see changes in the BAT weights (Hao et al., 2019). In our study, the mirabegron

dose was approximately 8mg/kg/day but ingested via drinking water (i.e. noncontinuous delivery) vs the continuous delivery with osmotic pumps used in the Hao et al. (2019) study. Further adding to these findings, Peres Valgas da Silva et al. (2021) recently conducted a study where mice were given a HFD for ten weeks prior to mirabegron being administered via oral gavage (10mg/kg) for two subsequent weeks (Peres Valgas da Silva et al., 2021). The two-week mirabegron treatment diminished the amount of LDs in the BAT and liver, increased the EE, and increased UCP1 protein expression in the BAT (Peres Valgas da Silva et al., 2021). However, the BAT UCP1 expression in the HFD group alone was not different from the control group (chow fed mice) and UCP1 expression was only increased when mirabegron was administered (Peres Valgas da Silva et al., 2021). Mirabegron did not increase ingWAT beiging (Peres Valgas da Silva et al., 2021), which is in concert with the results found in our study with corticosterone. Peres Valgas da Silva et al. (2021) explained the lack of mirabegron induced beiging in the ingWAT as a time-dependent finding with the two-week duration not being long enough to elicit the beiging change in the tissue (Peres Valgas da Silva et al., 2021). In our study, the treatment of concurrent GC and β3AR agonist administration resulted in virtually no change from the GC treatment alone in terms of body mass, weight gain, tissue appearance, histological examination and UCP1 protein expression. To our knowledge, our study is the first to examine these treatments concurrently for a mid-length amount of time, and the first study to illustrate that mirabegron could not induce beiging in WAT or counteract BAT whitening when corticosterone was present in levels equivalent to metabolic syndrome.

Table 1. A comparison of the dose of corticosterone received in each animal study where the target dose was 500μg/mouse/day and water consumption was measured twice a week.

	Animal Study #1		Animal Study #2			
	Corticosterone Treatment		Corticosterone Treatment		Combination Treatment Corticosterone Dose	
Length of Time in Treatment	Average Dose Received (μg/mouse/day)	% of Target Dose Achieved	Average Dose Received (μg/mouse/day)	% of Target Dose Achieved	Average Dose Received (μg/mouse/day)	% of Target Dose Achieved
Week 1	590	118%	554	111%	356	71%
	695	139%	486	97%	349	70%
Week 2	769	154%	549	110%	824	165%
	1031	206%	622	124%	379	76%
Week 3	1128	226%	926	185%	577	115%
	2038	408%	730	146%	364	73%
Week 4	360	72%	711	142%	390	78%
	219	44%	686	137%	382	76%
Overall Average % of Target Dose Achieved		171%		132%		91%

Table 2. A comparison of the dose of mirabegron received in each animal study where the target dose was 0.24mg/mouse/day and water consumption was measured twice a week.

	Animal Study #1		Animal Study #2			
	Mirabegron (High) Treatment		Mirabegron Treatment		Combination Treatment Mirabegron Dose	
Length of Time in Treatment	Average Dose Received (mg/mouse/day)	% of Target Dose Achieved	Average Dose Received (mg/mouse/day)	% of Target Dose Achieved	Average Dose Received (mg/mouse/day)	% of Target Dose Achieved
Week 1	0.20	82%	0.23	97%	0.23	94%
	0.19	81%	0.21	85%	0.22	93%
Week 2	0.20	82%	0.20	85%	0.55	231%
	0.20	84%	0.22	90%	0.24	101%
Week 3	0.19	77%	0.21	88%	0.40	165%
	0.20	81%	0.21	86%	0.23	97%
Week 4	0.18	74%	0.21	87%	0.25	102%
	0.18	77%	0.21	89%	0.24	101%
Overall Average % of Target Dose Achieved		80%		88%		123%

Oxidative stress and immune cell infiltration are not affected by corticosterone or mirabegron treatment, and mirabegron does not mitigate corticosterone induced increases in circulating leptin

Obesity can lead to suppressed mitochondrial activity and decreased biogenesis, leading to sustained oxidative stress (Masschelin et al., 2020). The AT implications of obesity are far-reaching and increased oxidative stress levels play a role in the pathogenesis of metabolic disease. Obese humans have higher oxidative stress levels in their WAT, and the tissue's ability to attenuate 4-HNE decreases in the obese state, further increasing its level of stress within AT (Masschelin et al., 2020). In this study, the protein adduct formation of 4-HNE was measured in both BAT and WAT as an indicator of oxidative stress. Similar to what was found for AS1, the BAT (Figure 56) and WAT (Figure 57) did not display differences in their level of 4-HNE protein adducts, an indicator of lipid peroxidation, between the treatments. Using a Pearson correlation, there was a moderate positive correlation (coefficient=0.6397), indicating again that the level of lipid peroxidation in one AT depot is related to the level in other depots (Figure 58). With the level of 4-HNE adducts not significantly different between our treatments, we could not determine if mirabegron was able to counteract the negative effects of corticosterone in terms of oxidative stress.

Immune cell infiltration in the form of CLSs were not observed in any treatments. As was stated with AS1, the four-week treatment may not have been of long enough duration to evoke the response in the AT depots studied. Many studies examining adipocytes use HFD rodent models where diets are composed of 60% fat and can last anywhere from 7 to 20 weeks in duration (Avtanski et al., 2019). A study where a HFD was given to male CL57BL/6J DIO mice for

nine weeks found significant ($p \leq 0.05$) increases in WAT and BAT weights, LD area, number of CLS, liver weight, hepatic lipid accumulation, fasting plasma glucose, insulin and leptin, and elevated circulating cytokines (Avtanski et al., 2019). While CLSs were not increased in our four-week treatment of chronic corticosterone, other parameters of the HFD studies were matched with IR, increased body mass, increased AT mass, and increased LD area. Do (2019) report different timelines for macrophage infiltration for gonadal and scWAT when under corticosterone-induced AT expansion (Do, 2019). Their study was eight weeks in duration in which they were able to detect macrophage markers in both subcutaneous and gonadal AT at the end of the treatment (Do, 2019). Gonadal AT macrophage infiltration was present after one week but was very delayed in the scWAT (Do, 2019). This increased macrophage infiltration preceded corticosterone induced obesity but was concurrent with induction of IR (Do, 2019). The current relationships between oxidative stress, macrophages and AT are not known due to the depot-specific nature of these responses. Peres Valgas da Silva et al. (2021) also investigated the effects of a two-week mirabegron treatment on inflammation after a 10-week HFD (Peres Valgas da Silva et al., 2021). Their findings of serum and epididymal AT TNFα levels being lowered when mirabegron was administered illustrate the ability of this β3AR agonist to interact with AT and systemic inflammation (Peres Valgas da Silva et al., 2021); however, further research needs to be conducted. The effects each AT depot has on whole-body health cannot be underscored. Additional knowledge into these areas is required to understand obesity-induced inflammation and the effects GCs can play in it. Without fully understanding these connections, treatment plans to combat GCs negative health implications cannot be thoroughly examined.

One of the most important adipokines for maintaining energy balance and signalling satiety is leptin (L. Chen et al., 2015; Guilherme et al., 2019; Kahn et al., 2019; Luo & Liu, 2016; Pan & Myers, 2018). The amount of leptin secreted by adipocytes is approximately proportional to the amount of TAG stored in the AT; its secretion influences the nutritional status of many other biological processes, including insulin signalling, inflammation, and other hormones (including GCs) (L. Chen et al., 2015; Guilherme et al., 2019; Kershaw & Flier, 2004a, 2004b; Kotzbeck et al., 2018; Luo & Liu, 2016; Pan & Myers, 2018). Leptin acts by binding to the leptin receptor in the brain to suppress food intake, increase EE, and deplete the stored TAG (Pan & Myers, 2018). Leptin can also act to reduce the production of adrenal corticosteroids by creating a feedback loop between the HPA axis and AT (Pan & Myers, 2018; Pralong et al., 1998). Leptin resistance is thought to be connected to increased circulating GCs where the effects of leptin are diminished, lead to increased food intake, and may be related to the obesity mechanism, connecting part of the dots between GCs and leptin (Pralong et al., 1998). In this study, the corticosterone and combination treatments had significantly ($p \leq 0.05$) greater plasma leptin concentrations than the vehicle control or mirabegron treatment (Figure 60). Elevated plasma leptin levels have been found in cases of obesity in both rodents and humans, where higher leptin levels correspond with increased adiposity. Many others have also found elevated plasma leptin levels with corticosterone treatment (Cassano et al., 2012; Karatsoreos et al., 2010; van Donkelaar et al., 2014). Hao et al. (2019) observed slight decreases in AT leptin mRNA expressions after mirabegron administration to mice fed a HFD (Hao et al., 2019). Sui et al. (2019) found that six weeks of mirabegron treatment in mice resulted in increased food consumption, lower body weight, increased UCP1 expression and decreased leptin

concentrations compared to vehicle treated mice (Sui et al., 2019). As mentioned earlier, Peres Valgas da Silva et al. (2021) recently completed a study where mice were given a HFD for ten weeks prior to mirabegron being administered via oral gavage (10mg/kg) for two subsequent weeks (Peres Valgas da Silva et al., 2021). They found that this two-week treatment could not lower the plasma leptin levels induced by the HFD (Peres Valgas da Silva et al., 2021). It is important to note that the method of drug delivery (i.e. through oral gavage, through osmotic pump, or through drinking water) will likely impact the results of the study. Oral gavage will deliver a one-time large treatment dose daily. While this will be similar to how humans ingest mirabegron, there may be limits to the absorption and amount of the drug that ends up in circulation. While osmotic pumps will deliver a continuous dose throughout the day, this is not physiological as it will still be delivered when the mouse is sleeping. Finally, through drinking water, the drug will only be delivered during the animal's awake hours, but the dose delivered will be smaller and noncontinuous.

While we anticipated the combination treatment to have reduced plasma leptin levels compared to the corticosterone treatment, this was not the case. Despite the findings by Hao et al. (2019) and Sui et al. (2019), the effects of corticosterone on leptin were stronger than that of mirabegron. In mice, a two-week mirabegron treatment after a HFD did not lower plasma leptin levels, further illustrating a limit to mirabegron's effect (Peres Valgas da Silva et al., 2021). When examining the effects of mirabegron in obese individuals, Finlin et al. (2020) reported that plasma leptin levels of patients with obesity were also not affected by the mirabegron treatment (Finlin et al., 2020). The findings by Finlin et al. (2020) and Peres Valgas da Silva et al. (2021), in combination with our study, illustrate that the β3AR agonist, mirabegron, cannot offset elevated

leptin secretion in models of obesity or excess GCs. The increase in plasma leptin in our combination and corticosterone treated mice are in concert with Hao et al. (2019)'s findings reporting increased leptin, lipid droplet size and weight gain. The increased leptin levels observed in corticosterone and combination mice further support the inducibility of GCs to amplify metabolic syndrome by increasing the amount of stored TAG within the AT depots and influence over whole-body health, independent of β3AR activation.

Mirabegron does not lower the level of insulin resistance when in combination with corticosterone

With IR being such a critical component of metabolic syndrome, fasting plasma glucose and insulin were also measured to determine if the mirabegron in our combination treatment could lower the amount of IR observed from corticosterone treatment. The plasma glucose concentrations were similar for all treatments (Figure 59A). The plasma insulin concentrations were significantly ($p \leq 0.05$) increased by the corticosterone and combination treatments (Figure 59B). This increased plasma insulin level illustrates the strong effect GCs have over insulin and its actions. The HOMA-IR was also increased in the corticosterone and combination treatments (Figure 59C). The altered insulin sensitivity by the corticosterone treatment was not entirely unexpected; however, the inability of mirabegron to lower the impact the GC had on insulin secretion was not anticipated.

The corticosterone-induced IR has been reported by others (Cassano et al., 2012; Karatsoreos et al., 2010; Kinlein et al., 2017; van Donkelaar et al., 2014) and is a hallmark of AT

whitening, which combines well with our other measured parameters, including increased LD area and AT mass (Kotzbeck et al., 2018). Mirabegron has been found to improve insulin sensitivity and glucose uptake in human trials (Finlin et al., 2020; O'Mara et al., 2020) and rodent studies (Hao et al., 2019; Peres Valgas da Silva et al., 2021). The fasting glucose concentrations were not altered from the HFD group in the study conducted by Peres Valgas da Silva et al. (2021) when mice were fed a HFD for ten weeks prior to mirabegron administration for two subsequent weeks (Peres Valgas da Silva et al., 2021). The fasting insulin concentrations in their study were increased with a HFD and the HFD with mirabegron treatment illustrated a 50% reduction in insulin resistance (Peres Valgas da Silva et al., 2021). The difference observed in our study where mirabegron is not able to remedy the increased insulin concentrations when in combination with corticosterone speaks to the fact that GCs may have a stronger impact on insulin resistance than those observed with DIO.

Like in patients with Cushing's syndrome, chronic GCs induce whole-body IR, whereas not all patients with obesity are IR (Geer et al., 2014). Patients with Cushing's syndrome develop IR through either increased gluconeogenesis in the liver or via decreased sensitivity to insulin in the liver or skeletal muscles (Pivonello et al., 2020). GC excess is thought to stimulate excess enzymes involved in gluconeogenesis, leading to increased glucose production (Pivonello et al., 2020). While we did not measure increased glucose production in our mice, we did see that fasting glucose concentrations which is the balance of gluconeogenesis and tissue-uptake, were not affected by our treatments. What likely could have occurred, producing such high circulating insulin concentrations, was an impairment in the sensitivity of the insulin receptor, its pathway, or increased production of insulin from the pancreatic beta cells in response to the excess GCs,

which led to IR (Ferris & Kahn, 2012; Pivonello et al., 2020). The pathogenicity of metabolic syndrome is strongly linked with AT IR and the development of impaired glucose metabolism (Longo et al., 2019; Pivonello et al., 2020). The inability of mirabegron to lower IR in the presence of GCs illustrates the strong force GCs play in AT metabolism and how more work will need to be conducted to utilize this β3AR agonist in a treatment plan for metabolic syndrome.

Specific Aim #4: Examine how mitochondrial content is impacted in the presence of the combination of corticosterone and β3AR stimulation

Mitochondria are the powerhouses of the cell and play key roles in many metabolic diseases, including diabetes, obesity, and IR (Boudina & Graham, 2014; Christe et al., 2013). Mitochondria are essential in AT as their function is linked to both lipid storage and mobilization within the adipocytes (Christe et al., 2013). Any alterations in the number and functionality of the mitochondria within adipocytes will lead to this organelle's impairment and further lead to the development of disease (Christe et al., 2013; Vieira & Valentine, 2009). Measurements of mitochondrial content have included the protein or enzyme expression of citrate synthase, a key enzyme in the Krebs cycle located in the mitochondrial matrix. Protein and enzyme expressions of citrate synthase have been validated for surrogate measures of mitochondrial content (Baldini et al., 2021; Larsen et al., 2012). Each tissue displays different mitochondrial properties and has its own metabolic demands that need to be met by this vital organelle (Holmström et al., 2012). In AT, the number of mitochondria is greater in BAT than in WAT; however, even with fewer

mitochondria, these organelles still play key roles in regulating energy production and responses to nutritional events (Boudina & Graham, 2014; Kusminski & Scherer, 2012). Many studies have found connections between obesity and impaired mitochondrial function, specifically in the adipocytes (Boudina & Graham, 2014; De Pauw et al., 2009; Holmström et al., 2012; Kusminski & Scherer, 2012). Baldini et al. (2021) illustrated how early adipocyte hypertrophy found in obesity can result in changes to mitochondrial respiration without altering mitochondrial mass or integrity (Baldini et al., 2021). A similar finding was also reported by Holmstrom et al. (2012), where they discovered that there was a tissue-specific control over mitochondrial respiration and that each tissue displays an altered response to obesity (Holmström et al., 2012). They also found that mitochondrial dysfunction was independent of skeletal muscle IR, further validating the idea that mitochondrial metabolism and control are altered differently under specific circumstances and diseases (Holmström et al., 2012). Sutherland et al. (2008) illustrated how rats fed a HFD for six weeks demonstrate impaired glucose tolerance prior to any reductions in mitochondrial content and biogenesis, shedding light on the sequences of events that take place in obesity (Sutherland et al., 2008). Therefore, severe adipocyte hypertrophy and reduced mitochondrial content found within previous studies of obesity illustrate a strong metabolic shift within AT, a response that does not occur quickly.

In this study, citrate synthase protein content was determined in both the BAT and WAT for each treatment group. The hypothesis was that mirabegron would mitigate adipocyte hypertrophy that occurs from corticosterone treatment and therefore increase the mitochondrial content for both AT depots. Surprisingly, the citrate synthase protein concentrations in both animal studies were similar, regardless of treatment (Figure 28) (Figure

29) (Figure 52) (Figure 53). With a lack of treatment effect observed in both animal studies, it is impossible to know if mirabegron was able to mitigate some of the effects caused by corticosterone in our combination treatment. To further understand if the mitochondrial content within each AT depot was altered, we then equated the citrate synthase protein expression back to the mass of each depot (Figure 55). In both the BAT and WAT depots, the corticosterone and combination treatments resulted in significantly ($p \leq 0.05$) less citrate synthase per gram of tissue than the vehicle control and mirabegron groups. This finding with less mitochondria per gram of AT is likely a result from increased lipid content (as evident through the increased LD area in these treatments), which may play a role in the overall function of the tissue.

A recent study where mirabegron was administered after a HFD for ten weeks showed that the β3AR agonist did not alter the mitochondrial transcription factor (TFAM) in BAT (Peres Valgas da Silva et al., 2021). Similar to the studies mentioned above, alterations in IR, early adipocyte hypertrophy, and altered metabolism can all occur before mitochondrial content is diminished (Baldini et al., 2021; Sutherland et al., 2008). This is not to imply that mitochondrial dysfunction did not occur. Excessive nutrient supply, ROS formation, IR, ER stress and proinflammatory markers have all been linked to the dysfunction of this organelle (Kusminski & Scherer, 2012; Longo et al., 2019). As mentioned previously, our study was of relatively short duration. It is possible that if the treatments in this study were substantially longer, in addition to CLS being observed in the AT depots, alterations in mitochondrial content or integrity may have also been found. In AS1, the BAT had increased UCP1 protein expression in the corticosterone group, even greater expression than the mirabegron treated groups (Figure 26). While this was

a surprise, the increased whitening that occurred in this tissue accompanying the increased uncoupling was likely a part of a compensatory response to overcome the excess lipids probably circulating from the excess GC treatment. Although the same increased UCP1 findings were not found in AS2 (Figure 50), the accumulated corticosterone dose was lower than AS1 based on the adjustments match the target dose (average doses received in AS1 and AS2 were 171% and 132% of the target respectively). It is possible that this had an impact on the adaptation of BAT in response to corticosterone. Although the oxidative capacity of BAT was not altered (Figure 50), there was less mitochondria per gram of tissue in the corticosterone and combination treated mice (Figure 55A). Increased BAT mass, LD area, and a decrease in mitochondrial content per gram of tissue all indicate that whitening of this depot occurred in both the corticosterone and the combination treatments. The increased LD area in the corticosterone group and the combination treatment, in combination with IR and increased leptin concentrations, indicate that both AT depots had adipocyte hypertrophy. Although these adipocytes were hypertrophic, they may not have become necrotic due to the lack of CLS and alterations to mitochondrial content (Longo et al., 2019). The fact that citrate synthase protein content did not change amongst the treatments in either animal study gives an indication that significant mitochondrial damage was not caused in our research. Although, the tissue functionality may have been altered due to less mitochondria per gram of tissue in both BAT and WAT of the corticosterone and combination treatments. It is possible that if the study was conducted over an increased time frame usually observed in HFD studies, for example, >10 weeks, different results for mitochondrial effects and inflammation may have occurred in these AT depots.

Further Comparisons of the Different Animal Studies

Two separate animal studies were conducted in this dissertation. The first animal study took place in the winter/spring months, and the second animal study took place in the late spring/summer months. While both studies were conducted at the same animal facility on the same breed of mice from the same distributor, a variety of factors could be responsible for the variety of differences observed. The first difference worth noting is the difference in temperature observed in the room the animals were housed in (Figure 61). Other than the first day, the second animal study was significantly ($p \leq 0.05$) lower than the first animal study (Figure 61A). This difference amounted to approximately a one-degree difference in the average room temperature (Figure 61B).

Conversely, the humidity of the room was significantly ($p \leq 0.05$) lower in AS1 when compared to AS2 (Figure 62). Again, after the first day, every other day of the study had significantly ($p \leq 0.05$) lower humidity values (Figure 62A), a difference which resulted in an average humidity that is lower than the desired humidity percentage for animal studies (i.e., lower than 40-60%) (Figure 62B). It is important to note that the temperature and humidity reported were for the room and not in a cage with bedding etc. The cage-level temperature and humidity were likely higher due to the micro-environment created within the cage (Rosenbaum et al., 2010) but this was not measured. The temperature and humidity variations could have been due to a variety of environmental factors given the different seasons and the HVAC system in the facility that these studies took place in, and these effects will be discussed below.

Even though pre-clinical studies are governed by regular light-dark cycles, constant temperatures and humidity levels, and are away from natural sunlight, seasonal variations in the

results still occur (Ferguson & Maier, 2013; Meyer et al., 2006) Time-of-year and time-of-day that an experiment is conducted will also play a large part in the results obtained in animal studies. Meyer et al. (2006) examined the impact of stress on laboratory mice during the different times of the year, which were similar time points to our studies (Meyer et al., 2006). They found that mice were more resistant to stress during the spring (April-May), as measured through a general slight increase in plasma corticosterone (Meyer et al., 2006). Whereas in the fall (November-December), mice were more susceptible to stress and had higher plasma corticosterone concentrations when presented with a stressor (Meyer et al., 2006). There is a seasonal-dependent effect on hormone levels and behavioural outputs, with mice being more curious in the spring and more reserved in the fall (Meyer et al., 2006). While Ferguson and Maier (2013) were skeptical of the behavioural findings with seasonal effects, current work supports this finding (Ferguson & Maier, 2013). A more recent study did, however, discern that laboratory mice kept under standard conditions do, in fact, show seasonal changes in their behavioural responses (Pernold et al., 2021). Most studies involving rodents do not report the time of year that an experiment was conducted, adding complications to fully understanding and reproducing any of the results obtained in similar experiments (Ferguson & Maier, 2013). This is a major flaw in current preclinical studies and should be a reporting requirement to ensure the results are interpreted correctly in the future.

Conventional housing room temperatures for mice (20-26°C) are below their thermoneutral zone (30°C), which implies that mice are always under a degree of stress in a cold environment (Canadian Council on Animal Care, 2019; Maloney et al., 2014). The room temperature is one factor that needs to be considered, but the importance of the

microenvironment in the cage is also critical (Reeb et al., 1998). The recommended cage temperature for rodents is between 18-26°C (Reeb et al., 1998). In their study, the room temperature of 22°C resulted in a cage temperature of 24°C when four male mice were housed per cage (Reeb et al., 1998). The warmer temperatures can produce greater humidity within the cage, but this can be mitigated with more air changes per hour (Reeb et al., 1998).

A review by Maloney et al. (2014) highlights many different aspects of housing animals below thermoneutral conditions, but a notable mention is what happens when mice are moved from 30°C to 21°C (Maloney et al., 2014). The metabolism of the mice change (increased EE and carbohydrate metabolism), increased lipid oxidation, increased lipid uptake in BAT and lower TAG circulating (Maloney et al., 2014). This is especially important in metabolic studies where mice housed at 30°C will display increased insulin concentrations in DIO models than those housed at standard housing temperatures (Dudele et al., 2015; Keijer et al., 2019). Numerous studies and reviews have been reported on the differences between mice housed at thermoneutrality and the recommended housing temperature (Keijer et al., 2019; Maloney et al., 2014; Small et al., 2018). The results from these studies are clear that temperature is a key variable that displays profound impacts on the physiology of mice and humans (Keijer et al., 2019). Housing mice at thermoneutral temperatures may actually present misleading results when attempting to extract the findings to humans (Keijer et al., 2019). Keijer et al. (2019) recommend housing mice at the optimum temperature of 23-25°C, which is the most translatable to humans, with the difference being 3-5°C below our critical temperature (Keijer et al., 2019). Anything lower than this optimal temperature just forces the animal to expend

energy beyond its basal EE level and is only more tolerable when mice are group-housed and can huddle to keep warm with ample insulation (Keijer et al., 2019).

The relative humidity for laboratory animals is recommended to be between 40-60%, with no less than 35% or more than 70% (Canadian Council on Animal Care, 2020). The average humidity in AS1 was significantly ($p \leq 0.05$) lower and hovered around 32.6%, whereas AS2 was approximately 45.2% (Figure 62). Rosenbaum et al. (2010) reported that humidity levels could significantly impact animal health. Low humidity is associated with ringtail and dermatitis, and high humidity promotes bacterial growth and subsequent infections (Rosenbaum et al., 2010).

Although differences were observed in the temperature and humidity for the animal studies conducted, there were no differences in the body weights of like treatments (Figure 63). The BAT weights were not significantly different alone, the ratio relative to body weight was increased in AS2 for the corticosterone group (Figure 64). There was a significant ($p \leq 0.05$) difference found in the WAT weights and ratios with the second animal study illustrating lower tissue masses for each repeated treatment (Figure 65). With the significant decrease in WAT weights from the second animal study, but without altered body weight, we attempted to discern how this could have occurred. With the BAT illustrating similar UCP1 values for all treatments in AS2, we directly compared vehicle control samples from AS1 to AS2 (Figure 66). To our surprise, AS2 controls expressed significantly ($p \leq 0.05$) more UCP1 than AS1 vehicle controls (Figure 66A) (Figure 66B) (Figure 66C). This increased UCP1 expression in the BAT of vehicle mice in AS2 illustrates a difference between the animal studies that may account for the diminished treatment effect is AS2. AS2 also illustrated a cooler room temperature, which could point to a slight decrease in the cage temperature, which may have been enough to activate

UCP1 in the AT to increase thermogenesis in all groups, including the vehicle controls group. However, we cannot concretely determine this was the causative effect within the studies conducted. With the UCP1 being increased across all treatments in the BAT, there appears to be an overarching force at play that equally affected all treatments, cooler temperatures. Although few animal studies have examined the effects of small housing temperature changes on BAT UCP1 expression and its effect on whole-body metabolism, this study illustrates the need for further investigations into how UCP1 influences overall AT health.

Animal Study #2 Conclusion

In order to further examine how excess corticosterone affects the β3AR stimulation and metabolic dysfunction of AT, we studied the interaction between these two treatments to determine if they can oppose each other at the whole-body level. The combination treatment mice had significantly ($p \leq 0.05$) increased body and tissue weights compared to the mirabegron alone or vehicle treatments. The similar weights between corticosterone and combination treatments were the first indication that the GC had a dominant effect over the mirabegron treatment. Histologically, the BAT and WAT depots were not affected by having mirabegron in the combination treatment as the LD areas were not significantly different from the corticosterone treatment. The increase in UCP1 in WAT of the vehicle control was a surprise, indicating again that there was no treatment effect found in this tissue. The lack of increased UCP1 from mirabegron illustrated that the β3AR agonist did not result in beiging. Citrate synthase and 4-HNE adducts were not significantly different between treatments for either

tissue in this animal study, and BAT UCP1 expressions were also similar between groups. The amount of mitochondria per gram of tissue was significantly ($p \leq 0.05$) less in both AT depots for the corticosterone and combination treatment groups, which likely played a role in these tissues functionality.

With the corticosterone response being dominant in all of our measurements, it is possible that the mirabegron is not potent enough to elicit an effect to oppose the negative effects of the GC when administered simultaneously. This brings to question what systemic effect mirabegron can have in cases of elevated GCs. The altered insulin sensitivity by the corticosterone treatment was not surprising, however, the inability of mirabegron to lower the impact the GC had on fasting insulin concentration was not anticipated. The inability of mirabegron to lower IR in the presence of GCs illustrates the strong force GCs play in AT metabolism and how more work will need to be conducted to utilize this β3AR agonist in a treatment plan for metabolic syndrome. The increased leptin levels observed in corticosterone and combination mice support the dominant role GCs can have in the development of metabolic syndrome. GC-induced increases of stored TAG within the AT depots can influence whole-body health independent of β3AR activation. This dose and duration of treatment in the present study was sufficient to induce increased lipid accumulation in AT and whole-body insulin resistance before the onset of overt disease. This allows for the study of mirabegron in early stages of progression of obesity related chronic disease. Other studies examining the effects of mirabegron on a HFD or the effects of corticosterone mentioned earlier induce disease first and then try to reverse it with a different treatment. To our knowledge, we were the first ones to administer corticosterone and mirabegron concurrently to examine the physiological effects of

these treatments. To our knowledge, this was the first study to examine these treatments concurrently for four weeks, and the first study to illustrate that mirabegron could not induce beiging in WAT or counteract BAT whitening when corticosterone was present in levels equivalent to metabolic syndrome

References

Alcala, M., Calderon-Dominguez, M., Bustos, E., Ramos, P., Casals, N., Sera, D., Viana, M., & Herrero, L. (2017). Increased inflammation, oxidative stress and mitochondrial respiration in brown adipose tissue from obese mice. *Scientific Reports*, *7*(16082). https://doi.org/10.1038/s41598-017-16463-6

Avtanski, D., Pavlov, V. A., Tracey, K. J., & Poretsky, L. (2019). Characterization of inflammation and insulin resistance in high-fat diet-induced male C57BL/6J mouse model of obesity. *Animal Models and Experimental Medicine*, *2*(4), 252–258. https://doi.org/10.1002/ame2.12084

Baldini, F., Fabbri, R., Eberhagen, C., Voci, A., Portincasa, P., Zischka, H., & Vergani, L. (2021). Adipocyte hypertrophy parallels alterations of mitochondrial status in a cell model for adipose tissue dysfunction in obesity. *Life Sciences*, *265*, 118812. https://doi.org/10.1016/j.lfs.2020.118812

Bartlet, A., & Heeren, J. (2013). Adipose Tissue Browning and Metabolic Health. *Nature Reviews Endocrinology*, *10*, 24–26. https://doi.org/doi:10.1038/nrendo.2013.204

Baskin, A. S., Linderman, J. D., Brychta, R. J., McGehee, S., Anflick-Chames, E., Cero, C., Johnson, J. W., O'Mara, A. E., Fletcher, L. A., Leitner, B. P., Duckworth, C. J., Huang, S., Cai, H., Garraffo, H. M., Millo, C. M., Dieckmann, W., Tolstikov, V., Chen, E. Y., Gao, F., … Cypess, A. M. (2018). Regulation of Human Adipose Tissue Activation, Gallbladder Size, and Bile Acid Metabolism by a β3-Adrenergic Receptor Agonist. *Diabetes*, *67*(10), 2113–2125. https://doi.org/10.2337/db18-0462

Beaupere, C., Liboz, A., Fève, B., Blondeau, B., & Guillemain, G. (2021). Molecular Mechanisms of Glucocorticoid-Induced Insulin Resistance. *International Journal of Molecular Sciences*, *22*(2), 623. https://doi.org/10.3390/ijms22020623

Bel, J. S., Tai, T. C., Khaper, N., & Lees, S. J. (2021). Mirabegron: The most promising adipose tissue beiging agent. *Physiological Reports*, *9*(5). https://doi.org/10.14814/phy2.14779

Bettini, S., Favaretto, F., Compagnin, C., Belligoli, A., Sanna, M., Fabris, R., Serra, R., Dal Prà, C., Prevedello, L., Foletto, M., Vettor, R., Milan, G., & Busetto, L. (2019). Resting Energy Expenditure, Insulin Resistance and UCP1 Expression in Human Subcutaneous and Visceral Adipose Tissue of Patients With Obesity. *Frontiers in Endocrinology*, *10*, 548. https://doi.org/10.3389/fendo.2019.00548

Bose, S. K., Hutson, I., & Harris, C. A. (2016). Hepatic Glucocorticoid Receptor Plays a Greater Role Than Adipose GR in Metabolic Syndrome Despite Renal Compensation. *Endocrinology*, *157*(12), 4943–4960. https://doi.org/10.1210/en.2016-1615

Boudina, S., & Graham, T. E. (2014). Mitochondrial function/dysfunction in white adipose tissue: Mitochondrial function/dysfunction in white adipose tissue. *Experimental Physiology*, *99*(9), 1168–1178. https://doi.org/10.1113/expphysiol.2014.081414

Burke, S. J., Batdorf, H. M., Eder, A. E., Karlstad, M. D., Burk, D. H., Noland, R. C., Floyd, Z. E., & Collier, J. J. (2017). Oral Corticosterone Administration Reduces Insulitis but Promotes Insulin Resistance and Hyperglycemia in Male Nonobese Diabetic Mice. *American Journal of Pathology*, 13.

Canadian Council on Animal Care. (2019). CCAC guidelines: Mice. *Https://Ccac.ca/Documents/Standards/Guidelines/CCAC_Guidelines_Mice.Pdf*, 127.

Canadian Council on Animal Care. (2020). *Guidelines on: Laboratory animal facilities - characteristics, design and development.* Canadian Council on Animal Care.

Cassano, A. E., White, J. R., Penraat, K. A., Wilson, C. D., Rasmussen, S., & Karatsoreos, I. N. (2012). Anatomic, Hematologic, and Biochemical Features of C57BL/6NCrl Mice Maintained on Chronic Oral Corticosterone. *Comparative Medicine by the American Association for Laboratory Animal Science*, *62*(5), 348–360.

Castillo-Campos, A., Gutiérrez-Mata, A., Charli, J.-L., & Joseph-Bravo, P. (2021). Chronic stress inhibits hypothalamus–pituitary–thyroid axis and brown adipose tissue responses to acute cold exposure in male rats. *Journal of Endocrinological Investigation*, *44*(4), 713–723. https://doi.org/10.1007/s40618-020-01328-z

Chait, A., & den Hartigh, L. J. (2020). Adipose Tissue Distribution, Inflammation and Its Metabolic Consequences, Including Diabetes and Cardiovascular Disease. *Frontiers in Cardiovascular Medicine*, *7*, 22. https://doi.org/10.3389/fcvm.2020.00022

Chen, K. Y., Brychta, R. J., Abdul Sater, Z., Cassimatis, T. M., Cero, C., Fletcher, L. A., Israni, N. S., Johnson, J. W., Lea, H. J., Linderman, J. D., O'Mara, A. E., Zhu, K. Y., & Cypess, A. M. (2020). Opportunities and challenges in the therapeutic activation of human energy expenditure and thermogenesis to manage obesity. *Journal of Biological Chemistry*, *295*(7), 1926–1942. https://doi.org/10.1074/jbc.REV119.007363

Chen, L., Chen, R., Wang, H., & Liang, F. (2015). Mechanisms Linking Inflammation to Insulin Resistance. *International Journal of Endocrinology*, *2015*, 1–9. https://doi.org/10.1155/2015/508409

Chen, Y., & Lyga, J. (2014). Brain-Skin Connection: Stress, Inflammation and Skin Aging. *Inflammation & Allergy-Drug Targets*, *13*(3), 177–190. https://doi.org/10.2174/1871528113666140522104422

Choromańska, B., Myśliwiec, P., Łuba, M., Wojskowicz, P., Dadan, J., Myśliwiec, H., Choromańska, K., Zalewska, A., & Maciejczyk, M. (2020). A Longitudinal Study of the Antioxidant Barrier and Oxidative Stress in Morbidly Obese Patients after Bariatric Surgery. Does the Metabolic Syndrome Affect the Redox Homeostasis of Obese People? *Journal of Clinical Medicine*, *9*(4), 976. https://doi.org/10.3390/jcm9040976

Christe, M., Hirzel, E., Lindinger, A., Kern, B., von Flüe, M., Peterli, R., Peters, T., Eberle, A. N., & Lindinger, P. W. (2013). Obesity Affects Mitochondrial Citrate Synthase in Human Omental Adipose Tissue. *ISRN Obesity*, *2013*, 1–8. https://doi.org/10.1155/2013/826027

Cummins, T. D., Holden, C. R., Sansbury, B. E., Gibb, A. A., Shah, J., Zafar, N., Tang, Y., Hellmann, J., Rai, S. N., Spite, M., Bhatnagar, A., & Hill, B. G. (2014). Metabolic remodeling of white adipose tissue in obesity. *American Journal of Physiology-Endocrinology and Metabolism*, *307*(3), E262–E277. https://doi.org/10.1152/ajpendo.00271.2013

Cypess, A. M., Weiner, L. S., Roberts-Toler, C., Elía, E. F., Kessler, S. H., Kahn, P. A., English, J., Chatman, K., Trauger, S. A., Doria, A., & Kolodny, G. M. (2015). Activation of Human Brown Adipose Tissue by a β3-Adrenergic Receptor Agonist. *Cell Metabolism*, *21*(1), 33–38. https://doi.org/10.1016/j.cmet.2014.12.009

De Pauw, A., Tejerina, S., Raes, M., Keijer, J., & Arnould, T. (2009). Mitochondrial (Dys)function in Adipocyte (De)differentiation and Systemic Metabolic Alterations. *The American Journal of Pathology*, *175*(3), 927–939. https://doi.org/10.2353/ajpath.2009.081155

Desarzens, S., & Faresse, N. (2016). Adipocyte glucocorticoid receptor has a minor contribution in adipose tissue growth. *Journal of Endocrinology*, 11.

Dham, D., Roy, B., Gowda, A., Pan, G., Sridhar, A., Zeng, X., Thandavarayan, R. A., & Palaniyandi, S. S. (2021). 4-Hydroxy-2-nonenal, a lipid peroxidation product, as a biomarker in diabetes and its complications: Challenges and opportunities. *Free Radical Research*, *55*(5), 547–561. https://doi.org/10.1080/10715762.2020.1866756

Do, T. T. H., Marie, G., Héloïse, D., Guillaume, D., Marthe, M., Bruno, F., & Marion, B. (2019). Glucocorticoid-induced insulin resistance is related to macrophage visceral adipose tissue infiltration. *The Journal of Steroid Biochemistry and Molecular Biology*, *185*, 150–162. https://doi.org/10.1016/j.jsbmb.2018.08.010

Dudele, A., Rasmussen, G. M., Mayntz, D., Malte, H., Lund, S., & Wang, T. (2015). Effects of ambient temperature on glucose tolerance and insulin sensitivity test outcomes in normal and obese C57 male mice. *Physiological Reports*, *3*(5), e12396. https://doi.org/10.14814/phy2.12396

Eltink, C., Lee, J., Schaddelee, M., Zhang, W., Kerbusch, V., Meijer, J., Marle, S. van, Grunenberg, N., Kowalski, D., Drogendijk, T., et al. (2012). Single dose pharmacokinetics and absolute bioavailability of mirabegron, a ?3-adrenoceptor agonist for treatment of overactive bladder. CP *50*, 838–850. https://doi.org/10.5414/CP201782.

Elrayess, M. A., Almuraikhy, S., Kafienah, W., Al-Menhali, A., Al-Khelaifi, F., Bashah, M., Zarkovic, K., Zarkovic, N., Waeg, G., Alsayrafi, M., & Jaganjac, M. (2017). 4-hydroxynonenal causes impairment of human subcutaneous adipogenesis and induction of adipocyte insulin resistance. *Free Radical Biology and Medicine*, *104*, 129–137. https://doi.org/10.1016/j.freeradbiomed.2017.01.015

Ferguson, S. A., & Maier, K. L. (2013). A review of seasonal/circannual effects of laboratory rodent behavior. *Physiology & Behavior*, *119*, 130–136. https://doi.org/10.1016/j.physbeh.2013.06.007

Ferris, H. A., & Kahn, C. R. (2012). New mechanisms of glucocorticoid-induced insulin resistance: Make no bones about it. *Journal of Clinical Investigation*, *122*(11), 3854–3857. https://doi.org/10.1172/JCI66180

Finlin, B. S., Memetimin, H., Zhu, B., Confides, A. L., Vekaria, H. J., El Khouli, R. H., Johnson, Z. R., Westgate, P. M., Chen, J., Morris, A. J., Sullivan, P. G., Dupont-Versteegden, E. E., & Kern, P. A. (2020). The β3-adrenergic receptor agonist mirabegron improves glucose homeostasis in obese humans. *Journal of Clinical Investigation*, *130*(5), 2319–2331. https://doi.org/10.1172/JCI134892

Furukawa, S., Fujita, T., Shimabukuro, M., Iwaki, M., Yamada, Y., Nakajima, Y., Nakayama, O., Makishima, M., Matsuda, M., & Shimomura, I. (2004). Increased oxidative stress in obesity

and its impact on metabolic syndrome. *Journal of Clinical Investigation*, *114*(12), 1752–1761. https://doi.org/10.1172/JCI21625

Gasparini, S. J., Weber, M.-C., Henneicke, H., Kim, S., Hong, Z., & Seibel, M. J. (2016). Continuous corticosterone delivery via the drinking water or pellet implantation: A comparative study in mice. *Steroids*, *116*, 76–82.

Geer, E. B., Islam, J., & Buettner, C. (2014). Mechanisms of Glucocorticoid-Induced Insulin Resistance. *Endocrinology and Metabolism Clinics of North America*, *43*(1), 75–102. https://doi.org/10.1016/j.ecl.2013.10.005

Glantschnig, C., Mattijssen, F., Vogl, E. S., Ali Khan, A., Rios Garcia, M., Fischer, K., Müller, T., Uhlenhaut, H., Nawroth, P., Scheideler, M., Rose, A. J., Pellegata, N., & Herzig, S. (2019). The glucocorticoid receptor in brown adipocytes is dispensable for control of energy homeostasis. *EMBO Reports*, *20*(11). https://doi.org/10.15252/embr.201948552

Guilherme, A., Henriques, F., Bedard, A. H., & Czech, M. P. (2019). Molecular pathways linking adipose innervation to insulin action in obesity and diabetes mellitus. *Nature Reviews Endocrinology*, *15*(4), 207–225. https://doi.org/10.1038/s41574-019-0165-y

Hao, L., Scott, S., Abbasi, M., Zu, Y., Khan, M. S. H., Yang, Y., Wu, D., Zhao, L., & Wang, S. (2019). Beneficial Metabolic Effects of Mirabegron In Vitro and in High-Fat Diet-Induced Obese Mice. *Journal of Pharmacology and Experimental Therapeutics*, *369*(3), 419–427. https://doi.org/10.1124/jpet.118.255778

Heeren, J., & Scheja, L. (2018). Brown adipose tissue and lipid metabolism: *Current Opinion in Lipidology*, *29*(3), 180–185. https://doi.org/10.1097/MOL.0000000000000504

Holmström, M. H., Iglesias-Gutierrez, E., Zierath, J. R., & Garcia-Roves, P. M. (2012). Tissue-specific control of mitochondrial respiration in obesity-related insulin resistance and diabetes. *American Journal of Physiology-Endocrinology and Metabolism*, *302*(6), E731–E739. https://doi.org/10.1152/ajpendo.00159.2011

Jaganjac, M., Almuraikhy, S., Al-Khelaifi, F., Al-Jaber, M., Bashah, M., Mazloum, N. A., Zarkovic, K., Zarkovic, N., Waeg, G., Kafienah, W., & Elrayess, M. A. (2017). Combined metformin and insulin treatment reverses metabolically impaired omental adipogenesis and accumulation of 4-hydroxynonenal in obese diabetic patients. *Redox Biology*, *12*, 483–490. https://doi.org/10.1016/j.redox.2017.03.012

Jeanson, Y., Carrière, A., & Casteilla, L. (2015). A New Role for Browning as a Redox and Stress Adaptive Mechanism? *Frontiers in Endocrinology*, *6*. https://doi.org/10.3389/fendo.2015.00158

Kahn, C. R., Wang, G., & Lee, K. Y. (2019). Altered adipose tissue and adipocyte function in the pathogenesis of metabolic syndrome. *The Journal of Clinical Investigation*, *129*(10), 12.

Karatsoreos, I. N., Bhagat, S. M., Bowles, N. P., Weil, Z. M., Pfaff, D. W., & McEwen, B. S. (2010). Endocrine and Physiological Changes in Response to Chronic Corticosterone: A Potential Model of the Metabolic Syndrome in Mouse. *Endocrinology*, *151*(5), 2117–2127. https://doi.org/10.1210/en.2009-1436

Keijer, J., Li, M., & Speakman, J. R. (2019). What is the best housing temperature to translate mouse experiments to humans? *Molecular Metabolism*, *25*, 168–176. https://doi.org/10.1016/j.molmet.2019.04.001

Kershaw, E. E., & Flier, J. S. (2004a). Adipose Tissue as an Endocrine Organ. *The Journal of Clinical Endocrinology & Metabolism*, *89*(6), 2548–2556. https://doi.org/10.1210/jc.2004-0395

Kershaw, E. E., & Flier, J. S. (2004b). Adipose Tissue as an Endocrine Organ. *The Journal of Clinical Endocrinology & Metabolism*, *89*(6), 2548–2556. https://doi.org/10.1210/jc.2004-0395

Kinlein, S. A., Shahanoor, Z., Romeo, R. D., & Karatsoreos, I. N. (2017). Chronic Corticosterone Treatment During Adolescence Has Significant Effects on Metabolism and Skeletal Development in Male C57BL6/N Mice. *Endocrinology*, *158*(7), 2239–2254.

Kotzbeck, P., Giordano, A., Mondini, E., Murano, I., Severi, I., Venema, W., Cecchini, M. P., Kershaw, E. E., Barbatelli, G., Haemmerle, G., Zechner, R., & Cinti, S. (2018). Brown adipose tissue whitening leads to brown adipocyte death and adipose tissue inflammation. *Journal of Lipid Research*, *59*(5), 784–794. https://doi.org/10.1194/jlr.M079665

Kusminski, C. M., & Scherer, P. E. (2012). Mitochondrial dysfunction in white adipose tissue. *Trends in Endocrinology & Metabolism*, *23*(9), 435–443. https://doi.org/10.1016/j.tem.2012.06.004

Larsen, S., Nielsen, J., Hansen, C. N., Nielsen, L. B., Wibrand, F., Stride, N., Schroder, H. D., Boushel, R., Helge, J. W., Dela, F., & Hey-Mogensen, M. (2012). Biomarkers of mitochondrial content in skeletal muscle of healthy young human subjects: Biomarkers of mitochondrial content. *The Journal of Physiology*, *590*(14), 3349–3360. https://doi.org/10.1113/jphysiol.2012.230185

Lee, M.J., Pramyothin, P., Karastergiou, K., & Fried, S. K. (2014). Deconstructing the roles of glucocorticoids in adipose tissue biology and the development of central obesity. *Biochimica et Biophysica Acta (BBA) - Molecular Basis of Disease*, *1842*(3), 473–481. https://doi.org/10.1016/j.bbadis.2013.05.029

Lee, J., Moy, S., Meijer, J., Krauwinkel, W., Sawamoto, T., Kerbusch, V., Kowalski, D., Roy, M., Marion, A., Takusagawa, S., et al. (2013). Role of Cytochrome P450 Isoenzymes 3A and 2D6 in the In Vivo Metabolism of Mirabegron, a β3-Adrenoceptor Agonist. Clin Drug Investig *33*, 429–440. https://doi.org/10.1007/s40261-013-0084-y.

Licholai, J. A., Nguyen, K. P., Fobbs, W. C., Schuster, C. J., Ali, M. A., & Kravitz, A. V. (2018). Why Do Mice Overeat High-Fat Diets? How High-Fat Diet Alters the Regulation of Daily Caloric Intake in Mice: Why Do Mice Overeat High-Fat Diets? *Obesity*, *26*(6), 1026–1033. https://doi.org/10.1002/oby.22195

Liu, J., Kong, X., Wang, L., Qi, H., Di, W., Zhang, X., Wu, L., Chen, X., Yu, J., Zha, J., Lv, S., Zhang, A., Cheng, P., Hu, M., Li, Y., Bi, J., Li, Y., Hu, F., Zhong, Y., … Ding, G. (2013). Essential roles of 11β-HSD1 in regulating brown adipocyte function. *Journal of Molecular Endocrinology*, *50*(1), 103–113. https://doi.org/10.1530/JME-12-0099

Longo, M., Zatterale, F., Naderi, J., Parrillo, L., Formisano, P., Raciti, G. A., Beguinot, F., & Miele, C. (2019). Adipose Tissue Dysfunction as Determinant of Obesity-Associated Metabolic Complications. *International Journal of Molecular Sciences*, *20*(9), 2358. https://doi.org/10.3390/ijms20092358

Luijten, I. H. N., Brooks, K., Boulet, N., Shabalina, I. G., Jaiprakash, A., Carlsson, B., Fischer, A. W., Cannon, B., & Nedergaard, J. (2019). Glucocorticoid-Induced Obesity Develops Independently of UCP1. *Cell Reports*, *27*(6), 1686-1698.e5. https://doi.org/10.1016/j.celrep.2019.04.041

Luijten, I. H. N., Cannon, B., & Nedergaard, J. (2019). Glucocorticoids and Brown Adipose Tissue: Do glucocorticoids really inhibit thermogenesis? *Molecular Aspects of Medicine*, *68*, 42–59. https://doi.org/10.1016/j.mam.2019.07.002

Luo, L., & Liu, M. (2016). Adipose tissue in control of metabolism. *Journal of Endocrinology*, *231*(3), R77–R99. https://doi.org/10.1530/JOE-16-0211

Maloney, S. K., Fuller, A., Mitchell, D., Gordon, C., & Overton, J. M. (2014). Translating Animal Model Research: Does It Matter That Our Rodents Are Cold? *Physiology*, *29*(6), 413–420. https://doi.org/10.1152/physiol.00029.2014

Manna, P., & Jain, S. K. (2015). Obesity, Oxidative Stress, Adipose Tissue Dysfunction, and the Associated Health Risks: Causes and Therapeutic Strategies. *Metabolic Syndrome and Related Disorders*, *13*(10), 423–444. https://doi.org/10.1089/met.2015.0095

Marín-Royo, G., Rodríguez, C., Pape, A. L., Jurado-Lopez, R., Luaces, M., Antequera, A., Martínez-Gonzalez, J., Souza-Neto, F. V., Nieto, M. L., Martínez-Martínez, E., & Cachofeiro, V. (2019). The role of mitochondrial oxidative stress in the metabolic alterations in diet-induced obesity in rats. *The FASEB Journal*, *33*(11), 12060–12072. https://doi.org/10.1096/fj.201900347RR

Masschelin, P. M., Cox, A. R., Chernis, N., & Hartig, S. M. (2020). The Impact of Oxidative Stress on Adipose Tissue Energy Balance. *Frontiers in Physiology*, *10*, 1638. https://doi.org/10.3389/fphys.2019.01638

Masuzaki, H., Paterson, J., Shinyam, H., Morton, N. M., Mullins, J. J., & Seckl, J. R. (2001). A transgenic model of visceral obesity and the metabolic syndrome. *Science*, *294*(5549), 2166–2170. https://doi.org/doi: 10.1126/science.1066285

Matoulková, P., Pávek, P., Malý, J., and Vlček, J. (2014). Cytochrome P450 enzyme regulation by glucocorticoids and consequences in terms of drug interaction. Expert Opinion on Drug Metabolism & Toxicology *10*, 425–435. https://doi.org/10.1517/17425255.2014.878703.

Meyer, L., Caston, J., & Mensahnyagan, A. (2006). Seasonal variation of the impact of a stressful procedure on open field behaviour and blood corticosterone in laboratory mice. *Behavioural Brain Research*, *167*(2), 342–348. https://doi.org/10.1016/j.bbr.2005.09.023

Mousovich-Neto, F., Matos, M. S., Costa, A. C. R., Melo Reis, R. A., Atella, G. C., Miranda-Alves, L., Carvalho, D. P., Ketzer, L. A., & Corrêa da Costa, V. M. (2019). Brown adipose tissue remodelling induced by corticosterone in male Wistar rats. *Experimental Physiology*, *104*(4), 514–528. https://doi.org/10.1113/EP087332

Mundell, L., Lindemann, R., and Douglas, J. (2017). Monitoring long-term oral corticosteroids. BMJ Open Qual *6*, e000209. https://doi.org/10.1136/bmjoq-2017-000209.

Murano, I., Barbatelli, G., Parisani, V., Latini, C., Muzzonigro, G., Castellucci, M., & Cinti, S. (2008). Dead adipocytes, detected as crown-like structures, are prevalent in visceral fat depots of genetically obese mice. *Journal of Lipid Research*, *49*(7), 1562–1568. https://doi.org/10.1194/jlr.M800019-JLR200

O'Mara, A. E., Johnson, J. W., Linderman, J. D., Brychta, R. J., McGehee, S., Fletcher, L. A., Fink, Y. A., Kapuria, D., Cassimatis, T. M., Kelsey, N., Cero, C., Sater, Z. A., Piccinini, F., Baskin, A. S., Leitner, B. P., Cai, H., Millo, C. M., Dieckmann, W., Walter, M., … Cypess, A. M. (2020). Chronic mirabegron treatment increases human brown fat, HDL cholesterol, and insulin sensitivity. *Journal of Clinical Investigation*, *130*(5), 2209–2219. https://doi.org/10.1172/JCI131126

Pan, W. W., & Myers, M. G. (2018). Leptin and the maintenance of elevated body weight. *Nature Reviews Neuroscience*, *19*(2), 95–105. https://doi.org/10.1038/nrn.2017.168

Peckett, A. J., Wright, D. C., & Riddell, M. C. (2011). The effects of glucocorticoids on adipose tissue lipid metabolism. *Metabolism*, *60*(11), 1500–1510. https://doi.org/10.1016/j.metabol.2011.06.012

Peres Valgas da Silva, C., Calmasini, F., Alexandre, E. C., Raposo, H. F., Delbin, M. A., Monica, F. Z., & Zanesco, A. (2021). The effects of mirabegron on obesity-induced inflammation and insulin resistance are associated with brown adipose tissue activation but not beiging in the subcutaneous white adipose tissue. *Clinical and Experimental Pharmacology and Physiology*, *48*(11), 1477–1487. https://doi.org/10.1111/1440-1681.13566

Pernold, K., Rullman, E., & Ulfhake, B. (2021). Major oscillations in spontaneous home-cage activity in C57BL/6 mice housed under constant conditions. *Scientific Reports*, *11*(1), 4961. https://doi.org/10.1038/s41598-021-84141-9

Petrick, H. L., Foley, K. P., Zlitni, S., Brunetta, H. S., Paglialunga, S., Miotto, P. M., Politis-Barber, V., O'Dwyer, C., Philbrick, D. J., Fullerton, M. D., Schertzer, J. D., & Holloway, G. P. (2020). Adipose Tissue Inflammation Is Directly Linked to Obesity-Induced Insulin Resistance, while Gut Dysbiosis and Mitochondrial Dysfunction Are Not Required. *Function*, *1*(2), zqaa013. https://doi.org/10.1093/function/zqaa013

Pivonello, R., Ferrigno, R., De Martino, M. C., Simeoli, C., Di Paola, N., Pivonello, C., Barba, L., Negri, M., De Angelis, C., & Colao, A. (2020). Medical Treatment of Cushing's Disease: An Overview of the Current and Recent Clinical Trials. *Frontiers in Endocrinology*, *11*, 648. https://doi.org/10.3389/fendo.2020.00648

Poggioli, R., Ueta, C. B., e Drigo, R. A., Castillo, M., Fonseca, T. L., & Bianco, A. C. (2013). Dexamethasone reduces energy expenditure and increases susceptibility to diet-induced obesity in mice. *Obesity*, n/a-n/a. https://doi.org/10.1002/oby.20338

Pralong, F. P., Roduit, R., Waeber, G., Castillo, E., Mosimann, F., Thorens, B., & Gaillard, R. C. (1998). Leptin Inhibits Directly Glucocorticoid Secretion by Normal Human and Rat Adrenal Gland**This work was supported by a grant from the Swiss National Science Foundation (No. 3100–050748.97/1). *Endocrinology*, *139*(10), 4264–4268. https://doi.org/10.1210/endo.139.10.6254

Ramage, L. E., Akyol, M., Fletcher, A. M., Forsythe, J., Nixon, M., Carter, R. N., van Beek, E. J. R., Morton, N. M., Walker, B. R., & Stimson, R. H. (2016). Glucocorticoids Acutely Increase Brown Adipose Tissue Activity in Humans, Revealing Species-Specific Differences in UCP-1 Regulation. *Cell Metabolism*, *24*(1), 130–141. https://doi.org/10.1016/j.cmet.2016.06.011

Reddy, N. L., Tan, B. K., Barber, T. M., & Randeva, H. S. (2014). Brown adipose tissue: Endocrine determinants of function and therapeutic manipulation as a novel treatment strategy for obesity. *BMC Obesity*, *1*(1), 13. https://doi.org/10.1186/s40608-014-0013-5

Reeb, C. K., Jones, R. B., Bearg, D. W., Bedigian, H., Myers, D. D., & Paigen, B. (1998). Microenvironment in Ventilated Animal Cages with Differing Ventilation Rates, Mice Populations, and Frequency of Bedding Changes. *Contemporary Topics in Laboratory Animal Science*, *32*(2), 43–49.

Rose, A. J., & Herzig, S. (2013). Metabolic control through glucocorticoid hormones: An update. *Molecular and Cellular Endocrinology*, *380*(1–2), 65–78. https://doi.org/10.1016/j.mce.2013.03.007

Rosenbaum, M. D., VandeWoude, S., Volckens, J., & Johnson, T. E. (2010). Disparities in Ammonia, Temperature, Humidity, and Airborne Particulate Matter between the Micro-

and Macroenvironments of Mice in Individually Ventilated Caging. *Journal of the American Association for Laboratory Animal Science*, *49*(2), 7.

Sefton, C., Davies, A., Allen, T.-J., Wray, J. R., Shoop, R., Adamson, A., Humphreys, N., Coll, A. P., White, A., & Harno, E. (2019). Metabolic Abnormalities of Chronic High-Dose Glucocorticoids Are Not Mediated by Hypothalamic AgRP in Male Mice. *Endocrinology*, *160*(5), 964–978. https://doi.org/10.1210/en.2019-00018

Sharma, A., Lavie, C. J., Borer, J. S., Vallakati, A., Goel, S., Lopez-Jimenez, F., Arbab-Zadeh, A., Mukherjee, D., & Lazar, J. M. (2015). Meta-Analysis of the Relation of Body Mass Index to All-Cause and Cardiovascular Mortality and Hospitalization in Patients With Chronic Heart Failure. *The American Journal of Cardiology*, *115*(10), 1428–1434. https://doi.org/10.1016/j.amjcard.2015.02.024

Small, L., Gong, H., Yassmin, C., Cooney, G. J., & Brandon, A. E. (2018). Thermoneutral housing does not influence fat mass or glucose homeostasis in C57BL/6 mice. *Journal of Endocrinology*, *239*(3), 313–324. https://doi.org/10.1530/JOE-18-0279

Strack, A. M., Bradbury, M. J., & Dallman, M. F. (1995). Corticosterone decreases nonshivering thermogenesis and increases lipid storage in brown adipose tissue. *American Journal of Physiology-Regulatory, Integrative and Comparative Physiology*, *268*(1), R183–R191. https://doi.org/10.1152/ajpregu.1995.268.1.R183

Sui, W., Li, H., Yang, Y., Jing, X., Xue, F., Cheng, J., Dong, M., Zhang, M., Pan, H., Chen, Y., Zhang, Y., Zhou, Q., Shi, W., Wang, X., Zhang, H., Zhang, C., Zhang, Y., & Cao, Y. (2019). Bladder drug mirabegron exacerbates atherosclerosis through activation of brown fat-mediated lipolysis. *Proceedings of the National Academy of Sciences*, *116*(22), 10937–10942. https://doi.org/10.1073/pnas.1901655116

Sutherland, L. N., Capozzi, L. C., Turchinsky, N. J., Bell, R. C., & Wright, D. C. (2008). Time course of high-fat diet-induced reductions in adipose tissue mitochondrial proteins: Potential mechanisms and the relationship to glucose intolerance. *American Journal of Physiology-Endocrinology and Metabolism*, *295*(5), E1076–E1083. https://doi.org/10.1152/ajpendo.90408.2008

Thuzar, M., Law, W. P., Ratnasingam, J., Jang, C., Dimeski, G., & Ho, K. K. (2018). Glucocorticoids Suppress Brown Adipose Tissue Function In Humans: A Double-Blind Placebo-Controlled Study : *Diabetes, Obesity and Metabolism*, *20*(4), 840–848.

UpToDate Inc (2022). Prednisone: Drug information. URL: https://www.uptodate.com/contents/prednisone-drug-information/print?topicRef=127454&source=see_link

van den Beukel, J. C., Boon, M. R., Steenbergen, J., Rensen, P. C. N., Meijer, O. C., Themmen, A. P. N., & Grefhorst, A. (2015). Cold Exposure Partially Corrects Disturbances in Lipid Metabolism in a Male Mouse Model of Glucocorticoid Excess. *Endocrinology*, *156*(11), 4115–4128. https://doi.org/10.1210/en.2015-1092

van den Beukel, J. C., Grefhorst, A., Quarta, C., Steenbergen, J., Mastroberardino, P. G., Lombès, M., Delhanty, P. J., Mazza, R., Pagotto, U., Lely, A. J., & Themmen, A. P. N. (2014). Direct activating effects of adrenocorticotropic hormone (ACTH) on brown adipose tissue are attenuated by corticosterone. *The FASEB Journal*, *28*(11), 4857–4867. https://doi.org/10.1096/fj.14-254839

van Donkelaar, E. L., Vaessen, K. R. D., Pawluski, J. L., Sierksma, A. S., Blokland, A., Cañete, R., & Steinbusch, H. W. M. (2014). Long-Term Corticosterone Exposure Decreases Insulin

Sensitivity and Induces Depressive-Like Behaviour in the C57BL/6NCrl Mouse. *PLoS ONE*, *9*(10), e106960. https://doi.org/10.1371/journal.pone.0106960

Vieira, V. J., & Valentine, R. J. (2009). Mitochondrial biogenesis in adipose tissue: Can exercise make fat cells 'fit'? *The Journal of Physiology*, *587*(14), 3427–3428. https://doi.org/10.1113/jphysiol.2009.175307

von Essen, G., Lindsund, E., Cannon, B., & Nedergaard, J. (2017). Adaptive facultative diet-induced thermogenesis in wild-type but not in UCP1-ablated mice. *American Journal of Physiology-Endocrinology and Metabolism*, *313*(5), E515–E527. https://doi.org/10.1152/ajpendo.00097.2017

Williams, D.M. (2018). Clinical Pharmacology of Corticosteroids. Respir Care *63*, 655–670. https://doi.org/10.4187/respcare.06314.

Winn, N. C., Vieira-Potter, V. J., Gastecki, M. L., Welly, R. J., Scroggins, R. J., Zidon, T. M., Gaines, T. L., Woodford, M. L., Karasseva, N. G., Kanaley, J. A., Sacks, H. S., & Padilla, J. (2017). Loss of UCP1 exacerbates Western diet-induced glycemic dysregulation independent of changes in body weight in female mice. *American Journal of Physiology-Regulatory, Integrative and Comparative Physiology*, *312*(1), R74–R84. https://doi.org/10.1152/ajpregu.00425.2016

Wu, H., & Ballantyne, C. M. (2020). Metabolic Inflammation and Insulin Resistance in Obesity. *Circulation Research*, *126*(11), 1549–1564. https://doi.org/10.1161/CIRCRESAHA.119.315896

Zhong, H., & Yin, H. (2015). Role of lipid peroxidation derived 4-hydroxynonenal (4-HNE) in cancer: Focusing on mitochondria. *Redox Biology*, *4*, 193–199. https://doi.org/10.1016/j.redox.2014.12.011

Chapter 6: Conclusions & Future Directions

Conclusions

With the incidence of metabolic diseases and obesity on the rise, the need to further understand AT and its role in metabolism is critical. The goal of this study was to determine how the effects of chronic corticosterone and β3AR stimulation impacts AT. Our central hypothesis was that the negative effects of excessive lipid accumulation and associated metabolic dysfunction induced by chronic corticosterone will be alleviated by β3AR agonists. Through various experiments and analyses, we determined that four weeks of exposure to high levels of corticosterone resulted in increased body and AT weights, BAT whitening, whole-body IR, and increased leptin concentrations without changes to oxidative stress markers or mitochondrial content. Treatment with β3AR agonist mirabegron did not impact body or AT weights, WAT beiging, glucose metabolism or leptin concentrations. Increased uncoupling protein UCP1 was observed in both chronic corticosterone and mirabegron treatments, relative to the control groups used in these studies. Mitochondrial content was not impacted by the presence of either corticosterone, mirabegron or the combination of corticosterone and mirabegron. However, when equated to tissue mass, the corticosterone and combination treatment groups contained less mitochondria per gram of tissue, which may have played a role in its function. This was the first study that reported whole-body metabolic effects in a short amount of time, without causing overt disease. Previous studies examining the effects of mirabegron on a HFD, or the effects of chronic doses of corticosterone, induce disease first and then attempt to reverse it with a different treatment. To our knowledge, the concurrent administration of corticosterone and mirabegron to study their interaction has also not been reported previously. When both treatments were combined, mirabegron failed to prevent any alterations in the body or AT

weights, alleviate corticosterone-induced IR, reduce high circulating leptin or increase UCP1 in the ATs. This was the first study to examine these treatments concurrently for four weeks, and the first study to illustrate that the highest approved dose of mirabegron could not induce beiging in WAT or counteract BAT whitening when corticosterone was present in levels equivalent to metabolic syndrome.

Future Directions

Our current work illustrated how the water consumption and dose of the treatment should also be reported in future drinking water drug delivery studies to ensure reproducibility and accuracy in interpreting results. Most studies involving rodents also do not report the time of year that an experiment was conducted, or specific data on actual room temperature (with most reporting the target temperature only), adding complexity to fully understanding and reproducing any of the results obtained in similar types of experiments. This is a flaw in current preclinical studies and should be a reporting requirement to ensure the results are interpreted correctly in the future. It is also important to investigate the effects of different routes of administration of mirabegron, for example through gavage compared to drinking water, in order to compare its effects systemically. It is currently understood that the metabolism of mirabegron is likely not dominated through one specific pathway, but it is known to be extensively cleared by the liver (Kashyap & Tyagi, 2013).

References

Kashyap, M., & Tyagi, P. (2013). The pharmacokinetic evaluation of mirabegron as an overactive bladder therapy option. *Expert Opinion on Drug Metabolism & Toxicology*, *9*(5), 617–627. https://doi.org/10.1517/17425255.2013.786700

Chapter 7: Limitations, Basic Assumptions, & Delimitations

Limitations and Basic Assumptions

As with any animal model, variability is inevitable, even with comprehensive monitoring. Our mice we housed at the Pre-Clinical Research facility following the Canadian Council on Animal Care guidelines (Canadian Council on Animal Care, 2020). The mice were assumed to be pathogen and disease-free when they arrived from Charles River and were maintained with ample food and water throughout the experiment. Even though the appropriate housing temperatures and humidity were targets, as explained previously, these were not achieved for both studies. The different seasons and room conditions may have played a role in the variabilities observed, but it is impossible to know the extent of these effects.

Lastly, the second animal study and all analyses were conducted during the COVID-19 pandemic. The pandemic presented unique challenges: initiating the second animal study after the pre-clinical research facility was closed for some time, wet laboratory capacity limits, acquiring supplies, and scheduling a team for tissue retrieval. While these limitations were in place, all experiments got completed, and the time of laboratory closure allowed for the project to expand for a more complete study.

Delimitations

While we strongly attempted to mitigate all known limitations, any biological model comes with certain constraints. The first is that this study was performed on mice. While mice serve as a great model for modelling disease and outcomes in humans (discussed previously in Experimental Design and Methods). Rodents serve as pre-clinical models for physiological experiments that allow for a much deeper understanding of the whole-body response than an *in vitro* cell culture model. In this dissertation, we used C57BL/6NCrl mice from Charles River Laboratories that belong to the strain of mice most commonly used in medical research (Jackson Laboratory, 2021). While there are strain differences between the C57BL/6NCrl strain and the more frequently reported sub-strain C57BL/6J, we chose this model due to the availability and treatment application (Bryant, 2011; Capri et al., 2019). The C57BL/6NCrl strain does not show the same increased ethanol consumption as the C57BL/6J strain, making the 6NCrl strain a better fit with our treatment delivery method (i.e., dissolved in ethanol) (Bryant, 2011). Another delimitation was the low blood volume retrieved from each mouse. This meant that only certain plasma measurements could be analyzed, and strategic selections needed to be made. This meant that other circulating inflammatory markers could not be analyzed. In order to reduce the number of animals needed for the experiment, no further animals were added for this single measure.

Another delimitation in our study is that we only used male mice. Historically, more stress research is conducted on males than females (Luine et al., 2017). Females also have a heightened stress reactivity when it comes to uncontrollable stress (Rincón-Cortés et al., 2019). In contrast, controllable stress (such as tail shock running wheels in rodents) did not affect

females overall (Rincón-Cortés et al., 2019). To successfully understand the effects of our treatment on beiging, the more challenging sex was chosen to be able to positively determine the use of mirabegron as a beiging agent and as a combination therapy to mitigate the effects of chronic stress.

Our model only used one timepoint in our experiments, and further studies involving longer study durations may have resulted in increased inflammatory responses or changes in oxidative stress markers. The four-week time point was determined based on previously reported studies. While we observed differences in many of our measurements, a longer duration may have allowed for further changes to occur within the AT.

Using a drinking water-based treatment delivery method is also a delimitation. Treatments were administered to the mice through water bottles that were pre-weighed in order to track water consumption. The amount of water consumed was then divided by the number of mice in the cage for approximate water amount consumed per mouse. While this method of delivery was chosen as the most optimal set-up for drug delivery to the animals, it resulted in an approximation for the dosage each animal received within the cage. Drinking water delivery methods offer poorer control over water consumption, as evident by the significant ($p \leq 0.05$) increase in the corticosterone group in our first animal study, which resulted in the mice receiving a dose greater than that which was targeted. Compared to other methods, such as oral gavage or injection, the same level of control cannot be achieved. The drinking water method of delivery does allow for the diurnal rhythm of corticosterone to be maintained and lower the amount of physical stress placed on the animals (since they did not need to be restrained to receive the treatments). While we did correct for the increased water

consumption in the corticosterone treatment water partway through the study, this may have impacted our results. We were able to deliver the target dose more accurately to the mice by correcting the concentration in the water in the second animal study. This further emphasizes how important reporting is for drug delivery via drinking water. Most studies do not report the animals' drinking water consumption, which may account for some discrepancies observed between previously published findings and our study.

References

Bryant, C. D. (2011). The blessings and curses of C57BL/6 substrains in mouse genetic studies: Bryant. *Annals of the New York Academy of Sciences*, *1245*(1), 31–33. https://doi.org/10.1111/j.1749-6632.2011.06325.x

Canadian Council on Animal Care. (2020). *Guidelines on: Laboratory animal facilities - characteristics, design and development.* Canadian Council on Animal Care.

Capri, K. M., Maroni, M. J., Deane, H. V., Concepcion, H. A., DeCourcey, H., Logan, R. W., & Seggio, J. A. (2019). Male C57BL6/N and C57BL6/J Mice Respond Differently to Constant Light and Running-Wheel Access. *Frontiers in Behavioral Neuroscience*, *13*, 268. https://doi.org/10.3389/fnbeh.2019.00268

Jackson Laboratory. (2021). *C57BL/6J*. https://www.jax.org/strain/000664

Luine, V., Gomez, J., Beck, K., & Bowman, R. (2017). Sex differences in chronic stress effects on cognition in rodents. *Pharmacology Biochemistry and Behavior*, *152*, 13–19. https://doi.org/10.1016/j.pbb.2016.08.005

Rincón-Cortés, M., Herman, J. P., Lupien, S., Maguire, J., & Shansky, R. M. (2019). Stress: Influence of sex, reproductive status and gender. *Neurobiology of Stress*, *10*, 100155. https://doi.org/10.1016/j.ynstr.2019.100155

Chapter 8: Appendix

Mirabegron Dose Calculations

As adapted from Nair and Jacob, 2016

K_m factor is the correction factor for converting animal and human doses by estimating the body weight (kg) of the species to its body surface area (m^2)

Converting Animal Dose to Human Dose (K_m factor= 0.081)

$Mirabegron_{High}$ = 8mg/kg

$Mirabegron_{Low}$ = 0.8mg/kg

$Mirabegron_{High}$ = 8mg/kg x 0.081 = 0.65mg/kg in humans

$Mirabegron_{Low}$ = 0.8mg/kg x 0.081 = 0.065mg/kg in humans

The $Mirabegron_{low}$ dose would be approximately equal to a 5mg dose in humans

Converting Human Dose to Animal Dose (K_m factor= 12.3)

Mirabegron doses are either 25mg/day or 50mg/day

If you assume the average person weighs 80kg

25mg/80kg =0.31mg/kg

50mg/80kg = 0.625mg/kg

25mg dose = 0.31mg/kg x 12.3 = 3.85mg/kg in mice

50mg dose = 0.625mg/kg x 12.3 = 7.68mg/kg in mice

The $Mirabegron_{high}$ dose would be approximately equal to a 50mg dose in humans

Mice Dose Received

If you assume the average mouse weighs 30g = 0.03kg

$Mirabegron_{High}$ = 8mg/kg

$Mirabegron_{Low}$ = 0.8mg/kg

$Mirabegron_{High}$ = 8mg/kg x 0.03kg/mouse = 0.048mg/ml

Each mouse drinks approximately 5ml of water per day = 0.24mg received per day

$Mirabegron_{Low}$ = 0.8mg/kg x0.03kg/mouse = 0.0048mg/ml

Each mouse drinks approximately 5ml of water per day = 0.025mg received per day

Example Power Analyses

The sample sizes were determined based on other studies being conducted using either corticosterone or mirabegron treatments in mice. Power analysis was performed using University of British Columbia's online statistics software (https://www.stat.ubc.ca/~rollin/stats/ssize/n2.html) with values reported by research in this area.

A power above 0.80 was desired from each analysis.

A sample size of 10 mice in each group, will provide an n value adequate to determine the treatment effects.

Example of power analysis for the mirabegron study described by Sui et al. (2019):

- UCP1 expression
  - Ms1=18, Ms2=30, sigma= 5, power = 0.97, alpha =0.05, n=5
- Body weight
  - Ms1=29, Ms2=26, sigma= 2 power = 0.92, alpha =0.05, n=10
- iBAT SUV-Body weight
  - Ms1=4, Ms2=8, sigma= 2, power = 0.89, alpha =0.05, n=5

Example of Power analysis for the corticosterone study van Donkelaar et al. (2014):

- HOMA-IR:
  - Ms1=37.1, Ms2=6.8, sigma= 4.5, power=0.99, alpha =0.05, n=5

Therefore, this study chose a sample group of 10 mice per group in order for the effects between treatments to be observed.

In order to complete all the measurements, additional animals were included in the study to ensure n=10 per group for each experiement.

Animal Care Committee
t: (807) 343-8283
research@lakeheadu.ca

MEMORANDUM

Date: October 25, 2019

To: Dr. Simon Lees, Neelam Khaper, Jocelyn Bel, Ashley Nemec-Bakk, Sarah Niccolli,

Subject: ACC Approval for ROMEO #1467270

Thank you for re-submitting your protocol titled, "*The Effects of Stress Hormones on Beiging and Inflammation of Adipose Tissue: Pilot Study*" to the Animal Care Committee (ACC) with the changes requested.

On behalf of the Animal Care Committee, I am pleased to inform you that the protocol has been **approved.**

Annual renewal is required each year with up to 3 renewals granted. The Office of Research Services will send you a reminder annually of your upcoming renewal.

If any serious animal incidents occur, the Animal Care Committee must be contacted immediately.

All the best for a successful research study.

Sincerely,

Dr. Christine Gottardo
Chair, Animal Care Committee

/scw

SOP # R-46-LUACF

Title: Ear Notching in Rodents

Species: Laboratory Rats and Mice

1. Purpose:

   1.1. To describe the use and method of ear notching in rodents.
   1.2. To provide a form of identification for mice and rats in the LUACF.

2. Responsibility:
   2.1. The responsibility for this procedure lies with the ACC-approved Animal users.

3. Minimum Qualifications/Training Required:
   3.1. Appropriate CCAC (Canadian Council on Animal Care) modules, facility orientation training, health and safety training, and species-specific animal handling training or experience.
   3.2. Training and experiences for carrying out ear notching in rodents.

4. Materials:
   4.1. Legend
   4.2. Ear punch
   4.3. Rodent restraining device
   4.4. Anesthetizing equipment and drugs
   4.5. 70% alcohol

5. Procedure:
   5.1. Ear notching may be used as a means of identification for laboratory rodents.
   5.2. The locations of the notches are determined by the ACC-approved animal users.
   5.3. The procedure for the notching is as follows:
      5.3.1. A legend for the notches is written up.
      5.3.2. An ear punch is tested on a piece of paper for effectiveness.
      5.3.3. The animal is restrained or anesthetized as necessary to prevent injury to the animal or the staff.
      5.3.4. An appropriate local anesthesia agent can be applied.
      5.3.5. The animal ear is swabbed with alcohol.
      5.3.6. The ear punch is swabbed with alcohol.
      5.3.7. The punch is placed over the pinna of the ear and positioned as described in the legend.
      5.3.8. The punch is squeezed in a quick firm motion to insure completeness of the punch.
      5.3.9. The animal is checked for bleeding and completeness and accuracy of the notch.
      5.3.10. The animal is returned to its cage.
      5.3.11. The ear punch is cleaned with alcohol.

6. References:

   6.1. University of Medicine & Dentistry of New Jersey, Ear Notching SOP: 1-21-95.

Review/Approval:

Veterinarian: P. Alderson — Date of review: January 16, 2018

ACC Chair: N. Luckai — Date of approval: January 16, 2018

SOP # R-18-LUACF

Title: Isofluorane Anaesthesia in Rodents

Species: Rats and Mice

1. Purpose:
   1.1. To describe the use of isofluorane anaesthesia to induce and maintain a surgical plane of inhalation anaesthesia in mice and rats.

2. Responsibility:
   2.1. Researcher
   2.2. Animal Care Technician or Veterinarian

3. Minimum Qualifications/Training Required:
   3.1. CCAC modules, Health & Safety Training, Facility Orientation
   3.2. Rodent handling training and/or experience
   3.3. Training and/or experience in general and inhalation anaesthesia of rodents

4. Materials:
   4.1. Anaesthesia machine (including vaporizer, tubing, breathing circuit (Mapleson E or other suitable for small rodents), oxygen tank, scavenger canister
   4.2. Nose cone, appropriate size for animal being anaesthetized
   4.3. Isofluorane anaesthesia, with key-fill adaptor
   4.4. Induction chamber
   4.5. Heating pad
   4.6. Eye lubricant (e.g. lacrilube, isoptotears)
   4.7. Subcutaneous fluids (0.9% saline or Lactate Ringers Solution), needles and syringes

5. Procedure:

For Occupational Health and Safety, isofluorane anaesthesia should be performed in a biosafety cabinet whenever possible. The nose cone should fit snugly to prevent gas from escaping. The induction chamber should be flushed with oxygen prior to opening. Refer to the MSDS sheets on the use of Isofluorane.

   5.1. Rodents do not need to be fasted prior to anaesthesia. However, to ensure their mouths are empty of food, and not potentially blocking their airway, food should be removed from the cage 1 hour prior to anaesthesia. Water does not need to be removed.

5.2. Do a pre-anaesthetic evaluation of the animal to be anaesthetized. If any health concerns are noted, contact the Veterinarian prior to proceeding.

5.3. Ensure anaesthesia system is properly connected

5.3.1. Induction chamber: inspect the chamber for cracks and ensure the lid closes securely. Attach one (blue) hose to the anaesthetic machine and one port on the induction chamber. Attach another hose (white) to the scavenger canister and the other port on the induction chamber.

5.3.2. Mapleson E circuit: Ensure it is intact and ready to use, but do not hook up until animal is anesthetised in the induction chamber. Attach appropriate sized mask to the T-end of the tubing. When ready to use, attach thin end to oxygen out port on the anaesthetic machine. Attach thicker end to the white hose attached to the scavenger canister.

5.3.3. Scavenger system: weigh canister without tubing before using, record weight. Do not use if the canister is over 50 grams from its original weight.

5.3.4. Fill vaporizer with isofluorane: Screw keyed adaptor onto isofluorane bottle collar. Unscrew top screw of vaporizer port. Place keyed adaptor into vaporizer port, ensuring that the holes are lined up. Tighten screw again. Lift isofluorane bottle and allow the liquid to pour into vaporizer. Fill to top line. Do not overfill. Loosen screw, remove keyed adaptor, and tighten screw. Remove keyed adaptor from isofluorane bottle and recap bottle with original cap. Keyed adaptor must remain with the vaporizer. Recheck the level of anaesthesia before starting. Recheck the level between animals or if the procedure is lengthy.

5.4. Turn oxygen on

5.4.1. Refer to SOP R-19-LUACF-Safe Oxygen Use

5.4.2. Ensure regulator is closed (turn counter clockwise until it feels loose)

5.4.3. Gauge should read zero

5.4.4. Turn tank valve on counter clockwise several turns to open

5.4.5. Turn regulator clockwise until the pressure on the gauge reads 55 psi (red line)

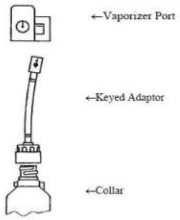

5.5. Place a drop of eye lubricant in each eye of the animal

5.6. Place animal in induction chamber and seal lid

5.7. Place induction chamber on heating pad

5.8. Turn oxygen on at the anaesthetic machine to about 1 to 1.5 L/min. Allow the rodent to acclimatize to the chamber for about 1 minute on oxygen.

5.9. Turn the isofluroane gas on by pressing down on the white button and turning the dial on the vaporizer to 1%. Allow the rodent to adjust to this amount of gas for about 1 minute.

5.10. Slowly turn the dial by 1% increments until you reach 4% to 5%. Allow the rodent to rest at this level until it is not responding to a gentle rocking of the induction

chamber. Monitor the breathing. It should go from rapid and shallow to slower, regular and deeper breaths as the animal goes under anaesthesia. Never leave an animal alone in the induction chamber.

5.11. Once the animal is under anaesthesia (not responding to gentle rocking, and breathing slow and regular), flush the chamber with oxygen by pressing the oxygen flush button on the anaesthesia machine several times. You will need to proceed quickly for the next steps so as not to allow sufficient time for the animal to wake up for anaesthesia.

5.12. Unplug the oxygen hose (blue) from the outflow port on the anaesthesia machine and plug in the smaller hose of the Mapleson E circuit. You can leave this blue hose attached to the induction chamber.

5.13. Unplug the scavenger (white) hose (leave it connected to the charcoal canister) from the induction chamber and attach it to the larger hose on the Mapleson E circuit.

5.14. Take the rodent out of the induction chamber and place the nose into the appropriate sized nose cone of the Mapleson E circuit. Set the induction chamber with the blue hose attached aside.

5.15. Keep the animal on the heating pad during the entire procedure to ensure warmth. Position and secure rodent for procedure as per AUP. Ensure that the nose is in the nose cone at all times. During the procedure, periodically check to ensure that the nose remains in the nose cone.

5.16. Turn the isofluorane gas down to about 1.5% to 2% to maintain the rodent under anaesthesia. Monitor breathing, heart rate, toe pinch reflex, eye blink response, and mucous membrane color to ensure proper anaesthesia. Adjust from 1.5% to 4% isoflourane as needed to maintain adequate plane of anaesthesia.

5.17. Administer subcutaneous fluids according to SOP R-20-LUACF-Subcutaneous Fluid Administration in Rodents. Place another drop of eye lubricant in each eye. Check the level of anaesthesia by toe pinch and blink response. If there is not response, and breathing is slow, deep and regular, you can proceed with the surgery or procedure intended. If there is a response, then wait and periodically check reflexes until there is no response and you have obtained a surgical plane of anaesthesia.

5.18. Continue to monitor the level of anaesthesia periodically during the surgery or procedure by checking breathing, heart rate, toe pink, eye blink and mucous membrane color. The surgical plane of anaesthesia is indicated by deep slow regular breathing, steady heart rate, and absence of toe pinch or eye blink reflex (see chart below). The mucous membrane should be pink.

5.19. Once the procedure is finished and you wish to recover the animal, turn the gas off (turn the dial on the vaporizer all the way to zero and ensure it clicks into place). Leave the oxygen on until the rodent's breathing becomes more rapid, about 1 to 2 minutes.

5.20. Place another drop of eye lubricant in each eye and place the animal back in the cage. It is best to recover the animals alone, with no other animal in the cage, if possible. Turn the oxygen off at the anaesthetic machine by turning the dial and

watching the silver ball fall all the way to the bottom. Keep the animal warm until it is able to walk around the cage normally without stumbling. Until the animal is fully recovered (approximately 10 to 30 minutes), it should not be left alone.

5.21. Clean your station, including the induction chamber, anaesthetic machine tubing, and nose cone. Use a mild detergent (e.g. dawn dish soap, Accel cleaner on the chamber, tubing and nose cone, and rinse thoroughly with water. Allow to dry adequately before storing. Hang the tubing up for several hours to dry thoroughly.

5.22. Ensure a record of anaesthesia is filled out for each animal.

5.23. Depending on the AUP, the rodent should be rechecked at least 4 to 6 hours post-anaesthesia to ensure full recovery.

6. Reference Chart:

Table 1. Parameters to gauge level of anaesthesia in rodents.

	Too light	Surgical Plane	Too deep or problem
Heart beat	Fast, regular	Slower, regular	Irregular, very slow, absent
Respirations	Fast, regular, shallow	Slower, regular, deep	Irregular, very slow, strained, absent
Toe pinch reflex	Present, animal will pull leg back	absent	absent
Eye blink reflex	Animal will blink	Absent	absent
Mucous membrane color	pink	pink	Red, pale, grey, white, blue

Review/Approval:

Author: P. Alderson

ACC Chair: N. Luckai Date of approval: March 27, 2015

SOP # R-09-LUACF

Title: Blood Collection Techniques in Rodents

Species: Mice and Rats

1. Purpose:
   1.1. To describe commonly used ACC acceptable procedures for taking blood samples from mice and rats.
   1.2. Retro-orbital bleeding, toe clip and tail tip amputation blood sampling are generally not used. These techniques are not described in this SOP. Prior ACC approval with strong scientific justification and a written SOP is required before these techniques can be used.

2. Responsibility:
   2.1. ACC approved Animal Users

3. Minimum Qualifications/Training Required:
   3.1. CCAC modules, Facility Orientation and Biosafety Training
   3.2. Training and experience with handling mice and rats
   3.3. Training and experience in blood collection in mice and rats

4. Materials:
   4.1. PPE (lab coat, gloves, mask, eye goggles)
   4.2. Masking Tape (optional)
   4.3. Animal weigh scale
   4.4. Scalpel blade (e.g. #22) or fur clippers
   4.5. Gauze and/or alcohol swab
   4.6. Antiseptic solution (e.g. Betadine solution or Chlorohexidine)
   4.7. Sterile needles (e.g. maximum 25G)
   4.8. Syringes (e.g. 1 – 3 mL)
   4.9. Collection tubes (see Table 2) +/- anticoagulant
   4.10. Animal restraint device or anaesthesia (see below)

   If using Anaesthesia:
   4.11. Anesthesia and delivery system
   4.12. Sterile Ophthalmic Ointment
   4.13. Heat lamp or temperature-control pad

5. Procedure:

General Guidelines:

5.1. VOLUME AND FREQUENCY OF SAMPLES:

5.1.1. For survival sampling: The approximate circulating blood volume of rodents is 55 to 70 ml/kg of body weight. Of the circulating blood volume, approximately 10% of the total volume can be safely removed every 3 to 4 weeks, 7.5% every 7 days, and 1% every 24 hours. Volumes greater than recommended should be justified in the AUP and appropriate fluid and/or cellular replacement provided. See Table 1 for more specific guidelines on sample volumes and frequency for a range of body weights.

5.1.2. Generally, samples 15% of circulating blood volume and greater are collected under anesthesia and are terminal procedures.

5.1.3. Sampling from the saphenous and tail can be repeated in a single animal if following the above guideline.

5.1.4. Due to potential complications, repeat sampling is not advised using the jugular vein technique.

5.1.5. Cardiac blood sampling can only be done once per animal, and is a terminal procedure.

5.1.6. Unsuccessful attempts or training sessions should be limited to 3 needle insertions per animal. If no blood has been collected after 3 attempts, the animal should be rested for a minimum of 24 hours. A longer rest period is required if a hematoma or bleeding occurs.

Table 1: Approximate Blood Sample Volumes and Frequency for a Range of Body Weights.

Body weight (g)	***CBV(ml)**	**1% CBV (ml)** ***every 24 hrs†***	**7.5% CBV (ml)** ***every 7 days†***	**10% CBV (ml)** ***every 3 - 4 wks†***	**> 15% CBV (ml)** ***once, terminal***
20	1.10 - 1.40	.011 - .014	.082 - .105	.11 - .14	> 0.21
25	1.37 - 1.75	.014 - .018	.10 - .13	.14 - .18	> 0.26
30	1.65 - 2.10	.017 - .021	.12 - .16	.17 - .21	> 0.31
35	1.93 - 2.45	.019 - .025	.14 - .18	.19 - .25	> 0.36
40	2.20 - 2.80	.022 - .028	.16 - .21	.22 - .28	> 0.42
125	6.88 - 8.75	.069 - .088	.52 - .66	.69 - .88	> 1.31
150	8.25 - 10.50	.082 - .105	.62 - .79	.82 - 1.0	> 1.57
200	11.00 - 14.00	.11 - .14	.82 – 1.05	1.1 - 1.4	> 2.10
250	13.75 - 17.50	.14 - .18	1.0 – 1.3	1.4 - 1.8	> 2.62
300	16.50 - 21.00	.17 - .21	1.2 – 1.6	1.7 - 2.1	> 3.15
350	19.25 - 24.50	.19 - .25	1.4 – 1.8	1.9 - 2.5	> 3.67

*Circulating blood volume In general: Mice CBV = 58.5 mL/kg Rat CBV = 64 mL/kg	†Maximum sample volume for that sampling frequency in healthy mouse. For obese animals, blood volume should be reduced to 7% CBV	Note: a survival volume of 10 – 15% CBV may be obtained once monthly with prior ACC approval with strong scientific justification.

5.2. TYPE OF SAMPLES:

5.2.1. No anticoagulant is needed for serum samples

5.2.2. Anticoagulants will be required if a plasma or whole blood sample is needed.

5.2.2.1. Syringes can be primed with anticoagulant prior to taking sample by drawing up the required amount of anticoagulant into the syringe through the needle. In most cases, heparin or EDTA can be drawn up into syringe and majority of volume expelled, just filling the syringe hub with anticoagulant.

5.2.2.2. Special collection tubes can also be purchased (see Table 2). If the collection tube contains an anticoagulant, the syringe need not be primed before taking the sample. Instead, collect blood sample and immediately transfer the sample to the collection tube. Gently rock the blood in the tube back and forth to mix well with the tube contents.

5.2.3. Confirm sample collection requirements prior to obtaining your blood samples.

Table 2. General Guideline of Contents and Uses of Common Blood Collection Tubes.

Contents of tube	***Typical color code**	***Typical laboratory use**
No anticoagulant: Plastic vials: clot activator Glass vials: no additive	Red	Serum collection, serology, blood chemistry
EDTA	Lavender Pink	Plasma, whole blood collection, hematology & blood typing
Sodium Citrate 3.2%	Light Blue	Coagulation assays
Lithium Heparin	Light Green	Plasma, blood chemistry
Sodium Heparin	Dark Green	Plasma, blood chemistry
Potassium Oxalate and Sodium Fluoride	Gray	Blood glucose
Potassium EDTA	Tan	Lead testing
Gel, clot activator	Gold	Serum
Sodium Heparin +/- EDTA	Dark Blue	Heavy metal testing
		*always confirm with supplier and/or laboratory

5.3 USE OF ANAESTHESIA:

5.3.1 Lateral saphenous and tail vein blood collection techniques can be performed safely and easily in non-anesthetized animals.

5.3.2 General anesthesia can decrease blood flow and make sampling more difficult from the saphenous vein.

5.3.3 A local anaesthesia, such as EMLA cream, can be used at the collection site in most cases.

5.3.4 General anesthesia is required for jugular vein and cardiac blood sampling.

5.4 SURVIVAL SAMPLING:

5.4.1 When larger volumes of blood are obtained, fluid volume should be replaced.

5.4.1.1 Mice: Give 1 mL warmed sterile lactated ringers solution (LRS) via SC or IP routes.

5.4.1.2 Rats: Give 3 to 10 mL warmed sterile lactated ringers solution (LRS)

5.4.2 Ensure bleeding has stopped before returning the animal to its cage.

5.4.3 Ensure all blood has been wiped from the animal, as this may cause fighting among cage mates.
5.4.4 Monitor the animal periodically for the next 24 hours to ensure bleeding does not restart, and that the animal is not chewing or licking excessively at the collection site.
5.4.5 Offer a reward (e.g. appropriate food treat) post-sampling whenever possible.

5.5 DISPOSAL OF SHARPS & BLOOD PRODUCTS:
5.5.1 Dispose of sharps in sharps container.
5.5.2 Dispose of all items containing or contacting blood into biohazard container.
5.5.3 See SOP R-55-LUACF-*Waste and Carcass Disposal*.

5.6 **Lateral Saphenous Vein Blood Collection:**

Figure 1. Insertion of needle and location of saphenous vein for blood collection of caudal limb.

5.6.1 Gently place the animal into a conical tube with small opening at opposite end to allow for breathing or other suitable restraint device.
5.6.1.1 For mice, a one person technique is easiest, when experienced.
5.6.1.2 For rats, it may be easier for 1 person to restrain and 1 person to do blood collection, especially when first learning.
5.6.2 LEFT SIDE COLLECTION: Extend the left hind leg and hold it in position by placing your thumb and index finger over the fold of skin between the tail and thigh. But applying firm pressure to this area, you can keep the leg in the proper position while occluding the saphenous vein.
5.6.3 RIGHT SIDE COLLECTION: Extend the right hind leg and hold the fold of skin between the abdomen and cranial thigh surface.
5.6.4 Using a small scalpel blade or clippers, shave a small area of dry hair (approximately 1 cm) off the lateral surface of the left hind leg proximal to the hind foot. The saphenous vein should now be visible on the surface of the thigh.
5.6.5 Use gauze dampened with lukewarm water or alcohol swab to smooth away any hair that is covering the phlebotomy site.
5.6.6 Use a sterile needle (e.g. 25 G) to puncture the saphenous vein.
5.6.7 A drop of blood will appear and can then be collected into a collection tube.

5.6.8 If the flow of blood stops, flex the foot or briskly rub the puncture site with a dry gauze swab.
5.6.9 Avoid re-puncture of the site whenever possible. However, if re-puncture is necessary, the same puncture site should be penetrated.
5.6.10 When the blood collection is completed, flex the foot towards the knee in order to reduce the flow of blood back to the puncture site.
5.6.11 By using a dry gauze square, apply firm pressure to the puncture site until the bleeding stops.
5.6.12 Ensure that bleeding has stopped before returning the animal to its cage.
5.6.13 If several small samples are required throughout the day, just remove the scab off the puncture site to initiate blood flow. If the flow does not start, flex the foot and/or briskly, but gently, rub the puncture site with a dry gauze.
5.6.14 No more than 4 samples within a 24 hour period should occur with this technique unless otherwise pre-approved by the ACC.
5.6.15 USE OF TOURNIQUET: a tourniquet can be applied to facilitate blood collection. This is especially helpful in the mouse.
5.6.16 A tourniquet for a mouse can be made from a syringe and suture material. (Figure 2 & 3)
5.6.17 Place tourniquet around limb just above stifle. (Figure 2)

Figure 2. Placement of tourniquet for saphenous blood collection in mouse.

5.6.18 Remove tourniquet immediately after blood sample has been collected and apply digital pressure to allow hemostasis. Tourniquet should not be left tightened for longer than 5 minutes as tissue damage will occur.

FIGURE 3. Instructions for making a mouse-sized tourniquet.

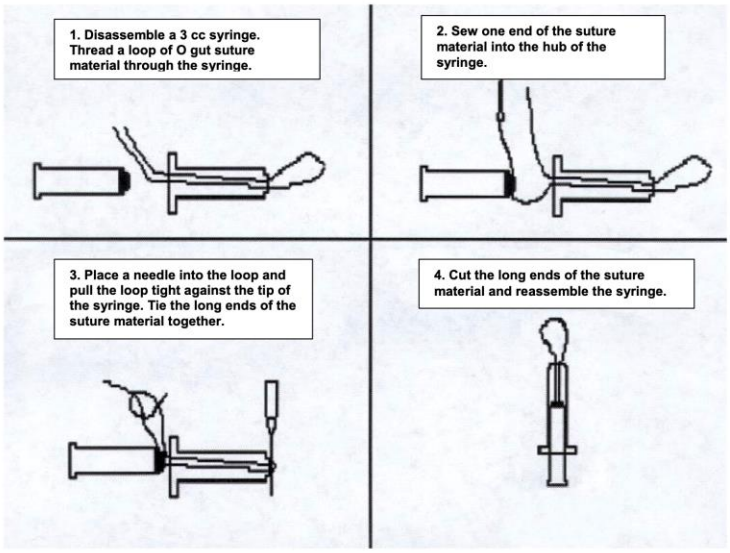

5.7 Tail Vein Blood Collection:

Figure 4. Restraint and insertion of needle for tail vein blood collection.

5.6.1 Warming the animal or the animal's tail prior to collection will make collection easier.

5.6.2 Place a heat lamp over the cage of the animals that you need to bleed. Monitor the animals closely to ensure they do not overheat. Do not place the heat lamp less than 50 cm above the cage, as they can become easily burned, especially albino strains.

5.6.3 Signs of overheating can include reddened ears and agitation.

5.6.4 Alternately, place animal's tail into warm water for 1 minute while it is inside the restraint device prior to taking sample. Take care that the water is not too hot as to scald the skin.
5.6.5 Remove one animal at a time from cage and place in restraint device.
5.6.6 Wipe the phlebotomy site with gauze moistened with warm water or an alcohol swab.
5.6.7 Puncture the lateral tail vein towards the tip of the tail (this ensures that you have more sites to bleed if the first site does not bleed well).
5.6.8 If bleeding stops, a gentle but brisk rub over the puncture site with a clean dry gauze square will stimulate bleeding.
5.6.9 If blood flow is limited, place a tourniquet over the vessel at the base of the tail. Ensure that you loosen or remove the tourniquet immediately after your sample has been collected. Tourniquet should not be left tightened for longer than 5 minutes as tissue damage will occur.
5.6.10 Collect the required volume of blood by drawing the blood droplets into a syringe directly from the tail vein. Do not milk the tail as this will haemolyse the sample.
5.6.11 Place direct pressure on the puncture site to stop the bleeding.
5.6.12 Ensure bleeding has stopped before returning the animal to its cage.
5.6.13 No more than 6 samples within a 24 hour period should occur with this technique unless otherwise pre-approved by the ACC.

5.7 Jugular Vein Blood Collection:

Figure 5. Location of the rodent jugular vein and site of needle insertion.

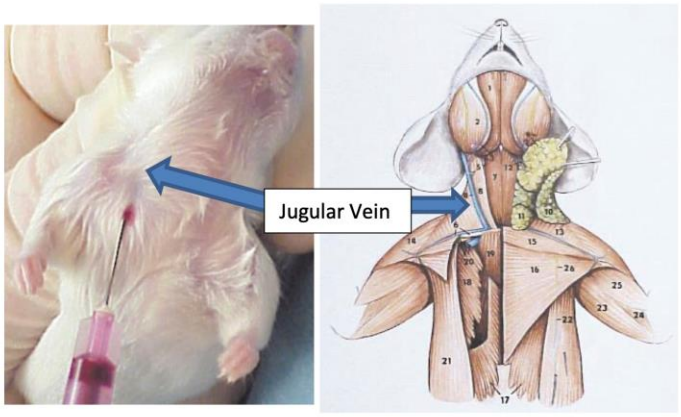

5.7.1 This technique is generally only used in rats by experienced personnel.
5.7.2 Complications can arise due to the positioning needed to obtain the sample. Some of these complications can include cessation of breathing, bleeding in the ears, forelimb lameness, and a hematoma at the bleeding site. Thus, this technique is limited to instances where alternate techniques cannot be used.
5.7.3 Anesthetize the rat as per study protocol and ensure a deep plane of anesthesia with a toe pinch test.

5.7.4 Apply sterile ophthalmic ointment to both eyes to prevent corneal ulceration.
5.7.5 Place animal in dorsal recumbency on insulating material or heating pad to help maintain body temperature.
5.7.6 The rodent is then secured with masking tape as per Figure 6 below. It is important that the rodent is positioned with is vertebra as straight as possible and the front limbs at approximately 45° angles to the spine. The forelimbs should extend, but not excessively stretched such that the anterior border of the pectoral muscle restricts venous return in the jugular vein, leading to distension and clear visualization.

Figure 6. Positioning of animal for jugular vein blood collection.

5.7.7 Shave the neck area around the phlebotomy site.
5.7.8 Prepare the site for blood collection by wetting the fur with a mixture of antiseptic soap (e.g. Chlorohexidine) and warm water. Avoid soaking the animal to prevent hypothermia.
5.7.9 Place a syringe underneath the neck of the animal to make the jugular vein more prominent. This hyperextends the neck and raises the jugular vein. Alternatively, experienced personnel may extend the neck digitally as indicated in Figure 5.
5.7.10 The jugular vein appears blue and lays 2 to 4 mm lateral to the sternoclavicular junction (Figure 5). This will be at approximately the middle point between the sternum and the ball of the shoulder.
5.7.11 Pull the skin taut and using a 1mL syringe and 23 to 25 G needle, approach the vein in a caudocephalic direction (from back to front). Insert the needle approx. 1 to 3 mm deep, 2 to 4 mm lateral of the sternoclavicular junction. (Figure 5)
5.7.12 Pull back on the plunger slightly once you have entered the skin to create a bit of suction to draw blood into the hub once you hit the vein.
5.7.13 Advance the needle slowly, a few millimeters at a time, through the skin and pectoral muscle into the vein.
5.7.14 If you hit the clavicle with the needle, pull back slightly and redirect it above the clavicle.
5.7.15 Once the needle is in the trunk of the vein, a very small drop of blood will appear in the needle hub. Stop advancing and steady the needle. Slowly "milk" back on the plunger until the required sample volume is obtained.
5.7.16 When the desired blood volume is obtained, apply slight digital pressure to the site before withdrawing the needle. This pressure should be held for a minimum of 30 seconds to prevent hematoma formation.

5.7.17 Ensure bleeding has stopped before recovering from anaesthesia.
5.7.18 Recover animal in a warm, quiet environment. Ensure fully recovered before returning animal to its home cage.
5.7.19 Repeat sampling using this method should be avoided.
5.7.20 NOTE: When learning this technique it may be helpful to initially perform a jugular cut down by incising the skin over the vein and gently teasing the subcutaneous fat away from the site. Visualization of the distended jugular greatly assists orientation and facilitates the "milking" procedure. This should be a non-recovery training technique only.

5.8 Cardiac Blood Collection:

Figure 7. Insertion of needle for cardiac blood collection.

5.8.1 Deeply anaesthetize or euthanize the mouse as per study protocol.
5.8.1.1 If euthanizing the animal prior to sampling, sampling must occur immediately after euthanasia.
5.8.1.2 If anaesthetized, perform a toe pinch test to ensure the animal is in a deep plane and unable to feel pain (surgical plane of anesthesia).
5.8.2 Place animal in dorsal recumbency and secure with masking tape (optional).
5.8.2.1 The forelimbs are taped separately and should be at a 90 degree angle to the body of the animal.
5.8.2.2 If experienced with the procedure, taping may not be necessary.
5.8.3 Before inserting needle into animal, pull back on the syringes plunger to ensure smooth movement.
5.8.3.1 For mice: Use a 1 mL to 3 mL syringe and a 21G or 22 G x 1" needle.
5.8.3.2 For rats: Use a 3 mL to 12 mL syringe and an 18 or 21 G x 1" to 1.5" needle.
5.8.4 Insert the needle at an approximate 5 to 15 degree angle immediately caudal to the xyphoid process (Figure 7). A larger animal will require a larger degree angle.
5.8.5 Place a slight negative pressure on the syringe, by pulling back on plunger, upon immediate entry into the skin.
5.8.6 Advance the needle forward until blood appears in the hub of the needle.

5.8.7 Once blood appears, stop advancing and steady the needle. Slowly "milk" back on the plunger until the required sample volume is obtained.
5.8.8 If blood flow stops, slowly and gently move your needle forward, back, up or down until blood flows again. This will take very small movements; otherwise you will exit the heart. Do not move the needle in a circular motion when inserted into the chest cavity.
5.8.9 Once adequate blood volume has been obtained, release pressure on the syringe before exiting the chest cavity.
5.8.10 If anesthetized, euthanize the animal via an ACC approved method once the sample has been obtained.
5.8.11 No more than 1 sample can occur with this technique and death of the animal must be assured once sample has been obtained.

6. References:

6.1. AALAS Learning Library. https://www.aalaslearninglibrary.org/ Free Animal Care and Use Courses. Mouse Biomethodology: Section 10. IV Injection and Blood Collection.
6.2. CCAC Guide to the Care and Use of Experimental Animals. Volume 1, 2nd Ed. 2017. http://www.ccac.ca/Documents/Standards/Guidelines/Experimental_Animals_Vol1.pdf
6.3. Hoff J. *Methods of Blood Collection in the Mouse*. 2000. Lab Animal: 29(10).
6.4. National Center for Replacement, Refinement and Reduction of Animals in Research. Blood Sampling Microsite. http://www.nc3rs.org.uk/bloodsamplingmicrosite/page.asp?id=313
6.5. NIH Guidelines for Survival Bleeding in Mice and Rats, 2010.

Review/Approval:

Author: P. Alderson

ACC Chair: N. Luckai Date of approval: May 14, 2018